

Regulation of vesicular trafficking in presence of mutations in contractile proteins

Dissertation
for the award of the degree
“Doctor rerum naturalium”
of the Georg-August-Universität Göttingen

within the doctoral program Molecular Biology of Cells
of the Georg-August University School of Science (GAUSS)

submitted by
YuanYuan Dai

from Nei Mongol, China
Göttingen 2022

Thesis Committee

PD Dr. Antje Ebert

Department of Cardiology and Pneumology
University Medical Center Göttingen

Prof. Dr. Henning Urlaub

Max-Planck-Institut für biophysikalische Chemie
Bioanalytische Massenspektrometrie Gruppe

Prof. Dr. Silvio O. Rizzoli

Department of Neuro- and Sensory Physiology
University Medical Center Göttingen

Members of the Examination Board

Referee: Prof. Dr. Ralf Dressel

Institut für Zelluläre und Molekulare Immunologie
University Medical Center Göttingen

2nd Referee: Prof. Dr. Dörthe Katschinski

Center for Physiology and Pathophysiology
Department of Cardiovascular Physiology
University Medical Center Göttingen

3rd Referee: Prof. Dr. André Fischer

Department for Psychiatry and Psychotherapy
German Center for Neurodegenerative Diseases (DZNE)
University Medical Center Göttingen

Date of oral examination:28-03-2022.....

Table of Contents

Table of Contents	I
Figure index	II
Abstract.....	III
List of abbreviations	V
1 Introduction.....	1
1.1 Membranes and the cytoskeleton are essential for cell function.....	1
1.2 Sarcomeres are basic functional units of cardiomyocytes	1
1.3 Troponin T	2
1.4 Tropomyosin	3
1.5 Troponin-tropomyosin (Tn-TPM) complexes on the sarcomeres	4
1.6 Sarcomeric microdomain organization is critical for the structure and function of cardiomyocytes	5
1.7 Intermediate filaments and microfilaments	6
1.8 Sarcomeres, microfilaments, and the PM are connected by costameres	6
1.9 Vinculin is an essential component of the costamere	7
1.10 PIP2 is regulated by RhoA functions	8
1.11 Functions of PIP2-enriched microdomains.....	9
1.12 Clathrin-mediated-endocytosis (CME)	9
1.13 Iron uptake via CME of transferrin receptor.....	11
1.14 Human iPSC-CMs as alternative model for molecular functional studies in DCM	13
2 Aims of this study	16
3 Publications	17
3.1 Pulication1	17
3.2 Pulication2	18
4 Discussion	19
4.1 Sarcomeric protein disorganisation results in microdomain dysfunction.....	21
4.2 Sarcomere disorganisation leads to impaired interactions with the PM	22
4.3 Defective sarcomere-microfilament-PM interactions cause impaired CME and abnormal early endosome distribution	23
4.4 Sarcomeric mutations result in impaired cargo uptake and depletion of iron levels in mitochondria.....	25
4.5 Novel therapeutic implications and directions of this study.....	25
4.6 Conclusions and outlook.....	26
5 Own contributions.....	29
6 List of publications	30
7 References	31
8 Acknowledgements	44

Figure index

Figure 1: Sarcomeres in cardiomyocytes are made up of thin filaments, thick filaments, and titin. 2

Figure 2: Tn-TPM complexes on thin filaments. 3

Figure 3: Conformational changes in Tn-TPM complexes upon Ca²⁺ binding to TnC. 4

Figure 4: Costameres connect sarcomeres, cytoskeleton, and the PM. 7

Figure 5: A schematic presentation of key steps in CME 10

Figure 6: Schematic illustrating the fate of iron at cellular levels. 13

Figure 7: Disorganized sarcomeric proteins result in dysfunction of sarcomeric microdomains. 21

Figure 8: Defective endocytosis and endosome distribution result in mitochondrial iron deficiency in presence of DCM mutations. 24

Abstract

The molecular and cellular mechanisms underlying disease phenotypes in dilated cardiomyopathy (DCM) are diverse and to date incompletely understood. Inherited mutations in genes encoding structural components of the sarcomere lead to DCM and have been studied previously. Moreover, induced pluripotent stem cell-derived cardiomyocytes (iPSC-CMs) from patients carrying familial DCM mutations have been shown to recapitulate disease phenotypes such as sarcomere misalignment and reduced contractility. In addition, impaired β -adrenergic signaling was reported to represent an important disease phenotype in DCM. However, the consequences of inherited DCM mutations on molecular pathological signaling in cardiomyocytes are not yet completely clear.

In presence of sarcomeric mutations, this study found disorganisation of sarcomeres to result in disturbed interactions between sarcomeric proteins, such as troponin T and tropomyosin. Moreover, interactions between sarcomeric proteins and proteins located at local microdomains, such as PKA (protein kinase A), were disturbed. Therefore, sarcomeric DCM mutations led to impaired local signaling and entailed reduced TnI phosphorylation upon β -adrenergic stimulation. Furthermore, interactions between sarcomeres and membrane-associated cytoskeleton-binding proteins, such as filament C and vinculin, were found to be disturbed. Together, these findings indicated that in presence of sarcomeric DCM mutations, defective interactions occur between sarcomeres and other cytoskeleton elements as well as the plasma membrane (PM).

Defects in sarcomere-cytoskeleton-PM interactions were also discovered to lead to impaired actin polymerization at the PM and reduced plasma membrane PIP2 levels. This was discovered to further result in impaired cargo uptake and abnormal early endosome distribution. Disturbed uptake of cargo such as transferrin-bound iron caused decreased iron levels in the mitochondria and defective cardiomyocyte functions, such as reduced contractility. Moreover, Rho A activation was found to

rescue these disease phenotypes, specifically the depletion of mitochondrial iron levels and the reduced contractility observed in presence of sarcomeric DCM mutations. This may represent a basis for potential future translational strategies. In addition, this study also showed that at cellular levels, replenishing intracellular iron could restore the depleted iron levels in mitochondria and rescue the impaired contractility in DCM iPSC-CMs. This provided further evidence for the benefits of iron supplementation, a treatment approach in patients with heart failure which is already in clinical use. Of note, left ventricular tissues from DCM patients with end-stage heart failure were found to display abnormal endosome distribution, compared to the left ventricular tissues from patients with preserved systolic left-ventricular function. This suggests that iron deficiency due to defective endocytosis may present a more general mechanism. Taken together, this study has discovered that disorganised sarcomere protein organization leads to impaired sarcomere-cytoskeleton-PM interactions, disturbed functions of cardiomyocyte signaling pathways, and defective uptake and distribution of cargo by clathrin-mediated endocytosis. This study provides potentially relevant directions for future translational therapeutic strategies.

List of abbreviations

AKAP	A-kinase anchoring protein
AMPK	AMP-activated protein kinase
AP2	adaptor protein 2
Arp2/3	actin related protein 2 and 3
BAR	Bin-Amphiphysin-Rvs
Ca ²⁺	calcium
cAMP	cyclic AMP
CCP	clathrin-coated pits
CME	clathrin-mediated endocytosis
CRISPR	clustered regularly interspaced short palindromic repeats
crRNAs	CRISPR RNAs
DCM	dilated cardiomyopathy
DMT1	divalent metal transporter 1
DSB	double-stranded break
EC	excitation–contraction
EEA1	early endosome antigen1
EHM	engineered heart muscle
F-actin	filamentous actin
FPN	ferroportin
FRET	fluorescence resonance energy transfer
G-actin	monomeric actin
GPCRs	G protein-coupled receptors
HCM	hypertrophic cardiomyopathy
HDR	high-fidelity homology-directed repair
hERG	human ether-a-go-go related gene
I/R injury	ischemia/reperfusion injury
IFs	Intermediate filaments
iPSC-CMs	induced pluripotent stem cell-derived cardiomyocytes
iPSCs	Induced pluripotent stem cells
IREs	iron regulatory elements
IRP1	Iron regulatory proteins 1
IRP2	Iron regulatory proteins 2
Lat-A	latrunculin-A
LDL	low-density lipoprotein
MIM	missing-in-metastasis
MyBPC	myosin binding protein C
MYH	myosin heavy chain
NHEJ	error-prone non-homologous end joining
PDEs	Phosphodiesterases
PIP2	Phosphatidylinositol 4,5-bisphosphate
PIP5K	Phosphatidylinositol 4-phosphate 5-kinase
PKA	protein kinase A
PKC	protein kinase C
PM	plasma membrane
RBPs	iron regulatory proteins
RhoA	Ras homolog gene family member A

List of abbreviations

SAA	α -actinin
Ser 23/24	Ser 23 and Ser 24
sgRNAs	single-guide RNAs
STEAP3	six-transmembrane epithelial antigen of the prostate 3
Tf	transferrin
TfR	transferrin receptor
TnC	troponin C
TnI	troponin I
TnT	troponin T
Tn-TPM	troponin-tropomyosin
TPM	Tropomyosin
WASH	Wiskott Aldrich Syndrome protein
WASP	Wiskott Aldrich Syndrome protein and scar homologue complex
β 2AR	β 2-adrenergic receptor
β -ARs	β -adrenergic receptors

The abbreviations used in the presented publications are shown within the articles.

1 Introduction

1.1 Membranes and the cytoskeleton are essential for cell function

Membranes comprise bilayers of phospholipids and membrane-associated proteins. Separating the intracellular space from the extracellular environment, membranes substantially define the structure and function of cells and their organelles, including e.g. the nucleus, mitochondria, as well as the cytoskeleton¹. The cytoskeleton includes intermediate filaments, microtubules and actin filaments (microfilaments) which perform nutrient uptake and signal transduction in cells in a coordinated way. For example, endocytosis is a process through which the plasma membrane (PM) invaginates into cells with the aid from a complex protein machinery including also cytoskeleton elements². Endocytosis includes different types of uptake, such as clathrin-mediated endocytosis (CME), caveolae-mediated endocytosis and others. β 2-adrenergic receptor (β 2AR) undergoes agonist-induced endocytosis through clathrin-coated pits and sequentially couples with Gs and Gi to transmit signals. It has been reported that the carboxyl-terminal PDZ-binding motif of the β 2AR is essential for β 2AR endocytic uptake in cardiomyocytes³. A further example is β -arrestin, which functions as an endocytic adaptor and scaffold protein by binding to β 2AR and clathrin^{4,5}. In addition, endocytosis is an important part of the mechanism mediating turnover of ion channels at the plasma membrane in cardiomyocytes⁶. For example, cells internalize the hERG (human ether-a-go-go related gene) potassium channel (Kv11.1) involved in the repolarisation phase of the cardiac action potential through a clathrin-independent endocytic mechanism⁷. Taken together, endocytosis as a process is essential for cells to uptake nutrients such as iron and lipids, and to mediate signal transduction.

1.2 Sarcomeres are basic functional units of cardiomyocytes

The cytoskeleton in cardiomyocytes contributes to structure integrity, mechanical resistance and signaling transduction⁸. Sarcomeres belong to the cytoskeleton and are the structural building blocks of heart muscle. Their particularly specialized functions depend on a highly organized cell structure. In cardiomyocytes, sarcomeres comprise three principal important components: actin-containing thin filaments, myosin-containing thick filaments, and titin (Figure 1)⁹. The thick filaments contain myosin and other proteins, such as myosin binding protein C (MyBPC). The thin filaments contain the troponin-tropomyosin (Tn-TPM) complex decorating the actin filaments. Contraction of cardiomyocytes is conducted via excitation–contraction (EC) coupling,

which is regulated by the coordination of highly organized sarcomere and the level of intracellular Ca^{2+} (Figure 1)¹⁰. Ca^{2+} binds to troponin, resulting in sliding of the thick and thin filaments, as well as cell shortening, and force generation¹⁰.

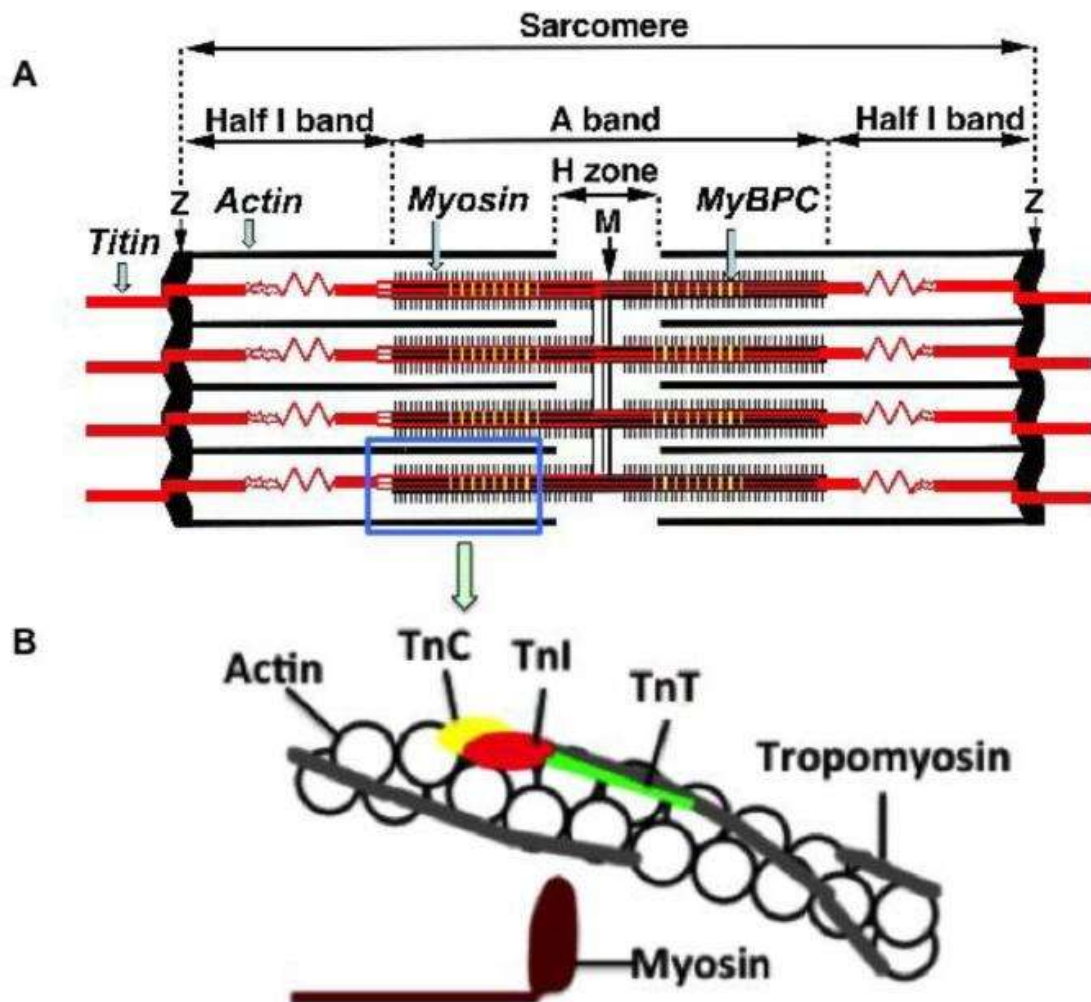


Figure 1: Sarcomeres in cardiomyocytes are made up of thin filaments, thick filaments, and titin.

A schematic showing sarcomeres comprise three principal components including actin-containing thin filaments, myosin-containing thick filaments and titin in cardiomyocytes. Contraction of cardiomyocytes is conducted via excitation–contraction (EC) coupling, which is regulated by the coordination of highly organized sarcomere and the level of intracellular Ca^{2+} . This image is adapted after Yin Z et al. *Biochim Biophys Acta*. 2015 Jan;1852(1):47-52.¹¹

1.3 Troponin T

The troponin (TnT) molecule serves to couple troponin complexes to thin filaments. TnT is composed of a N-terminal variable domain, a conserved middle domain, and a conserved C-terminal domain^{12,13}. The T1 region which consists of N-terminal domain

interacts with tropomyosin (TPM). The T2 region, which comprises the middle and the C-terminal domains, interacts with TnC and TnI to anchor the troponin complexes onto the thin filaments^{12,13}. Amino acid substitutions due to genetic mutations of sarcomeric proteins result in severe cardiac diseases such as dilated cardiomyopathy (DCM) and hypertrophic cardiomyopathy (HCM). Most of the pathogenic mutations in TnT, which include TnT-R173W and TnT-R141W, occur within the T1 region which is known to interact with TPM¹⁴. So far, many studies have crystalized large part of the TnT protein, but no published crystal structures cover yet the complete C-terminal domain of TnT¹⁵⁻¹⁷.

1.4 Tropomyosin

Tropomyosin (TPM) proteins are encoded by the four genes, TPM1, TPM2, TPM3, and TPM4. However, by alternative splicing of gene products, multiple isoforms are produced¹⁸. A crystal structure has been reported for a complex of TPM and the N-terminal segment of TnT¹⁹. The crystal structure of TPM has been resolved at a 7 Å resolution²⁰. TPM1 mutations such as E40K/E54K inhibit the actin-myosin interactions and cross-bridge cycling, ultimately resulting in DCM. The TPM1 mutations E62Q and L185R result in increased stability and ultimately lead to HCM²¹. TPM1-L185F, a TPM1 mutation, is located in a region where interaction of the troponin complex-TPM occurs (Figure 2)¹⁸.

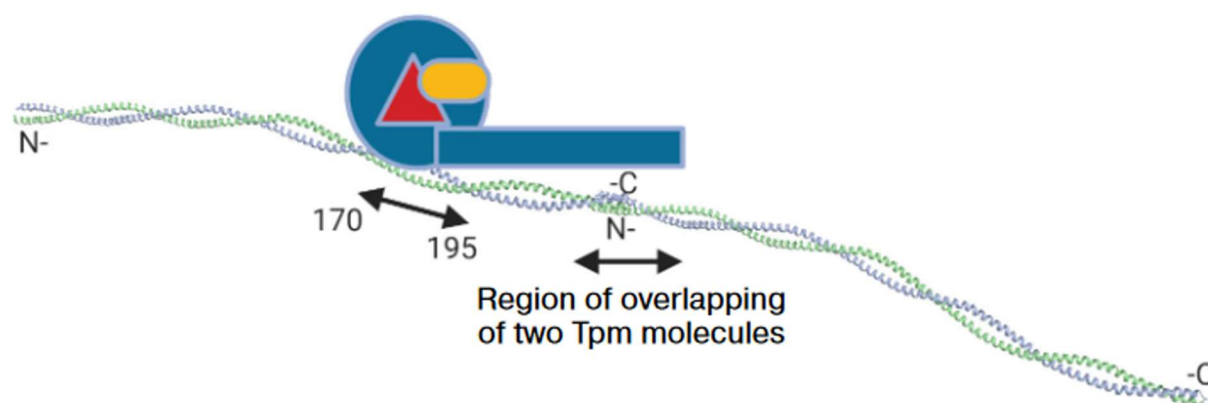


Figure 2: Tn-TPM complexes on thin filaments.

TnT is shown as a blue shape, TnI in red and TnC in yellow. Actin filaments are shown in green helix and TPM is shown in light blue. Arrows indicate the sites of TnT interacted with TPM. This image is adapted after A M Matyushenko et al. *Biochemistry (Mosc)*. 2020 Jan;85(Suppl 1): S20-S33.¹⁸

1.5 Troponin-tropomyosin (Tn-TPM) complexes on the sarcomeres

The troponin-tropomyosin (Tn-TPM) complex on thin filaments is a critical component for EC coupling. During the systolic state, cytosolic Ca^{2+} is increased and consequently, binding of cytosolic Ca^{2+} to troponin C (TnC) induces conformational changes of troponin I (TnI). This results in dissociation of an inhibitory domain of TnI from actin and allows TPM to expose the myosin-binding sites on actin, promoting actin/myosin formation and contraction¹². In diastole, Ca^{2+} dissociates from the N-terminal domain of TnC. This restores the inhibitory action of TnI, disturbing the actomyosin interaction. TPM blocks the interaction site of actin with myosin. The C-terminal domain of TnT interacts with actin and TPM as well, providing stability and anchoring of the Tn-TPM complex on thin filaments (Figure 3)¹².

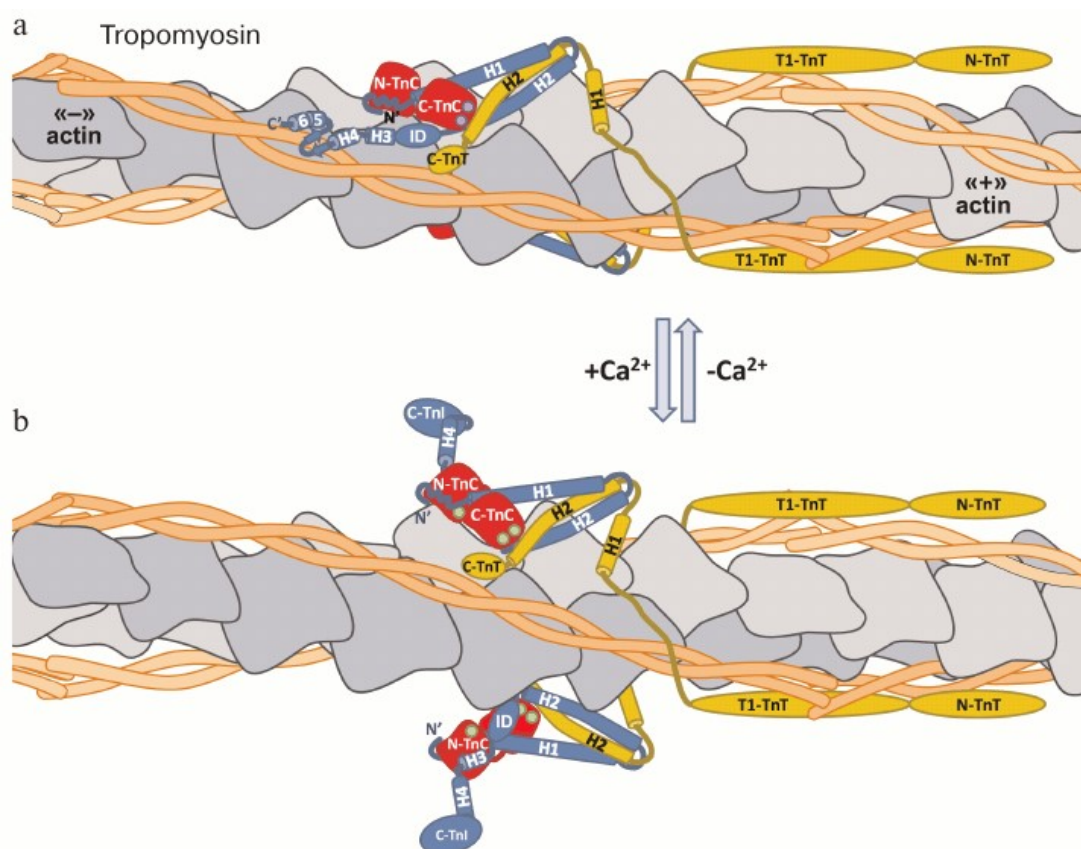


Figure 3: Conformational changes in Tn-TPM complexes upon Ca^{2+} binding to TnC.

The binding of increased cytosolic Ca^{2+} to troponin C (TnC) induces conformational changes in troponin I (TnI). This results in dissociation of an inhibitory domain of TnI from actin and allows TPM to expose the myosin-binding sites on actin, promoting actin/myosin formation and contraction¹². In contrast, dissociation of Ca^{2+} from the N-terminal domain of TnC restores the inhibitory action of TnI, disturbing the actomyosin interaction. TPM blocks the interaction site of actin with myosin. The C-terminal domain of troponin T (TnT) interacts with actin and TPM as well, providing the stability and anchoring of the Tn-TPM complex on thin filaments¹². This image is adapted after I A Katrukha. *Biochemistry (Mosc)*. 2013 Dec;78(13):1447-65.¹²

The barbed ends of the actin filaments are covered by CapZ which interacts with α -actinin (SAA), forming an important part of the z-discs^{22,23}. Z-discs are the lateral boundaries of the sarcomere and serve as anchoring sites for thin filaments and titin⁹. Intermediate filaments proteins such as vimentin connect adjacent myofibrils to the PM by interacting with z-discs⁹. Because of those properties, z-discs achieve proper force transmission and signal transduction from the sarcomere to the PM⁹.

1.6 Sarcomeric microdomain organization is critical for the structure and function of cardiomyocytes

Sarcomeric microdomain organization is important for the maintenance of cardiomyocyte functions²⁴⁻²⁸. For example, L-type calcium channels in caveolin-3 enriched microdomains play an important role in Ca^{2+} signaling²⁴. Sarcomeres are fine-tuned by post-translational modifications, such as PKA-mediated phosphorylation of TnI in response to the activation of β -adrenergic receptors (β -ARs)²⁹. The stimulation of β -ARs activates cyclic AMP (cAMP) generation by adenylate cyclase²⁹. In response to increased cAMP concentrations, PKA phosphorylates and alters the function of cardiac proteins including L-type calcium channels, phospholamban, sarcoplasmic reticulum ryanodine receptor channels, and TnI²⁹. PKA phosphorylates TnI at residues Ser 23 and Ser 24 (Ser 23/24). These residues are located in the N-terminal domain of TnI which is present uniquely in cardiomyocytes²⁹. The phosphorylation decreases the affinity of Ca^{2+} for TnC as well as the Ca^{2+} sensitivity of the myofilaments³⁰⁻³³. A reduction of this PKA-dependent TnI phosphorylation can contribute to reduced cross-bridge cycling rates³¹⁻³⁴. β -agonist-induced lusitropy is significantly impaired in cardiomyocytes from transgenic mice expressing slow skeletal TnI that lacks PKA phosphorylation sites³⁵. Consistently, local coordination of the cAMP signal around sarcomeres maximizes enhancement of contraction and reduces Ca^{2+} sensitivity of myofilaments following β -AR-induced stimulation³⁶. Phosphodiesterases (PDEs) belong to a superfamily of enzymes that hydrolyze phosphodiester bonds of cyclic nucleotides and therefore regulate the cyclic nucleotide-mediated signaling pathway³⁷. It has been shown that inhibition of PDE2A and PDE3A restores cAMP levels and recovers the impaired β -adrenergic signaling in DCM³⁸.

Besides TnI, also TnT has been reported as a sarcomeric AKAP (A-kinase anchoring protein) interacting with PKA at the myofilaments³⁹. In addition, both TnI and TnT can be phosphorylated by protein kinase C (PKC), a family of serine/threonine kinases⁴⁰.

1.7 Intermediate filaments and microfilaments

Intermediate filaments (IFs), including filamin C, vimentin, plectin, desmin, and lamins are essential elements to regulate cellular structure and plasticity⁴¹. IFs link the PM, sarcomeres, and microfilaments in the myocardium^{42,43}. The disturbance of the IF network results in cardiac diseases⁴². Filamin C (also known as γ -Filamin), an actin-binding protein, represents a critical link between the PM and the sarcomere^{9,44}. In cardiomyocytes, filamin C interacts with the z-disc as well as a variety of membrane-associated proteins, such as caveolin-1^{45,46}. Loss of filamin C leads to severe defects in myogenesis and maintenance of structural integrity in muscle cells⁴⁷. Mutations in the gene encoding filamin C have been associated with DCM⁴⁸.

Actin can switch from the monomeric (G-actin) and filamentous (F-actin) state to form microfilaments⁴⁹. Several drugs are known to inhibit actin polymerization, such as latrunculin-A(Lat-A), a drug derived from the Red Sea sponge can bind to G-actin⁵⁰. A core set of proteins, including actin-depolymerizing factors such as profilin, gelsolin and cofilin, regulate actin organization⁴⁹. Gelsolin-mediated actin-severing plays a critical role in actin remodeling in cardiomyocytes⁵¹. F-actin together with myosin comprises an important basis for muscle contraction. Moreover, the Arp2/3 (actin related protein 2 and 3) complex modulates generation of branched actin networks⁵²⁻⁵⁴. The WASH complex, a member of the Wiskott Aldrich Syndrome protein and scar homologue complex (WASP) family of proteins, activates the Arp2/3 complex in endocytosis to control branched actin formation⁵⁵.

An example for central regulatory proteins regulating actin dynamics is adenosine monophosphate-activated protein kinase (AMPK), a conserved serine/threonine⁵⁶⁻⁵⁸. AMPK presents a cytoskeleton remodeling factor via its interaction with myosin heavy chain proteins (MYH)⁵⁷⁻⁵⁹. Furthermore, myosin heavy chain 7 (MYH7) has been documented to interact with troponin⁶⁰. AMPK is a well-known energy sensor in cardiomyocytes due to its role to monitor metabolic activities via the phosphorylation of multiple proteins⁵⁹. AMPK regulates mitochondrial function, mitophagy, and other cellular processes⁵⁹.

1.8 Sarcomeres, microfilaments, and the PM are connected by costameres

Costameres bridge the sarcomere and the PM by interacting with IFs such as filamin C. Filamin C interacts with components of the dystrophin-glycoprotein complex and

the integrin–vinculin–talins complex, two principal protein complexes in the costamere^{61,62}. Costameres are sub-membranous structures which engage both the z-disc and the PM (Figure 4)⁶³. They resemble focal adhesions, which ensure adhesion to the extracellular matrix in non-muscle cells⁶⁴. In addition, costameres are essential for bidirectional signal transmission and force transduction from the sarcomere to the PM⁶³.

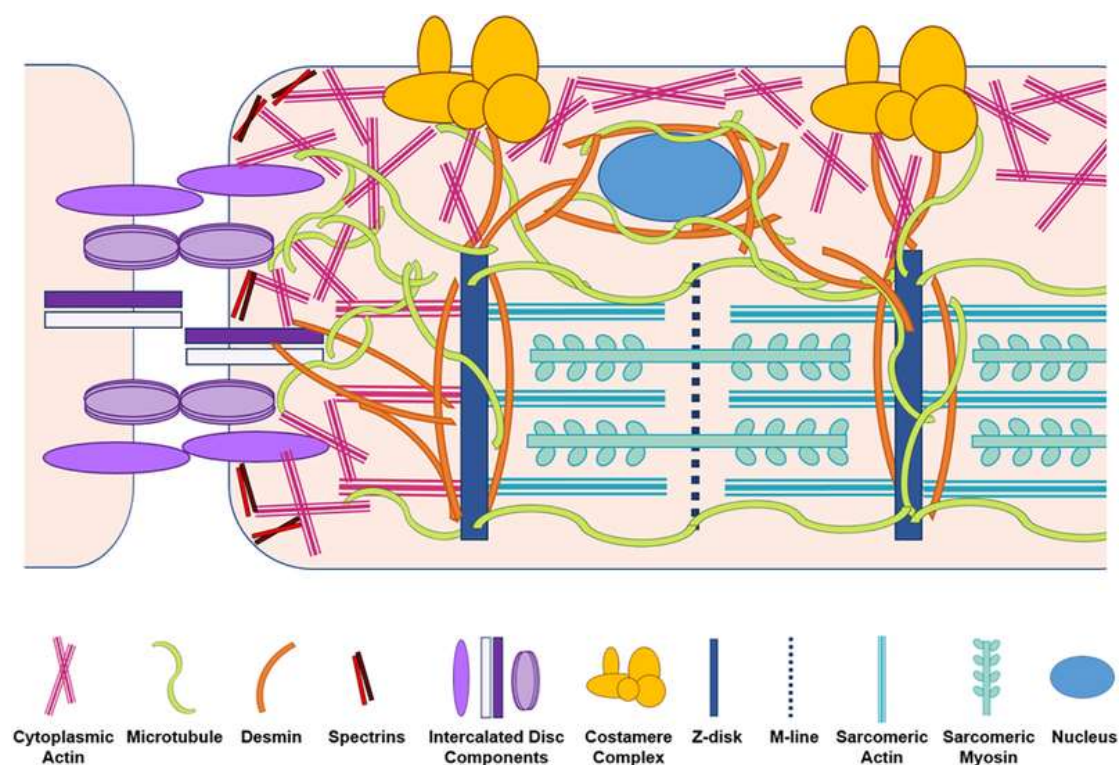


Figure 4: Costameres connect sarcomeres, cytoskeleton, and the PM.

Interactions among sarcomeres, cytoskeleton, and the PM. IFs such as desmin, actin, and microtubules all serve as linkages from sarcomeres to the PM and costameres. Adapted after Kelly M Grimes et al. *J Mol Cell Cardiol.* 2019 Jun; 131:187-196⁶⁵.

1.9 Vinculin is an essential component of the costamere

Vinculin, a membrane-associated actin-binding protein, is critical for the structural integrity of cardiomyocytes and preservation of normal cardiac function⁶⁴. A crystal structure of full-length vinculin molecule has been reported previously^{66,67}. Vinculin contains five domains (D1-5). The D1 domain interacts with SAA and talin. The D5 domain (also known as tail domain) connects to microfilaments and phosphatidylinositol 4,5 bisphosphate (PIP₂). Therefore, vinculin presents a connection among the sarcomeres, actin cytoskeleton and the PM^{68,69}. Vinculin

manipulates the dynamics of the branched actin network via the Arp2/3 complex⁷⁰. Moreover, vinculin binds transiently and directly to Arp2/3, playing a role in integrin-mediated adhesion⁷¹. In addition, vinculin can directly bind to Rab5, a small GTPase associated with vesicular trafficking and fusion, and affect the uptake of pathogens^{72,73}. Direct interactions with PIP2 are essential for activation and localization of vinculin^{74,75}. PIP2 induces conformational changes in vinculin to promote anchoring of the actin cytoskeleton to the PM⁷⁶.

1.10 PIP2 is regulated by RhoA functions

Although PIP2 makes up a minor part of membrane phospholipids and found primarily in the PM^{77,78}, it has several critical functions. PIP2 accounts for less than 1% of membrane phospholipids⁷⁷ and is an essential element in actin dynamics, membrane structure, intracellular trafficking, and signal transduction⁷⁹. Phosphatidylinositol 4-phosphate 5-kinase (PIP5K) is the primary enzyme that generates PIP2 from PIP4 (phosphatidylinositol 4 phosphate) inside cells⁸⁰. RhoA manipulates PIP2 production and F-actin polymerization via PIP5K activation^{81,82}. RhoA (Ras homolog gene family member A), a member of Rho GTPase superfamily, regulates phosphoinositide synthesis, cytoskeleton dynamics, and protein kinase activation⁸³. On the one hand RhoA, is activated by the binding to GTP catalysed by the guanine nucleotide exchange factors⁸⁴. On the other hand, GTPase-activating proteins accelerate the hydrolysis of GTP to GDP and promote the release of the bound effector⁸⁴.

RhoA plays an important role in cardiac remodeling and cardiomyopathies. Previous studies demonstrate that in response to chronic pressure overload, cardiomyocyte-specific deletion of RhoA results in accelerated DCM and increases the severity of heart failure outcome⁸⁵. Low levels of activated RhoA in cardiomyocytes lead to increased tolerance to ischemia/reperfusion (I/R) injury⁸⁶. However, sustained overactivation of RhoA results in pathological consequences⁸⁷. An example is cardiac-specific overexpression of RhoA ultimately induces DCM with impaired contractility⁸⁸. ROCKs (Rho-associated protein kinases) are effector proteins of RhoA⁸⁹. The treatment with a ROCK inhibitor, Y-27632, protects the heart against I/R injury⁹⁰. It has been reported that ROCKs play a role in the development of cardiac fibrosis, hypertrophy, and subsequent heart failure⁹¹. Therefore, a basal amount of RhoA activity is required for normal cardiac function.

1.11 Functions of PIP2-enriched microdomains

PIP2-enriched microdomains are important for membrane curvature sensing and regulation of ion channels^{79,92}. PIP2 is the dominant inner-leaflet lipid of the PM forming microdomains and comprises a size of about 73 nm⁹³. Those domains are essential for protein-PIP2 interactions which are affected by local fluxes of divalent metal ions⁹⁴. PIP2 interacts with many transmembrane proteins, in particular with those containing Bin-Amphiphysin-Rvs (BAR) domains. BAR domain proteins can sense and generate membrane curvature in cooperation with the cytoskeleton and with metabolic changes within the phospholipid bilayer⁹⁵. Actin-binding protein MIM (missing-in-metastasis), a member of the inverse BAR-domain protein family, directly binds PIP2-enriched membranes and deforms them into tubular structures⁹⁶. The ability of full-length BIN1, also known as amphiphysin2, to sense and generate membrane curvature is inhibited on membranes lacking PIP2⁹⁷. PIP2 is necessary for functions of many ion channels and ion transporters on the PM and the depletion of PIP2 can cause defects in their functions⁷⁸. For example, PIP2 is required for the function of the Na⁺-Ca²⁺ exchanger and the ATP-inhibited potassium channels on the PM in cardiac myocytes from guinea pigs⁹⁸.

1.12 Clathrin-mediated-endocytosis (CME)

PIP2-mediated actin polymerization on the PM is critical for the initiation of endocytosis⁹⁹. Endocytosis is a process through which plasma membrane invaginates into the cells so that various cargo molecules can be transported into the cytoplasm¹⁰⁰. Two of the most-studied endocytosis pathways are clathrin-mediated endocytosis (CME) and caveolae-dependent endocytosis. CME is involved in a wide variety of physiological processes including nutrient uptake and cell signaling^{99,101}. For example, CME of transferrin receptor (TfR) is essential for iron homeostasis¹⁰². CME of LDL (low-density lipoprotein) receptor is required for lipid metabolism in cardiomyocytes¹⁰³.

CME demands the spatial and temporal coordination of a complex protein machinery to conduct initiation, cargo loading, membrane bending, scission and uncoating (Figure 5). Firstly, early-arriving proteins including F-BAR domain proteins, adaptor protein 2 (AP2), and cargo adaptors, initiate endocytic events by interacting with clathrin. Those proteins work in a network to form clathrin-coated pits (CCP). Many endocytic proteins are recruited to the PM by interacting with PIP2, and this interaction is necessary for the initiation and stabilization of the CCP^{104,105}. PIP5K catalyses PIP2 production to recruit players involved in endocytic initiation^{99,106}. Secondly, the clathrin coat binds to

the cytosolic parts of transmembrane cargo proteins, resulting in the enrichment of certain cargoes in the region where vesicles were formed. Many proteins including AP2 recognize sorting signals to mediate the cargo loading process¹⁰⁷. Thirdly, several proteins contribute to membrane bending during vesicle formation such as the clathrin coat, actin filaments, and scission proteins. Actin polymerisation is necessary to complete membrane deformation into a CCP on the PM¹⁰⁸. Actin filaments cooperate with the clathrin coat to transmit force and bend the membrane⁹⁹. Furthermore, it has been demonstrated that actin propels vesicles from the PM into the cytoplasm¹⁰⁹⁻¹¹¹. Fourthly, dynamin, a large GTPase, assembles at the neck of the CCP and dissociates it from the PM⁹⁹. Other proteins such as BAR proteins which interact with dynamin are also involved in this process⁹⁹. Lastly, the breakdown of clathrin coat by the chaperone HSC70 probably coordinates the dephosphorylation of PIP2 to conduct uncoating⁹⁹. Inositol polyphosphate 5-phosphatase can be recruited to the endosomes to degrade the remaining PIP2 on the endosomal membrane¹¹².

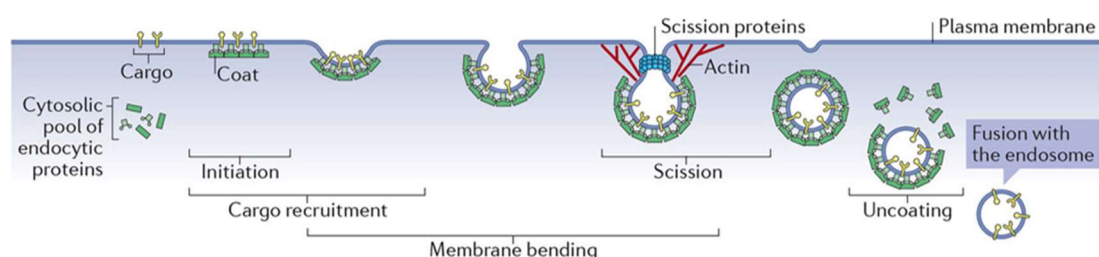


Figure 5: A schematic presentation of key steps in CME

Multiple proteins collaborate to conduct the CME process including nucleation, cargo selection, maturation, scission, and uncoating. Adapted after Kaksonen, M et al. *Nat Rev Mol Cell Biol.* 2018 May;19(5):313-326.⁹⁹

Rab5 and phosphatidylinositol 3-phosphate (PI3P) are produced by VPS34 on the endosomal membranes. These proteins work in a coupled manner to recruit other factors required for membrane tethering and fusion, such as early endosome antigen 1 (EEA1)^{113,114}. A tight control of PIP2 and actin polymerization at the endosomal membranes is essential for cargo sorting¹¹⁵. Retromer complex, a key endosomal protein sorting machinery, requires WASH complex/Arp2/3-mediated actin polymerization to achieve its function¹¹⁶. Wiskott Aldrich Syndrome protein and scar homologue complex (WASH complex) is a complex protein machinery, consisting of KIAA1033, strumpellin, FAM21, WASH1 and CCDC53¹¹⁷. WASP proteins stimulate the Arp2/3 complex to form branched actin filaments^{118,119}. CCDC53 is essential for actin

assembly in response to local PIP2 levels at the surface of endosomal membranes^{117,120}.

1.13 Iron uptake via CME of transferrin receptor

TfR1 and divalent metal transporter 1 (DMT1) are essential for the process of iron uptake¹²¹. Internalization of TfR complexed to ferric transferrin (Tf-Fe³⁺) is conducted through CME¹²². Once TfR is internalized, low pH within the endosomes is generated via proton pumps¹²³. This results in the dissociation of iron from transferrin. A ferric reductase on endosomal membrane, six-transmembrane epithelial antigen of prostate 3 (STEAP3), can reduce free ferric iron (Fe³⁺) to ferrous iron (Fe²⁺)¹²⁴⁻¹²⁶. Ferrous iron is then transported across the endosomal membrane by DMT1 to enter the cytosol^{121,127}. Excessive iron is collected and sequestered by ferritin, a ubiquitous and highly conserved protein (Figure 6)¹²⁸.

Clinically, iron deficiency is a prevalent comorbidity with heart failure, affecting up to 50% of patients¹²⁹. A definition of iron deficiency is that iron availability is insufficient to meet the body's needs, which occur with or without the presence of anemia^{130,131}. The intravenous administration of iron has been documented to improve conditions of patients with heart failure, such as the 6-minute-walking distance and quality of life¹³².

However, the underlying mechanisms of iron deficiency are complex. Iron homeostasis is controlled at both cellular and systemic levels. At systemic levels, duodenal enterocytes play significant roles in dietary iron absorption¹³³. Subsequently, iron can be transported by binding to transferrin (Tf) in the serum. The bone marrow is the major consumer of iron because of its function in haematopoiesis¹³³. The liver is a crucial regulator for iron homeostasis at the system-wide level by secreting hepcidin, an iron hormone^{133,134}. At cellular levels, iron availability is achieved through well-coordinated uptake, utilization, storage and export of iron. In cardiomyocytes, iron uptake is primarily conducted by CME-dependent transferrin uptake. Excessive intracellular iron is stored by ferritin^{128,135,136}. Iron export was performed by ferroportin (FPN, also known as SLC40A1), a transmembrane iron-exporting protein whose activities are controlled by hepcidin¹³⁷⁻¹⁴⁰. Hepcidin orchestrates iron metabolism by inducing the internalization and degradation of ferroportin¹³⁷. IRP1 (iron regulatory protein1, also known as ACO1) represses ferritin mRNA translation under low intracellular iron conditions^{141,142}. Under low levels of intracellular iron, the stability of mRNAs encoding TfR1 is increased to assist iron uptake. Meanwhile, the translation of mRNAs encoding

ferritin and ferroportin is decreased to reduce iron sequestration and export^{143,144}. This adaptation is conducted via iron regulatory proteins (RBPs)/ iron regulatory elements (IREs) system^{143,144}. IRP1 and IRP2 (iron regulatory protein 2, also known as IREB2) can bind to IREs located at the 5' UTR IREs of ferritin and ferroportin mRNAs to prevent their translation, and 5' UTR IREs of the TFR1 mRNA to inhibit its degradation at low iron levels^{144,145}.

Mitochondria are major recipients of iron in the cell^{146,147} and require iron for electron transport in the mitochondrial respiratory chain as well as oxygen transport¹⁴⁸. Iron imbalance particularly in the mitochondria is deleterious as their essential functions require a fine balance of mitochondrial iron¹⁴⁷. Mice lacking TfR 1 in the heart have severely reduced iron levels in the cardiomyocytes, resulting in poor cardiac function and failure of mitochondrial respiration¹⁴⁹. This phenotype can only be rescued by a substantial iron supplementation¹⁴⁹. Studies in human cardiomyocytes indicates iron deficiency is accompanied by impaired contractility, while re-supplementation of iron rescues cardiomyocyte contractility¹⁵⁰.

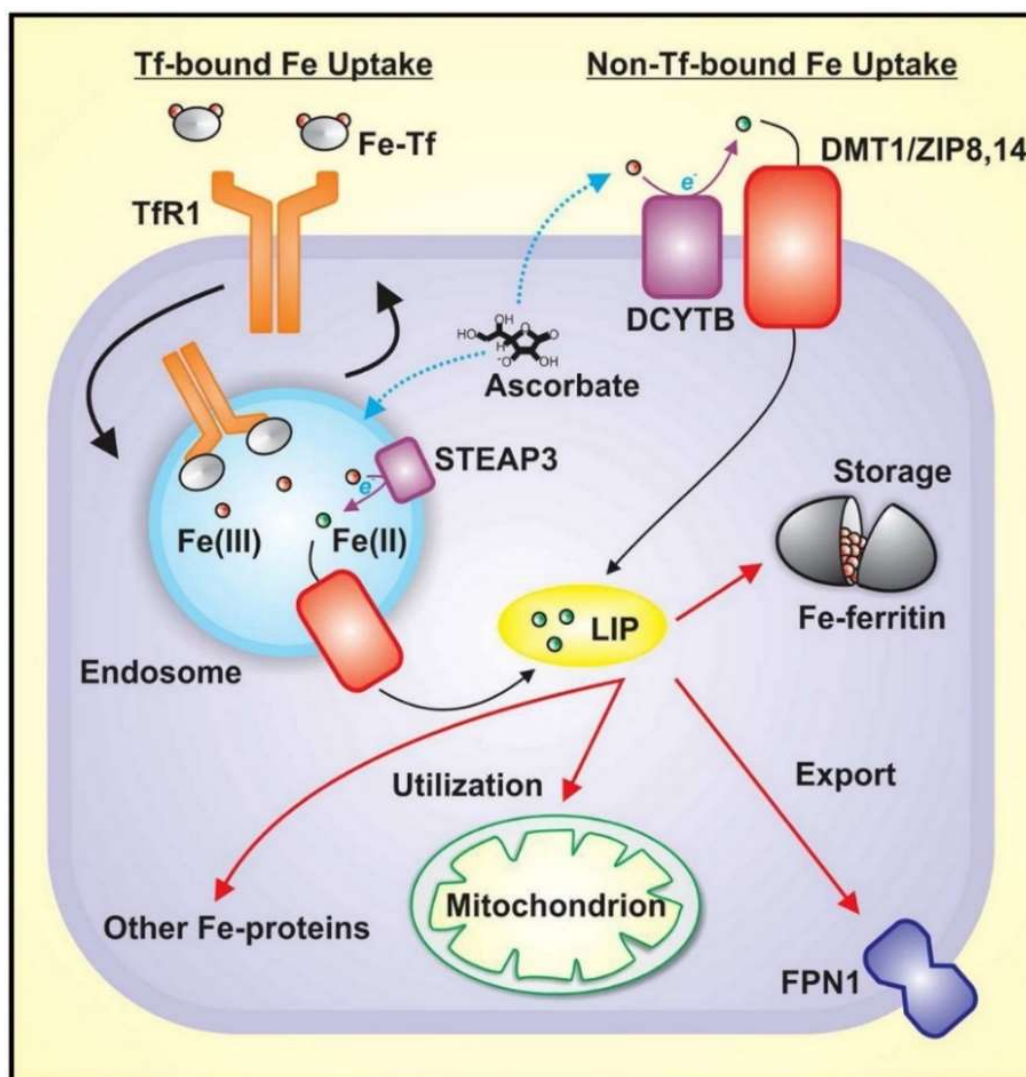


Figure 6: Schematic illustrating the fate of iron at cellular levels.

Iron can enter cardiomyocytes by binding to TfR1 and CME of transferrin receptor. Other ion channels and transporters can assist cells to uptake iron. The acidic environment of the endosomes liberates the iron from the transferrin (Tf)-TfR1 complexes and reduces ferric iron (Fe^{3+}) to ferrous iron (Fe^{2+}). The ferrous iron is then transported across the endosomal membrane and becomes part of labile iron pool (LIP) in the cytosol. Storage is conducted by ferritin. Mitochondria are the major destination for iron utilization. Iron is crucial for the biogenesis of heme and Fe-S clusters, which are key elements for mitochondrial function. Excessive iron is exported by ferroportin (FPN). Adapted after D J R Lane et al. *Biochim Biophys Acta*. 2015 May;1853(5):1130-44.¹⁰²

1.14 Human iPSC-CMs as alternative model for molecular functional studies in

DCM

Despite deep insights into the disease mechanism of DCM provided by animal models, significant species differences are considered to present a limitation to these data¹⁵¹. In addition, human adult cardiomyocytes are a limited resource and not available in sufficient amounts to fulfil the needs of research. This gap may be bridged by additional

human disease models to better understand the molecular and cellular pathogenesis of DCM. Yamanaka and his colleagues identified 4 factors (Oct3/4, Sox2, Klf4, and c-Myc) that are sufficient for reprogramming of somatic cells into iPSCs¹⁵². Human iPSCs can proliferate unlimitedly and have the potential to generate in principle cells of all three germ layers¹⁵³. An additional advantage of this system is to allow the application of gene editing technologies which enhances its potential for applications in biotechnology and translational medicine. iPSCs can be cultured and maintained in a defined medium consisting of eight components (E8)¹⁵⁴. Highly efficient differentiation methods have been established to drive cardiomyocyte differentiation from iPSCs by modulating the Wnt signaling pathway, which is essential for cardiogenesis in vivo and in vitro^{155,156}. Induction of canonical Wnt signaling at early stages combined with suppression of canonical Wnt signaling at later stages of differentiation achieves a high yield of cardiomyocytes^{155,156}.

A number of gene editing techniques have been discovered, including the RNA-guided CRISPR (clustered regularly interspaced short palindromic repeats)/Cas nuclease system^{157,158}. CRISPR/Cas is part of an adaptive immune system defence against foreign nucleic acids in bacteria such as archaea¹⁵⁹. Foreign DNA (protospacers) are acquired and integrated into the CRISPR locus. Cas proteins use the short CRISPR RNAs (crRNAs) transcribed from the CRISPR locus and are cleaved by a protein or protein complex to target the invading DNA^{159,160}. Three types (I-III) of CRISPR systems have been identified, among which the type II utilizing Cas9 nuclease is one of the best characterized ones^{158,161}. The Cas9 nuclease can target genomic DNA via a single-guide RNAs (sgRNAs)^{159,160}. Cas9-sgRNA complexes conduct genome editing by binding to the target DNA sequence and creating a double-stranded break (DSB) at around 3 bp upstream of the protospacer adjacent motif (PAM)¹⁵⁹. Subsequently, both strands of the targeted DNA sequence are repaired by one of two major pathways: the error-prone non-homologous end joining (NHEJ) or the high-fidelity homology-directed repair (HDR) pathway^{158,162-164}. In the absence of a repair template, the NHEJ pathway can introduce random deletions or insertions at the DSB^{162,165}. This can lead to knock-out mutations in the gene of interest/targeted gene. The HDR pathway enables the genomic knock-in of mutations such as single amino acid changes in presence of an exogenously introduced repair template^{163,164}.

Model systems employed for studying heart diseases comprise in vivo and in vitro models. In vivo models include small animal models such as mouse and rat, and big

animal models such as swine. In vitro models include engineered heart muscle (EHM) approaches, 2D tissue culture and so on¹⁶⁶. Genetic models of DCM¹⁶⁷ have been employed to discover molecular dysfunctions in the presence of DCM mutations, such as sarcomere protein misalignment, defective contractility and abnormal Ca²⁺ handling¹⁶⁸⁻¹⁷¹. Human iPSC-CMs have been used to elucidate causes of cellular disease phenotypes and pathogenesis of DCM^{38,171,172}. Using CRISPR/Cas9 genome editing, mutation-introduced and mutation corrected iPSC-CMs were created and utilized to introduce and reverse the molecular pathway's dysfunctions, respectively. Previous studies have shown that DCM iPSC-CMs recapitulate cellular disease phenotypes such as disrupted sarcomere protein organization, defective contractility, and Ca²⁺ handling^{38,171-173}. β -adrenergic signaling is blunted in iPSC-CMs carrying the DCM mutation TnT-R173W. Inhibition of PDE2A and PDE3A restores cAMP levels and rescues the impaired β -adrenergic signaling of DCM iPSC-CMs³⁸. The TnT-R141W mutation decreases the Ca²⁺ sensitivity of contraction, resulting in DCM^{174,175}. Mutations in the gene encoding the large protein titin result in sarcomere insufficiency, defective force generation and impaired β -adrenergic signaling¹⁷⁶. TPM, which anchors the troponin complex on thin filaments, is critical for cross-bridge formation and force generation in cardiomyocytes^{16,18,177,178}. It has been shown that TPM1 mutations reduce force generation and Ca²⁺ sensitivity in cardiomyocytes^{21,179,180}. TPM1-L185F, a TPM1 mutation, is located in a region where the troponin complex interacts with tropomyosin^{16,18}. Therefore, it is possible that sarcomeric mutations such as TnT-R173W, TnT-R141W or TPM1-L185F may disrupt sarcomere organization and filament stability^{171,173-175}. Here, a human iPSC model for sarcomeric DCM mutations, such as TnT-R173W, TnT-R141W or TPM1-L185F, was employed to discover further consequences of disorganised sarcomere protein organization. This study showed that sarcomere disorganization led to dysfunction of sarcomere microdomains, as well as defective interactions with the cytoskeleton and the PM. Consequently, this disturbed the uptake of cargoes such as transferrin which is necessary for the maintenance of proper cellular functions. Impaired transferrin uptake was shown to contribute to reduced iron levels in mitochondria in presence of sarcomeric mutations. Overall, iron deficiency negatively affected cardiomyocyte functions and could be modulated and partially rescued by supplementation of iron or small peptide treatments. Thereby, this study contributed new insights into molecular functional (patho-) mechanisms in human cardiomyocytes carrying DCM mutations.

2 Aims of this study

The goals listed below comprise central parts of this work and will be addressed in the next chapter by articles that are published or presently submitted to the journal, *Circulation Research*.

1. Sarcomeric DCM mutations cause sarcomere misalignment and impaired contractility in cardiomyocytes. However, how sarcomere disorganization contributes to the dysfunction of sarcomeric microdomains is not yet clear. Interactions at local sarcomeric domains, such as PKA-mediated TnI phosphorylation upon stimulation of β -AR, play an essential role for cardiomyocyte functions. Additionally, sarcomeres interact closely with other cytoskeleton proteins, such as filamin C, for signaling and mechano-transduction. Therefore, this study aims to characterize the protein interactions at sarcomeric microdomains in presence of sarcomeric DCM mutations, and their effects on cardiomyocyte functions.

2. Sarcomeric protein-protein interactions play an essential role in linking the cytoskeleton to the plasma membrane. In presence of sarcomeric DCM mutations, sarcomere interactions with the plasma membrane may be disturbed. Moreover, in DCM cardiomyocytes, additional consequences of disturbed sarcomere-cytoskeleton interactions with the PM on cardiomyocyte signaling pathways are not yet fully clear. Therefore, this study aimed to elucidate related patho-mechanisms using DCM patient-specific and CRISPR/Cas-edited iPSC-CMs. Functional effects that were to be studied include cytoskeleton interactions and signaling at the plasma membrane relevant for cargo uptake as well as cargo distribution. This study aims to provide insights into disease mechanisms at the cellular level and provide a basis for potential directions for future translational strategies.

3 Publications

3.1 Publication1

Troponin destabilization impairs sarcomere-cytoskeleton interactions in iPSC-derived cardiomyocytes from dilated cardiomyopathy patients

Yuanyuan Dai, Asset Amenov, Nadezda Ignatyeva, Andreas Koschinski, Hang Xu, Poh Loong Soong, Malte Tiburcy, Wolfgang A. Linke, Manuela Zaccolo, Gerd Hasenfuss, Wolfram-Hubertus Zimmermann, Antje Ebert

Heart Research Center Goettingen, Department of Cardiology and Pneumology, University Medical Center Goettingen, Georg-August University of Goettingen, Goettingen, Germany;

DZHK (German Center for Cardiovascular Research), partner site Goettingen, Germany.

OPEN

Troponin destabilization impairs sarcomere-cytoskeleton interactions in iPSC-derived cardiomyocytes from dilated cardiomyopathy patients

Yuanyuan Dai^{1,3}, Asset Amenov^{1,3}, Nadezda Ignatyeva^{1,3}, Andreas Koschinski⁵, Hang Xu^{1,3}, Poh Loong Soong^{2,3}, Malte Tiburcy^{2,3}, Wolfgang A. Linke^{1,3,4}, Manuela Zaccolo⁵, Gerd Hasenfuss^{1,3}, Wolfram-Hubertus Zimmermann^{2,3} & Antje Ebert^{1,3*}

The sarcomeric troponin-tropomyosin complex is a critical mediator of excitation-contraction coupling, sarcomeric stability and force generation. We previously reported that induced pluripotent stem cell-derived cardiomyocytes (iPSC-CMs) from patients with a dilated cardiomyopathy (DCM) mutation, troponin T (TnT)-R173W, display sarcomere protein misalignment and impaired contractility. Yet it is not known how TnT mutation causes dysfunction of sarcomere microdomains and how these events contribute to misalignment of sarcomeric proteins in presence of DCM TnT-R173W. Using a human iPSC-CM model combined with CRISPR/Cas9-engineered isogenic controls, we uncovered that TnT-R173W destabilizes molecular interactions of troponin with tropomyosin, and limits binding of PKA to local sarcomere microdomains. This attenuates troponin phosphorylation and dysregulates local sarcomeric microdomains in DCM iPSC-CMs. Disrupted microdomain signaling impairs MYH7-mediated, AMPK-dependent sarcomere-cytoskeleton filament interactions and plasma membrane attachment. Small molecule-based activation of AMPK can restore TnT microdomain interactions, and partially recovers sarcomere protein misalignment as well as impaired contractility in DCM TnT-R173W iPSC-CMs. Our findings suggest a novel therapeutic direction targeting sarcomere-cytoskeleton interactions to induce sarcomere re-organization and contractile recovery in DCM.

Sarcomeres are the basic contractile unit of cardiac cells, whose particularly specialized function depends on a highly organized structure. The troponin-tropomyosin (Tn-Tm) complex at sarcomeric thin filaments is a critical component for excitation-contraction coupling. Stability and anchoring of the Tn-Tm complex on sarcomeres is provided by binding of the troponin T (TnT) subunit to Tm and the troponin I subunit (TnI) on actin myofilaments. Tropomyosin (TPM) together with TnI regulates actin/myosin binding and ATPase function in presence of micromolar, cytosolic Ca²⁺, which is bound by the troponin C subunit (TnC). This highly sensitive mechanism is fine-tuned by post-translational modifications, such as PKA-mediated phosphorylation of TnI. Mutations in the Tn-Tm complex lead to severe disease, such as dilated cardiomyopathy (DCM). DCM is featured by left ventricular dilatation, contractile dysfunction, and arrhythmias¹ and represents a frequent cause of heart failure. More than 25% of DCM cases are caused by inherited mutations, particularly in sarcomeric proteins². Recently, human iPSC-derived cardiomyocytes (iPSC-CMs) have been utilized for human genetic disease modeling³⁻⁶ and drug testing⁷. Here, we analyze a sarcomeric mutation in cardiac troponin T (TnT), TnT-R173W. This mutation is located within one of the two tropomyosin binding regions of TnT, the T1 domain⁸ and was the first DCM mutation reported in a human patient-specific iPSC-derived cardiomyocyte model⁹. This report

¹Heart Center, Department of Cardiology and Pneumology, Goettingen, Germany. ²Institute of Pharmacology, University of Goettingen, Robert-Koch-Str. 40, 37075, Goettingen, Germany. ³DZHK (German Center for Cardiovascular Research), partner site Goettingen, Germany. ⁴Institute of Physiology II, University of Muenster, Muenster, Germany. ⁵Department of Physiology, Anatomy and Genetics, University of Oxford, Oxford, OX1 3PT, UK. *email: antje.ebert@med.uni-goettingen.de

demonstrated DCM patient-specific iPSC-CMs to display molecular disease-specific phenotypes such as abnormal sarcomeric structure, dysregulated Ca^{2+} signaling, and impaired contractility⁹. More recently, disturbed beta-adrenergic signaling due to epigenetic modulation has been attributed as a source for PDE2A and PDE3A upregulation, as well as dysregulated Ca^{2+} handling¹⁰. These and other studies^{11–14} show that sarcomeric microdomain organization plays an important role in maintenance of cardiomyocyte structure and function. Likewise, sarcomeric microdomains are critical for cytoskeleton filament integrity and mediate attachment with the plasma membrane¹⁵. Previously, cytoskeletal interactions with caveolin-enriched plasma membrane domains have been implied in sarcomere attachment as well as in signal transduction during heart failure¹⁶. Novel proteins contributing to these processes have been recently characterized, such as AMP-activated protein kinase (AMPK)^{17,18}. The regulation of metabolism by AMPK in various cell types is well recognized, as well as the ability of AMPK to sense ATP levels^{18–20}. Of note, AMPK has been shown to also act as a cytoskeleton remodeling protein^{21–23}. Despite this progress, the contribution of cardiomyopathy mutations, such as DCM TnT-R173W, to dysfunction of local sarcomeric microdomains and their cytoskeleton/plasma membrane interactions is not yet clear.

Here, we uncover novel mechanistic features underlying disorganization of sarcomeric protein- and microdomain array, as well as reduced contractility in DCM patient-specific iPSC-CMs. We generated CRISPR/Cas9 gene edited troponin T knock-out (TnT-KO) iPSC-CMs as an isogenic control for specificity. We report disturbed molecular interactions of troponin and tropomyosin in patient-specific iPSC-CMs carrying the DCM-TnT-R173W mutation, compared to gene edited TnT-KO iPSC-CMs and healthy controls (TnT-WT). Importantly, the DCM mutation TnT-R173W destabilizes TnT interactions with PKA, resulting in diminished troponin I (TnI) phosphorylation. This contributes to impaired force generation as well as reduced contractility, which we validated in a 3D engineered heart muscle (EHM) model. A Foerster Resonance Electron Transfer (FRET)-based molecular sensor and interrogation of sarcomeric PDE activity revealed dysregulation of local TnT microdomains in presence of DCM-TnT-R173W, which results in impaired interactions with cytoskeleton filaments as well as reduced plasma membrane attachment. We identified AMPK to assist in cytoskeleton filament interactions with both sarcomere- and plasma membrane junctions via myosin heavy chain 7 (MYH7) in DCM iPSC-CMs. We showed that AMPK activation can in part overcome destabilized microdomain interactions, as well as sarcomere protein misalignment and impaired contractility in presence of the TnT-R173W mutation. Our studies present new information regarding disturbed troponin complex interactions in patient-specific iPSC-CMs carrying an inherited DCM mutation. We contribute to novel understanding of local signal regulation in sarcomeric microdomains as well as sarcomere interactions with other cytoskeleton filament proteins and plasma membrane compartments. These findings may be exploited in the future for therapeutic manipulation of molecular disease mechanisms.

Results

Patient-specific iPSC-CMs and engineered heart muscle (EHM) recapitulate sarcomere protein misalignment and impaired contractility in presence of DCM-TnT-R173W. We employed DCM patient-specific iPSCs from a family cohort carrying an inherited DCM mutation, TnT-R173W (Fig. 1A)⁹ as well as healthy control (WT) iPSCs. We generated an isogenic TnT knock-out iPSC line as a negative control, using site-specific CRISPR-Cas9 gene editing to induce a frameshift mutation at exon 2 (Fig. 1A, Supplementary Fig. 1A,B). Human iPSC lines displayed regular expression of pluripotency markers (Supplementary Fig. 1C). Next, TnT-KO as well as DCM TnT-R173W and WT iPSCs were differentiated to iPSC-CMs using a small molecule-based monolayer protocol described earlier^{24–26} (Fig. 1, Supplementary Fig. 1D,E).

While beating iPSC-CMs were observed for healthy control and DCM TnT-R173W patient-specific iPSC-CM lines, differentiated iPSC-CMs from TnT-KO iPSCs did not express TnT (Fig. 1A) and did not display any beating (Movies S1–3). To establish DCM-specific phenotypic features in DCM TnT-R173W iPSC-CMs compared to TnT-KO and healthy controls, we first analyzed sarcomere protein arrangement. The number of cells with severely abnormal sarcomeres was significantly increased in DCM TnT-R173W iPSC-CMs compared to healthy controls (Fig. 1A,B). No cells with organized sarcomeres were found in TnT-KO iPSC-CMs (Fig. 1A,B). Of note, DCM TnT-R173W iPSC-CMs showed significantly reduced sarcomere length (Fig. 1C) and a less negative correlation coefficient corresponding to diminished sarcomere protein regularity (Supplementary Fig. 1F), compared to healthy controls.

Contractility of DCM TnT-R173W iPSC-CMs was analyzed by an automated high-speed imaging platform, MuscleMotion²⁷ (Fig. 1D–F). DCM TnT-R173W iPSC-CMs displayed significantly prolonged contraction duration (Fig. 1D), reduced amplitude (Fig. 1E) and increased time-to-peak (Fig. 1F), compared to healthy control (TnT-WT) iPSC-CMs. Contractility analysis confirmed TnT-KO iPSC-CMs to be unable to contract. To further corroborate that destabilization of TnT complex interactions in presence of TnT-R173W results in reduced contractile force, we utilized a 3D model of contracting human engineered heart muscle (Fig. 1G–J). EHMs from both DCM TnT-R173W iPSC-CMs and healthy control iPSC-CMs (TnT-WT) stained in cross-sections for cardiac marker proteins such as sarcomeric alpha-actinin (Fig. 1G,H). TnT-KO iPSC-CMs were unable to condense into EHM rings, likely due to poor stability and integrity of TnT-KO iPSC-CM sarcomeres. Therefore, TnT-KO EHMs could not be generated. The contraction force in EHMs was determined over a range of Ca^{2+} concentrations (Fig. 1I,J). EHMs from DCM TnT-R173W iPSC-CMs showed significantly reduced force of contraction, compared to WT controls (Fig. 1I), and the response to electrical stimulation was slightly lower in DCM EHMs versus WT control EHMs following pacing at 1 Hz (Fig. 1J).

Interactions of the TnT complex are disturbed in DCM TnT-R173W iPSC-CMs. We next compared consequences of the disease-specific mutation TnT-R173W versus TnT-KO for the expression of the troponin complex subunits in iPSC-CMs at the gene and protein levels. First, we confirmed that mRNA expression of TNNT2, TNNI3, TNNC1 and TPM1 in DCM TnT-R173W iPSC-CMs was not significantly different from WT

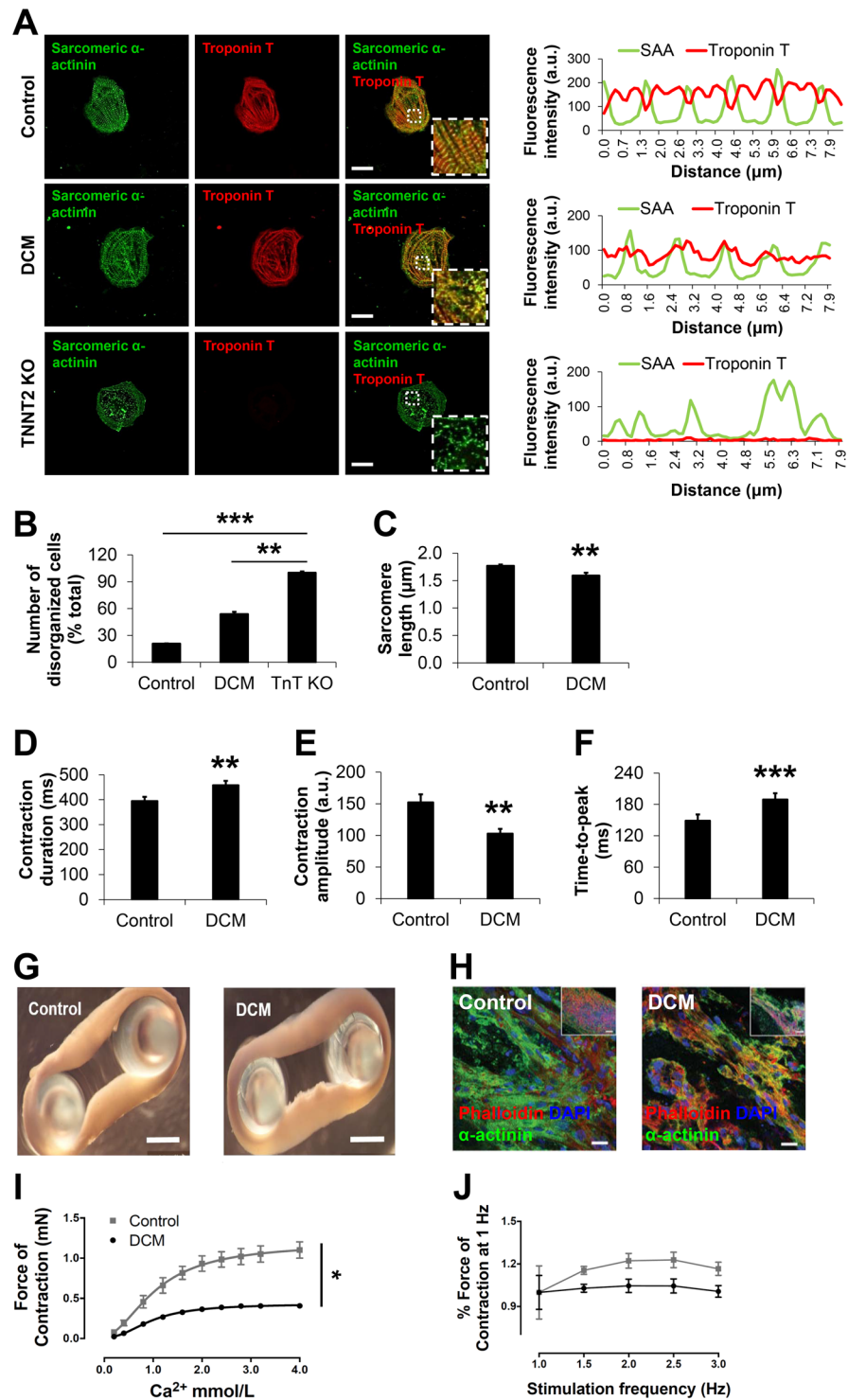


Figure 1. DCM iPSC-CMs display impaired sarcomeric protein alignment and reduced contractility. **(A,B)** Analysis of sarcomere protein alignment in DCM and TnT KO iPSC-CMs, compared to healthy controls. **(A)** Immunohistochemistry for sarcomeric alpha-actinin (SAA) and cardiac troponin T (TnT), followed by confocal imaging (scale bar, 20 μm). Line scans show striation patterns for SAA and TnT sarcomeric distributions (y-axis, fluorescence intensity in arbitrary units; x-axis, distance in μm). **(B)** Quantification of disorganized iPSC-CMs using confocal images as shown in Fig. 1A. Control, n = 70 cells, 3 cell lines; DCM, n = 92 cells, 3 cell lines; TnT KO, n = 36 cells, 1 cell line. **P < 0.01, ***P < 0.001 (one-way ANOVA and Sidak's multiple comparisons test). **(C)** DCM TnT-R173W iPSC-CMs display significantly reduced sarcomere length, compared to healthy controls. Data are expressed as mean ± s.e.m. Control (WT), n = 3 cell lines and 39 images were analyzed; DCM (TnT-R173W), n = 3 cell lines and 42 images were analyzed. **(D–F)** Motion-based contractility analysis of iPSC-CMs revealed significantly prolonged contraction duration **(D)**, P = 0.01; reduced contraction amplitude **(E)**, P = 0.01; and prolonged time to peak **(F)**, ***P < 0.001. Data are expressed as mean ± sem. Control (WT), n = 3 cell lines; DCM, n = 3 cell lines. **P < 0.01 as calculated by Student's t-test. **(G–J)** TnT-R173W results in

impaired contraction force in human iPSC-derived engineered heart muscle (EHM) from DCM iPSC-CMs and healthy controls. **(G)** Mechanical loading of control and DCM EHMs on PDMS stretchers before force testing (scale bars: 2 mm). **(H)** Immunofluorescence images of EHMs show distribution and alignment of iPSC-CMs (sarcomeric alpha-actinin) for healthy control and DCM (scale bars: 20 μm ; inset: 100 μm). **(I)** EHMs were attached to force transducers and pre-stretched to reach optimal sarcomere length (maximal isometric active tension according to Frank-Starling-mechanism). DCM EHMs demonstrate reduced force of contraction (FOC) under isometric conditions and addition of increasing Ca^{2+} concentrations ($P < 0.05$). **(J)** Shown is the response to electrical stimulation for control- and DCM EHMs ($P = \text{ns}$). $n = 8$ EHMs per group. Data are expressed as mean \pm sem. * $P < 0.05$ and ns, not significant as calculated by two-way ANOVA and Tukey's post-hoc test.

controls (Supplementary Fig. 2A–D). In contrast, TNNT2 KO iPSC-CMs were found to not express TNNT2. In line with previous publications²⁸, we found TNNT2 KO to result in loss of TnI expression at both mRNA and protein levels (Supplementary Fig. 2,D–H)²⁸. TnT-KO iPSC-CMs also displayed a substantial loss of TnC (Supplementary Fig. 2,B–F)²⁸ and Tm (Supplementary Fig. 2C–G) at mRNA and protein levels. On the other hand, protein expression levels of TnI, TnC and Tm were not significantly altered in DCM patient-specific iPSC-CMs versus controls (Supplementary Fig. 2E–H).

We next probed if the troponin complex subunits and tropomyosin would interact in presence of the TnT-R173W mutation and following TnT-KO in the same manner as in healthy control iPSC-CMs (TnT-WT). Co-immunoprecipitation experiments indicated reduced binding capacity of TnT-R173W towards Tm, compared to iPSC-CMs (Supplementary Fig. 3A–C). TnT-KO iPSC-CMs were utilized as a control for binding specificity (Supplementary Fig. 3,A–D). To further corroborate these findings, we employed *in-vitro* interaction studies with recombinant flag (DYK)-tagged TnT-WT and TnT-R173W. TnT-WT-DYK, TnT-R173W-DYK or DYK as a negative control were expressed in HEK 293 T cells, immobilized on flag-decorated beads (Fig. 2A) and incubated with iPSC-CM lysate from healthy controls (Supplementary Fig. 4A). Binding of TnC, TnI and Tm was determined in bound fractions via immunoblot (Fig. 2B–D, Supplementary Fig. 4A). A flag-tag encoding vector was utilized as a negative control for overexpression- and binding studies (Fig. 2A–E, Supplementary Fig. 4A). Of note, TnT-binding to Tm, which anchors the troponin complex on the actin myofilaments, was significantly reduced in presence of the TnT-R173W mutation, compared to TnT-WT (Fig. 2B). Particularly, tropomyosin binding is critical for force transduction by gate-keeping the myosin-binding site on actin, as well as sarcomere stability²⁹. Our findings suggest that the DCM TnT-R173W mutation destabilizes the troponin-tropomyosin interaction.

Dysregulated sarcomeric PKA function and elevated sarcomeric cAMP are consequences of the DCM mutation TnT-R173W. The troponin complex is a key regulator of calcium binding and contractility in cardiomyocytes, to which PKA-mediated phosphorylation contributes. TnT acts as an A-kinase anchoring protein (AKAP)³⁰. We thus investigated if the DCM TnT-R173W mutation impairs PKA binding on sarcomeric myofilaments. Immunoprecipitation studies showed that TnT-R173W binds significantly less PKA than WT-TnT (Fig. 2E, Supplementary Fig. 4A). Moreover, these data are in line with a previous study reporting lower PKA activity in DCM TnT-R173W iPSC-CMs¹⁰.

These findings pointed to a local modulation of sarcomeric functions at the TnT complex in presence of the DCM mutation TnT-R173W. As PKA directly interacts with the troponin complex and phosphorylates TnI, we considered that altered PKA levels at the sarcomere would affect phosphorylation levels of TnI, which in turn contributes to regulating contractility³¹. We therefore tested phosphorylation of TnI-Ser 23/24 in DCM patient-specific TnT-R173W iPSC-CMs, compared to healthy control iPSC-CMs and TnT-KO iPSC-CMs. In DCM iPSC-CMs, substantially reduced phosphorylation of TnI was detected (Fig. 3A, Supplementary Fig. 4B). In TnT-KO iPSC-CMs, low phosphorylation of TnI-Ser 23/24 was observed (Fig. 3A), in line with very low baseline expression of TnI in TnT-KO iPSC-CMs (Supplementary Fig. 2H). Of note, reduced sarcomeric target phosphorylation was not a ubiquitous effect. PKA-dependent phosphorylation of phospholamban (Pln) was not significantly altered in presence of TnT-R173W in DCM patient-specific iPSC-CMs, compared to WT iPSC-CMs (Fig. 3B).

To further explore local regulation of TnT complex function in relation to PKA, we next tested if DCM-TnT-R173W leads to alterations in local cAMP levels at the sarcomere in comparison to cytosolic cAMP. We employed a FRET (Foerster Resonance Electron Transfer)-based readout for detection of locus-specific cAMP levels at the TnT complex. A targeted cAMP FRET-biosensor, CUTie, which has the PKA cyclic nucleoside binding domain fused to TnI (TnI-CUTie)¹⁴ was utilized for measurement of cAMP at sarcomeric myofilaments. The TnI-CUTie sensor recapitulated correctly targeted TnI-CUTie biosensor in patient-specific and healthy control iPSC-CMs (Fig. 3C–E) while in contrast, severely disorganized sarcomeric structure was detected in TnT-KO iPSC-CMs (Supplementary Fig. 4C,D). Investigation of local sarcomeric cAMP levels in DCM TnT-R173W iPSC-CMs versus healthy controls revealed a slight increase of sarcomeric cAMP (Fig. 3D,E). This may present a local compensatory reaction in DCM iPSC-CMs to increase PKA activity and TnI phosphorylation. However, given diminished PKA anchoring and resulting reduced phosphorylation of TnI in presence of TnT-R173W, slightly elevated sarcomeric cAMP is not sufficient to activate the remaining AKAP-bound sarcomeric PKA. These findings highlight local microdomain regulation of PKA function at the sarcomere in presence of the DCM TnT-R173W mutation.

Local dysfunction at the TnT complex in presence of TnT-R173W results in disrupted sarcomere-cytoskeleton filament- and plasma membrane interactions. In line with a previous report¹⁰ we found increased phosphodiesterase PDE3A in TnT-R173W iPSC-CMs, compared to healthy controls (Fig. 4A). Adenylyl cyclase (AC) expression levels were not significantly altered between DCM iPSC-CMs

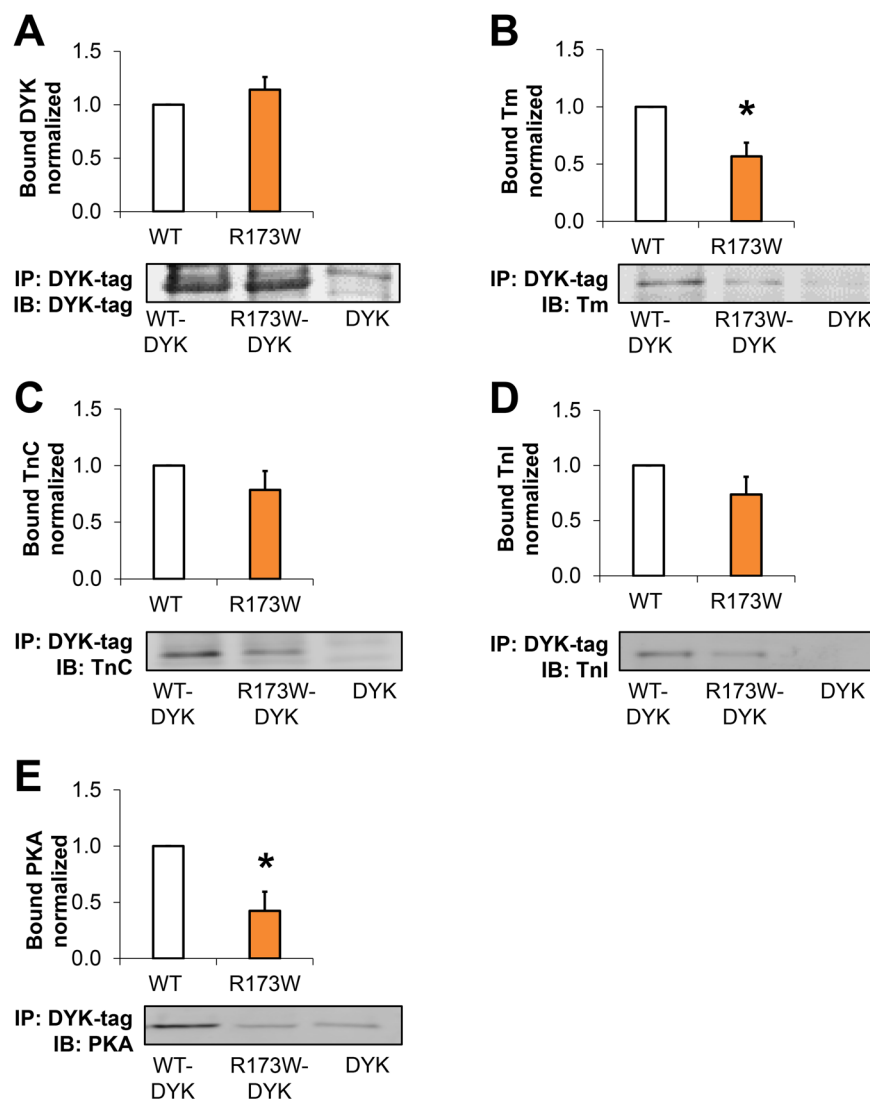


Figure 2. Troponin complex interactions are disturbed in presence of DCM-TnT-R173W. (A–D) Co-immunoprecipitation showed reduced capacity of TnT-R173W to bind to tropomyosin, compared to TnT-WT. Human TnT-R173W-DYK, TnT-WT-DYK or DYK (negative control) was overexpressed in HEK cells and immobilized on DYK-antibody-decorated beads. Human iPSC-CM lysate from healthy controls was used for co-immunoprecipitation to test the binding capacity of TnT-WT or TnT-R173W towards troponin complex subunits and tropomyosin. (A) Binding of TnT-WT-DYK and TnT-R173W-DYK to DYK-coated beads is comparable. TnT-R173W binding to tropomyosin (Tm) (B) is significantly reduced compared to TnT-WT. (C) Binding of TnT-DYK to TnC (D) Binding of TnT-DYK to TnI. (E) PKA binding is significantly reduced in TnT-R173W-DYK, compared to TnT-WT-DYK. Representative membrane scans are shown. Bargraphs show averages of $n = 8$ experiments for TnT-DYK; $n = 5$ experiments for Tm; $n = 6$ experiments for TnC; $n = 5$ experiments for TnI; $n = 4$ experiments for PKA. Groups in (A–E) are shown following subtraction of respective DYK negative controls. Bound protein was normalized by immobilized TnT-WT-DYK or TnT-R173W-DYK (see also Supplementary Fig. 4A,B). Data are expressed as mean \pm sem. * $P < 0.05$ (one sample t- and Wilcoxon test).

and healthy controls (Supplementary Fig. 5A). We speculated that upregulation of sarcomeric cAMP in DCM TnT-R173W iPSC-CMs may be mediated by local regulation at sarcomeric microdomains due to disrupted sarcomere protein alignment. To test this hypothesis, we first assessed sarcomeric PDE enzymatic activity by measuring 5'AMP released in DCM TnT-R173W iPSC-CMs as well as healthy controls and TnT-KO (Fig. 4B, Supplementary Fig. 5B). Overall sarcomeric (Fig. 4B) PDE activity was significantly increased in DCM TnT-R173W iPSC-CMs, compared to healthy controls (Figure 4B), while cytosolic PDE activity was not found to be significantly altered (Supplementary Figure. 6C). These experiments reveal that beta-adrenergic responsiveness in DCM iPSC-CMs is not only limited by generic cellular cAMP levels. Importantly, DCM TnT-R173W results in reduced binding of PKA to TnT-R173W as well as lower TnI phosphorylation¹¹ and causes impaired sarcomeric microdomain function in DCM iPSC-CMs. This cannot be overcome by a compensatory minor increase of local sarcomeric cAMP

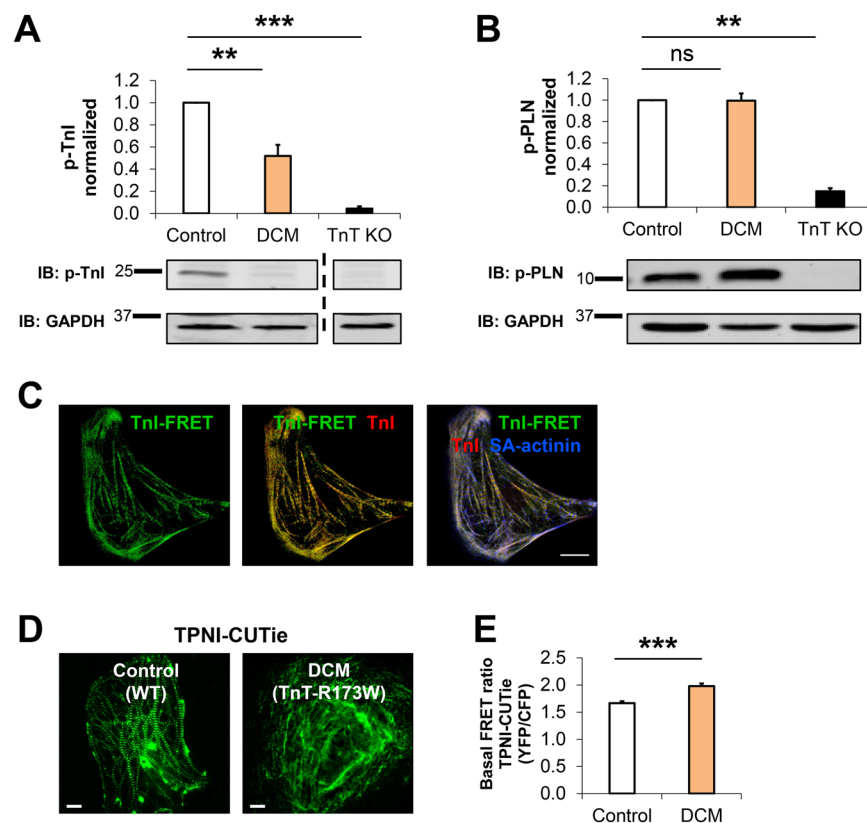


Figure 3. Reduced PKA-mediated TnI phosphorylation in TnT-R173W iPSC-CMs cannot be compensated by local sarcomeric cAMP modulation. **(A)** PKA-mediated phosphorylation of TnI at Ser 23/24 is reduced in DCM iPSC-CMs, as well as TnT KO iPSC-CMs. Bargraph presents averages of $n = 5$ experiments for control (WT, $n = 3$ cell lines), DCM (TnT-R173W, $n = 3$ cell lines), and TnT KO ($n = 1$ cell line); shown below are representative immunoblots. Data are expressed as mean \pm sem. $**P < 0.01$, $***P < 0.001$ and ns, not significant (one sample t- and Wilcoxon test). **(B)** Phosphorylation of PLN is not altered in DCM iPSC-CMs compared to healthy controls. Bar graph presents averages of $n = 6$ experiments for control (WT, $n = 3$ cell lines), DCM (TnT-R173W, $n = 3$ cell lines), and TnT KO ($n = 1$ cell line); representative immunoblots are shown below. Data are expressed as mean \pm sem. $**P < 0.01$ and ns, not significant (one sample t- and Wilcoxon test). **(C–E)** TPNI-FRET-sensor-based detection of cAMP levels in TnT-WT and TnT-R173W iPSC-CMs. Shown are basal FRET ratios (emission YFP/emission CFP following background subtraction). **(C)** Sarcomeric localization of the TPNI-CUTie FRET-sensor in iPSC-CMs. TPNI-FRET signal co-localizes with TnI co-staining in immunohistochemistry. Co-staining for sarcomeric alpha-actinin is shown. Scale bar, $10 \mu\text{m}$. **(D,E)** Detection of local cAMP upregulation at the Tn complex via the TPNI-FRET-sensor in DCM-TnT-R173W iPSC-CMs, compared to control iPSC-CMs (WT). **(D)** Representative images are shown; scale bar, $10 \mu\text{m}$. **(E)** Quantification of **(D)**. WT iPSC-CMs (healthy control), $n = 45$ cells; TnT-R173 iPSC-CMs (DCM), $n = 45$ cells. $***P < 0.001$ (Student's t- test). Data are shown as mean \pm sem.

(Fig. 3C,D). Moreover, these findings are in line with a previous report confirming that elevated PDE2A/3A caused impaired beta- adrenergic signaling in DCM iPSC-CMs¹⁰. We speculated that altered sarcomeric microdomain function in DCM TnT-R173W iPSC-CMs could affect sarcomere protein alignment and interactions with other cytoskeleton filament proteins as well as the plasma membrane (PM). We therefore assessed interactions of sarcomere microdomains with cytoskeleton filament proteins and the PM in more detail. Of note, we found impaired integrity of sarcomere-cytoskeleton filament junctions in DCM TnT-R173W iPSC-CMs versus healthy controls (Fig. 4C–I). Immunoprecipitation studies revealed an interaction of the cytoskeleton attachment protein, filamin-C, with TnT in healthy control (WT) iPSC-CMs (Fig. 4C–E, Supplementary Fig. 6A–C). Filamin-C localizes to the sarcomeric z-disc but also to other subcellular sites, such as cytoskeleton filament microdomains and is suggested to be involved in cytoskeleton signaling and remodeling¹⁶. The dynamic distribution of filamin-C suggests it is exposed to TnT at z-disc interaction zones with TnT-decorated actin filaments. Interestingly, the interaction of filamin-C with TnT-R173W was significantly reduced in DCM iPSC-CMs, compared to TnT-WT controls (Fig. 4C–E, Supplementary Fig. 6A–C). We also confirmed reduced co-localization of TnT and filamin-C in DCM TnT-R173W iPSC-CMs, compared to TnT-WT controls (Fig. 4F,G). No significant difference in filamin-C expression was observed in DCM iPSC-CMs compared to healthy controls and TnT KO-iPSC-CMs (Supplementary Fig. 6B,C).

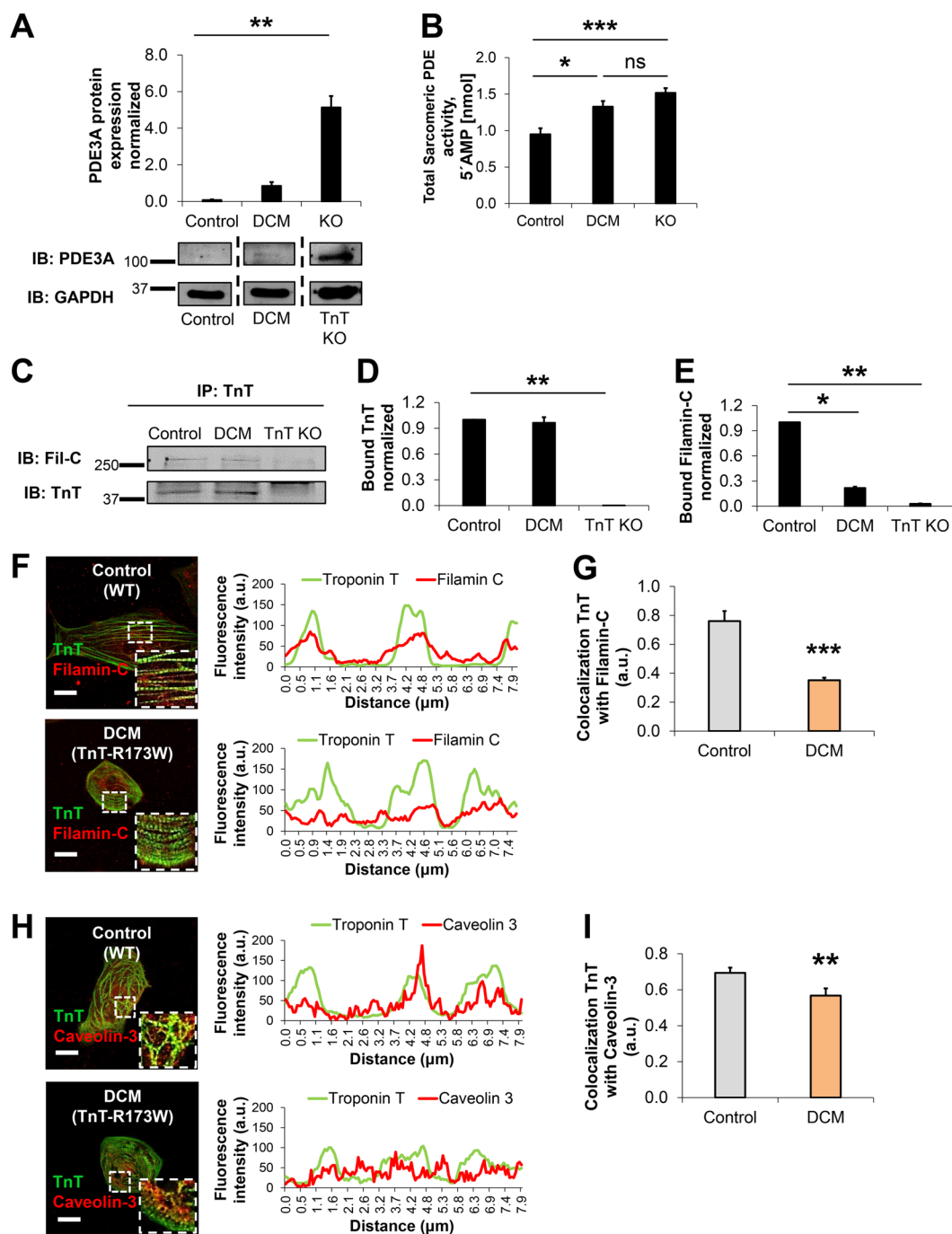


Figure 4. Sarcomeric microdomain regulation and interactions with cytoskeleton filament proteins are disturbed in DCM-TnT-R173W iPSC-CMs. **(A)** PDE3A protein expression levels are increased in DCM iPSC-CMs compared to healthy controls. **(B)** Total sarcomeric PDE activity is significantly increased in DCM- and TnT KO iPSC-CMs, compared to healthy controls. **(A,B)** Averages of 3 experiments are shown for control ($n = 2$ cell lines), DCM ($n = 2$ cell lines) and TnT- KO ($n = 1$ cell line). Representative membrane scans are shown. Data are shown as mean \pm sem. $*P < 0.05$, $***P < 0.01$, $**P < 0.001$, ns = not significant as calculated by Kruskal-Wallis test and Dunn's multiple comparisons test. **(C–E)** Interactions of sarcomeric TnT with the z-disc and cytoskeleton protein, filamin-C, were assessed by immunoprecipitation using a TnT-specific antibody. **(C)** Representative membrane scans for immunoprecipitation of filamin-C with TnT are shown. **(D)** Equal amounts of TnT-WT and TnT- R173W were immunoprecipitated from lysates of healthy control and DCM iPSC-CMs. **(E)** Binding of filamin-C to DCM-TnT-R173W is reduced, compared to healthy control WT-TnT. Bargraphs shown averages of $n = 2$ experiments for control (WT, $n = 2$ cell lines), DCM (TnT- R173W, $n = 3$ cell lines), and TnT KO ($n = 1$ cell line). Bound TnT was normalized by input and GAPDH (see also Supplementary Fig. 6A). $*P < 0.05$, $**P < 0.01$, $***P < 0.001$ and ns, not significant (one sample t- and Wilcoxon test). Data are expressed as mean \pm sem. **(F–I)** Co-localization of TnT with the z-disc and cytoskeleton attachment protein, filamin-C, and caveolin-3 is reduced in DCM iPSC-CMs compared to healthy controls. Immunostainings, confocal images and corresponding ImageJ-based quantifications are shown. Line scans show striation patterns

for sarcomeric distribution of TnT (y-axis, fluorescence intensity in arbitrary units; x-axis, distance in μm). (F) Co-localization of filamin-C with TnT and (G) Quantification of (F). Analysis was done for WT healthy control, $n = 1$ cell line and $n = 17$ cells, 16 images, as well as DCM, $n = 1$ cell line and $n = 48$ cells, 25 images. (H) Co-localization of TnT with caveolin-3 and (I) Quantification of (H). Analysis was done for WT healthy control, $n = 2$ cell lines and $n = 38$ cells, 31 images, and DCM, $n = 2$ cell lines and $n = 44$ cells, 35 images. Data are shown as mean \pm sem. $**P < 0.01$, $***P < 0.001$, as calculated by Student's t-test.

Together, these data indicate in presence of DCM TnT-R173W impaired interactions of cytoskeleton filaments with TnT-enriched sarcomere microdomains. These junctions also contribute to attachment of sarcomere- and other cytoskeleton elements to the plasma membrane, which contains caveolin-3-enriched microdomains¹⁶. Co-localization of caveolin-3 with filamin-C at plasma membrane microdomains has been previously reported¹⁶. Therefore, we compared co-localization of TnT with caveolin-3 (Fig. 4H,I) in DCM TnT-R173W iPSC-CMs versus TnT-WT controls. Interestingly, TnT-caveolin-3 co-localization was significantly reduced in DCM iPSC-CM compared to healthy controls (Fig. 4H,I). Overall, these data suggest reduced attachment of sarcomere microdomains with cytoskeleton filaments as well as the plasma membrane in DCM TnT-R173W iPSC-CMs. Disturbed sarcomere microdomain attachment is likely a consequence of the impaired interaction of TnT with tropomyosin in presence of TnT-R173W (Fig. 2A,B,E) and the resulting disrupted sarcomere protein alignment (Fig. 1A-C, Supplementary Fig. 1F).

AMPK activation improves sarcomere-cytoskeleton attachment as well as sarcomere protein alignment.

To further investigate the impaired sarcomere-cytoskeleton filament microdomain interactions in presence of the TnT-R173W mutation, we assessed molecular factors known to regulate sarcomere interactions with cytoskeleton filament proteins. AMP-activated protein kinase (AMPK) is an established modulator of cytoskeleton filament interactions, which is known to regulate cardiomyocyte metabolism^{23,32}. AMPK-mediated metabolic regulation has been recently studied also in iPSC-CMs³³. Of note, AMPK has been shown to act as a cytoskeleton remodeling factor mediating cytoskeleton rearrangement and polarity, via interaction with myosin heavy chain proteins (MYH7-9)^{17,23,32}. As myosin heavy chain 7 (MYH7) could also interact with troponin³⁴, we speculated that the presence of the DCM mutation TnT-R173W may impair TnT interaction with MYH7. Destabilization of the TnT-MYH7 interaction could in turn affect AMPK-mediated regulation of cytoskeleton filaments. To probe integrity of MYH7 binding to TnT in DCM and control iPSC-CMs, we used immunoprecipitation from iPSC-CM cell lysates (Fig. 5A-C, Supplementary Fig. 7A). In presence of DCM TnT-R173W, MYH7 binding to TnT was significantly reduced, compared to WT controls (Fig. 5A-C, Supplementary Fig. 7A), confirming that the DCM TnT-R173W mutation causes disruption of sarcomere-cytoskeleton filament interactions. We next sought to test if this would affect AMPK-mediated regulation of cytoskeleton stability and integrity. To explore if sarcomere-cytoskeleton attachment would respond to AMPK modulation, we cultured DCM iPSC-CMs in presence of a small-molecule AMPK activator, A-769662³⁵, or control vehicle (Fig. 5D,E). Interestingly, while AMPK activation via A-769662 increased AMPK activity in both healthy control and DCM iPSC-CMs, the increase of AMPK activity was substantially higher in DCM iPSC-CMs than in healthy controls (DCM control vehicle vs. DCM A-769662, 14.6-fold and healthy control A-769662 vs. DCM A-769662, 2.1-fold, Fig. 5D,E). AMPK protein expression was comparable in DCM TnT-R173W iPSC-CMs and healthy controls (Supplementary Fig. 7B).

We next probed if increased AMPK activation in DCM iPSC-CMs could contribute to sarcomere microdomain organization as well as cytoskeleton-plasma membrane attachment in human iPSC-CMs. Interestingly, quantitative immunohistochemistry studies showed significantly reduced co-localization of MYH7 and AMPK in DCM iPSC-CMs compared to healthy controls (Fig. 5F,G). Following activation of AMPK via A-769662 in DCM iPSC-CMs, MYH7-AMPK co-localization was recovered (Fig. 5F,G). In addition, co-localization of the cytoskeleton intermediate filament protein vimentin with AMPK was significantly reduced in DCM TnT-R173W iPSC-CMs versus controls (Fig. 5H,I) and was restored by small molecule-based AMPK activation in DCM iPSC-CMs (Fig. 5H,I). These findings are in line with the diminished interaction of TnT-R173W with MYH7 (Fig. 5A-C) in DCM iPSC-CMs. We thus speculated that in DCM iPSC-CMs, the substantial increase in AMPK activity following activation via A-769662 may convene recovery of reduced sarcomere-cytoskeleton attachment. We found that following A-769662 treatment, co-localization of TnT with filamin-C (Fig. 6A,B) and caveolin-3 (Fig. 6C,D) in DCM iPSC-CMs was significantly increased, suggesting that AMPK activation supports recovery of both sarcomere-cytoskeleton- and sarcomere-PM attachment.

We next tested if AMPK activation could also recover the impaired contractility in DCM iPSC-CMs (Fig. 1D-F). Following small molecule-based activation of AMPK, we observed significantly improved contraction duration as well as amplitude and time-to-peak (Fig. 6E-G). In addition, AMPK activation recovered disrupted sarcomere protein alignment in DCM iPSC-CMs (Fig. 6H,I). Conversely, AMPK inhibition via BML-275³⁶ in WT iPSC-CMs (Supplementary Fig. 8A-C) phenocopied contractile parameters observed in DCM iPSC-CMs (Fig. 1D-F), such as significantly reduced contraction amplitude, increased time-to-peak and prolonged contraction duration.

Together, our data suggest that in DCM iPSC-CMs with a sarcomeric mutation, TnT-R173W, loss of sarcomere organization due to reduced T_m and PKA binding contributes to disrupted cytoskeleton- and plasma membrane interactions in iPSC-CMs (Fig. 7). We identified AMPK as a cytoskeleton organization protein which regulates stability of cytoskeleton filament-sarcomere interactions via MYH7. Activation of AMPK can ameliorate disrupted sarcomeric microdomain interactions in DCM patient-derived iPSC-CMs. Importantly, this recovers also DCM disease phenotypes such as reduced sarcomere protein alignment and impaired contractility in presence of a DCM mutation, TnT-R173W.

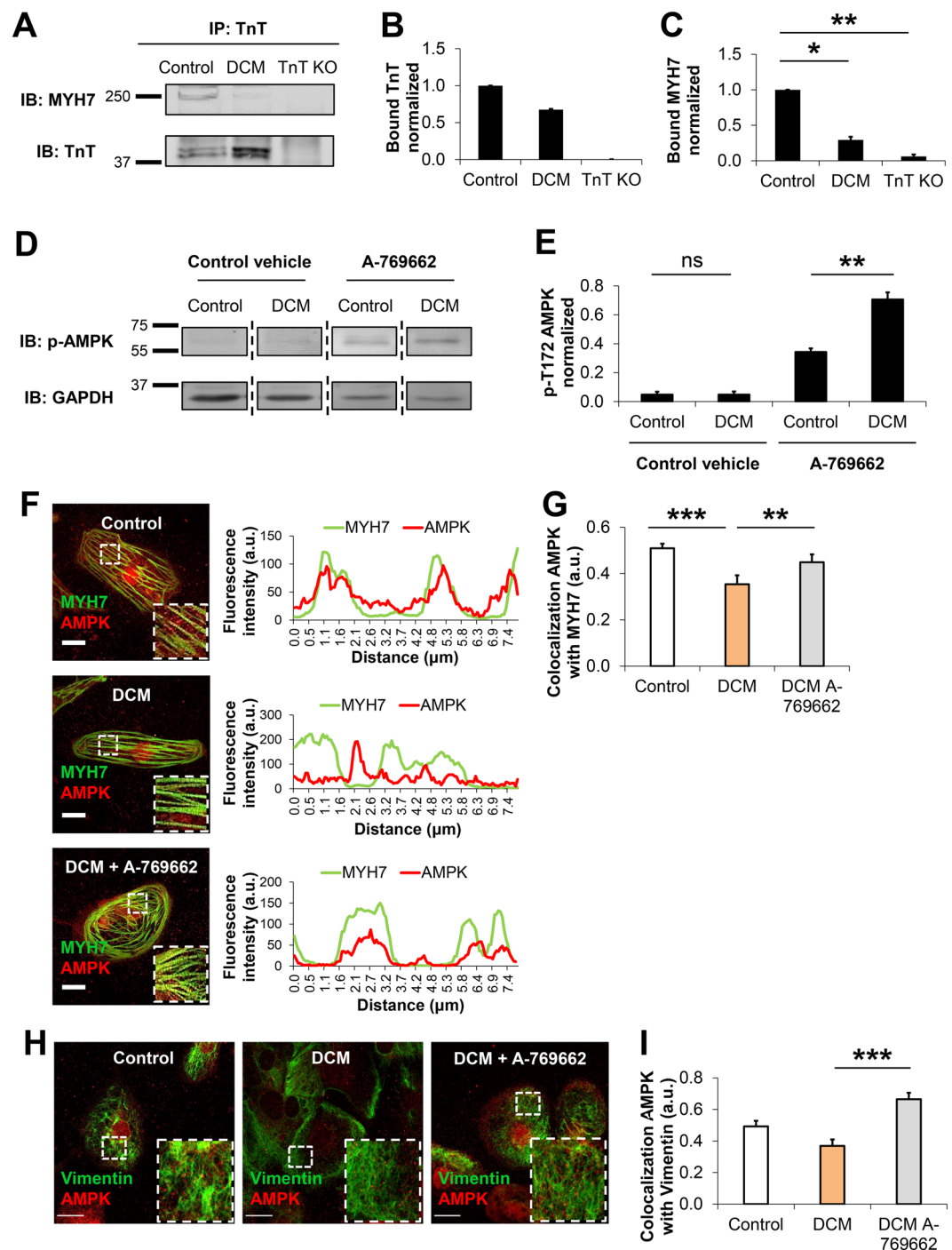


Figure 5. AMPK is a positive regulator of sarcomere-cytoskeleton filament interactions. (A–C) Immunoprecipitation of MYH7 with TnT is shown, using cell lysates from DCM iPSC-CMs, healthy controls and TnT KO. Interaction of TnT with MYH7 was assessed by immunoprecipitation using a TnT-specific antibody. (A) Representative membrane scans for immunoprecipitation of TnT and MYH7 are shown. (B) Comparable amounts of TnT-WT and TnT-R173W were immunoprecipitated from lysates of healthy control and DCM iPSC-CMs. (C) Binding of MYH7 to DCM-TnT-R173W is reduced, compared to healthy controls. Bargraphs show signal from bound IP fractions following normalization for input in each group for input and loading control. Shown are averages of 2 experiments for control (WT, $n = 3$ cell lines), DCM (TnT-R173W, $n = 3$ cell lines) and TnT KO ($n = 1$ cell line); input and loading control are shown in Supplementary Fig. 7A. $*P < 0.05$, $**P < 0.01$ (one sample t - and Wilcoxon test). Data are expressed as mean \pm sem. (D–E) AMPK activity in DCM versus healthy control iPSC-CMs measured via a phospho-AMPK α (Thr172)-specific antibody. Following treatment with A-769662, AMPK activity in DCM iPSC-CMs is significantly increased, compared to control vehicle (DMSO). (D) Representative membrane scans are shown. (E) Quantification of (D). Shown are averages of 4 experiments for control (WT, $n = 3$ cell lines), DCM (TnT-R173W, $n = 3$ cell lines) and TnT KO ($n = 1$ cell line); $**P < 0.01$ and ns, not significant (one-way ANOVA and Sidak's multiple

comparison test) data are expressed as mean \pm sem. **(F–I)** Co-localization of AMPK with MYH7 and vimentin is reduced in DCM iPSC-CMs compared to healthy controls and is recovered following AMPK activation via A-769662. Immunostaining and confocal images (scale bar, 20 μ m) as well as corresponding ImageJ-based quantifications are shown. Line scans show striation patterns for sarcomeric distribution of TnT (y-axis, fluorescence intensity in arbitrary units; x-axis, distance in μ m). **(F)** Co-localization of AMPK with MYH7 and **(G)** Quantification of **(F)**, *** $P < 0.001$ for WT control vehicle vs. DCM control vehicle, ** $P < 0.01$ for DCM control vehicle vs. DCM-A-769662 and WT control vehicle vs. DCM-A-769662, $P =$ not significant (one-way ANOVA and Sidak multiple comparison test). Analysis was performed for WT healthy control, $n = 2$ cell lines and $n = 68$ cells; DCM, $n = 1$ cell line and $n = 49$ cells; and DCM A-769662, $n = 2$ cell lines and $n = 74$ cells. **(H)** Co-localization of AMPK with vimentin. Scale bar, 20 μ m. **(I)** Quantification of **(H)**, *** $P < 0.001$ for DCM control vehicle versus DCM-A-769662 (one-way ANOVA and Sidak multiple comparison test) WT healthy control, $n = 2$ cell lines and $n = 38$ cells; DCM, $n = 1$ cell line and $n = 23$ cells; and DCM A-769662, $n = 1$ cell line and $n = 14$ cells. Data are shown as mean \pm sem.

Discussion

The molecular consequences of inherited mutations causing familial dilated cardiomyopathy (DCM) have been studied previously^{2,37}. Human iPSC-CMs have been utilized for disease modeling and have revealed cellular phenotypic features of DCM in patient-derived models^{9,38}. Specifically, these phenotypes comprise disrupted sarcomeric structure and abnormal calcium handling, as published earlier in a human iPSC-CM model for the DCM mutation TnT-R173W^{9,10}. Moreover, impaired beta-adrenergic signaling has been characterized as an important molecular mechanism in cardiomyopathy^{10,39,40}. A previous study reconstituted myofilaments containing TnT-WT or TnT-R173W and found depressed ATPase rates in presence of TnT-R173W⁴¹. Moreover, TnT-R173W iPSC-CMs treated with the sarcomere activator omecamtiv mecarbil⁴² showed recovered sarcomere shortening⁴¹. Despite this progress, many features of the molecular basis underlying these phenotypes at the sarcomere protein level are not fully understood.

Here, we utilized human patient-specific iPSC-CMs to characterize sarcomere microdomain interactions in presence of the DCM TnT-R173W mutation. We discovered binding of TnT-R173W to Tm to be reduced, which limits troponin anchoring on sarcomere filaments and destabilizes sarcomere protein alignment. A previous study which used recombinant pyrene-labeled tropomyosin did not detect any differences in the binding affinity of recombinant TnT-R173W compared to WT⁴³. To our best knowledge, this is the first time a cell-based assay with iPSC-CMs is used to examine TnT binding in presence of the TnT-R173W mutation. We found in this experimental system significantly reduced binding of TnT-R173W to tropomyosin compared to WT. In addition, we found lower PKA binding at sarcomeric microdomains in presence of TnT-R173W, resulting in diminished TnI phosphorylation. Moreover, presence of the TnT-R173W mutation disturbed sarcomere microdomain-cytoskeleton filament interactions via MYH7 and AMPK, contributing to disrupted sarcomere protein alignment and impaired contractility.

Firstly, biochemical assessment revealed reduced binding of mutated TnT-R173W with Tm, which stabilizes the troponin complex on sarcomeric myofilaments. This may directly lead to the disrupted sarcomere protein alignment and regularity observed in DCM iPSC-CMs, compared to healthy controls. Moreover, reduced force generation may be an important consequence of limited TnT-Tm interaction since Tm occupies the myosin-binding site on actin filaments under low intracellular $[Ca^{2+}]$. Reduced interaction with TnT in presence of DCM-TnT-R173W may affect correct relocation of Tm following Ca^{2+} binding to TnC as well as complete freeing of myosin-binding sites on actin, thereby limiting the initiation of contraction. We confirmed impaired force generation and contractility in presence of the DCM mutation using automated high-speed imaging-based analysis of contractility as well as a 3D engineered heart muscle (EHM) model.

Secondly, we discovered that the DCM mutation TnT-R173W contributes to dysregulation of local sarcomeric microdomains by limiting PKA binding and resulting in decreased PKA-mediated TnI phosphorylation at Ser-23/24. PKA-mediated phosphorylation is a critical regulatory switch for modulation of cardiac contraction^{44,45}. Previously, TnT was identified as an A-kinase anchoring protein (AKAP) which brings PKA at the thin filaments into close proximity with its sarcomeric substrates, including TnI³⁰. Generally, beta-adrenergic stimulation leads to a cell-wide increase of cAMP, which is important for local regulation of cAMP-PKA responses¹⁴. Using a sarcomeric TnI-localized FRET biosensor, we determined dysregulation of local sarcomeric cAMP/PKA pools in presence of the TnT-R173W mutation. DCM iPSC-CMs attempt an upregulation of local sarcomeric cAMP, likely to compensate for reduced PKA binding in presence of the TnT-R173W mutation, which limits TnI phosphorylation at local sarcomere microdomains, thereby diminishing contractility. On the other hand, we found a substantial upregulation of sarcomeric PDE activity in DCM TnT-R173W iPSC-CMs, in line with a recent report proposing upregulation of PDE isoform expression as a basis for deficient beta-adrenergic activation in DCM iPSC-CMs¹⁰. Thus, the observed slight increase in sarcomeric cAMP levels in DCM TnT-R173W iPSC-CMs may present a compensatory reaction and long-term-adaptation of cardiomyocyte signaling. Importantly, sarcomeric cAMP alterations could not counterbalance reduced PKA binding to TnT in presence of TnT-R173W, which may contribute to the impaired contractility observed in DCM TnT-R173W iPSC-CMs.

Together, these findings indicate a highly sensitive balance of sarcomere microdomain regulation, which is disrupted in presence of DCM TnT-R173W. Consequently, as our results show, sarcomere-cytoskeleton filament attachment is mediated via MYH7 and AMPK and is impaired in DCM iPSC-CMs. Binding of cytoskeleton attachment proteins, such as MYH7 and filamin-C, with TnT was significantly diminished in presence of the TnT-R173W mutation. Also, sarcomere attachment with plasma membrane junctions appears to be impaired in DCM iPSC-CMs compared to healthy controls. Particularly, TnT binding to MYH7 implies a critical link

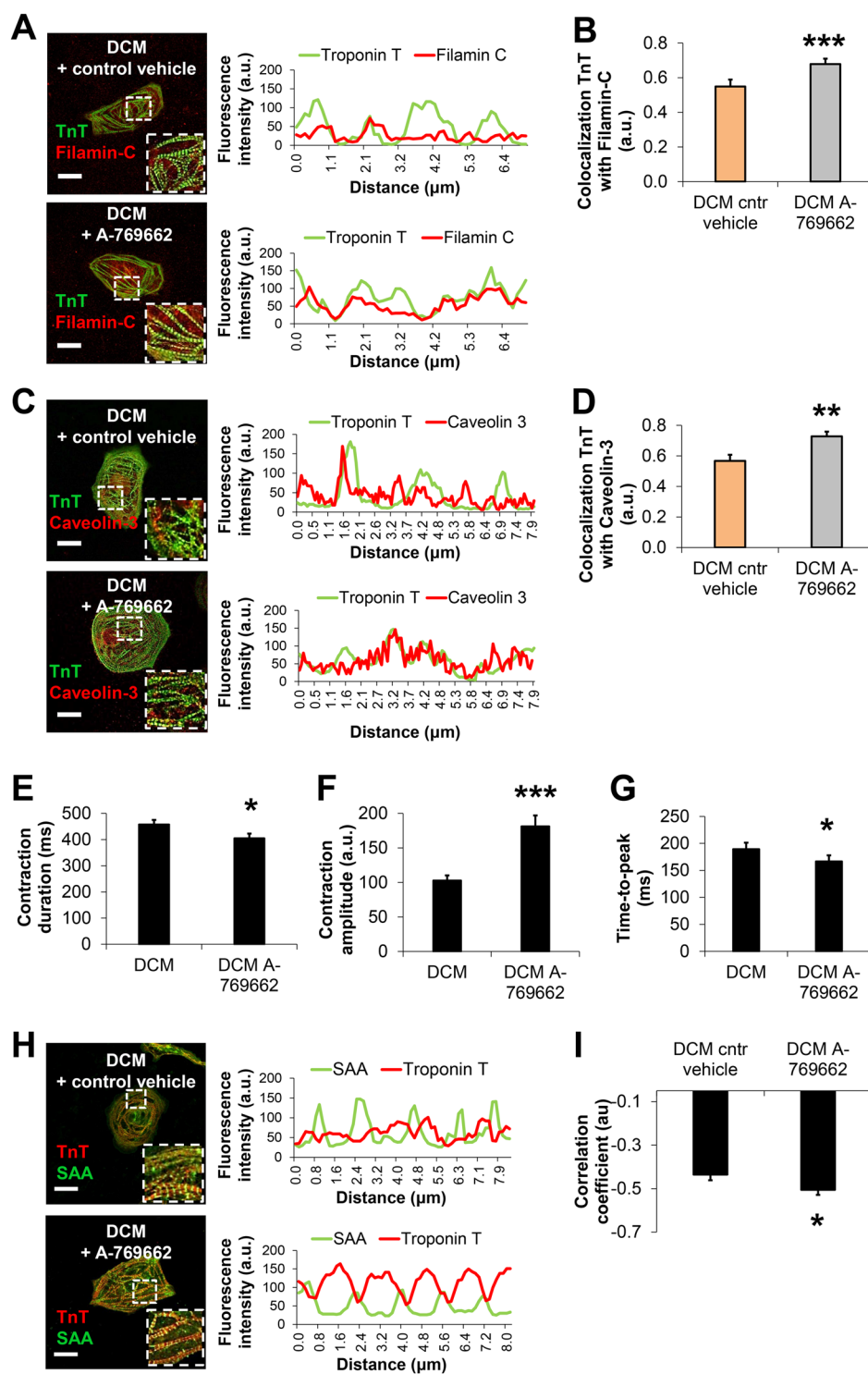


Figure 6. Activation of AMPK improves cytoskeleton attachment as well as sarcomere length in DCM TnT-R173W iPSC-CMs. (A–D) Immunostaining and confocal imaging are shown for sarcomere-cytoskeleton filament proteins in DCM iPSC-CMs following treatment with A-769662 (3 μM) or control vehicle (DMSO). Line scans show striation patterns for sarcomeric distribution of TnT (y-axis, fluorescence intensity in arbitrary units; x-axis, distance in μm). (A) Shown is co-localization of TnT and filamentin-C. (B) Quantification of (A). Analysis was performed for DCM control vehicle, n = 2 cell lines and n = 75 cells; and DCM A-769662, n = 2 cell lines and n = 35 cells. ****P* < 0.001 as calculated by Student’s t-test. Data are shown as mean ± sem. (C) Co-localization of TnT and caveolin-3. Scale bar, 20 μm. (D) Quantification of (C). Analysis was performed for DCM control vehicle, n = 2 cell lines and n = 44 cells; and DCM A-769662, n = 2 cell lines and n = 23 cells. Data are shown as mean ± sem. ***P* < 0.01, as calculated by Student’s t-test. (E–G) Motion-based contractility analysis of iPSC-CMs revealed following A-769662 treatment in DCM iPSC-CMs significantly reduced contraction duration (E), *P* = 0.01; increased contraction amplitude (F); ****P* < 0.001; and decreased

time to peak (G), $P = 0.01$. Data are expressed as mean \pm sem. Control (WT), $n = 3$ cell lines; DCM, $n = 3$ cell lines. $*P < 0.05$, and $***P < 0.001$ as calculated by Student's t-test. (H,I) Analysis of sarcomere protein regularity is shown for confocal images of immunohistochemistry performed for DCM iPSC-CMs following 7 days of culture in presence of A-769662 or control vehicle. Line scans show striation patterns for sarcomeric distribution of TnT and SAA (y-axis, fluorescence intensity in arbitrary units; x-axis, distance in μm). (H) Representative confocal images are shown. Scale bar, 20 μm . (I) Analysis of TnT and SAA signals via Fast Fourier transformation show following A-769662 treatment improved regularity of sarcomere protein arrangement (H) in DCM iPSC-CMs. Analyzed were $n = 31$ cells for control vehicle and $n = 31$ cells for A-769662, $n = 2$ cell lines per group. Data are shown as mean \pm sem. $*P < 0.05$ as calculated by Student's t-test.

of sarcomere protein alignment and organization to cytoskeleton filament stability and function. Our data suggest that disturbed binding of TnT-R173W to MYH7 directly destabilizes MYH7-AMPK interactions and AMPK-mediated modulation of cytoskeleton integrity. AMPK, a protein which assists cytoskeleton remodeling, was found to regulate sarcomere-cytoskeleton filament interactions in iPSC-CMs. Small molecule-based AMPK activation could ameliorate disruption of sarcomere-cytoskeleton protein interaction sites in DCM TnT-R173W iPSC-CMs. Importantly, activation of AMPK leads to improved contractility and sarcomeric protein alignment in DCM iPSC-CMs. Our findings suggest that in DCM TnT-R173W iPSC-CMs, disturbed interactions of TnT and resulting reduced sarcomere protein alignment and interactions require a substantial activation of AMPK to overcome the consequences of the TnT-R173W mutation. In line with a previous publication⁴⁶, we observe that AMPK activation improves contractility in cardiomyocytes. In our study, we utilize a recently developed, direct AMPK activator, A-769662, which is not expected to exert side-effects on e.g. metabolism-related enzymes^{35,47,48}.

Figuratively, these signaling events resemble a “molecular seesaw”, in which the DCM mutation causes disturbed binding of TnT-R173W to MYH7, which in turn directly translates into impaired MYH7-AMPK interactions and AMPK-mediated modulation of cytoskeleton integrity. Conversely, activation of AMPK causes a recovery shift in the opposite “seesaw” direction, by restoring cytoskeleton-sarcomere interactions and thus partially recovering sarcomere protein alignment as well as contractility. Overall, our study reveals impaired sarcomere microdomain regulation in DCM iPSC-CMs such as disrupted binding of mutated TnT-R173W with tropomyosin as well as PKA, affecting sarcomeric protein alignment and local sarcomeric cAMP/PKA regulation. These molecular functions are modulated by AMPK and contribute to reduced sarcomere protein regularity and defective force generation observed in DCM iPSC-CMs. Moreover, our findings provide novel insight into the tightly regulated interplay of sarcomeric microdomains with cytoskeleton- as well as plasma membrane junctions in iPSC-CMs from DCM patients. Further studies of these molecular functions may assist the development of novel therapeutic strategies exploiting these regulatory mechanisms to combat cardiac disease.

Materials and Methods

Cardiac differentiation of iPSCs. Human iPSCs were grown to 80–90% confluence using matrigel-coating and chemically defined E8 medium^{26,49}. Subsequently, iPSCs were differentiated into beating cardiomyocytes with a small molecule-based monolayer method described previously^{24,25}. In short, a GSK inhibitor, Chir (Selleckchem) was applied for 48 h, followed by addition of the canonical Wnt-signaling inhibitor, IWR2 (Selleckchem). Beating iPSC-derived cardiomyocytes (iPSC-CMs) were observed from day 7–10 onwards. Following differentiation, human iPSC-CMs were cultured in RPMI medium plus B-27 Supplement (Life Technologies). Human iPSC-CMs expressed typical cardiac markers such as cardiac troponin T (TNNT2), sarcomeric α -actinin (SAA), and myosin light chain 2a (MYL2a). Following 25 days of cardiac differentiation, beating iPSC-CM monolayers were dissociated using Accutase and plated in the required assay format. All protocols required for this study were approved by the Goettingen University Ethical Board. Informed consent was obtained from all participants and all research was performed in accordance with relevant guidelines and regulations.

CRISPR/Cas9 genetic engineering and plasmid generation. CRISPR/Cas9-mediated gene editing was performed as described before^{50–53}. Briefly, ATG knock-out of troponin T was performed by oligonucleotide annealing the sgRNA sequences (5'-GACCATGTCTGACATAGAAG-3', 5'-CTTCTATGTCTAGACATGGTC-3'), subcloning into the pSpCas9(BB)-2A-Puro plasmid and subsequent iPSC transfection and single clone isolation. pcDNA 3.1 plasmids carrying the full-length TNNT2-C-terminal-DYK sequence were purchased from GenScript. The TNNT2-R173W was generated by PCR-based site-directed mutagenesis as described before⁵⁴.

Immunoprecipitation and immunoblotting. TnT-specific antibody (Thermo Fisher Scientific) was immobilized on IgG1 Protein G Sepharose beads (GE Healthcare) according to the manufacturer's instructions. Subsequently, iPSC-CMs lysates were prepared in immunoprecipitation binding and wash buffer as described before⁵⁴ with protease and phosphatase inhibitors. Eluted protein solutions as well as lysate input were subjected to immunoblot. For visualization of phosphorylated TnI (p-TnI), a phospho-TnI-Ser23/24 antibody (Cell Signaling cat. no. 4004 S) was used. In addition, phos-tag acrylamide was used^{55,56}. Non-phosphorylated and phosphorylated cTnI species were separated in one-dimensional SDS-PAGE with containing phos-tag acrylamide and transferred to Western blots.

Generation of engineered heart muscle (EHM) tissues. Human ESC-CMs (2.5×10^6) were first gently mixed on ice with collagen type I and serum-free EHM medium and casted into custom-made molds according to a previously published protocol⁵⁷. Following 5 days condensation in casting molds, EHM were transferred onto mechanical stretchers for functional maturation for an additional 12–14 days. EHM media was changed

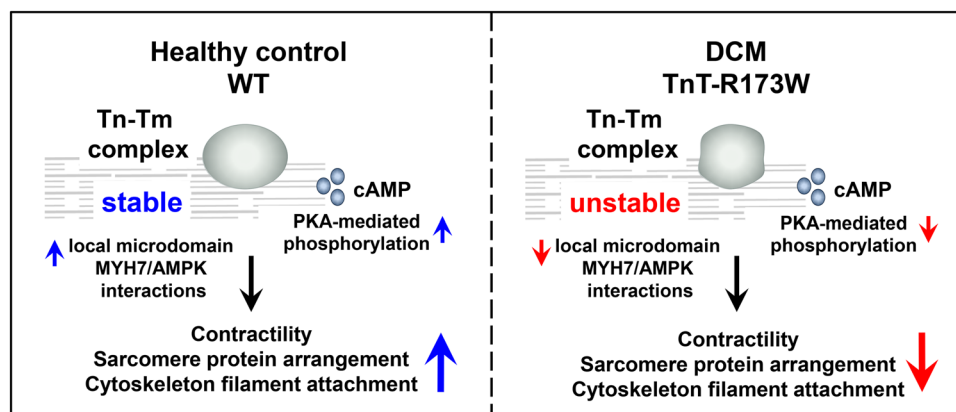


Figure 7. Schematic model showing consequences of impaired TnT interactions at sarcomere microdomains in presence of the DCM mutation TnT-R173W. In DCM iPSC-CMs, reduced TnT-R173W binding to tropomyosin and PKA destabilizes sarcomere protein alignment, limits TnI phosphorylation and impairs local microdomain signaling. This disrupts sarcomere-cytoskeleton filament interactions via MYH7 and AMPK, contributing to sarcomere misalignment and lowered contractility. These molecular disease phenotypes can be partially overcome by activation of AMPK.

every other day. Contractile forces generated by EHM were measured in organ baths in Tyrode's solution containing 1.8 mmol/L calcium under 1.5 Hz field stimulation.

Statistical analysis. Statistical significance was determined using an unpaired Student's t-test for comparison of two normally distributed data sets. A one-way or two-way ANOVA was used as appropriate to compare multiple data sets, together with post-hoc tests for pairwise comparisons according to the Sidak or Tukey methods, depending on the properties of the data sets. For non-parametric tests, Mann-Whitney- or Kruskal-Wallis tests were used together with Dunn's post-hoc multiple-comparison test. P-values < 0.05 were considered as statistically significant. Data are presented as mean \pm standard error of mean (sem).

An expanded Methods section is available in the online Data Supplement.

Received: 29 May 2019; Accepted: 13 September 2019;

Published online: 14 January 2020

References

- Maron, B. J. *et al.* Contemporary definitions and classification of the cardiomyopathies: an American Heart Association Scientific Statement from the Council on Clinical Cardiology, Heart Failure and Transplantation Committee; Quality of Care and Outcomes Research and Functional Genomics and Translational Biology Interdisciplinary Working Groups; and Council on Epidemiology and Prevention. *Circulation* **113**, 1807–1816 (2006).
- McNally, E. M., Golbus, J. R. & Puckelwartz, M. J. Genetic mutations and mechanisms in dilated cardiomyopathy. *J Clin Invest* **123**, 19–26 (2013).
- Moretti, A. *et al.* Patient-specific induced pluripotent stem-cell models for long-QT syndrome. *N Engl J Med* **363**, 1397–1409 (2010).
- Yazawa, M. *et al.* Using induced pluripotent stem cells to investigate cardiac phenotypes in Timothy syndrome. *Nature* **471**, 230–234 (2011).
- Kim, C. *et al.* Studying arrhythmogenic right ventricular dysplasia with patient-specific iPSCs. *Nature* **494**, 105–110 (2013).
- Lan, F. *et al.* Abnormal calcium handling properties underlie familial hypertrophic cardiomyopathy pathology in patient-specific induced pluripotent stem cells. *Cell Stem Cell* **12**, 101–113 (2013).
- Liang, P. *et al.* Drug screening using a library of human induced pluripotent stem cell-derived cardiomyocytes reveals disease-specific patterns of cardiotoxicity. *Circulation* **127**, 1677–1691 (2013).
- Katrakha, I. A. Human cardiac troponin complex. Structure and functions. *Biochemistry (Mosc)* **78**, 1447–1465 (2013).
- Sun, N. *et al.* Patient-specific induced pluripotent stem cells as a model for familial dilated cardiomyopathy. *Sci Transl Med* **4**, 130ra147 (2012).
- Wu, H. *et al.* Epigenetic Regulation of Phosphodiesterases 2A and 3A Underlies Compromised beta-Adrenergic Signaling in an iPSC Model of Dilated Cardiomyopathy. *Cell Stem Cell* **17**, 89–100 (2015).
- Glukhov, A. V. *et al.* Direct Evidence for Microdomain-Specific Localization and Remodeling of Functional L-Type Calcium Channels in Rat and Human Atrial Myocytes. *Circulation* **132**, 2372–2384 (2015).
- Balycheva, M., Faggian, G., Glukhov, A. V. & Gorelik, J. Microdomain-specific localization of functional ion channels in cardiomyocytes: an emerging concept of local regulation and remodeling. *Biophys Rev* **7**, 43–62 (2015).
- Pasqualini, F. S., Nesmith, A. P., Horton, R. E., Sheehy, S. P. & Parker, K. K. Mechanotransduction and Metabolism in Cardiomyocyte Microdomains. *Biomed Res Int* **2016**, 4081638 (2016).
- Surdo, N. C. *et al.* FRET biosensor uncovers cAMP nano-domains at beta-adrenergic targets that dictate precise tuning of cardiac contractility. *Nat Commun* **8**, 15031 (2017).
- Sequeira, V., Nijenkamp, L. L., Regan, J. A. & van der Velden, J. The physiological role of cardiac cytoskeleton and its alterations in heart failure. *Biochim Biophys Acta* **1838**, 700–722 (2014).
- Head, B. P. *et al.* Microtubules and actin microfilaments regulate lipid raft/caveolae localization of adenylyl cyclase signaling components. *J Biol Chem* **281**, 26391–26399 (2006).
- Moon, S. *et al.* Interactome analysis of AMP-activated protein kinase (AMPK)-alpha1 and -beta1 in INS-1 pancreatic beta-cells by affinity purification-mass spectrometry. *Sci Rep* **4**, 4376 (2014).

18. Bairwa, S. C., Parajuli, N. & Dyck, J. R. The role of AMPK in cardiomyocyte health and survival. *Biochim Biophys Acta* **1862**, 2199–2210 (2016).
19. Barnes, B. R. & Zierath, J. R. Role of AMP-activated protein kinase in the control of glucose homeostasis. *Curr Mol Med* **5**, 341–348 (2005).
20. Scott, J. W. *et al.* CBS domains form energy-sensing modules whose binding of adenosine ligands is disrupted by disease mutations. *J Clin Invest* **113**, 274–284 (2004).
21. Viollet, B. *et al.* AMPK inhibition in health and disease. *Crit Rev Biochem Mol Biol* **45**, 276–295 (2010).
22. Wang, Y. *et al.* Deoxyphalloidin suppresses tumor vasculature in HUVECs by promoting cytoskeleton remodeling through LKB1-AMPK dependent Rho A activation. *Oncotarget* **6**, 29497–29512 (2015).
23. Miranda, L. *et al.* AMP-activated protein kinase induces actin cytoskeleton reorganization in epithelial cells. *Biochem Biophys Res Commun* **396**, 656–661 (2010).
24. Lian, X. *et al.* Robust cardiomyocyte differentiation from human pluripotent stem cells via temporal modulation of canonical Wnt signaling. *Proc Natl Acad Sci USA* **109**, E1848–E1857 (2012).
25. Lian, X. *et al.* Directed cardiomyocyte differentiation from human pluripotent stem cells by modulating Wnt/beta-catenin signaling under fully defined conditions. *Nat Protoc* **8**, 162–175 (2013).
26. Ebert, A. D. *et al.* Characterization of the molecular mechanisms underlying increased ischemic damage in the aldehyde dehydrogenase 2 genetic polymorphism using a human induced pluripotent stem cell model system. *Sci Transl Med* **6**, 255ra130 (2014).
27. Sala, L. *et al.* MUSCLEMOTION: A Versatile Open Software Tool to Quantify Cardiomyocyte and Cardiac Muscle Contraction *In Vitro* and *In Vivo*. *Circ Res* **122**, e5–e16 (2018).
28. Sehnert, A. J. *et al.* Cardiac troponin T is essential in sarcomere assembly and cardiac contractility. *Nat Genet* **31**, 106–110 (2002).
29. Jin, J. P. & Chong, S. M. Localization of the two tropomyosin-binding sites of troponin T. *Arch Biochem Biophys* **500**, 144–150 (2010).
30. Sumandea, C. A. *et al.* Cardiac troponin T, a sarcomeric AKAP, tethers protein kinase A at the myofilaments. *J Biol Chem* **286**, 530–541 (2011).
31. Layland, J., Solaro, R. J. & Shah, A. M. Regulation of cardiac contractile function by troponin I phosphorylation. *Cardiovasc Res* **66**, 12–21 (2005).
32. Chatterjee, A., Villarreal, G. Jr., Oh, D. J., Kang, M. H. & Rhee, D. J. AMP-activated protein kinase regulates intraocular pressure, extracellular matrix, and cytoskeleton in trabecular meshwork. *Invest Ophthalmol Vis Sci* **55**, 3127–3139 (2014).
33. Hinson, J. T. *et al.* Integrative Analysis of PRKAG2 Cardiomyopathy iPS and Microtissue Models Identifies AMPK as a Regulator of Metabolism, Survival, and Fibrosis. *Cell Rep* **19**, 2410 (2017).
34. Johnston, J. R., Chase, P. B. & Pinto, J. R. Troponin through the looking-glass: emerging roles beyond regulation of striated muscle contraction. *Oncotarget* **9**, 1461–1482 (2018).
35. Goransson, O. *et al.* Mechanism of action of A-769662, a valuable tool for activation of AMP-activated protein kinase. *J Biol Chem* **282**, 32549–32560 (2007).
36. Duong, H.-Q., Hwang, J. S., Kim, H. J., Seong, Y.-S. & Bae, I. BML-275, an AMPK inhibitor, induces DNA damage, G2/M arrest and apoptosis in human pancreatic cancer cells. *International Journal of Oncology* **41**(6), 2227–2236 (2012).
37. Lu, Q. W. *et al.* Cardiac troponin T mutation R141W found in dilated cardiomyopathy stabilizes the troponin T-tropomyosin interaction and causes a Ca²⁺ desensitization. *J Mol Cell Cardiol* **35**, 1421–1427 (2003).
38. Hinson, J. T. *et al.* HEART DISEASE. Titin mutations in iPS cells define sarcomere insufficiency as a cause of dilated cardiomyopathy. *Science* **349**, 982–986 (2015).
39. Lowes, B. D. *et al.* Myocardial gene expression in dilated cardiomyopathy treated with beta-blocking agents. *N Engl J Med* **346**, 1357–1365 (2002).
40. Lohse, M. J., Engelhardt, S. & Eschenhagen, T. What is the role of beta-adrenergic signaling in heart failure? *Circ Res* **93**, 896–906 (2003).
41. Broughton, K. M. *et al.* A myosin activator improves actin assembly and sarcomere function of human-induced pluripotent stem cell-derived cardiomyocytes with a troponin T point mutation. *Am J Physiol Heart Circ Physiol* **311**, H107–H117 (2016).
42. Malik, F. I. *et al.* Cardiac myosin activation: a potential therapeutic approach for systolic heart failure. *Science* **331**, 1439–1443 (2011).
43. Sommese, R. F. *et al.* Effects of troponin T cardiomyopathy mutations on the calcium sensitivity of the regulated thin filament and the actomyosin cross-bridge kinetics of human beta-cardiac myosin. *PLoS One* **8**, e83403 (2013).
44. Kentish, J. C. *et al.* Phosphorylation of troponin I by protein kinase A accelerates relaxation and crossbridge cycle kinetics in mouse ventricular muscle. *Circ Res* **88**, 1059–1065 (2001).
45. Schillinger, W. & Kogler, H. Altered phosphorylation and Ca²⁺-sensitivity of myofilaments in human heart failure. *Cardiovasc Res* **57**, 5–7 (2003).
46. Oliveira, S. M. *et al.* AMP-activated protein kinase phosphorylates cardiac troponin I and alters contractility of murine ventricular myocytes. *Circ Res* **110**, 1192–1201 (2012).
47. Cool, B. *et al.* Identification and characterization of a small molecule AMPK activator that treats key components of type 2 diabetes and the metabolic syndrome. *Cell Metab* **3**, 403–416 (2006).
48. Guma, M., Wang, Y., Viollet, B. & Liu-Bryan, R. AMPK Activation by A-769662 Controls IL-6 Expression in Inflammatory Arthritis. *PLoS One* **10**, e0140452 (2015).
49. Chen, G. *et al.* Chemically defined conditions for human iPSC derivation and culture. *Nat Methods* **8**, 424–429 (2011).
50. Kodo, K. *et al.* iPSC-derived cardiomyocytes reveal abnormal TGF-beta signalling in left ventricular non-compaction cardiomyopathy. *Nat Cell Biol* **18**, 1031–1042 (2016).
51. Bak, R. O. Dever, D. P. & Porteus, M. H. CRISPR/Cas9 genome editing in human hematopoietic stem cells. *Nature Protocols* **13**(2), 358–376 (2018).
52. Hendel, A. *et al.* Chemically modified guide RNAs enhance CRISPR-Cas genome editing in human primary cells. *Nature Biotechnology* **33**(9), 985–989 (2015).
53. Liang, P. *et al.* Patient-Specific and Genome-Edited Induced Pluripotent Stem Cell-Derived Cardiomyocytes Elucidate Single-Cell Phenotype of Brugada Syndrome. *Journal of the American College of Cardiology* **68**(19), 2086–2096 (2016).
54. Ebert, A. D. *et al.* Tec-kinase-mediated phosphorylation of fibroblast growth factor 2 is essential for unconventional secretion. *Traffic* **11**, 813–826 (2010).
55. Kinoshita, E., Kinoshita-Kikuta, E., Takiyama, K. & Koike, T. Phosphate-binding tag, a new tool to visualize phosphorylated proteins. *Mol Cell Proteomics* **5**, 749–757 (2006).
56. Hamdani, N. *et al.* More severe cellular phenotype in human idiopathic dilated cardiomyopathy compared to ischemic heart disease. *J Muscle Res Cell Motil* **31**, 289–301 (2010).
57. Tiburcy, M., Meyer, T., Soong, P. L. & Zimmermann, W. H. Collagen-based engineered heart muscle. *Methods Mol Biol* **1181**, 167–176 (2014).

Acknowledgements

This work was supported by the Deutsche Forschungsgemeinschaft (German Research Foundation) Sonderforschungsbereich 1002, Projekt A12 (A.E.), the German Academic Exchange Service (DAAD, N.I.) as well as British Heart Foundation grant RG/17/6/32944 (M.Z.). We are grateful for support by the Heidenreich von Siebold program at the University Medical Center Goettingen, as well as the DZHK (German Center for Cardiovascular Research), partner site Goettingen, Germany, and the Clinic for Cardiology and Pneumology at the University Medical Center, Goettingen University.

Author contributions

Y.D. performed biochemical experiments including troponin expression, interaction, local PKA signaling, AMPK activation, and microdomain interaction; A.A. and N.I. performed experiments on microdomain interaction and sarcomere analysis; H.X. performed cell contractility experiments; P.L.S., M.T., Y.D., A.E. and W.H.Z. performed EHM experiments; A.K., Y.D. and M.Z. performed FRET sensor experiments; G.H., W.A.L. and M.Z. provided critical suggestions and equipment use; A.E. designed and supervised the study and wrote the manuscript.

Competing interests

The authors declare no competing interests.

Additional information

Supplementary information is available for this paper at <https://doi.org/10.1038/s41598-019-56597-3>.

Correspondence and requests for materials should be addressed to A.E.

Reprints and permissions information is available at www.nature.com/reprints.

Publisher's note Springer Nature remains neutral with regard to jurisdictional claims in published maps and institutional affiliations.



Open Access This article is licensed under a Creative Commons Attribution 4.0 International License, which permits use, sharing, adaptation, distribution and reproduction in any medium or format, as long as you give appropriate credit to the original author(s) and the source, provide a link to the Creative Commons license, and indicate if changes were made. The images or other third party material in this article are included in the article's Creative Commons license, unless indicated otherwise in a credit line to the material. If material is not included in the article's Creative Commons license and your intended use is not permitted by statutory regulation or exceeds the permitted use, you will need to obtain permission directly from the copyright holder. To view a copy of this license, visit <http://creativecommons.org/licenses/by/4.0/>.

© The Author(s) 2020

SUPPLEMENTAL MATERIALS

Troponin destabilization impairs sarcomere-cytoskeleton interactions in iPSC-derived cardiomyocytes from dilated cardiomyopathy patients

Yuanyuan Dai^{1,3}, Asset Amenov^{1,3}, Nadezda Ignatyeva^{1,3}, Andreas Koschinski⁵, Hang Xu^{1,3}, Poh Loong Soong^{2,3}, Malte Tiburcy^{2,3}, Wolfgang A. Linke^{1,3,4}, Manuela Zaccolo⁵, Gerd Hasenfuss^{1,3}, Wolfram-Hubertus Zimmermann^{2,3}, Antje Ebert^{1,3}

¹Heart Center, Department of Cardiology and Pneumology; ²Institute of Pharmacology, University Medical Center, University of Goettingen, Robert-Koch-Str. 40, 37075 Goettingen, Germany; ³DZHK (German Center for Cardiovascular Research), partner site Goettingen, Germany; ⁴Institute of Physiology II, University of Muenster, Germany; ⁵Department of Physiology, Anatomy and Genetics, University of Oxford, Oxford OX1 3PT, UK.

SUPPLEMENTAL METHODS

Culture and maintenance of human iPSCs. The human iPSC lines described earlier (1-3) were grown on Matrigel-coated plates (ES qualified, BD Biosciences, San Diego) as described previously (4, 5) using chemically defined E8 medium (4). Culture medium for iPSCs was changed daily. Cells were passaged every 4 days using Accutase (Global Cell Solutions). Healthy control and DCM iPSCs as published in (1, 2) were a kind gift from Joseph C. Wu (Stanford University, CA). Protocols for human biomaterial studies required for this study were approved by the Goettingen University Ethical Board.

Pluripotency marker analysis. Human iPSC colonies were grown in 6-well plate format (Sigma Aldrich) and stained as described previously (1, 5) for Oct3/4 (Cell Signaling Technology), Tra-1-60 (Sigma-Aldrich/Chemicon), SSEA4 (Santa Cruz Biotechnology) and Nanog (Santa Cruz Biotechnology). Images were acquired with a brightfield microscope (Leica).

Flow cytometry. Assessment of TnT expression in human iPSC-CMs by flow cytometry was performed as described before (6). Briefly, iPSC-CMs were detached as described above, and subsequently fixed and permeabilized (5, 6). Cells were incubated with a primary anti-cardiac TnT antibody (Thermo Scientific) for 2 h at 4°C, and a secondary Alexa Fluor-488 antibody (Life Technologies) for 45 min at 4°C. Cells were washed and analyzed by fluorescent activated cell sorting (FACS; BD Aria II), and data were analyzed using FlowJo software.

Immunofluorescence staining and confocal microscopy. Differentiated iPSC-CMs were passaged on matrigel-coated glass coverslips. Cells were stained as described before with mouse

anti-human antibodies for cardiac troponin T (Thermo Scientific and Abcam) and sarcomeric alpha-actinin (Sigma). DAPI was used for staining of nuclei. Coverslips were mounted on glass slides using Fluoromount-G. Pictures were taken with 10x, 40x (plan apochromat), and 63x (plan apochromat oil) objectives using an inverted confocal microscope (Carl Zeiss, LSM 710 Meta, Göttingen, Germany) and ZEN software (Carl Zeiss).

Quantification of protein co-localization. Confocal images generated as described above were analyzed for protein co-localization analysis using the ImageJ function Coloc2. Background correction was performed using Fiji-ImageJ. For individual cells, ROIs were selected. Coloc2 was used for background subtraction, and analysis for obtaining Manders' correlation was performed as described before (7-9).

Co-immunoprecipitation with DYK-tagged TnT and immunoblot. HEK 293T cells overexpressing in a pcDNA 3.1 backbone either TnT-WT-DYK, TnT-R173W-DYK or DYK tag alone as a negative control were lysed and input was kept for analysis. Cell lysates were bound with DYK-antibody-decorated magnetic beads and subsequently, immobilized TnT-DYK was incubated for co-immunoprecipitation (10) with cell lysate from healthy control iPSC-CMs. The bound fraction was analyzed by immunoblot. The following antibodies were purchased from Abcam: Tropomyosin (ab7785), troponin C (ab137130), troponin I (ab52862), phospholamban (ab2865). Myosin heavy chain antibody was purchased from DSHB.

PDE activity assay. Human iPSC-CM lysates were prepared as described (5). Sarcomere-containing fractions were obtained by pelleting pre-cleared lysates (10). The cytosolic supernatant

was transferred to a new tube and analyzed separately. Both cytosolic and sarcomere-containing fractions were subsequently analyzed using a PDE activity assay kit (Abcam, ab139460) according to the manufacturer's instructions.

Analysis of AMPK activity via phosphorylation of T172. Human iPSC-CM lysates were prepared as described (5) from healthy control (n=2 cell lines) and DCM (n=3 cell lines) groups. To determine AMPK activity based on phosphorylation of Thr-172 in the AMPK catalytic subunit, cell lysates were incubated with A-769662 or control vehicle (DMSO) and subsequently subjected to immunoblot analysis.

Fluorescent resonance energy transfer (FRET) measurements and analysis. All FRET-measurements were performed with a Nikon Eclipse FN-1 microscope. An Opto-Led fluorescent light source (Cairn-Research) was used for excitation at 436 ± 25 nm, the excitation / emission dichroic was 455 nm (long pass). Emitted light was split with a Dual-View beam splitter (Optical Insights) and recorded with a CoolSnap HQ² camera (Photometrix). Emission light was split with a 505 nm longpass dichroic and was then filtered at 480 ± 15 nm for CFP emission and 535 ± 20 nm for YFP emission. Extracellular buffer for the measurements was a modified and CO₂ supplemented Ringer-solution with NaCl (140 mM), KCl (3 mM), MgCl₂ (2 mM), CaCl₂ (2 mM), Glucose (15 mM), HEPES (10 mM), pre-adjusted to pH 7.2 with NaOH, then supplemented with NaHCO₃ (10 mM) and finally pH-adjusted to pH 7.2. Acquisition and analysis were performed using Optofluor software (Cairn Research). All ratios were calculated as emission at 535 nm / emission at 480 nm. The TPNI-CUTie FRET-sensor was developed before (11). Adenoviruses were used to infect cells 24-48h before the measurements.

SUPPLEMENTAL FIGURE LEGENDS

Supplementary Figure 1: Characterization of DCM and TnT-KO iPSC-CMs. (A) Sanger sequencing chromatogram of genomic DNA from healthy control and DCM-TnT-R173W iPSCs. Arrow indicates site of mutation. (B) Strategy for generation of a troponin T knock-out in iPSC via CRISPR/Cas9-mediated targeting of *TNNT2* exon 2. Underlined corresponds to sequence of the sgRNA employed for targeting of exon 2 (red highlight, ATG). (C) Immunohistochemistry and wide-field imaging show expression of the indicated pluripotency markers. (D) Healthy control and DCM iPSC-CMs express standard sarcomeric marker proteins. Expression of MYL2 (MYL) and MYH7 is reduced in TnT-KO iPSC-CMs. * $P < 0.05$, ** $P < 0.01$, *** $P < 0.001$ and ns, not significant, as calculated by Kruskal-Wallis test and Dunn's multiple comparisons test. (E) Representative analysis of TnT expression in human iPSC-CMs via flow cytometry. (F) Immunohistochemistry for sarcomeric alpha-actinin and cardiac troponin T, followed by confocal imaging was performed (shown in Fig 1A) and sarcomeric alpha-actinin and TnT signals were analyzed by Pearson's correlation and Fast Fourier transformation, to obtain correlation coefficients in DCM iPSC-CMs (94 cells) than in healthy controls (n=78 cells). The difference between the groups is not statistically significant as calculated by Mann-Whitney test. TnT KO iPSC-CMs could not be reliably analyzed due to lack of signal for TnT. Data are expressed as mean \pm sem.

Supplementary Figure 2: Expression levels of TNNT2, TNNC1, TNNI3 and TPM1 are not significantly altered in TnT-R173W iPSC-CMs. (A-D) Expression of TNNT2 (A), TNNC1(B), TPM1 (C) and TNNI3 (D) was determined at the mRNA level via quantitative real-time PCR (qRT-PCR). WT control vs DCM, not significant (ns) and *** $P < 0.001$ towards all other groups, as

calculated by Kruskal-Wallis test and Dunn's multiple comparisons test. **(E-H)** Expression levels of the troponin complex were comparable in DCM-R173W iPSC-CMs and healthy controls. Immunoblot analysis for protein expression of troponin T (TnT) **(E)**, troponin C (TnC) **(F)**, tropomyosin (Tm) **(G)**, and troponin I (TnI) **(H)** was performed for DCM R173W iPSC-CMs compared to healthy control- (WT) and TnT KO iPSC-CMs. Control (WT), n=3 cell lines; DCM (TnT-R173W), n=3 cell lines; TnT KO, n=1 cell line. Bargraphs display averages of n=3 experiments and shown below are representative immunoblots; ns, not significant as calculated by one-way ANOVA and multiple comparisons tests (Dunn and Sidak methods). Data are expressed as mean \pm sem.

Supplementary Figure 3, relating to Figure 2: Interactions within the troponin complex are affected by the DCM mutation TnT-R173W. **(A-C)** Protein-protein interactions within the troponin-tropomyosin complex were assessed by immunoprecipitation using a TnT-specific antibody. **(A)** Equal amounts of TnT-WT and TnT-R173W were immunoprecipitated from lysates of healthy control and DCM. No substantial binding is detected for TnT-KO iPSC-CMs (negative control). TnC **(B)**, Tm **(C)** and TnI **(D)** binding to TnT is shown. Tm-binding to TnT-R173W is reduced in DCM TnT-R173W iPSC-CMs, compared to WT controls. TnT KO iPSC-CMs are employed as negative control. Bargraphs are shown for control (WT, n= 3 cell lines), DCM (TnT-R173W, n=3 cell lines), and TnT KO (n=1 cell line). TnT, averages of n=8 experiments; TnC, averages of n=8 experiments; Tm, averages of n=7 experiments; and TnI, averages of n=2 experiments. Representative immunoblots are shown. ns=not significant as calculated by one-way ANOVA and Dunn's multiple comparison test. Data are expressed as mean \pm sem.

Supplementary Figure 4, relating to Figure 2-3: Disturbed interactions within the troponin complex in presence of DCM-TnT-R173W. (A) Input for TnT-WT-DYK and TnT-R173W-DYK (MUT) as well as DYK-negative control (NC) from HEK cell lysates prior to coupling to DYK-decorated beads; and input for human iPSC-CM WT cell lysate used for co-immunoprecipitation of TnC, Tm, TnI as well as PKA. GAPDH was used as a loading control. (B) Phos-tag gel analysis of DCM- and healthy control iPSC-CM cell lysates is shown. TnI phosphorylation in DCM TnT-R173W is reduced compared to healthy control iPSC-CMs. Shown is 2-P-phosphorylated TnI as reported previously (50). Averages of 3 independent experiments are shown for control (n=3 cell lines), DCM (n=3 cell lines); *** $P < 0.001$ (Mann-Whitney test). Data are shown as mean \pm sem. Representative membrane scans are shown. Reduced PKA-mediated TnI phosphorylation was also analyzed with a TnI-Ser 23/24 specific antibody (Figure 3A). (C-D) FRET-based analysis of cAMP levels in TnT-KO iPSC-CMs versus WT controls. (C) Disorganized sarcomeric structure in TnT-KO iPSC-CMs results in corresponding mislocalization of the sarcomeric FRET-sensor TPNI-CUTie. Respectively, no significant difference in sarcomeric cAMP levels is detected in TnT-KO iPSC-CMs, compared to WT. Representative images are shown; scale bar, 10 μ m. (D) Quantification of TPNI-CUTie FRET analysis shown in (C). No significant difference is detected between WT control and TnT-KO ($P = 0.0981$). WT iPSC-CMs (healthy control), n=45 cells; TnT-KO iPSC-CMs, n=89 cells. ns = not significant (Student's t-test). Data are shown as mean \pm sem.

Supplementary Figure 5: Total cytosolic PDE activity is elevated in DCM TnT-R173W iPSC-CMs. (A) Adenylyl cyclase protein expression levels are not significantly changed in DCM iPSC-CMs and healthy controls as well as TnT-KO iPSC-CMs. Bargraphs indicate averages of n=2

experiments for n=2 cell lines (WT, DCM) and n=1 cell line (TnT-KO), representative immunoblots are shown below. Differences are not statistically significant (one-way ANOVA and Dunn's multiple comparison test). **(B-C)** Measurements of cytosolic PDE activity in DCM iPSC-CMs compared to healthy controls as well as TnT-KO iPSC-CMs, using a PDE activity assay kit (Abcam). **(B)** Measurement of PDE activity via 5'AMP release, using a standard curve for absorbance at 620 nm. **(C)** Differences in total cytosolic PDE activity were not significantly altered between DCM- and TnT-KO iPSC-CMs, compared to healthy controls. Averages of n=2 experiments for n=2 cell lines (WT, DCM) and n=1 cell line (TnT-KO) are shown. Differences are not statistically significant, as calculated by Kruskal-Wallis test and Dunn's multiple comparisons test. Data are shown as mean \pm sem.

Supplementary Figure 6, relating to Figure 4: Interaction of TnT with cytoskeleton filament proteins. Input for TnT IP from healthy control (WT), DCM (TnT-R173W) and TnT-KO iPSC-CMs is shown. Input was collected from cell lysates prior to coupling to TnT antibody-decorated beads **(A)** mouse TnT, relating to Figure 4C-E and **(B)** Immunoblot analysis for filamin-C expression in DCM-TnT-R173W iPSC-CMs and WT controls using input fractions from immunoprecipitation of TnT with filamin-C shown in Fig 4C-E. A representative membrane scan is shown. **(C)** Quantification of **(B)**, n=3 experiments. *P*= not significant (one-way ANOVA and Dunn's multiple comparisons test). Data are shown as mean \pm sem.

Supplementary Figure 7, relating to Fig. 5: Interaction of TnT with cytoskeleton filament proteins. **(A)** Input for relevant proteins in TnT IP with MYH7 is shown for healthy control (WT), DCM (TnT-R173W) and TnT-KO iPSC-CM cell lysates. Input was collected from cell lysates

prior to coupling to TnT antibody-decorated beads (mouse TnT). GAPDH was used as a loading control. **(B)** Western blot indicates total protein expression levels of AMPK to be comparable in DCM and healthy control iPSC-CMs. Quantification of 2 experiments is shown. Control, n=2 cell lines; DCM, n=3 cell lines. P = not significant (Mann-Whitney test); data are shown as mean \pm sem.

Supplementary Figure 8, relating to Fig. 6: AMPK inhibition in WT iPSC-CMs results in impaired contractility as observed in DCM iPSC-CMs. Motion-traction analysis of WT iPSC-CMs treated for 24h with an AMPK inhibitor, BML-275. **(A)** Time-to-peak; **(B)** Contraction amplitude; **(C)** Contraction duration. Quantification is shown for n=2 cell lines; ** P <0.01 and *** P <0.001 as calculated by Student's t-test. Data are shown as mean \pm sem.

Supplementary Table 1, relating to Fig. 1: Numerical values represented in the error bars in Fig. 1I (standard error of mean) showing force-of-contraction measurements in EHM from WT control and DCM TnT-R173W iPSC-CMs. n=8 EHM per group. * P < 0.05 and ns, not significant as calculated by two-way ANOVA and Tukey's post-hoc test.

REFERENCES

1. N. Sun *et al.*, Patient-specific induced pluripotent stem cells as a model for familial dilated cardiomyopathy. *Sci Transl Med* **4**, 130ra147 (2012).
2. F. Lan *et al.*, Abnormal calcium handling properties underlie familial hypertrophic cardiomyopathy pathology in patient-specific induced pluripotent stem cells. *Cell Stem Cell* **12**, 101-113 (2013).

3. H. Wu *et al.*, Epigenetic Regulation of Phosphodiesterases 2A and 3A Underlies Compromised beta-Adrenergic Signaling in an iPSC Model of Dilated Cardiomyopathy. *Cell Stem Cell* **17**, 89-100 (2015).
4. G. Chen *et al.*, Chemically defined conditions for human iPSC derivation and culture. *Nat Methods* **8**, 424-429 (2011).
5. A. D. Ebert *et al.*, Characterization of the molecular mechanisms underlying increased ischemic damage in the aldehyde dehydrogenase 2 genetic polymorphism using a human induced pluripotent stem cell model system. *Sci Transl Med* **6**, 255ra130 (2014).
6. P. E. de Almeida *et al.*, Transplanted terminally differentiated induced pluripotent stem cells are accepted by immune mechanisms similar to self-tolerance. *Nat Commun* **5**, 3903 (2014).
7. E. M. M. Manders, V. F.J., A. J.A., Measurement of co-localization of objects in dual-colour confocal images *Journal of Microscopy* **169**, 375-382 (1993).
8. J. Oswald *et al.*, Leptin affects filopodia and cofilin in NK-92 cells in a dose- and time-dependent manner. *Eur J Histochem* **62**, 2848 (2018).
9. V. Zinchuk, O. Zinchuk, T. Okada, Quantitative colocalization analysis of multicolor confocal immunofluorescence microscopy images: pushing pixels to explore biological phenomena. *Acta Histochem Cytochem* **40**, 101-111 (2007).
10. A. D. Ebert *et al.*, Tec-kinase-mediated phosphorylation of fibroblast growth factor 2 is essential for unconventional secretion. *Traffic* **11**, 813-826 (2010).
11. N. C. Surdo *et al.*, FRET biosensor uncovers cAMP nano-domains at beta-adrenergic targets that dictate precise tuning of cardiac contractility. *Nat Commun* **8**, 15031 (2017).

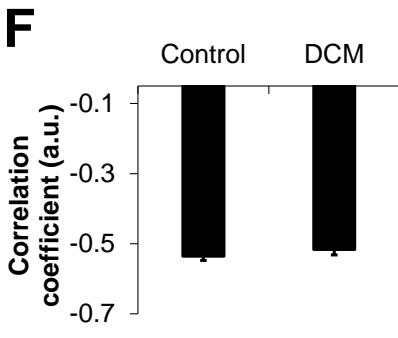
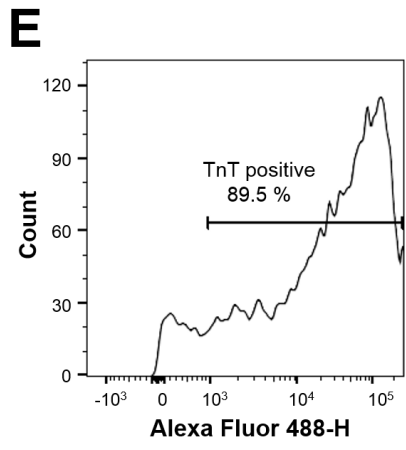
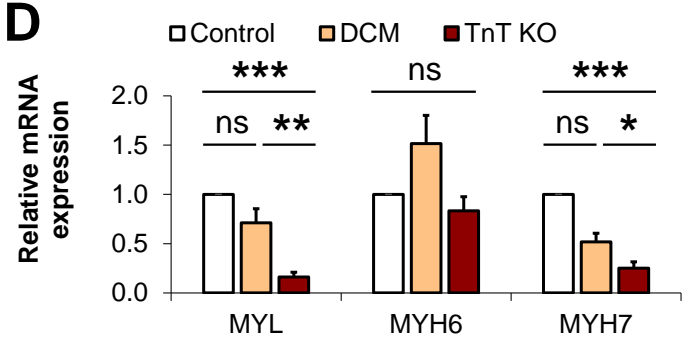
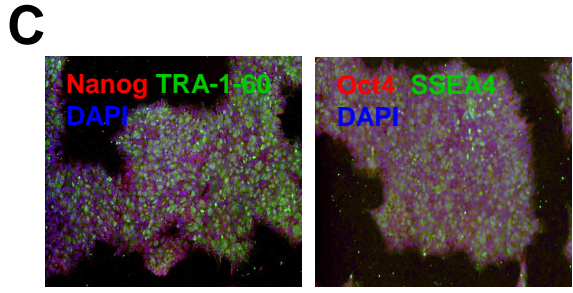
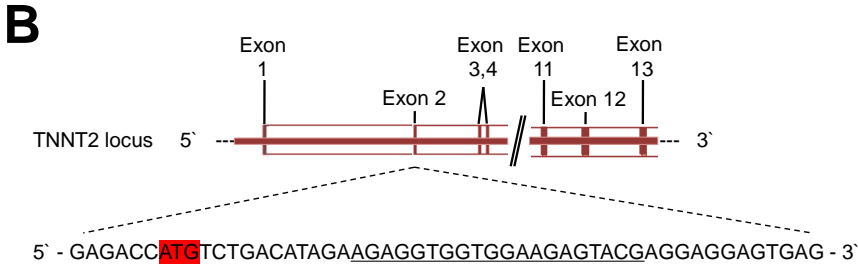
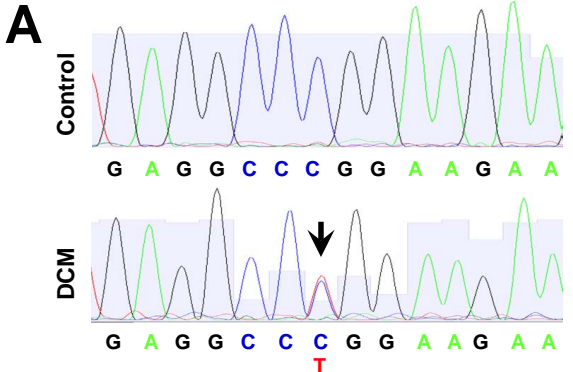
SUPPLEMENTAL FIGURES

Troponin destabilization impairs sarcomere-cytoskeleton interactions in iPSC-derived cardiomyocytes from dilated cardiomyopathy patients

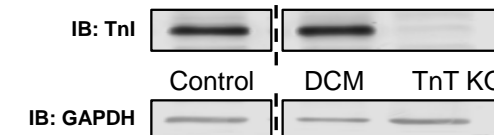
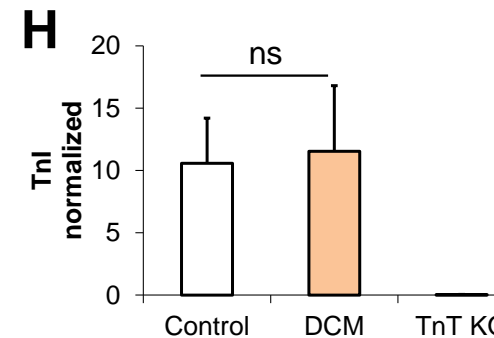
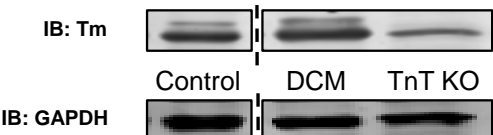
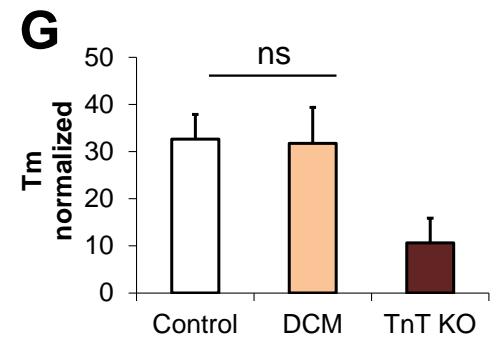
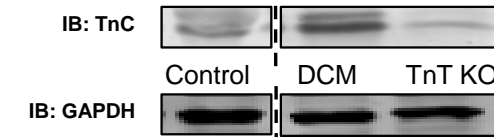
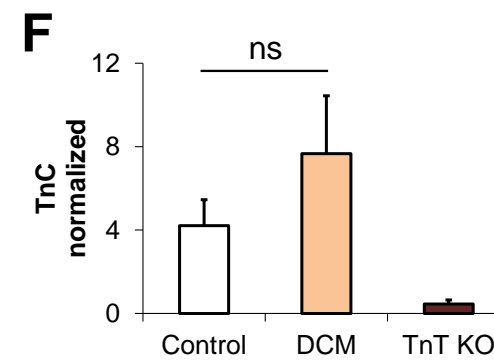
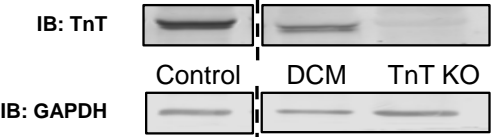
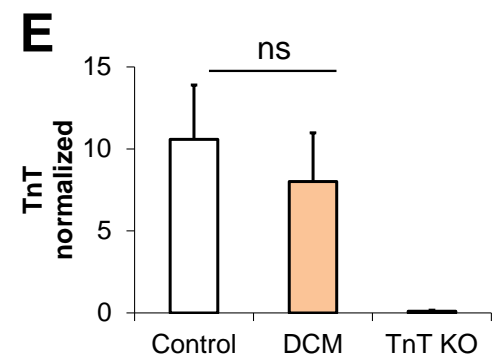
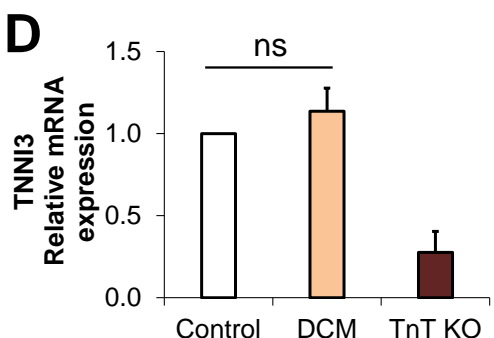
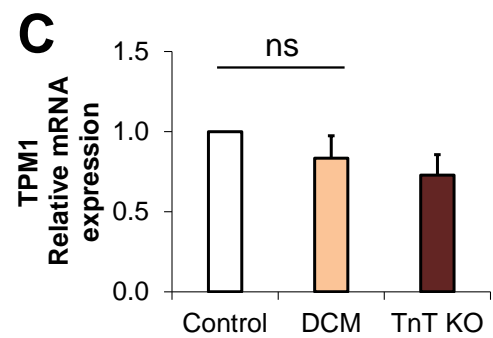
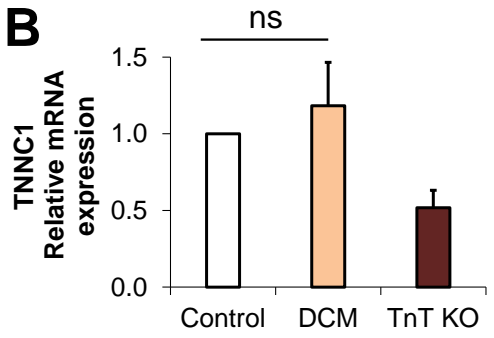
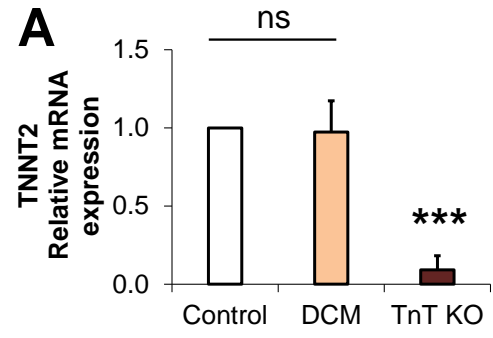
Yuanyuan Dai^{1,3}, Asset Amenov^{1,3}, Nadezda Ignatyeva^{1,3}, Andreas Koschinski⁵, Hang Xu^{1,3},
Poh Loong Soong^{2,3}, Malte Tiburcy^{2,3}, Wolfgang A. Linke^{1,3, 4}, Manuela Zaccolo⁵,
Gerd Hasenfuss^{1,3}, Wolfram-Hubertus Zimmermann^{2,3}, Antje Ebert^{1,3}

¹Heart Center, Department of Cardiology and Pneumology; ²Institute of Pharmacology, University of Goettingen, Robert-Koch-Str. 40, 37075 Goettingen, Germany; ³DZHK (German Center for Cardiovascular Research), partner site Goettingen, Germany; ⁴Institute of Physiology II, University of Muenster, Germany; ⁵Department of Physiology, Anatomy and Genetics, University of Oxford, Oxford OX1 3PT, UK.

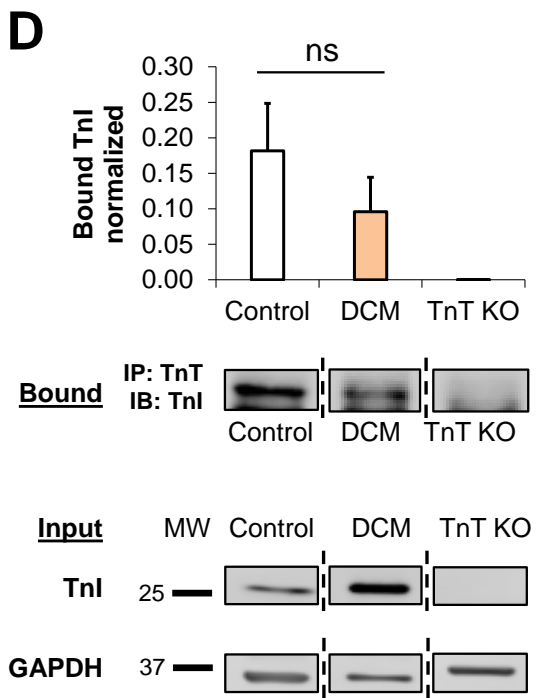
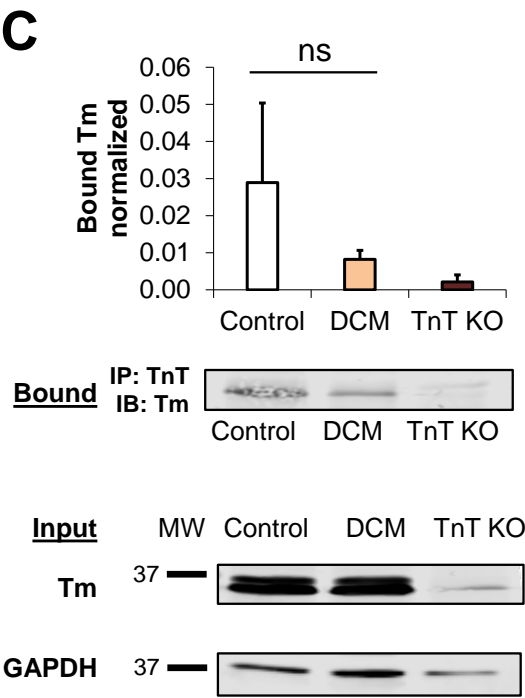
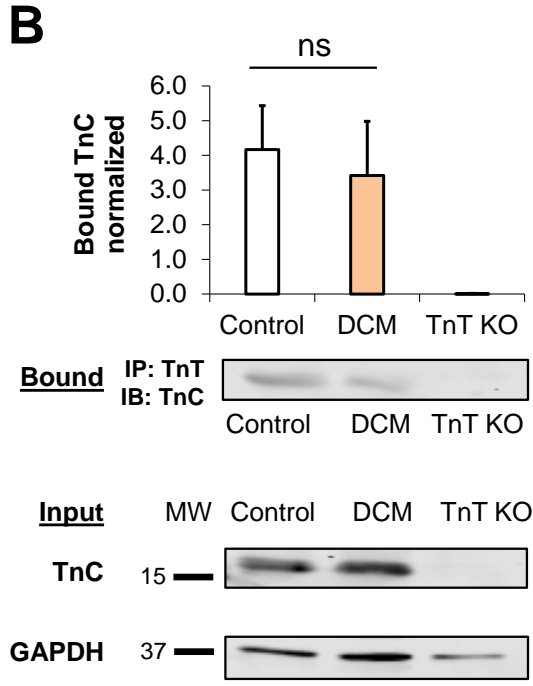
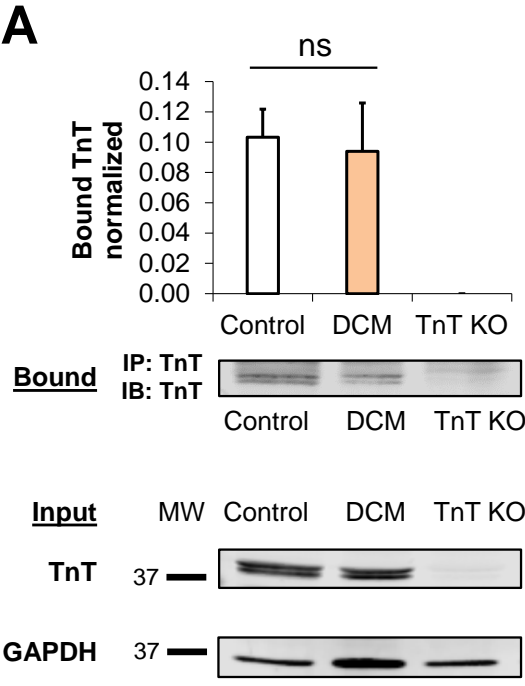
Supplementary Figure 1



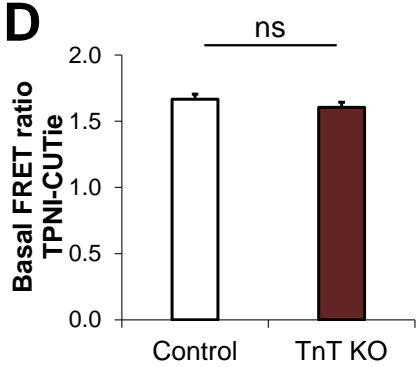
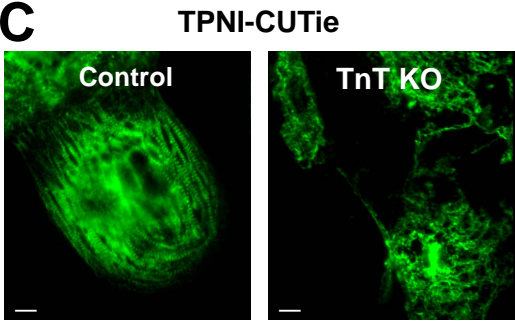
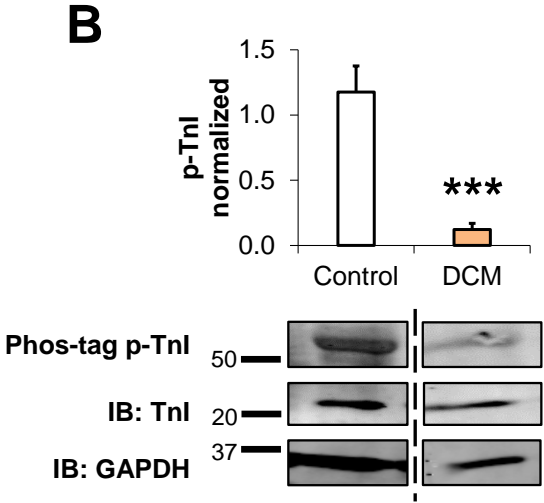
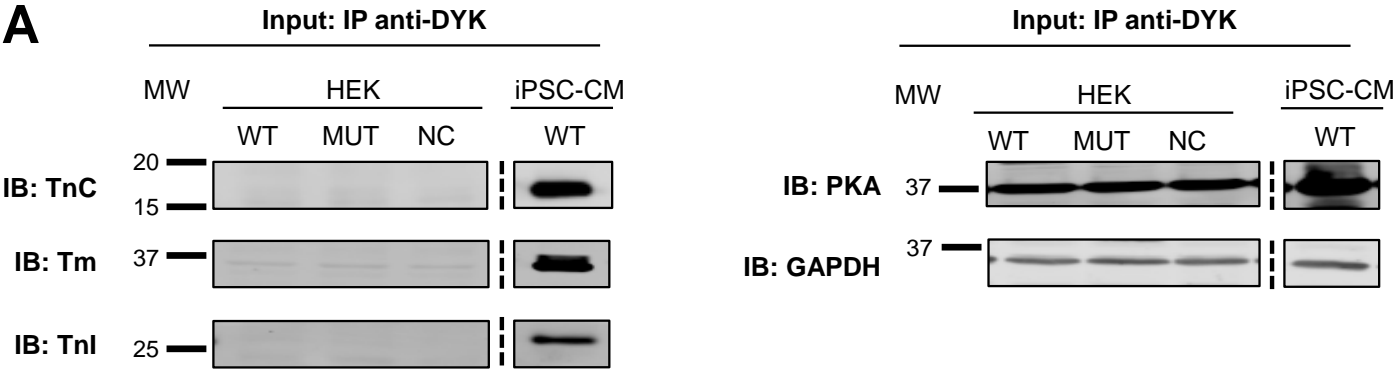
Supplementary Figure 2



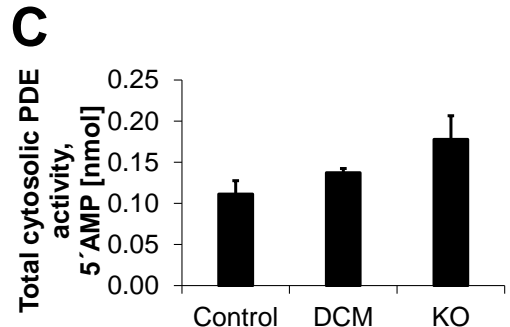
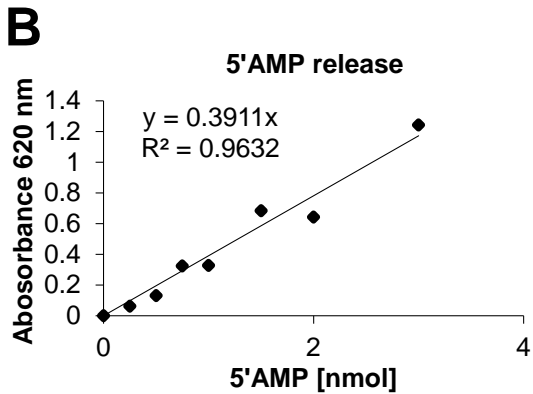
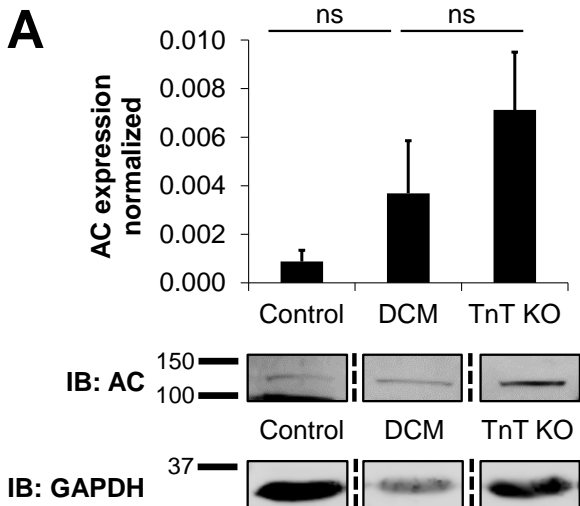
Supplementary Figure 3



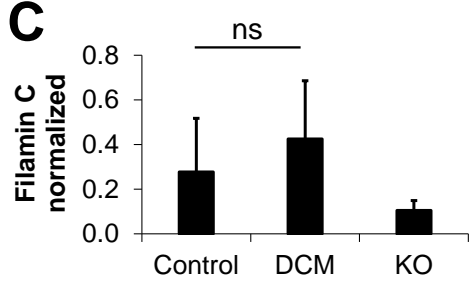
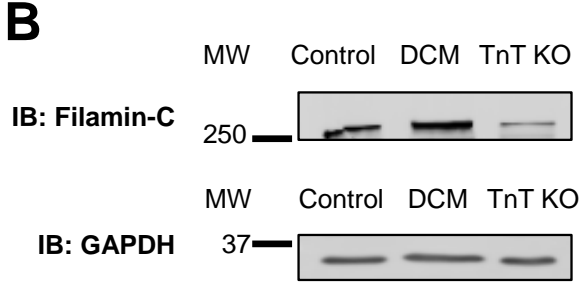
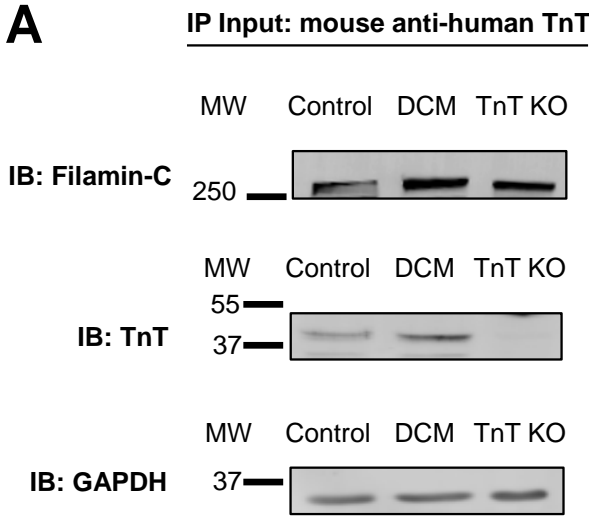
Supplementary Figure 4



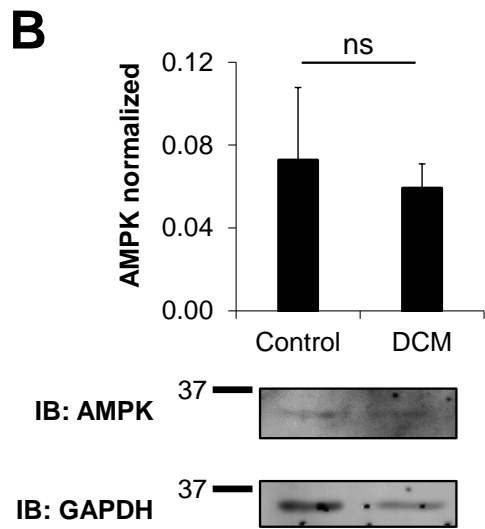
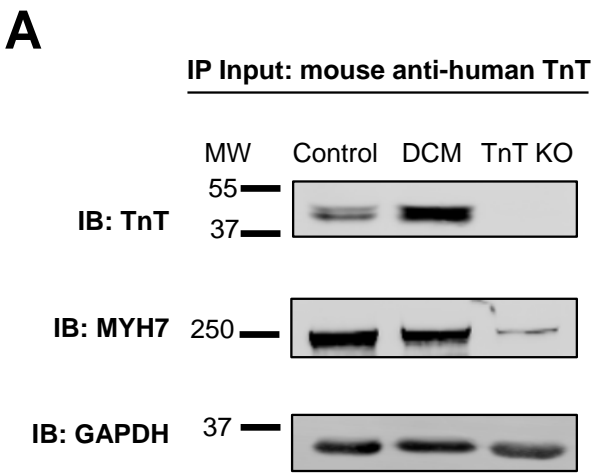
Supplementary Figure 5



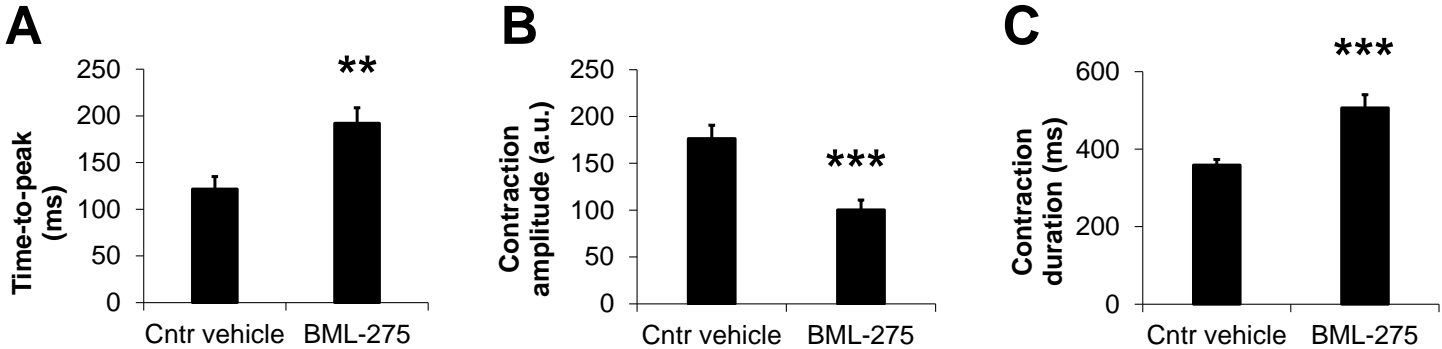
Supplementary Figure 6



Supplementary Figure 7



Supplementary Figure 8



Supplementary Table 1

Ca²⁺[mmol/l]	Control (WT) EHMs			DCM (TnT-R173W) EHMs		
	Mean	SEM	N	Mean	SEM	N
0.2	0.079	0.014	8	0.025	0.003	8
0.4	0.194	0.036	8	0.066	0.006	8
0.8	0.458	0.077	8	0.181	0.023	8
1.2	0.660	0.096	8	0.267	0.029	8
1.6	0.817	0.081	8	0.327	0.023	8
2	0.933	0.096	8	0.365	0.021	8
2.4	0.984	0.096	8	0.389	0.019	8
2.8	1.020	0.100	8	0.404	0.019	8
3.2	1.052	0.102	8	0.405	0.019	8
4	1.102	0.102	8	0.407	0.021	8

3.2 Pulication2

An alternative mechanism of subcellular iron uptake deficiency in cardiomyocytes and treatment approach in heart failure

Yuanyuan Dai, Nadezda Ignatyeva, Hang Xu, Ruheen Wali, Karl Toischer, Sören Brandenburg, Christof Lenz, Samuel Sossalla, Niels Voigt, Elisabeth M. Zeisberg, Andreas Janshoff, Henning Urlaub, Torsten Bloch Rasmussen, Jens Mogensen, Stephan E. Lehnart, Gerd Hasenfuss, Antje Ebert

Heart Research Center Goettingen, Department of Cardiology and Pneumology, University Medical Center Goettingen, Georg-August University of Goettingen, Goettingen, Germany;

DZHK (German Center for Cardiovascular Research), partner site Goettingen, Germany.

**An alternative mechanism of subcellular iron uptake deficiency in cardiomyocytes
and treatment approach in heart failure**

Yuanyuan Dai^{1,2}, Nadezda Ignatyeva^{1,2}, Hang Xu^{1,2}, Ruheen Wali^{1,2}, Karl Toischer^{1,2,3}, Sören Brandenburg^{1,2,3}, Christof Lenz⁴, Samuel Sossalla⁵, Niels Voigt^{2,6,7}, Elisabeth M. Zeisberg^{1,2},
Andreas Janshoff⁸, Henning Urlaub^{4,9}, Torsten Bloch Rasmussen¹⁰, Jens Mogensen¹¹,
Stephan E. Lehnart^{1,2,7}, Gerd Hasenfuss^{1,2,3}, Antje Ebert^{1,2}

¹ Heart Research Center Goettingen, Department of Cardiology and Pneumology, University Medical Center Goettingen, Georg-August University of Goettingen, Goettingen, Germany;
²DZHK (German Center for Cardiovascular Research), partner site Goettingen, Germany;
³Heart Center, Department of Cardiology and Pneumology, University Medical Center Goettingen, Goettingen University, Germany; ⁴Institute of Clinical Chemistry, University Medical Center, Goettingen University; ⁵Department for Internal Medicine II, University Medical Center Regensburg; ⁶Institute of Pharmacology and Toxicology University Medical Center, Goettingen University; ⁷Cluster of Excellence “Multiscale Bioimaging: from Molecular Machines to Networks of Excitable Cells” (MBExC), Goettingen University;
⁸Institute for Physical Chemistry, Goettingen University, Germany; ⁹Bioanalytical Mass Spectrometry, Max Planck Institute for Biophysical Chemistry, Goettingen; ¹⁰Department of Cardiology, Regional Hospital West Jutland, Herning, Denmark; ¹¹Department of Cardiology, Aalborg University Hospital, Aalborg, Denmark.

Total word count: 4,600

Keywords: Human iPSCs/ sarcomeres/ microdomains/ iron deficiency/ signal transduction/
cardiovascular disease/ dilated cardiomyopathy/heart failure

Correspondence: Antje Ebert, Goettingen University Medical Center, Goettingen University,
Robert-Koch-Strasse 40, 37075 Goettingen, Germany. Email: antje.ebert@med.uni-goettingen.de

ABSTRACT

Systemic defects in intestinal iron absorption, circulation, and retention cause iron deficiency in 50% of patients with heart failure (HF). Defective subcellular iron uptake mechanisms that are independent of systemic absorption are incompletely understood. We investigated these mechanisms in patient-derived and CRISPR/Cas-edited induced pluripotent stem cell-derived cardiomyocytes (iPSC-CMs) as well as patient-derived heart tissue using an integrated platform of MS-SWATH-based proteomics and signaling pathway interrogation. We employed a genetic iPSC model of two inherited mutations (troponin T, TnT-R141W and tropomyosin, TPM1-L185F) that lead to dilated cardiomyopathy (DCM), a frequent cause of HF, to study the underlying molecular dysfunctions of DCM mutations. We identified a molecular patho-mechanism of impaired subcellular iron deficiency that is independent of systemic iron metabolism. Clathrin-mediated endocytosis (CME) defects as well as impaired endosome distribution and cargo transfer were identified as a basis for subcellular iron deficiency in DCM iPSC-CMs. The CME defects were also confirmed in the hearts of DCM patients with end-stage HF. Correction of the TPM1-L185F mutation in DCM patient-derived iPSCs, treatment with a small compound, RhoA activator II, or iron supplementation rescued the molecular disease pathway and recovered contractility. Pheno-copying the effects of the TPM1-L185F mutation into WT iPSC-CMs could be ameliorated by iron supplementation. Our findings suggest that impaired endocytosis and cargo transport resulting in subcellular iron deficiency could be a relevant patho-mechanism for DCM patients carrying inherited mutations. Insight into this molecular mechanism may contribute to the development of treatment strategies and risk management in HF.

INTRODUCTION

Iron deficiency is a frequent co-morbidity in heart failure affecting 50% of patients with HF (1, 2) and has been linked to cardiovascular disease as well (3-5). The physiological basis of iron deficiency has been described by duodenal blockage of iron absorption, iron retention in the reticuloendothelial system, as well as circulation-related absorption defects (2, 6). Long-term intravenous iron therapy showed beneficial effects to patients with heart failure in clinical trials (4, 7-10) and compensation of iron levels reduces morbidity and mortality. In contrast, the subcellular iron uptake mechanisms that are independent of systemic absorption, as well as the adverse consequences of defects in these processes were previously not examined in patient-derived cardiomyocytes. Subcellular iron uptake occurs by clathrin-mediated endocytosis (CME) of the iron carrier protein transferrin (11, 12). An essential step for initiation of CME events is the formation of plasma membrane (PM) microdomain hubs enriched for phosphatidylinositol 4,5-bisphosphate (PIP2) and F-actin (13, 14). Importantly, decreased F-actin content at the PM of cardiomyocytes from dilated cardiomyopathy (DCM) patients with end-stage heart failure has been highlighted as a critical disease feature in myocardial dysfunction (15). Moreover, loss-of-function mutations in cytoskeletal proteins are known to contribute to alteration of the actin cytoskeleton and the progression of DCM and heart failure in humans (16-18). Nevertheless, the understanding of subcellular dysfunctions in presence of inherited DCM mutations remains incomplete.

To better understand the molecular disease mechanisms associated with DCM mutations, we employed a genetic iPSC model of two inherited mutations in recognized DCM genes, troponin T (R141W) and tropomyosin (TPM1, L185F). Interestingly, we found defective intracellular

iron uptake in iPSC-derived cardiomyocytes from DCM patients with inherited mutations. The defective iron uptake was due to disrupted sarcomere organization in DCM cardiomyocytes which impaired the linkage and formation of F-actin-enriched PM microdomains as a basis for CME-mediated iron uptake.

DCM is a major cause of heart failure and characterized clinically by ventricular dilation and contractile dysfunction (19). Inherited mutations, frequent causes of DCM affecting 30% of patients (20), presented a basis for disease modelling using human induced pluripotent stem cell-derived cardiomyocytes (iPSC-CMs). Human iPSC-CMs have been employed to study causes of subcellular disease phenotypes in DCM (21-23) such as disrupted sarcomere protein organization and defective contractility. Goal of this study was to identify druggable pathogenic molecular signalling defects altered in the presence of DCM mutations due to defective sarcomere organization and function. We utilized two different DCM iPSC models, the troponin mutation TnT-R141W (24-26) and a novel DCM-causing variant, tropomyosin (TPM1)-L185F. TPM1, a critical regulator of force generation in cardiomyocytes, anchors the troponin complex on actin myofilaments (27-30). Previous reports demonstrated the pathogenicity of TPM1 mutations in DCM, which reduce force generation and Ca²⁺ sensitivity of cardiomyocytes (31-33). TPM1-L185F is located in a mutational hot spot of TPM1 within the troponin complex-interacting region (27, 30). Due to their location, the DCM mutations TPM1-L185F as well as TnT-R141W were likely to disrupt sarcomere function. Accordingly, the DCM TPM1-L185F patient-specific and CRISPR/Cas9 mutation-introduced iPSC-CMs displayed altered sarcomere organization, contractility, and force generation as well as cytoskeleton filament interactions.

Here, we identified a molecular pathway altered in DCM cardiomyocytes due to defective sarcomere organization and function, which is present in DCM models but also in the heart tissues of patients suffering from other forms of systolic HF. We show a new mechanistic defect in iron uptake in DCM cardiomyocytes, which results in subcellular iron deficiency and mitochondrial iron-depletion dysfunctions. This pathway is not related to physiological and systemic iron absorption defects in heart failure.

Our findings show that sarcomere disorganization in DCM cardiomyocytes disrupted vinculin-based linkage and formation of plasma membrane (PM) hubs enriched for F-actin and PIP2. Consequently, disruption of PM microdomains limited the initiation of endocytosis and thereby reduced the uptake of critical cargo such as transferrin-bound iron. Particularly in the mitochondria, iron imbalance is deleterious as mitochondrial functions require fine-balanced iron levels (34). Both the inappropriate elevation as well as reduction of iron levels are associated with cardiac disease (34, 35). Previous studies showed that in the murine heart, lack of transferrin receptor 1 (TfR1), the key iron transport protein, resulted in severely reduced iron levels in cardiomyocytes, causing poor cardiac function and failure of mitochondrial respiration (36). In this study, we describe a molecular regulatory patho-mechanism which depletes intracellular iron levels in cardiomyocytes carrying DCM mutations. We employed CRISPR/Cas9 genome editing together with whole-proteome mapping technologies and delivered genetic and pharmacological rescue strategies to reverse the molecular pathway's dysfunction. CRISPR/Cas9-based correction of the DCM mutation, re-supplementation of iron, or treatment with a small peptide molecule (Rho A activator II) rescued endosome distribution, mitochondrial iron levels, contractility, and sarcomere protein organization in iPSC-CMs.

We confirmed that this molecular disease pathway is not limited to DCM iPSC-CMs but occurs also in the heart tissue of DCM patients with end-stage heart failure. Therefore, defective endocytosis and impaired endosome distribution may present pathogenic and functional defects that are more generally representative of DCM and systolic heart failure. Our approach to therapeutically target the molecular defects in this pathway may suggest an alternative opportunity for development of future treatment directions in patients with DCM and HF due to inherited mutations.

RESULTS

A TPM1 mutation causes defective contractility, force generation and sarcomere connections with the plasma membrane in DCM patient-specific iPSC-CMs

We recruited a family cohort of DCM patients carrying the point mutation TPM1-L185F which caused ventricular dilatation, sinus rhythm abnormalities, and non-sustained ventricular tachycardia in the patients (**Fig. 1A, Fig. S1A to C**). We generated iPSCs from a 15-year-old male carrier, III-5 (DCM patient, MUT/WT) who received a heart transplantation due to end-stage heart failure, as well as from a non-affected family member, II-4 (healthy donor, HD, WT/WT) (**Fig. 1A, Fig. S1 A to C**). WT/WT and WT/MUT iPSCs displayed regular expression of pluripotency markers (**Fig. S2A to E**). We differentiated iPSCs into beating iPSC-CMs and found patient-specific (MUT/WT) and HD control (WT/WT) iPSC-CMs to express comparable levels of TPM1 and other cardiac markers at the gene expression and protein expression levels (**Fig. S3A to K**). Patient-specific (MUT/WT) iPSC-CMs recapitulated significantly reduced sarcomere length, beating force, and contractility, compared to HD control (WT/WT) iPSC-CMs (**Fig. 2B to E, Fig. S4A to E**). We also noted reduced field potential duration and amplitude in the presence of TPM1-L185F (**Fig. S4F to G**).

To determine differential regulation of signaling pathways altered in the presence of TPM1-L185F, we utilized label-free SWATH-MS whole-proteome analysis (**Fig. 1B to G**). Between HD (WT) control and DCM patient-specific iPSC-CMs, 1206 proteins were found to be upregulated and 1357 proteins to be downregulated (**Fig. 1B**). Venn diagram of differentially expressed protein profiles for HD control and DCM iPSC-CM groups (**Fig. 1C**). Principal component analysis (PCA) demonstrated distinct segregation of DCM and WT groups (**Fig.**

1D). The proteomic profiling for 2563 proteins displayed differences between WT control and DCM iPSC-CMs (**Fig. 1E**). Protein enrichment assessment and signaling pathway mapping showed among the top 15 significantly changed pathways mitochondrial dysfunction and, interestingly, clathrin-mediated endocytosis (**Fig. 1F**). This prompted us to investigate the molecular mechanisms underlying endocytosis in the presence of DCM-TPM1-L185F in more detail. Of note, subsequent bioinformatic analysis revealed in DCM iPSC-CMs differentially regulated protein expression profiles in the signaling pathways controlling actin cytoskeleton functions, clathrin-mediated endocytosis, as well as iron homeostasis in addition to DCM (**Fig. 1G**).

To assess the molecular dysfunctions in endocytosis and iron homeostasis in the presence of the DCM mutation TPM1-L185F in more detail, we generated mutation-introduced iPSCs. Isogenic iPSC lines with genetically identical background present substantial advantages for assessing genotype-phenotype relationships in human model systems. We used CRISPR-Cas9 gene editing to introduce the TPM1-L185F mutation into WT iPSCs, producing an isogenic MUT-introduced iPSC line (MUT-int/MUT-int) (**Fig. 2A**). MUT-int/MUT-int iPSCs express regular levels of pluripotency markers (**Fig. S2A to E**) and following cardiac differentiation, regular expression of cardiac markers (**Fig. S3A to K**). Like DCM TPM1-L185F patient-derived iPSC-CMs, the isogenic mutation-introduced iPSC-CMs displayed significantly reduced sarcomere length, beating force, and contractility, as well as field potential duration and amplitude, compared to HD control (WT/WT) iPSC-CMs (**Fig. 2B to E, Fig. S4A to G**). Disrupted sarcomere organization is a key phenotype in presence of DCM mutations (23, 37, 38). We tested if impaired sarcomere regularity in presence of TPM1-L185F interrupted

sarcomere interactions with the plasma membrane via vinculin, a plasma membrane-associated protein critical for normal cardiac function (39-41). Vinculin is known to interact with sarcomeric alpha-actinin (SAA) at the sarcomeres and mediates a connection to F-actin-organizing hubs at the plasma membrane (42-44). We performed immunoprecipitation of SAA and vinculin using WT/MUT, MUT-int/MUT-int versus WT/WT iPSC-CMs and Igg as a negative control (**Fig. 2F to H, Fig. S5A to C**). In presence of TPM1-L185F, we identified a reduced interaction of SAA and vinculin (**Fig. 2F to H, Fig. S5D to G**) as well as disturbance of additional sarcomere-plasma membrane interactions, such as vinculin-TPM and vinculin-troponin T (TnT) (**Fig. 2F to L, Fig. S5D to L**). To test if disrupted sarcomere-plasma membrane interactions are observed in presence of different DCM mutations, we employed a isogenic iPSC line carrying the DCM mutation TnT-R141W (MUT2-int/MUT2-int) described earlier (26). We established significantly reduced co-localization of vinculin and sarcomeric TnT (**Fig. 2M to N**) in patient-specific iPSC-CMs (MUT1/WT) and mutation-introduced iPSC-CMs carrying TPM1-L185F (MUT1-int/MUT1-int) or TnT-R141W (MUT2-int/MUT2-int) as well as isogenic WT controls (WT/WT). Taken together, our data demonstrate that in presence of two different DCM mutations, TPM1-L185F and TnT-R141W, sarcomere interactions with the plasma membrane are significantly disrupted.

Impaired F-actin polymerization is linked to defective clathrin-mediated endocytosis and endosome distribution in presence of DCM mutations

We speculated that disrupted vinculin interactions in DCM iPSC-CMs might be accompanied by disfunction of the vinculin/F-actin interface, a major hub for organization of F-actin

filaments and phosphatidylinositol 4,5-bisphosphate (PIP2)-enriched microdomains at the PM. To test if actin microfilament polymerization was altered, we measured the ratio of polymerized F-actin and monomeric G-actin. In DCM iPSC-CMs (patient-specific WT/MUT and Cas9-mutation-introduced MUT-int/MUT-int), reduced F/G actin ratios were detected, compared to WT/WT controls (**Fig. 3A**) while total beta-actin protein levels were not significantly changed between the groups (**Fig. S6A**). As PIP2-enriched microdomains at the PM are critical for actin polymerization (45-47), we quantified PIP2 levels in the presence of the two DCM mutations, TPM1-L185F and TnT-R141W. DCM patient-specific and Cas9-mutation-introduced iPSC-CMs contained a reduced amount of PM-localized PIP2, compared to WT/WT iPSC-CMs (**Fig. 3B and C**). To confirm our findings, we next sought to introduce the molecular phenotype observed in DCM iPSC-CMs, reduced PIP2 levels, into WT/WT iPSC-CMs. We utilized chemical inhibition of PIP5K, a major PIP2 synthesizing enzyme at the PM (48), via UNC3230, a PIP5K-specific inhibitor (49). UNC3230-treated WT/WT iPSC-CMs showed reduced PIP2 levels at the PM (**Fig. S6B and C**). As expected, UNC3230 treatment resulted also in reduced F-actin levels in WT/WT iPSC-CMs (**Fig. S6D and E**), thereby recapitulating the molecular phenotype observed in DCM iPSC-CMs. These findings demonstrate decreased actin polymerization and PM-localized PIP2 levels in DCM patient-specific and Cas9 mutation-introduced iPSC-CMs. This is yet more relevant as a main route for cellular cargo import, clathrin-mediated endocytosis (CME), is regulated at actin-assembling plasma membrane hubs controlling PIP2 synthesis and turnover (50-52). In cardiomyocytes, critical cargo such as iron (Fe III+) is internalized via the transferrin receptor by CME and distributed by endosomes (34). Considering the importance of PIP2-mediated F-actin assembly for CME, we assessed if CME-

dependent cargo uptake was altered in the presence of DCM mutations. We examined continuous uptake of transferrin-bound iron in live iPSC-CMs and observed a significant reduction of CME-based transferrin uptake in DCM patient-specific and Cas9-mutation-introduced iPSC-CMs (**Fig. 3D and E, Fig. S6F**) while expression levels of the transferrin receptor were not significantly changed between groups (**Fig. S6G**). To exclude the possibility that the observed reduction of CME-dependent cargo uptake was limited to the transferrin receptor, we analysed internalization of low-density lipoprotein (LDL) receptor, which was also significantly reduced in DCM iPSC-CMs (**Fig. S7A and B**). LDL receptor expression levels were not significantly altered between groups (**Fig. S7C**). Next, we tested if endosome-dependent distribution of CME-internalized cargo, such as transferrin-bound iron, was altered in iPSC-CMs carrying DCM mutations. To first test if endosome distribution is affected by impaired actin polymerization, spatial localization of endosomes was tracked using the early endosome (EE) marker EEA1. While in WT iPSC-CMs, early endosome cargo carriers were evenly distributed throughout the cells, no regular distribution of EEs was observed in DCM iPSC-CMs (patient-specific WT/MUT and Cas9-edited MUT-int/MUT-int). Instead, in the presence of DCM mutations, cargo-carrying EEs arrested at the plasma membrane (**Fig. 3F and G, Fig. S7D**). Moreover, this new DCM disease phenotype, defective distribution of cargo-carrying early endosomes, could be successfully introduced into WT iPSC-CMs via a potent inhibitor of actin polymerization, latrunculin A (Lat-A). Lat-A treatment resulted in a reduced F/G actin ratio (**Fig. S8A**) as well as accumulation of EEs at the PM in WT iPSC-CMs (**Fig. S8B and C**), thereby phenocopying the presentation of DCM iPSC-CMs (**Fig. 3F and G**). Our data demonstrate defective cargo uptake and distribution in DCM patient-specific iPSC-CMs

as well as isogenic controls carrying two different DCM mutations, TPM1-L185F and TnT-R141W.

Iron deficiency in the presence of DCM mutations causes mitochondrial dysfunction and reduced contractility in DCM iPSC-CMs

Mitochondria, a major recipient of iron (Fe) in the cell (34, 53) require Fe for electron transport in the mitochondrial respiratory chain as well as oxygen transport (54). Iron imbalance specifically in the mitochondria is deleterious as its critical functions require a fine balance of mitochondrial iron (34). Iron deficiency has been associated with cardiovascular disease and heart failure (5). Therefore, we assessed the effects of impaired uptake of transferrin-bound iron and impaired early endosome distribution on mitochondria function. We examined Fe levels in mitochondria in live cells and found that mitochondria of DCM iPSC-CMs (patient-specific WT/MUT and Cas9-mutation-introduced MUT-int/MUT-int) display significantly depleted iron levels, compared to control (**Fig. 4A and B**). This was true for both DCM mutations, TPM1-L185F and TnT-R141W (**Fig. 4A and B**) and was accompanied by a reduction of mitochondrial membrane potential, supporting reduced function of iron-deficient mitochondria in DCM iPSC-CMs (**Fig. S9A and B**).

Clinical trials demonstrated increased iron supply in iron-deficient heart failure patients to be beneficial for cardiac function (8). We thus first confirmed that iron supplementation recovered reduced mitochondrial iron levels in DCM iPSC-CMs (patient-specific WT/MUT and Cas9-engineered MUT-int/MUT-int) (**Fig. S10D to G**). Importantly, replenishing iron levels rescued impaired contractility in DCM patient-specific iPSC-CMs (WT/MUT) as well as in Cas9-

mutation-introduced iPSC-CMs carrying two different DCM mutations, TPM1-L185F and TnT-R141W (**Fig. 4C to E**). To confirm that iron deficiency due to impaired endocytosis and endosome distribution is linked to actin polymerization defects in the presence of DCM mutations, we quantified Fe levels of Lat-A-treated WT iPSC-CMs. Our data show that Lat-A-induced actin polymerization defects can introduce imbalance of Fe levels into WT control iPSC-CMs (**Fig. S9H**) which could be recovered by subsequent Fe treatment (**Fig. S9H**).

Fe deficiency has been associated with increased reactive oxygen species (ROS) production in heart failure (55). To test if this molecular disease phenotype is recapitulated in DCM iPSC-CMs, we measured total ROS levels in live iPSC-CMs. As expected, we observed elevated mitochondrial superoxide levels in DCM iPSC-CMs (WT/MUT and MUT1-int/MUT1-int) (**Fig. S9C**) which could be rescued by Fe supplementation (**Fig. S9I and J**). This confirmed that Fe deficiency may result in elevated ROS levels in the presence of DCM mutations.

Together, our data indicated reduced iron levels in DCM iPSC-CMs due to defective actin polymerization, impaired endocytosis, and defective endosome distribution. These molecular causes of iron deficiency exacerbate defective contractility in the presence of DCM mutations.

Recovering actin polymerization via RhoA activation rescues PM-localized PIP2 levels and uptake of transferrin-bound iron

To rescue the molecular DCM disease phenotypes resulting in mitochondrial iron deficiency in DCM iPSC-CMs, we turned to RhoA, a Rho GTPase which regulates PIP2 production via PIP5K activation and F-actin polymerization (56, 57). Under chronic stress, loss of RhoA in cardiomyocytes leads to decreased contractility (58). We applied a RhoA activating peptide,

Rho activator II (RhoA II), which has been shown previously to increase PIP2 production in mammalian cells (59). Following RhoA II treatment, PIP2 levels at the PM were significantly increased in DCM iPSC-CMs (patient-specific WT/MUT and Cas9-mutation-introduced MUT-int/MUT-int) (**Fig. S10A to C**). Moreover, RhoA activation increased endocytosis-dependent uptake of the transferrin receptor (**Fig. 5A and B**) and rescued endosome distribution in mutation-introduced iPSC-CMs to the levels observed in WT control (WT/WT) iPSC-CMs (**Fig. 5C and D**). Importantly, treatment with RhoA II rescued mitochondrial iron levels in DCM iPSC-CMs (**Fig. 5E to G**) as well as sarcomere-plasma membrane interactions such as TnT-vinculin (**Fig. S10D to F**). This highlights the critical role PIP2 plays at the sarcomere/F-actin/PM regulatory hub. Consequently, Rho activator II treatment improved contractility in DCM iPSC-CMs, such as amplitude and maximal decay (**Fig. 5H, Fig. S10G to I**) and significantly recovered sarcomere protein organization in DCM iPSC-CMs (patient-specific WT/MUT and Cas9-engineered MUT-int/MUT-int) (**Fig. 5I to K**). Our findings stress the intricate molecular mechanisms controlled by sarcomere interactions with F-actin and PM-localized PIP2 and their dysfunction in DCM iPSC-CMs.

CRISPR/Cas9-correction of the patient-specific DCM mutation TPM1-L185F rescues endosome distribution and mitochondrial iron levels in DCM-corrected iPSC-CMs

Isogenic cell lines are a valuable tool to ascertain molecular disease mechanisms and genotype-phenotype correlations. To further demonstrate that the DCM mutation TPM1-L185F causes defective uptake and distribution of transferrin-bound iron, resulting in mitochondrial iron deficiency and reduced contractility, we corrected the DCM mutation via CRISPR/Cas9 gene

editing. We generated an isogenic mutation-corrected (WT-cor/ WT-cor) iPSC line, using site-specific CRISPR-Cas9 gene editing (**Fig. 6A** and **Fig. S11A to E**) and differentiated the mutation-corrected iPSCs (WT-cor/ WT-cor) into iPSC-CMs (**Fig. S11F to P**). Firstly, we confirmed that actin polymerization was recovered in mutation-corrected iPSC-CMs (WT-cor/ WT-cor) compared to DCM patient-specific iPSC-CMs (**Fig. 6B**). Importantly, compared to DCM patient-specific iPSC-CMs, uptake of the transferrin receptor (**Fig. 6C and D**) as well as distribution of endosomes was rescued in isogenic mutation-corrected iPSC-CMs (**Fig. 6E and F**). Consequently, we noted mitochondrial iron levels to be more than 2-fold increased (DCM patient: 0.21 ± 0.01 vs mutation-corrected: 0.52 ± 0.03) following correction of the DCM mutation (**Fig. 6G and H**). In line with this, mutation-corrected iPSC-CMs displayed significantly improved sarcomere protein organization (**Fig. 6I and J**) as well as recovered beating force (**Fig. 6K**), compared to DCM patient-specific iPSC-CMs.

Heart tissues from DCM patients with end-stage heart failure display defective endosome distribution

We considered that the mitochondrial iron deficiency due to defective endocytosis and endosome distribution observed in DCM iPSC-CMs may be present more generally in patients with heart failure (HF). To test this, we analyzed vinculin-positive plasma membrane (PM) junctions, the sites of CME initiation and endosome formation, in cardiomyocytes of left ventricular tissues from patients with end-stage HF due to DCM versus patients with preserved systolic left-ventricular function in the control group (**Fig. 7A to C** and **Fig. S12** provide detailed clinical patient information). We found the vinculin-positive PM domains in DCM

patients with end-stage HF to be significantly more disorganized and less regular than in the controls (**Fig. 7C**). Moreover, we quantified the endosome distribution in cardiomyocytes of left ventricular tissues from DCM patients with end-stage HF versus patients with preserved systolic left-ventricular function in the control group. We utilized as an endosome marker CCDC53, a subunit of the WASH complex localized on endosomes (60). In heart tissues from both patient groups, standard expression of TnT and CCDC53 was observed (**Fig. S13A and B**). Strikingly, cardiomyocytes in left-ventricular tissues from HF patients were characterized by significantly higher levels of PM-localized endosomes, compared to controls with preserved left-ventricular function (**Fig. 7D to F and Fig. S14A to E**). Hence, these data closely recapitulate both the disrupted PM-localized microdomains that present the basis for endosome formation, as well as the ectopic PM-localized endosome distribution in the heart tissue of HF patients. Thus, these findings suggest that the molecular dysfunctions caused by defective endocytosis and iron deficiency in the presence of DCM mutations may present a more general feature in patients with heart failure. Overall, our findings suggest a new patho-mechanism in patients with DCM due to inherited mutations as well as in DCM patients with systolic HF. Sarcomere protein misalignment may destabilize protein-protein interactions linking sarcomeres and other cytoskeleton filaments to the plasma membrane and contribute to defective functions of PIP2-enriched PM microdomains critical for CME. Consequently, endosome formation and distribution are impaired, resulting in reduced uptake of critical cargo such as transferrin-bound iron and lower mitochondrial iron levels (**Fig. 8**). These molecular defects can contribute to reduced energy supply and impaired contractility of cardiomyocytes in patients with DCM and heart failure.

DISCUSSION

Iron deficiency is a co-morbidity in 50% of patients with heart failure (1) and may present a therapeutic target (6). Main causes for iron deficiency at the organ level are intestinal iron absorption and circulation-related defects as well as impaired iron retention in heart failure. In addition, despite insights into molecular disease mechanisms at the cellular level, DCM remains a main cause of heart failure and new therapeutic directions are needed. Mutations in genes encoding sarcomere proteins have been identified to cause 30% of DCM cases (20, 61). Genetic models of DCM (62-64) have been employed to elucidate the molecular causes of primary dysfunctions observed in the presence of DCM mutations, such as disrupted sarcomere protein organization and defective contractility (23, 64-66). Recently, impaired protein-based interactions of the sarcomeres with other cytoskeleton filaments have been shown to contribute to DCM disease phenotypes in patient-specific iPSC-CMs (23, 40). However, the subcellular dysfunctions in presence of DCM mutations at the molecular and signalling levels are to date still incompletely understood. Based on this, we generated here a human iPSC-CM model of the new DCM-causing mutation TPM1-L185F, combined with CRISPR/Cas9-based gene editing to elucidate molecular dysfunctions in the presence of DCM mutations, such as consequences of defective sarcomere organization and functions. We identified sarcomere interactions via the stabilizing plasma membrane-binding protein vinculin to be disrupted in the presence of two different DCM mutations, TPM1-L185F and TnT-R141W. Consequently, this disrupted vinculin-containing and F-actin-organizing PM hubs enriched for PIP2 in DCM iPSC-CMs. Altered F-actin-binding PIP2 microdomains at the PM, in turn, resulted in defective clathrin-mediated endocytosis (CME) of critical cargo such as transferrin-bound iron in DCM

iPSC-CMs. These findings establish defective endocytosis and impaired distribution of endosome cargo carriers as a molecular basis for mitochondrial iron deficiency in the presence of DCM mutations. Importantly, we could rescue this pathogenic mechanism in a three-fold way in our human iPSC-CM model: Firstly, by treatment with RhoA activator II (57) which replenished plasma membrane PIP2 levels and rescued CME, endosome distribution, as well as mitochondrial iron levels and DCM iPSC-CM contractility. Secondly, supplying iron externally could overcome depletion of mitochondrial iron deficiency and rescued contractility in DCM iPSC-CMs. Thirdly, these phenotypic dysfunctions were recovered in iPSC-CMs following CRISPR/Cas9-based correction of the inherited DCM mutation, TPM1-L185F, in patient-specific iPSCs. Moreover, we pheno-copied the patho-mechanistic defects found in presence of the TPM1-L185F mutation into WT control iPSC-CMs via drug treatments targeting the disease pathway: Application of a small molecule inhibitor of actin polymerization (latrunculin-A, Lat-A) introduced defective endosome distribution in WT control iPSC-CMs. Furthermore, treatment with a PIP5K inhibitor (UNC3230) introduced in WT control iPSC-CMs disruption of F-actin/PIP2-containing PM microdomains, the sites of CME and endosome formation

Interestingly, cardiac-specific overexpression of RhoA ultimately induces DCM with impaired contractility (67) and treatment with an inhibitor of the well-characterized downstream effector of RhoA, ROCK, protected the heart against ischemia/reperfusion (I/R) injury (68). Treatment with an inhibitor of ROCK benefited patients with cardiac hypertrophy in clinical trials (69, 70). However, the complete deletion of RhoA from cardiomyocytes results in accelerated DCM and increases the severity of heart failure outcome following chronic pressure overload (58).

These reports indicate the critical need for fine-tuned modulation of RhoA activity as a basis for cardiomyocyte homeostasis and recovery in disease models. In line with this, low levels of constitutively active RhoA in cardiomyocytes protected mouse hearts against I/R injury and improved contractile function (71). Consistently, our findings showed that low-dose activation of RhoA improved sarcomere-PM interactions via vinculin and F-actin. Concomitantly, RhoA treatment replenished PIP2 content at the PM and recovered CME and endosome distribution in DCM iPSC-CMs.

The signalling mechanisms associated with systemic iron deficiency in heart failure due to absorption defects are complex (2, 6, 7, 72). It should be noted that both the inappropriate elevation and reduction of iron levels are associated with cardiac disease (34, 35), indicating the importance of intact iron homeostasis. Abnormally high iron levels lead to iron overload cardiomyopathy (35) while abnormally low levels of iron were linked to cardiovascular disease as well (3-5). Iron homeostasis at the systemic level, including the storage and export of excess iron, is mediated by ferritin, ferroportin, and iron regulatory proteins IRP1 (ACO1) and IRP2 (IREB2) (3, 73-75). Low iron levels have been shown to induce IRP1/2-modulated increase of iron uptake via stabilization of TfR1-encoding mRNAs, while IRP-dependent repression of ferritin and ferroportin mRNA translation reduces iron sequestration as well as export (76). Mitochondria utilize a major amount of intracellular iron in Fe/S clusters as well as heme groups essential for the function of electron transport chain complexes (77). Insufficient iron levels impair mitochondrial function in cardiomyocytes (3, 78) which may occur by enhanced degradation of mRNAs encoding mitochondrial Fe/S-cluster-containing proteins (78) (79). In line with this, we found iron supplementation to rescue both mitochondrial iron levels as well

as iPSC-CM contractility in DCM iPSC-CMs. Importantly, clinical trials demonstrated intravenous iron administration to improve endpoint outcomes in heart failure patients, including improvement of NYHA class, increased 6-minute-walking distance and improved quality of life (8-10, 80). These results were independent of the presence of anaemia.

Here, we describe a new molecular iron uptake defect in cardiomyocytes unrelated to systemic iron absorption defects: the impaired subcellular uptake of transferrin-bound iron. This molecular patho-mechanism is linked to the sarcomere disorganization observed in presence of DCM mutations but also in the heart tissues of patients suffering from other forms of systolic HF. Our findings show that sarcomere disorganization results in disrupted vinculin-based linkage and formation of plasma membrane (PM) hubs enriched for F-actin and PIP2. These PM microdomain hubs are critical for initiation of endocytosis and uptake of cargo such as transferrin-bound iron. Indeed, it could be expected that other patho-physiological dysfunctions may also interfere with endocytosis and cargo uptake, e.g., by causing defective formation and/or function of F-actin and PIP2-enriched PM microdomains in other ways.

The majority of cardiomyocyte iron demand is served by TfR1-mediated internalization of the iron-carrier transferrin. We observed in DCM iPSC-CMs defective F-actin/PIP2-enriched microdomains at the PM, resulting in impaired endocytosis of transferrin-bound iron and, ultimately, reduced mitochondria iron levels. This patho-mechanism could be reversed by rescue of F-actin/PIP2 microdomain function via Rho activator II treatment, which consequently recovered uptake of transferrin and distribution of endosomes. This resulted in significantly improved mitochondrial iron levels as well as contractility in DCM iPSC-CMs.

Moreover, this disease mechanism was confirmed by introducing defective F-actin/PIP2-dependent microdomain function via Lat-A treatment into WT iPSC-CMs. Concomitantly, Lat-A treatment induced impaired endosome distribution and decreased mitochondrial iron levels in the healthy donor-derived iPSC-CMs.

Of note, supplementation of iron also improved contractility in DCM iPSC-CMs while expression levels of transferrin receptor and gene products regulating iron homeostasis, such as ferritin (FTH1), were not significantly changed. These results might suggest that DCM patients carrying inherited mutations could profit from iron supplementation also if their blood levels of transferrin and ferritin are not abnormal. Yet it should be noted that iron supplementation may not completely recover phenotypic consequences of heart failure in cases where the defects are located further downstream of the patho-mechanism described here. Moreover, and in line with previous findings, our data support a balanced intracellular iron homeostasis in cardiomyocytes to be essential for proper cardiovascular functions. Beyond this study, it is possible that mechanisms exist which link sarcomeric mutations to regulation of iron homeostasis genes. While the investigation of such mechanisms exceeds the frame of this study, this could be an interesting topic for future research.

We showed that RhoA treatment significantly improved contractility as well as sarcomere protein organization and interactions as well as PM microdomain function in DCM iPSC-CMs. These findings suggest a potential benefit of fine-tuned therapeutic modulation of RhoA activity for patients carrying inherited DCM mutations. Subsequent studies to validate therapeutic targeting of CME and endosome cargo distribution defects should include animal models of sarcomeric DCM mutations.

We also showed that heart tissues from DCM patients with end-stage heart failure display abnormal distribution of endosome cargo carriers as well. These data suggest that iron deficiency due to defective endocytosis might be present more generally in DCM patients with heart failure. Together, the patho-mechanism of defective CME and endosome cargo distribution described here may possibly play a role in the pathophysiology of cardiomyopathy and heart failure and might be a prevalent mechanism in presence of DCM mutations. Based on these findings, it will be relevant to explore if this disease mechanism may be true also for other forms of systolic heart failure. Overall, drug treatments addressing defects in this molecular mechanistic pathway may present promising future therapeutic directions for DCM patients with inherited sarcomeric mutations.

MATERIALS AND METHODS

A detailed description of the Methods is available in the Supplementary Materials.

Study design

The objective of the study was to investigate molecular patho-mechanisms in presence of inherited DCM mutations causing disturbed sarcomere organization and function. We employed a combined model of patient-derived and CRISPR/Cas-edited induced pluripotent stem cell-derived cardiomyocytes (iPSC-CMs) as well as patient-derived heart tissue. We used an integrated platform of MS-SWATH-based proteomics and signaling pathway interrogation and identified from this analysis a molecular patho-mechanism, impaired subcellular iron deficiency. We next confirmed this molecular disease mechanism in both DCM iPSC-CMs and clinical specimens from DCM patients with end-stage HF. To rescue the molecular disease pathway, we employed correction of the TPM1-L185F mutation in DCM patient-derived iPSCs or treatment with a small compound, RhoA activator II, recovering PM-localized PIP2 levels, uptake of transferrin-bound iron, endosome distribution, mitochondrial iron levels, sarcomere length, and/or contractility. Moreover, we pheno-copied the effects of the TPM1-L185F mutation (abnormal F/G actin ratio, reduced PIP2 levels, endosome distribution defects) into WT iPSC-CMs by treatment with lat-A or UNC3230. Biochemical and cell biology experiments (Western blotting, immunoprecipitation, uptake assay, image analysis) were conducted in an unblinded fashion for ≥ 2 independent experiments to ensure reproducibility, and end points were determined from the literature and pilot studies, respectively. The numbers of independent experiments performed for each figure are listed in Supplementary Table 1. We

employed an iPSC model covering n=2 inherited mutations in different proteins that lead to dilated cardiomyopathy (DCM), troponin T (TnT-R141W) and tropomyosin (TPM1-L185F). Clinical specimens were employed from n=5 patients with DCM and end-stage heart failure and n=4 patients with preserved LV function that underwent aortic valve replacement (severe valve stenosis) and coronary artery bypass graft surgery in the control group.

Generation, culture, and cardiac differentiation of human iPSCs

The protocols for studies with iPSC were approved by the Goettingen University Ethical Board (15/2/20 and 20/9/16An) and the Odense University Ethical Board (Projekt ID S-20140073HLP). Informed consent was obtained from all participants and all research was performed in accordance with relevant guidelines and regulations. Approval for the study of human myocardial samples was granted by the Goettingen University Ethical Board (No. 21/10/00 and 31/9/00), and written informed consent was obtained from all patients. The procedures used in this study adhere to the tenets of the Declaration of Helsinki. A family cohort with carriers of the novel pathogenic variant within the TPM1 gene, TPM1-L185F, was recruited. Human fibroblasts from five mutation carriers and four healthy donors from this family were reprogrammed to hiPSCs using the CytoTune™-iPS 2.0 Sendai Reprogramming Kit (Thermo Fisher Scientific). Human induced pluripotent stem cells (iPSCs) were grown on Matrigel-coated plates (ES qualified, BD Biosciences) using chemically defined E8 medium as described previously(81, 82). The culture medium was changed every day, and iPSCs were passaged every four days using EDTA (Life Technologies). The iPSC lines have been deposited at the Goettingen University Medical Center Biobank (WT1, DCM) or the Stanford

Cardiovascular Institute Biobank (WT2). For cardiac differentiation of iPSCs, a small molecule-based monolayer protocol based on previous reports was utilized(83, 84). At day 20-25 of cardiac differentiation, beating iPSC-CM cultures were dissociated using trypleE (Life Technologies) and plated in the required assay format. Human iPSC-CMs were cultured in RPMI (Life Technologies) complemented with B27 supplement (Life Technologies) prior to experimental analysis.

LC/MS/MS SWATH analysis. Tryptic gel-extracted peptides were prepared as described(85). Proteomics Protein digests were analyzed on a nanoflow chromatography system (Eksigent nanoLC425) hyphenated to a hybrid triple quadrupole-TOF mass spectrometer (TripleTOF 5600+) equipped with a Nanospray III ion source and controlled by Analyst TF 1.7.1 software build 1163 (all AB Sciex). Qualitative LC/MS/MS SWATH (Sequential Window Acquisition of all Theoretical Mass Spectra) analysis was performed using a Top30 data-dependent acquisition method and two biological replicates per sample were analyzed. MS/MS data were acquired as described(86, 87) and analyzed using ProteinPilot Software version 5.0 build 4304 (AB Sciex) and PeakView Software version 2.1 build 11041 (AB Sciex) was used.

F/G-actin measurements. Human iPSC-CMs were fixed in 4% PFA for 20 min at room temperature (RT) following a PBS wash. Cells were incubated with 0.2 % triton X-100 at RT for 60 min followed by a blocking step with 5% BSA. Subsequently, cells were incubated with DnaseI-488 (Thermo Fisher Scientific), Phalloidin-488 (Thermo Fisher Scientific), DAPI-405

(Thermo Fisher Scientific) according to the manufacturer's description. Fluorescence was measured via a Cytation 3 reader (BioTek).

Atomic force microscopy (AFM) and contractility measurements. iPSC-CMs were seeded on coverslips 2-3 days before AFM or contractility measurements. AFM recordings were performed using a NanoWizard 3 (JPK Instruments) as described previously(26). Briefly, the cantilever mounted on a glass block was dipped in cell medium for 30 - 60min to equilibrate. A calibration was done to measure the spring constant and sensitivity of the used cantilever. The cells were probed with a nonconductive silicon nitride cantilever (Bruker). Contractility measurements were performed using an Olympus microscope with Olympus IX2-UCB software as described earlier(23, 26).

Drug treatments. Human iPSC-CMs were treated with 3 μ M Latrunculin A (Cayman) for 20min, UNC3230 (Cayman) 10 μ M for 24h, SAR405 (Cayman) 10 μ M for 24h, 3 μ g/mL Rho activator II (Cytoskeleton) for 3 hours or overnight.

Human heart tissue. Clinical data for patients are presented in Fig. S12. LV heart tissue from patients with dilated cardiomyopathy who received a heart transplantation due to end-stage heart failure (indicated as "heart failure", HF, or heart transplantation) was analyzed. In comparison, LV heart tissue from patients with preserved LV function that underwent aortic valve replacement (severe valve stenosis) and coronary artery bypass graft surgery was used in the control group ("control"). Human heart tissue slides were prepared and stained based on a

previously published protocol (88, 89). Slides were incubated with primary antibodies overnight, such as TnT (Thermo Fisher Scientific), vinculin (Sigma) or CCDC53 (ProteinTech). Wheat germ agglutinin (WGA, Alexa Fluor™ 594 Conjugate, Thermo Fisher Scientific), DAPI and secondary antibodies such as Alexa Fluor 488 goat anti-Rabbit antibody (Thermo Fisher Scientific), Alexa Fluor 568 goat anti-Rabbit antibody (Thermo), Alexa Fluor 488 goat anti-mouse antibody (Thermo Fisher Scientific) were applied afterwards. Slides were mounted with FluroMount mounting medium (Thermo Fisher Scientific). Images were taken with 63x (plan apochromat oil) objectives from a confocal microscope (Carl Zeiss, LSM 710, Göttingen, Germany) and ZEN software (Carl Zeiss). Relative controls for staining specificity were performed (Fig. S14). ImageJ-based analysis was used for image analysis. ImageJ was used to calculate the regularity of orientation for vinculin-positive structures. Data display the standard error of mean of angles from vinculin-positive areas in each image. To analyze the location of CCDC53, automated threshold setting in WGA staining was used to define PM-localized ROIs. Data were normalized by the total CCDC53 signal per image.

Statistical analysis

Statistical significance was processed using GraphPad Prism v.8.4.2 (GraphPad). An unpaired Student's t-test is used for comparison of two normally distributed data sets. Ordinary one-way ANOVA together with Sidak's multiple comparisons test were employed for comparison of three or more normally distributed data sets. For non-parametric tests, Mann-Whitney or one-way ANOVA and Dunn's multiple comparisons test were used. P-values < 0.05 were considered as statistically significant. Data are presented as mean \pm standard error of mean

(sem). The numbers of independent experiments performed for each figure are listed in Supplementary Table 1. Unless indicated otherwise, number of independent experiments equals number of independent iPSC cardiac differentiation.

Data Availability

A detailed description of the Methods is available in the Supplemental Materials section.

The data, analytic methods, and study materials are available to other researchers for purposes of reproducing the results or replicating the procedures on request. Because of the sensitive nature of the data collected for this study, requests to access the dataset from qualified researchers may be sent to the corresponding author.

List of Supplementary Materials

1. Supplementary Figures
2. Supplementary Methods
3. Supplementary Tables

ACKNOWLEDGEMENTS

This work was supported by the Deutsche Forschungsgemeinschaft (German Research Foundation) Sonderforschungsbereich 1002, projects A09 (S.B., C.L., S.E.L.), A12 (A.E.), S02 (S.E.L); and under Germany's Excellence Strategy - EXC 2067/1- 390729940; the Deutsche Stiftung für Herzforschung (DSHF) Projekt F/13/20 (A.E.), and the German Academic Exchange Service (DAAD, N.I.). S.E.L. is a principal investigator of DZHK (German Centre

for Cardiovascular Research). We are grateful for support by the DZHK (German Center for Cardiovascular Research), partner site Goettingen, Germany, and the Clinic for Cardiology and Pneumology at the University Medical Center, Goettingen University. We thank the Central Service Unit for Cell Sorting at the University Medical Center, Goettingen University for their support, and the Stem Cell Unit at the University Medical Center, Goettingen University for supporting fibroblast-based reprogramming.

DISCLOSURE

The authors declare no conflict of interest.

REFERENCES

1. C. Rizzo, R. Carbonara, R. Ruggieri, A. Passantino, D. Scrutinio, Iron Deficiency: A New Target for Patients With Heart Failure. *Front Cardiovasc Med* **8**, 709872 (2021).
2. K. Ghafourian, J. S. Shapiro, L. Goodman, H. Ardehali, Iron and Heart Failure: Diagnosis, Therapies, and Future Directions. *JACC Basic Transl Sci* **5**, 300-313 (2020).
3. S. Lakhal-Littleton, Mechanisms of cardiac iron homeostasis and their importance to heart function. *Free Radic Biol Med* **133**, 234-237 (2019).
4. B. M. L. Rocha, G. J. L. Cunha, L. F. Menezes Falcao, The Burden of Iron Deficiency in Heart Failure: Therapeutic Approach. *J Am Coll Cardiol* **71**, 782-793 (2018).
5. S. von Haehling, E. A. Jankowska, D. J. van Veldhuisen, P. Ponikowski, S. D. Anker, Iron deficiency and cardiovascular disease. *Nat Rev Cardiol* **12**, 659-669 (2015).
6. P. Ponikowski, E. A. Jankowska, Targeting Iron Deficiency in Heart Failure: Existing Evidence and Future Expectations. *Circ Heart Fail* **14**, e008299 (2021).
7. S. von Haehling, N. Ebner, R. Evertz, P. Ponikowski, S. D. Anker, Iron Deficiency in Heart Failure: An Overview. *JACC Heart Fail* **7**, 36-46 (2019).
8. S. D. Anker, J. Comin Colet, G. Filippatos, R. Willenheimer, K. Dickstein, H. Drexler, T. F. Lüscher, B. Bart, W. Banasiak, J. Niegowska, B. A. Kirwan, C. Mori, B. von Eisenhart Rothe, S. J. Pocock, P. A. Poole-Wilson, P. Ponikowski, F.-H. T. Investigators, Ferric carboxymaltose in patients with heart failure and iron deficiency. *N Engl J Med* **361**, 2436-2448 (2009).
9. P. Ponikowski, D. J. van Veldhuisen, J. Comin-Colet, G. Ertl, M. Komajda, V. Mareev, T. McDonagh, A. Parkhomenko, L. Tavazzi, V. Levesque, C. Mori, B. Roubert, G. Filippatos, F. Ruschitzka, S. D. Anker, C.-H. Investigators, Beneficial effects of long-term intravenous iron therapy with ferric carboxymaltose in patients with symptomatic heart failure and iron deficiency†. *Eur Heart J* **36**, 657-668 (2015).
10. D. J. van Veldhuisen, P. Ponikowski, P. van der Meer, M. Metra, M. Böhm, A. Doletsky, A. A. Voors, I. C. Macdougall, S. D. Anker, B. Roubert, L. Zakin, A. Cohen-Solal, E.-H. Investigators, Effect of Ferric Carboxymaltose on Exercise Capacity in Patients With Chronic Heart Failure and Iron Deficiency. *Circulation* **136**, 1374-1383 (2017).
11. A. Dautry-Varsat, Receptor-mediated endocytosis: the intracellular journey of transferrin and its receptor. *Biochimie* **68**, 375-381 (1986).
12. K. M. Mayle, A. M. Le, D. T. Kamei, The intracellular trafficking pathway of transferrin. *Biochim Biophys Acta* **1820**, 264-281 (2012).
13. E. Boucrot, S. Saffarian, R. Massol, T. Kirchhausen, M. Ehrlich, Role of lipids and actin in the formation of clathrin-coated pits. *Exp Cell Res* **312**, 4036-4048 (2006).
14. C. J. Merrifield, M. Kaksonen, Endocytic accessory factors and regulation of clathrin-mediated endocytosis. *Cold Spring Harb Perspect Biol* **6**, a016733 (2014).
15. V. B. Patel, P. Zhabyeyev, X. Chen, F. Wang, M. Paul, D. Fan, B. A. McLean, R. Basu, P. Zhang, S. Shah, J. F. Dawson, W. G. Pyle, M. Hazra, Z. Kassiri, S. Hazra, B. Vanhaesebroeck, C. A. McCulloch, G. Y. Oudit, PI3K α -regulated gelsolin activity is a critical determinant of cardiac cytoskeletal remodeling and heart disease. *Nat Commun* **9**, 5390 (2018).
16. S. Shah, H. Yogasundaram, R. Basu, F. Wang, D. I. Paterson, T. P. Alastalo, G. Y. Oudit, Novel Dominant-Negative Mutation in Cardiac Troponin I Causes Severe Restrictive Cardiomyopathy. *Circ Heart Fail* **10**, (2017).

17. E. M. McNally, J. R. Golbus, M. J. Puckelwartz, Genetic mutations and mechanisms in dilated cardiomyopathy. *J Clin Invest* **123**, 19-26 (2013).
18. D. S. Herman, L. Lam, M. R. Taylor, L. Wang, P. Teekakirikul, D. Christodoulou, L. Conner, S. R. DePalma, B. McDonough, E. Sparks, D. L. Teodorescu, A. L. Cirino, N. R. Banner, D. J. Pennell, S. Graw, M. Merlo, A. Di Lenarda, G. Sinagra, J. M. Bos, M. J. Ackerman, R. N. Mitchell, C. E. Murry, N. K. Lakdawala, C. Y. Ho, P. J. Barton, S. A. Cook, L. Mestroni, J. G. Seidman, C. E. Seidman, Truncations of titin causing dilated cardiomyopathy. *N Engl J Med* **366**, 619-628 (2012).
19. H. P. Schultheiss, D. Fairweather, A. L. P. Caforio, F. Escher, R. E. Hershberger, S. E. Lipshultz, P. P. Liu, A. Matsumori, A. Mazzanti, J. McMurray, S. G. Priori, Dilated cardiomyopathy. *Nat Rev Dis Primers* **5**, 32 (2019).
20. A. N. Chang, J. D. Potter, Sarcomeric protein mutations in dilated cardiomyopathy. *Heart Fail Rev* **10**, 225-235 (2005).
21. N. Sun, M. Yazawa, J. Liu, L. Han, V. Sanchez-Freire, O. J. Abilez, E. G. Navarrete, S. Hu, L. Wang, A. Lee, A. Pavlovic, S. Lin, R. Chen, R. J. Hajjar, M. P. Snyder, R. E. Dolmetsch, M. J. Butte, E. A. Ashley, M. T. Longaker, R. C. Robbins, J. C. Wu, Patient-specific induced pluripotent stem cells as a model for familial dilated cardiomyopathy. *Sci Transl Med* **4**, 130ra147 (2012).
22. H. Wu, J. Lee, L. G. Vincent, Q. Wang, M. Gu, F. Lan, J. M. Churko, K. I. Sallam, E. Matsa, A. Sharma, J. D. Gold, A. J. Engler, Y. K. Xiang, D. M. Bers, J. C. Wu, Epigenetic Regulation of Phosphodiesterases 2A and 3A Underlies Compromised beta-Adrenergic Signaling in an iPSC Model of Dilated Cardiomyopathy. *Cell Stem Cell* **17**, 89-100 (2015).
23. Y. Dai, A. Amenov, N. Ignatyeva, A. Koschinski, H. Xu, P. L. Soong, M. Tiburcy, W. A. Linke, M. Zaccolo, G. Hasenfuss, W. H. Zimmermann, A. Ebert, Troponin destabilization impairs sarcomere-cytoskeleton interactions in iPSC-derived cardiomyocytes from dilated cardiomyopathy patients. *Sci Rep* **10**, 209 (2020).
24. D. Li, G. Z. Czernuszewicz, O. Gonzalez, T. Tapscott, A. Karibe, J. B. Durand, R. Brugada, R. Hill, J. M. Gregoritch, J. L. Anderson, M. Quinones, L. L. Bachinski, R. Roberts, Novel cardiac troponin T mutation as a cause of familial dilated cardiomyopathy. *Circulation* **104**, 2188-2193 (2001).
25. K. M. Dieseldorff Jones, Y. Koh, R. S. Weller, R. S. Turna, F. Ahmad, S. Huke, B. C. Knollmann, J. R. Pinto, H. S. Hwang, Pathogenic troponin T mutants with opposing effects on myofilament Ca. *Arch Biochem Biophys* **661**, 125-131 (2019).
26. H. Xu, R. Wali, C. Cheruiyot, J. Bodenschatz, G. Hasenfuss, A. Janshoff, M. Habeck, A. Ebert, Non-negative blind deconvolution for signal processing in a CRISPR-edited iPSC-cardiomyocyte model of dilated cardiomyopathy. *FEBS Lett*, (2021).
27. A. M. Matyushenko, D. I. Levitsky, Molecular Mechanisms of Pathologies of Skeletal and Cardiac Muscles Caused by Point Mutations in the Tropomyosin Genes. *Biochemistry (Mosc)* **85**, S20-S33 (2020).
28. T. M. Gupte, F. Haque, B. Gangadharan, M. S. Sunitha, S. Mukherjee, S. Anandhan, D. S. Rani, N. Mukundan, A. Jambekar, K. Thangaraj, R. Sowdhamini, R. F. Sommese, S. Nag, J. A. Spudich, J. A. Mercer, Mechanistic heterogeneity in contractile properties of α -tropomyosin (TPM1) mutants associated with inherited cardiomyopathies. *J Biol Chem* **290**, 7003-7015 (2015).
29. A. N. Chang, K. Harada, M. J. Ackerman, J. D. Potter, Functional consequences of hypertrophic

- and dilated cardiomyopathy-causing mutations in alpha-tropomyosin. *J Biol Chem* **280**, 34343-34349 (2005).
30. J. C. Tardiff, Thin filament mutations: developing an integrative approach to a complex disorder. *Circ Res* **108**, 765-782 (2011).
 31. A. N. Chang, N. J. Greenfield, A. Singh, J. D. Potter, J. R. Pinto, Structural and protein interaction effects of hypertrophic and dilated cardiomyopathic mutations in alpha-tropomyosin. *Front Physiol* **5**, 460 (2014).
 32. F. Bai, H. L. Groth, M. Kawai, DCM-related tropomyosin mutants E40K/E54K over-inhibit the actomyosin interaction and lead to a decrease in the number of cycling cross-bridges. *PLoS One* **7**, e47471 (2012).
 33. N. K. Lakdawala, L. Dellefave, C. S. Redwood, E. Sparks, A. L. Cirino, S. Depalma, S. D. Colan, B. Funke, R. S. Zimmerman, P. Robinson, H. Watkins, C. E. Seidman, J. G. Seidman, E. M. McNally, C. Y. Ho, Familial dilated cardiomyopathy caused by an alpha-tropomyosin mutation: the distinctive natural history of sarcomeric dilated cardiomyopathy. *J Am Coll Cardiol* **55**, 320-329 (2010).
 34. D. R. Richardson, D. J. Lane, E. M. Becker, M. L. Huang, M. Whitnall, Y. Suryo Rahmanto, A. D. Sheftel, P. Ponka, Mitochondrial iron trafficking and the integration of iron metabolism between the mitochondrion and cytosol. *Proc Natl Acad Sci U S A* **107**, 10775-10782 (2010).
 35. D. T. Kremastinos, D. Farmakis, Iron overload cardiomyopathy in clinical practice. *Circulation* **124**, 2253-2263 (2011).
 36. W. Xu, T. Barrientos, L. Mao, H. A. Rockman, A. A. Sauve, N. C. Andrews, Lethal Cardiomyopathy in Mice Lacking Transferrin Receptor in the Heart. *Cell Rep* **13**, 533-545 (2015).
 37. A. C. Garfinkel, J. G. Seidman, C. E. Seidman, Genetic Pathogenesis of Hypertrophic and Dilated Cardiomyopathy. *Heart Fail Clin* **14**, 139-146 (2018).
 38. C. C. Yuan, K. Kazmierczak, J. Liang, Z. Zhou, S. Yadav, A. V. Gomes, T. C. Irving, D. Szczesna-Cordary, Sarcomeric perturbations of myosin motors lead to dilated cardiomyopathy in genetically modified. *Proc Natl Acad Sci U S A* **115**, E2338-E2347 (2018).
 39. V. Sequeira, L. L. Nijenkamp, J. A. Regan, J. van der Velden, The physiological role of cardiac cytoskeleton and its alterations in heart failure. *Biochim Biophys Acta* **1838**, 700-722 (2014).
 40. S. Hein, S. Kostin, A. Heling, Y. Maeno, J. Schaper, The role of the cytoskeleton in heart failure. *Cardiovasc Res* **45**, 273-278 (2000).
 41. T. M. Olson, S. Illenberger, N. Y. Kishimoto, S. Huttelmaier, M. T. Keating, B. M. Jockusch, Metavinculin mutations alter actin interaction in dilated cardiomyopathy. *Circulation* **105**, 431-437 (2002).
 42. B. M. Jockusch, G. Isenberg, Interaction of alpha-actinin and vinculin with actin: opposite effects on filament network formation. *Proc Natl Acad Sci U S A* **78**, 3005-3009 (1981).
 43. P. R. Bois, R. A. Borgon, C. Vornrhein, T. Izard, Structural dynamics of alpha-actinin-vinculin interactions. *Mol Cell Biol* **25**, 6112-6122 (2005).
 44. P. R. Bois, B. P. O'Hara, D. Nietlispach, J. Kirkpatrick, T. Izard, The vinculin binding sites of talin and alpha-actinin are sufficient to activate vinculin. *J Biol Chem* **281**, 7228-7236 (2006).
 45. Y. Sun, A. C. Martin, D. G. Drubin, Endocytic internalization in budding yeast requires coordinated actin nucleation and myosin motor activity. *Dev Cell* **11**, 33-46 (2006).
 46. V. Sirotkin, C. C. Beltzner, J. B. Marchand, T. D. Pollard, Interactions of WASp, myosin-I, and

- verprolin with Arp2/3 complex during actin patch assembly in fission yeast. *J Cell Biol* **170**, 637-648 (2005).
47. C. J. Merrifield, B. Qualmann, M. M. Kessels, W. Almers, Neural Wiskott Aldrich Syndrome Protein (N-WASP) and the Arp2/3 complex are recruited to sites of clathrin-mediated endocytosis in cultured fibroblasts. *Eur J Cell Biol* **83**, 13-18 (2004).
 48. I. van den Bout, N. Divecha, PIP5K-driven PtdIns(4,5)P₂ synthesis: regulation and cellular functions. *J Cell Sci* **122**, 3837-3850 (2009).
 49. D. N. Silachev, L. S. Khailova, V. A. Babenko, M. V. Gulyaev, S. I. Kovalchuk, L. D. Zorova, E. Y. Plotnikov, Y. N. Antonenko, D. B. Zorov, Neuroprotective effect of glutamate-substituted analog of gramicidin A is mediated by the uncoupling of mitochondria. *Biochim Biophys Acta* **1840**, 3434-3442 (2014).
 50. M. G. Roth, Integrating actin assembly and endocytosis. *Dev Cell* **13**, 3-4 (2007).
 51. C. N. Antonescu, F. Aguet, G. Danuser, S. L. Schmid, Phosphatidylinositol-(4,5)-bisphosphate regulates clathrin-coated pit initiation, stabilization, and size. *Mol Biol Cell* **22**, 2588-2600 (2011).
 52. Z. Kadlecova, S. J. Spielman, D. Loerke, A. Mohanakrishnan, D. K. Reed, S. L. Schmid, Regulation of clathrin-mediated endocytosis by hierarchical allosteric activation of AP2. *J Cell Biol* **216**, 167-179 (2017).
 53. S. Cerri, C. Milanese, P. G. Mastroberardino, Endocytic iron trafficking and mitochondria in Parkinson's disease. *Int J Biochem Cell Biol* **110**, 70-74 (2019).
 54. J. J. Braymer, R. Lill, Iron-sulfur cluster biogenesis and trafficking in mitochondria. *J Biol Chem* **292**, 12754-12763 (2017).
 55. V. Melenovsky, J. Petrak, T. Mracek, J. Benes, B. A. Borlaug, H. Nuskova, T. Pluhacek, J. Spatenka, J. Kovalcikova, Z. Drahotka, J. Kautzner, J. Pirk, J. Houstek, Myocardial iron content and mitochondrial function in human heart failure: a direct tissue analysis. *Eur J Heart Fail* **19**, 522-530 (2017).
 56. Y. Shibasaki, H. Ishihara, N. Kizuki, T. Asano, Y. Oka, Y. Yazaki, Massive actin polymerization induced by phosphatidylinositol-4-phosphate 5-kinase in vivo. *J Biol Chem* **272**, 7578-7581 (1997).
 57. P. A. Oude Weernink, P. Schulte, Y. Guo, J. Wetzel, M. Amano, K. Kaibuchi, S. Haverland, M. Voss, M. Schmidt, G. W. Mayr, K. H. Jakobs, Stimulation of phosphatidylinositol-4-phosphate 5-kinase by Rho-kinase. *J Biol Chem* **275**, 10168-10174 (2000).
 58. J. Lauriol, K. Keith, F. Jaffré, A. Couvillon, A. Saci, S. A. Goonasekera, J. R. McCarthy, C. W. Kessinger, J. Wang, Q. Ke, P. M. Kang, J. D. Molkentin, C. Carpenter, M. I. Kontaridis, RhoA signaling in cardiomyocytes protects against stress-induced heart failure but facilitates cardiac fibrosis. *Sci Signal* **7**, ra100 (2014).
 59. B. Ronan, O. Flamand, L. Vescovi, C. Dureuil, L. Durand, F. Fassy, M. F. Bachelot, A. Lambertson, M. Mathieu, T. Bertrand, J. P. Marquette, Y. El-Ahmad, B. Filoche-Romme, L. Schio, C. Garcia-Echeverria, H. Goulaouic, B. Pasquier, A highly potent and selective Vps34 inhibitor alters vesicle trafficking and autophagy. *Nat Chem Biol* **10**, 1013-1019 (2014).
 60. D. Jia, T. S. Gomez, Z. Metlagel, J. Umetani, Z. Otwinowski, M. K. Rosen, D. D. Billadeau, WASH and WAVE actin regulators of the Wiskott-Aldrich syndrome protein (WASP) family are controlled by analogous structurally related complexes. *Proc Natl Acad Sci U S A* **107**, 10442-10447 (2010).

61. M. Kamisago, S. D. Sharma, S. R. DePalma, S. Solomon, P. Sharma, B. McDonough, L. Smoot, M. P. Mullen, P. K. Woolf, E. D. Wigle, J. G. Seidman, C. E. Seidman, Mutations in sarcomere protein genes as a cause of dilated cardiomyopathy. *N Engl J Med* **343**, 1688-1696 (2000).
62. Y. Ikeda, J. Ross, Models of dilated cardiomyopathy in the mouse and the hamster. *Curr Opin Cardiol* **15**, 197-201 (2000).
63. M. Nonaka, S. Morimoto, Experimental models of inherited cardiomyopathy and its therapeutics. *World J Cardiol* **6**, 1245-1251 (2014).
64. K. E. Yutzey, J. Robbins, Principles of genetic murine models for cardiac disease. *Circulation* **115**, 792-799 (2007).
65. F. Rudolph, C. Fink, J. Hüttemeister, M. Kirchner, M. H. Radke, J. Lopez Carballo, E. Wagner, T. Kohl, S. E. Lehnart, P. Mertins, M. Gotthardt, Deconstructing sarcomeric structure-function relations in titin-BiOLD knock-in mice. *Nat Commun* **11**, 3133 (2020).
66. S. Swist, A. Unger, Y. Li, A. Vöge, M. von Frieling-Salewsky, Å. Skärlén, N. Cacciani, T. Braun, L. Larsson, W. A. Linke, Maintenance of sarcomeric integrity in adult muscle cells crucially depends on Z-disc anchored titin. *Nat Commun* **11**, 4479 (2020).
67. V. P. Sah, S. Minamisawa, S. P. Tam, T. H. Wu, G. W. Dorn, 2nd, J. Ross, Jr., K. R. Chien, J. H. Brown, Cardiac-specific overexpression of RhoA results in sinus and atrioventricular nodal dysfunction and contractile failure. *J Clin Invest* **103**, 1627-1634 (1999).
68. W. Bao, E. Hu, L. Tao, R. Boyce, R. Mirabile, D. T. Thudium, X. L. Ma, R. N. Willette, T. L. Yue, Inhibition of Rho-kinase protects the heart against ischemia/reperfusion injury. *Cardiovasc Res* **61**, 548-558 (2004).
69. T. Shimizu, J. K. Liao, Rho Kinases and Cardiac Remodeling. *Circ J* **80**, 1491-1498 (2016).
70. M. Surma, L. Wei, J. Shi, Rho kinase as a therapeutic target in cardiovascular disease. *Future Cardiol* **7**, 657-671 (2011).
71. S. Y. Xiang, D. Vanhoutte, D. P. Del Re, N. H. Purcell, H. Ling, I. Banerjee, J. Bossuyt, R. A. Lang, Y. Zheng, S. J. Matkovich, S. Miyamoto, J. D. Molkenin, G. W. Dorn, J. H. Brown, RhoA protects the mouse heart against ischemia/reperfusion injury. *J Clin Invest* **121**, 3269-3276 (2011).
72. G. Loncar, D. Obradovic, H. Thiele, S. von Haehling, M. Lainscak, Iron deficiency in heart failure. *ESC Heart Fail* **8**, 2368-2379 (2021).
73. F. M. Torti, S. V. Torti, Regulation of ferritin genes and protein. *Blood* **99**, 3505-3516 (2002).
74. E. Nemeth, M. S. Tuttle, J. Powelson, M. B. Vaughn, A. Donovan, D. M. Ward, T. Ganz, J. Kaplan, Hepcidin regulates cellular iron efflux by binding to ferroportin and inducing its internalization. *Science* **306**, 2090-2093 (2004).
75. A. Donovan, C. A. Lima, J. L. Pinkus, G. S. Pinkus, L. I. Zon, S. Robine, N. C. Andrews, The iron exporter ferroportin/Slc40a1 is essential for iron homeostasis. *Cell Metab* **1**, 191-200 (2005).
76. T. A. Rouault, The role of iron regulatory proteins in mammalian iron homeostasis and disease. *Nat Chem Biol* **2**, 406-414 (2006).
77. O. Stehling, A. D. Sheftel, R. Lill, Chapter 12 Controlled expression of iron-sulfur cluster assembly components for respiratory chain complexes in mammalian cells. *Methods Enzymol* **456**, 209-231 (2009).
78. T. Sato, H. C. Chang, M. Bayeva, J. S. Shapiro, L. Ramos-Alonso, H. Kouzu, X. Jiang, T. Liu, S. Yar, K. T. Sawicki, C. Chen, M. T. Martínez-Pastor, D. J. Stumpo, P. T. Schumacker, P. J.

- Blackshear, I. Ben-Sahra, S. Puig, H. Ardehali, mRNA-binding protein tristetraprolin is essential for cardiac response to iron deficiency by regulating mitochondrial function. *Proc Natl Acad Sci U S A* **115**, E6291-E6300 (2018).
79. M. F. Hoes, N. Grote Beverborg, J. D. Kijlstra, J. Kuipers, D. W. Swinkels, B. N. G. Giepmans, R. J. Rodenburg, D. J. van Veldhuisen, R. A. de Boer, P. van der Meer, Iron deficiency impairs contractility of human cardiomyocytes through decreased mitochondrial function. *Eur J Heart Fail* **20**, 910-919 (2018).
80. I. R. Mordi, A. Tee, C. C. Lang, Iron Therapy in Heart Failure: Ready for Primetime? *Card Fail Rev* **4**, 28-32 (2018).
81. G. Chen, D. R. Gulbranson, Z. Hou, J. M. Bolin, V. Ruotti, M. D. Probasco, K. Smuga-Otto, S. E. Howden, N. R. Diol, N. E. Propson, R. Wagner, G. O. Lee, J. Antosiewicz-Bourget, J. M. Teng, J. A. Thomson, Chemically defined conditions for human iPSC derivation and culture. *Nat Methods* **8**, 424-429 (2011).
82. A. D. Ebert, K. Kodo, P. Liang, H. Wu, B. C. Huber, J. Riegler, J. Churko, J. Lee, P. de Almeida, F. Lan, S. Diecke, P. W. Burridge, J. D. Gold, D. Mochly-Rosen, J. C. Wu, Characterization of the molecular mechanisms underlying increased ischemic damage in the aldehyde dehydrogenase 2 genetic polymorphism using a human induced pluripotent stem cell model system. *Sci Transl Med* **6**, 255ra130 (2014).
83. X. Lian, C. Hsiao, G. Wilson, K. Zhu, L. B. Hazeltine, S. M. Azarin, K. K. Raval, J. Zhang, T. J. Kamp, S. P. Palecek, Robust cardiomyocyte differentiation from human pluripotent stem cells via temporal modulation of canonical Wnt signaling. *Proc Natl Acad Sci U S A* **109**, E1848-1857 (2012).
84. X. Lian, J. Zhang, S. M. Azarin, K. Zhu, L. B. Hazeltine, X. Bao, C. Hsiao, T. J. Kamp, S. P. Palecek, Directed cardiomyocyte differentiation from human pluripotent stem cells by modulating Wnt/beta-catenin signaling under fully defined conditions. *Nat Protoc* **8**, 162-175 (2013).
85. I. Atanassov, H. Urlaub, Increased proteome coverage by combining PAGE and peptide isoelectric focusing: comparative study of gel-based separation approaches. *Proteomics* **13**, 2947-2955 (2013).
86. J. P. Lambert, G. Ivosev, A. L. Couzens, B. Larsen, M. Taipale, Z. Y. Lin, Q. Zhong, S. Lindquist, M. Vidal, R. Aebersold, T. Pawson, R. Bonner, S. Tate, A. C. Gingras, Mapping differential interactomes by affinity purification coupled with data-independent mass spectrometry acquisition. *Nat Methods* **10**, 1239-1245 (2013).
87. Y. Zhang, A. Bilbao, T. Bruderer, J. Luban, C. Strambio-De-Castillia, F. Lisacek, G. Hopfgartner, E. Varesio, The Use of Variable Q1 Isolation Windows Improves Selectivity in LC-SWATH-MS Acquisition. *J Proteome Res* **14**, 4359-4371 (2015).
88. T. Wilhelmi, X. Xu, X. Tan, M. S. Hulshoff, S. Maamari, S. Sossalla, M. Zeisberg, E. M. Zeisberg, Serelaxin alleviates cardiac fibrosis through inhibiting endothelial-to-mesenchymal transition via RXFP1. *Theranostics* **10**, 3905-3924 (2020).
89. S. Brandenburg, T. Kohl, G. S. Williams, K. Gusev, E. Wagner, E. A. Rog-Zielinska, E. Hebisch, M. Dura, M. Didié, M. Gotthardt, V. O. Nikolaev, G. Hasenfuss, P. Kohl, C. W. Ward, W. J. Lederer, S. E. Lehnart, Axial tubule junctions control rapid calcium signaling in atria. *J Clin Invest* **126**, 3999-4015 (2016).

FIGURE LEGENDS

Fig. 1. TPM1-L185F causes defective contractility and force generation in DCM patient-specific iPSC-CMs

(A) Pedigree of the family carrying the DCM-associated variant TPM1-L185F variant. Human iPSCs were generated for four mutation carriers and four healthy donors. Squares, male and circles, female gender; filled symbols, affected; cross bars, deceased individuals; arrow, proband; *, skin biopsy obtained. Ages at time of diagnosis and last follow-up for gene carriers and age at evaluation for genotype negative control are shown. The healthy donor, individual II-4 (L185F $-/-$, 55 yr*) as well as patient III-5 (L185F $+/-$, (HTx) /27 yr*) analyzed in this study are indicated (blue and red, respectively). HTx, heart transplantation. *, age at first and last evaluation, death, or heart transplantation. (B) Label-free SWATH-MS whole-proteome analysis was used to analyze significantly differently expressed proteins in healthy donor (HD) control iPSC-CMs (WT/WT) (WT) vs DCM patient-derived iPSC-CMs (WT/MUT) (Pat). 1206 proteins were found to be upregulated and 1357 proteins to be downregulated. (C) Venn diagram of differentially expressed protein profiles for HD control and DCM iPSC-CM groups. (D) Principal component analysis (PCA) for proteomic expression profiling detected for WT control and DCM iPSC-CMs. (E) Heatmap of proteomic profiling for WT control and DCM iPSC-CMs (n=4 replicates each). Cluster analysis was performed for 2563 proteins (rows) via Euclidean distance assessment by clustermap (Seaborn). (F) Bargraph for the top 15 significantly changed pathways between WT control and DCM iPSC-CMs retrieved via ingenuity pathway analysis (IPA). (G) Volcano plot showing up- vs. down-regulated protein expression profiles in the signaling pathways for actin cytoskeleton (purple), clathrin-mediated

endocytosis (blue), iron homeostasis (green), as well as DCM (yellow) between WT (healthy donor) and DCM groups.

Fig. 2. TPM1-L185F disrupts sarcomere connections with plasma membrane microdomains in DCM patient-specific iPSC-CMs

(A) CRISPR-Cas genome editing to generate TPM1-L185F MUT-introduced iPSCs. (B-C) Reduced sarcomere length in patient and MUT-int/MUT-int compared with WT iPSC-CMs. (B) Representative images from cells stained with TnT and SAA antibodies. (C) Quantification of (B). *** $P < 0.001$ for WT vs. patient (Pat) and WT vs. Mut-int1 (one-way ANOVA and Dunn's multiple comparisons test). (D) Reduced beating force in WT/MUT and TPM1-L185F MUT-introduced iPSC-CMs. ** $P < 0.01$ for WT vs. patient (Pat); *** $P < 0.001$ WT vs. Mut-int1 (one-way ANOVA and Dunn's multiple comparisons test). (E) WT/MUT and TPM1-L185F MUT-introduced iPSC-CMs display impaired contractility indicated by reduced $\Delta F/F_0$. * $P < 0.05$ for WT vs. patient (Pat); *** $P < 0.001$ WT vs. Mut-int1 (one-way ANOVA and Dunn's multiple comparisons test). (F-I) In presence of TPM1-L185F, a lower amount of sarcomeric alpha-actinin (SAA, ACTN2) and TPM (TPM1) bind to vinculin. (F) Representative images of immunoblot membranes are shown. (G) No significant difference was observed in the amount of vinculin bound with beads. ns, not significant for WT vs. patient (Pat) and WT vs. Mut-int1. (H) Reduced binding of SAA to vinculin in presence of TPM1-L185F. Data were normalized by bound vinculin from corresponding groups, respectively. * $P < 0.05$ for WT vs. patient (Pat), ** $P < 0.01$ WT vs. Mut-int1. (I) Reduced binding of TPM to vinculin in presence of TPM1-L185F. Data were normalized by bound vinculin from corresponding groups, respectively.

***P<0.001 for WT vs. patient (Pat) and WT vs. Mut-int1 calculated by one-way ANOVA and Sidak's multiple comparisons test. Data were normalized by WT (WT1, WT2). (J-L) Reduced binding of TnT to vinculin in presence of TPM1-L185F. (J) Representative images of immunoblot membranes. (K) The amount of vinculin bound to anti-vinculin-antibody decorated beads was comparable between groups. ns, not significant for WT vs. patient (Pat) and WT vs. Mut-int1. (L) Reduced binding of TnT to vinculin in presence of TPM1-L185F. Bound TnT was normalized by corresponding amount of bound vinculin for the respective groups. *P<0.05 for WT vs. patient (Pat), **P<0.01 for WT vs. Mut-int1. Statistics were calculated by one-way ANOVA and Sidak's multiple comparisons test. Data were normalized by WT (WT1, WT2). (M-N) Reduced amount of TnT-localized vinculin localized in presence of sarcomeric mutations, TPM1-L185F (Mut-int 1) and TnT-R141W (Mut-int 2). (M) Representative confocal images following immunostaining for vinculin and TnT. Scale bar, 20 μ m. (N) Quantification of (M). **P<0.01 for WT1 vs. patient (Pat) and WT1 vs. Mut-int1, ***P<0.001 for WT2 vs. Mut-int2 (one-way ANOVA and Dunn's multiple comparisons test). Data are shown as mean \pm sem.

Fig. 3. Impaired F-actin polymerization is linked to defective clathrin-mediated endocytosis and endosome distribution in presence of DCM mutations

(A) Reduced F-actin content in WT/MUT and MUT-int/MUT-int iPSC-CMs. Actin polymerization was measured via detection of phalloidin (F-actin) and DNase I (G-actin) immunostaining using a high-content plate reader. DAPI was used to normalize total cell numbers. ***P<0.001 for WT1 vs. patient (Pat) and WT1 vs. Mut-int1; *P<0.05 for WT2 vs.

Mut-int2 (one-way ANOVA and Sidak's multiple comparisons test). (B, C) Reduced PIP2 levels on the PM in WT/MUT and MUT-int/MUT-int iPSC-CMs. (B) Representative confocal images following PIP2-specific immunostaining. (C) Quantification of (B). ***P<0.001 WT1 vs. patient (Pat), WT1 vs. Mut-int1 and WT2 vs. Mut-int2 (one-way ANOVA and Dunn's multiple comparisons test). (D-E) Impaired transferrin uptake in WT/MUT and MUT-int/MUT-int iPSC-CMs. (D) Representative 63x confocal images of continuous transferrin uptake at 5min. Scale bar, 20 μ m. (E) Quantification of 20x confocal Z stack images of continuous transferrin uptake at 5 min normalized by uptake at 0 min. ***P<0.001 for WT1 vs. patient (Pat), WT1 vs. Mut-int1, and WT2 vs. Mut-int2 (one-way ANOVA and Dunn's multiple comparisons test). (F-G) Abnormal early endosome distribution in WT/MUT and MUT-int/MUT-int iPSC-CMs. (F) Representative 63x confocal images and (G) quantification of confocal images following immunostaining with an anti-EEA1 antibody. Scale bar, 20 μ m. ***P<0.001 for WT1 vs. patient (Pat), WT1 vs. Mut-int1 and WT2 vs. Mut-int2 (one-way ANOVA and Sidak's multiple comparisons test). Data are shown as mean \pm sem.

Fig. 4. Iron deficiency in the presence of DCM mutations causes mitochondrial dysfunction and reduced contractility in DCM iPSC-CMs

(A-B) Mitochondrial Fe (II) levels are reduced in WT/MUT and MUT-int/MUT-int iPSC-CMs. Representative 63x confocal images (A) and ROI based quantification (B) following Mitotracker and FerroOrange labelling. Scale bar, 20 μ m. *P<0.05 for WT1 vs. patient (Pat); ***P<0.001 for WT1 vs. Mut-int1 and WT2 vs. Mut-int2 (one-way ANOVA and Dunn's multiple comparisons test). (C-E) Fe (II) treatment rescued the contraction amplitude in

WT/MUT and MUT-int/MUT-int iPSC-CMs. Contractility was measured via video-based motion-traction analysis. ***P<0.001 for control vehicle (CV) vs. Fe (II) in DCM patient (Pat) iPSC-CMs, CV vs. Fe(II) in Mut-int1 iPSC-CMs and CV vs. Fe(II) Mut-int2, calculated by Mann-Whitney test. Data are shown as mean \pm sem.

Fig. 5. Recovering actin polymerization via RhoA activation rescues PM-localized PIP2 levels and uptake of transferrin-bound iron

(A-B) Rho activator II treatment assists transferrin uptake in Mut-int1 iPSC-CMs. (A) Representative confocal images of Mut-int1 iPSC-CMs after control vehicle (CV) and RhoA II (3 μ g/mL, 3 h) treatment followed by incubation with Alexa 488 labeled transferrin (20 μ g/mL, 5min). (B) Quantification of (A). Data are normalized by 0min; scale bar, 20 μ m. ***P<0.01 for CV vs. RhoA II in Mut-int1 iPSC-CMs. (C-D) Abnormal early endosome distribution is rescued by RhoA II treatment in Mut-int1 iPSC-CMs. Confocal images (C) and quantification (D) of immuno-staining with an anti-EEA1 antibody following CV and RhoA II (3 μ g/mL, 3 h) treatment. Scale bar, 20 μ m. ***P<0.001 for CV vs. RhoA II. (E-G) Mitochondrial Fe (II) levels in DCM patient-derived WT/MUT (Pat) and TPM1-L185F MUT-int/MUT-int iPSC-CMs were replenished following RhoA II treatment. (E) CV or RhoA II (3 μ g/mL, 3 h) treatment followed by Mitotracker and FerroOrange staining. Representative 63x confocal images are shown; scale bar, 20 μ m. (F-G) ROI based quantification of (E). ***P<0.001 for control vehicle (CV) vs. RhoA II in DCM patient-derived iPSC-CMs (Pat) and CV vs. RhoA II in Mut-int1 iPSC-CMs. (H) Contractility in TPM1-L185F MUT-int/MUT-int iPSC-CMs. Delta F/F0 are improved by RhoA II treatment was recovered after RhoA II

treatment (3 μ g/mL, 3 h). ***P<0.001, CV vs. RhoA II in Mut-int1 iPSC-CMs. (I-K) RhoA II treatment results in increased sarcomere length in DCM patient-derived WT/MUT (Pat) iPSC-CMs and MUT-int/MUT-int TPM1-L185F iPSC-CMs, compared to respective control vehicle (CV); scale bar, 20 μ m. (I) Representative 63X confocal images of DCM patient-derived WT/MUT (Pat) and TPM1-L185F MUT-int/MUT-int iPSC-CMs treated with CV and RhoA II (3 μ g/mL, 16 h) followed by co-immunostaining with TnT and SAA antibodies. (J-K) Quantification of (I). *P<0.05, CV vs. RhoA II in patient and CV vs. RhoA II in Mut-int1 iPSC-CMs as calculated by Mann-Whitney test. Data are shown as mean \pm sem.

Fig. 6. CRISPR/Cas9-correction of the patient-specific DCM mutation TPM1-L185F rescues endosome distribution and mitochondrial iron levels in DCM-corrected iPSC-CMs

(A) CRISPR/Cas9 gene editing strategy to generate TPM1-L185F MUT-corrected iPSCs (WT-cor/WT-cor) iPSCs. (B) Increased F-actin content in WT-cor/WT-cor iPSC-CMs compared to DCM TPM1-L185F patient-derived WT/MUT (Pat) iPSC-CMs. Actin polymerization was measured via phalloidin (to stain F-actin) and DNase I (to stain G-actin) labelling in a high-content plate reader. Normalization to cell numbers labeled by DAPI is performed. ***P<0.001 for DCM patient-derived (Pat) vs. mutation-corrected (mut-cor) iPSC-CMs (unpaired t test). Data of mutation-corrected (mut-cor) iPSC-CMs were compared to data from DCM patient-derived (Pat) group in Fig. 3A. (C-D) Increased transferrin uptake in WT-cor/WT-cor iPSC-CMs. (C) Representative images of DCM patient-derived (Pat, WT/MUT) and patient-derived, Cas9-mutation-corrected (WT-cor/WT-cor) iPSC-CMs after incubation with Alexa 488-

labeled transferrin (20 $\mu\text{g}/\text{mL}$, 5min). (D) Quantification of (C). Data are normalized by uptake at 0 min; scale bar, 20 μm . *** $P < 0.001$ for DCM patient-derived (Pat) vs. mutation-corrected mut-cor iPSC-CMs (Mann-Whitney test). Data of mutation-corrected (mut-cor) iPSC-CMs were compared to data from DCM patient-derived (Pat) group in Fig. 3E. (E-F) Abnormal early endosome distribution is rescued mutation-corrected iPSC-CMs. Confocal images (E) and quantification (F) of cells immuno-stained with an anti-EEA1 antibody. Scale bar, 20 μm . *** $P < 0.001$ for DCM patient-derived (Pat) vs. mutation-corrected (mut-cor) iPSC-CMs (unpaired t test). Data of mutation-corrected (mut-cor) iPSC-CMs were compared to data from DCM patient-derived (Pat) group in Fig. 3G. (G-H) Increased mitochondrial Fe (II) levels in mutation-corrected iPSC-CMs. (G) Representative 63x confocal images following Mitotracker and FerroOrange staining; scale bar, 20 μm . (H) ROI-based quantification of (G). *** $P < 0.001$ for DCM patient-derived (Pat) vs. mutation-corrected (mut-cor) iPSC-CMs (Mann-Whitney test). (I-J) Increased sarcomere length observed in mutation-corrected iPSC-CMs (WT-cor/WT-cor) compared to DCM patient-derived (WT/MUT) iPSC-CMs. (I) Representative 63x confocal images of DCM patient-derived (WT/MUT) and mutation-corrected iPSC-CMs following immunostaining with anti-TnT and anti-SAA antibodies. (J) Quantification of (I). Scale bar, 20 μm . ** $P < 0.01$ for DCM patient-derived (Pat) vs. mutation-corrected (mut-cor) iPSC-CMs (Mann-Whitney test). Data of mutation-corrected (mut-cor) iPSC-CMs were compared to data from DCM patient-derived (Pat) group in Fig. 2C (K) Increased contractile force in mutation-corrected (WT-cor/WT-cor) compared to DCM patient-derived (WT/MUT) iPSC-CMs. *** $P < 0.001$ for DCM patient-derived (Pat) vs. mutation-corrected (mut-cor) iPSC-CMs (Mann-Whitney test). Data of mutation-corrected (mut-cor) iPSC-CMs were compared

to data from DCM patient-derived (Pat) group in Fig. 2D. Data are shown as mean \pm sem.

Fig. 7. Heart tissues from DCM patients with end-stage heart failure display defective endosome distribution

Assessment of vinculin-positive plasma membrane (PM) junctions that are sites of CME initiation and endosome formation, as well as analysis of the intracellular distribution of endosomes by immunostaining were performed in human heart tissue. LV heart tissue from patients with dilated cardiomyopathy who received a heart transplantation due to severe heart failure (indicated as “heart failure”, HF, or heart transplantation) was analyzed. In comparison, LV heart tissue from patients with preserved LV function that underwent aortic valve replacement (severe valve stenosis) and coronary artery bypass graft surgery was used in the control group (“control”). (A-C) Left-ventricular tissues from DCM patients with HF show disorganized PM-localized vinculin structures compared to controls. Representative 63x confocal images of tissues from control (A) versus HF (B) stained with wheat germ agglutinin (WGA, Alexa Fluor™ 594 Conjugate) and a vinculin antibody. Scale bar, 20 μ m. (C) Quantification of (A-B) using ImageJ. Data display the standard error of mean of angles from vinculin-positive areas in each image. Control, n=45 images, n=4 patients; HF, n=52 images, n=5 patients. (D-F) Left-ventricular tissues from DCM patients with HF show abnormal early endosome (EE) distribution with the EEs localizing to the PM compared to controls. Representative 63x confocal images of tissues from control (D) versus HF (E) stained with wheat germ agglutinin (WGA, Alexa Fluor™ 594 Conjugate) and a CCDC53 antibody. Scale bar, 20 μ m (scale bar in enlarged sections, 5 μ m). (F) Quantification of immunostaining and

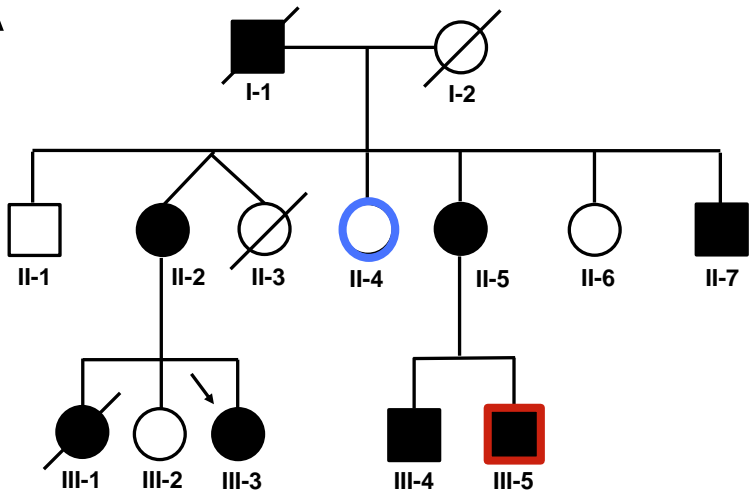
confocal images as described in (D-E) using ROI-based image quantification via ImageJ. Control, n=61 images, n=4 patients; HF, n=76 images, n=5 patients. **P<0.01 for control vs. HF (Mann-Whitney test). Data are shown as mean \pm sem.

Fig. 8. Defective endocytosis and endosome distribution result in mitochondrial iron deficiency in presence of DCM mutations.

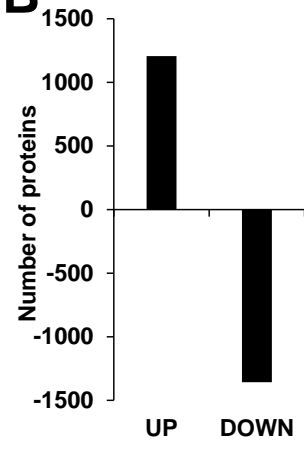
Schematic indicating patho-mechanisms associated with dysfunctional sarcomere links via vinculin to F-actin/PIP2-enriched PM microdomains, resulting in impaired clathrin-mediated endocytosis (CME) of cargo such as transferrin-bound iron, as well as altered endosome distribution. These molecular dysfunctions cause lower mitochondrial iron levels and reduced mitochondrial function, as well as impaired contractility and force generation. Disrupted sarcomere organization and function is observed in presence of sarcomeric DCM mutations as well as in cardiomyocytes from patients with systolic heart failure. IF, intermediate filaments; MF, actin filaments around the PM (red); PM, plasma membrane; PIP2, PIP2-enriched PM microdomains; green circles, endosomes containing transferrin-bound iron.

Fig. 1

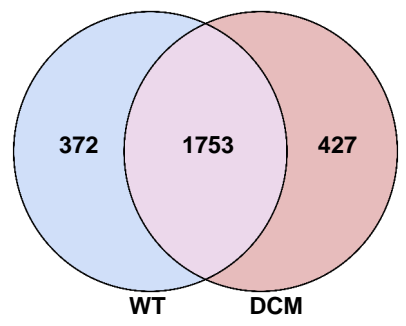
A



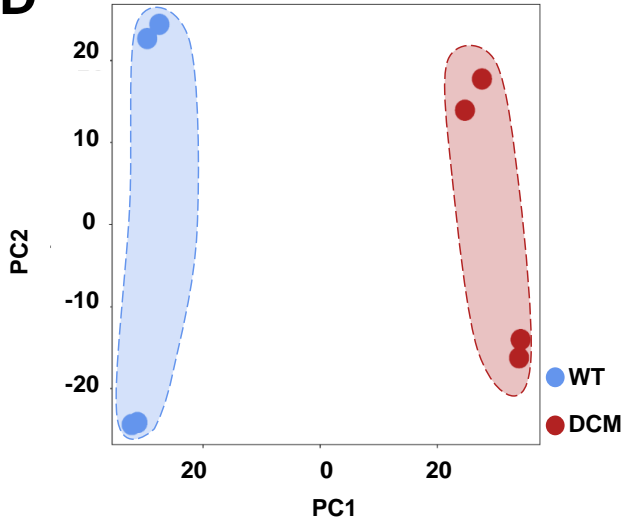
B



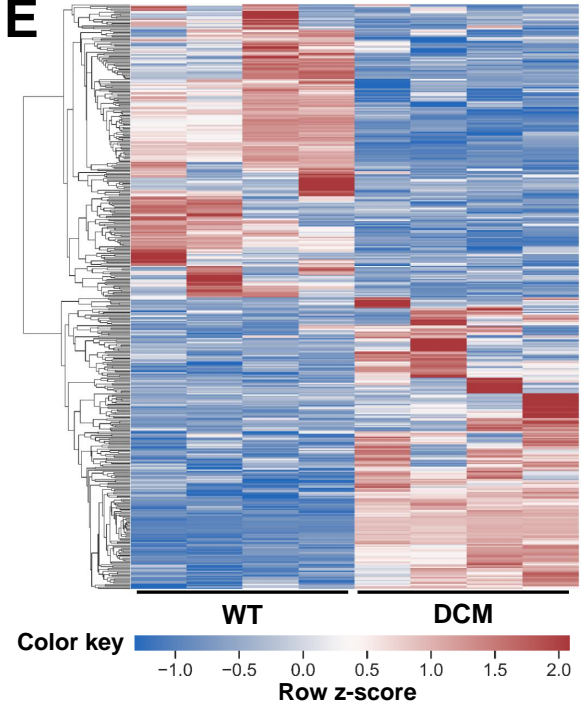
C



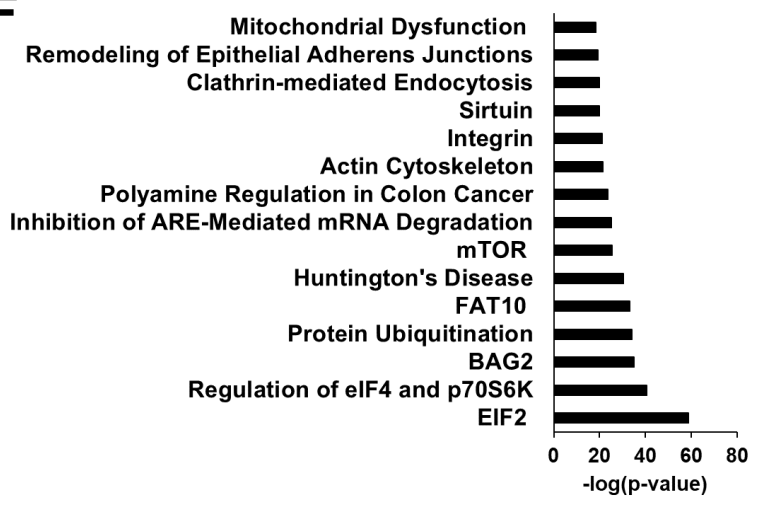
D



E



F



G

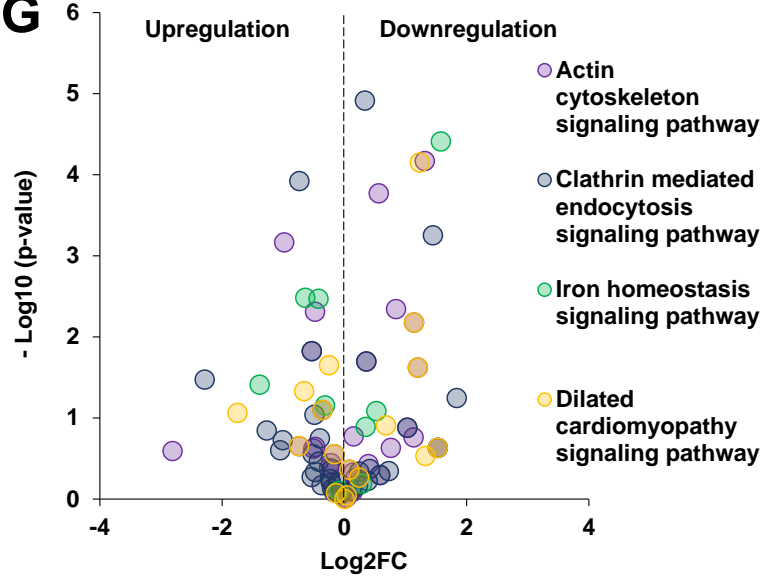


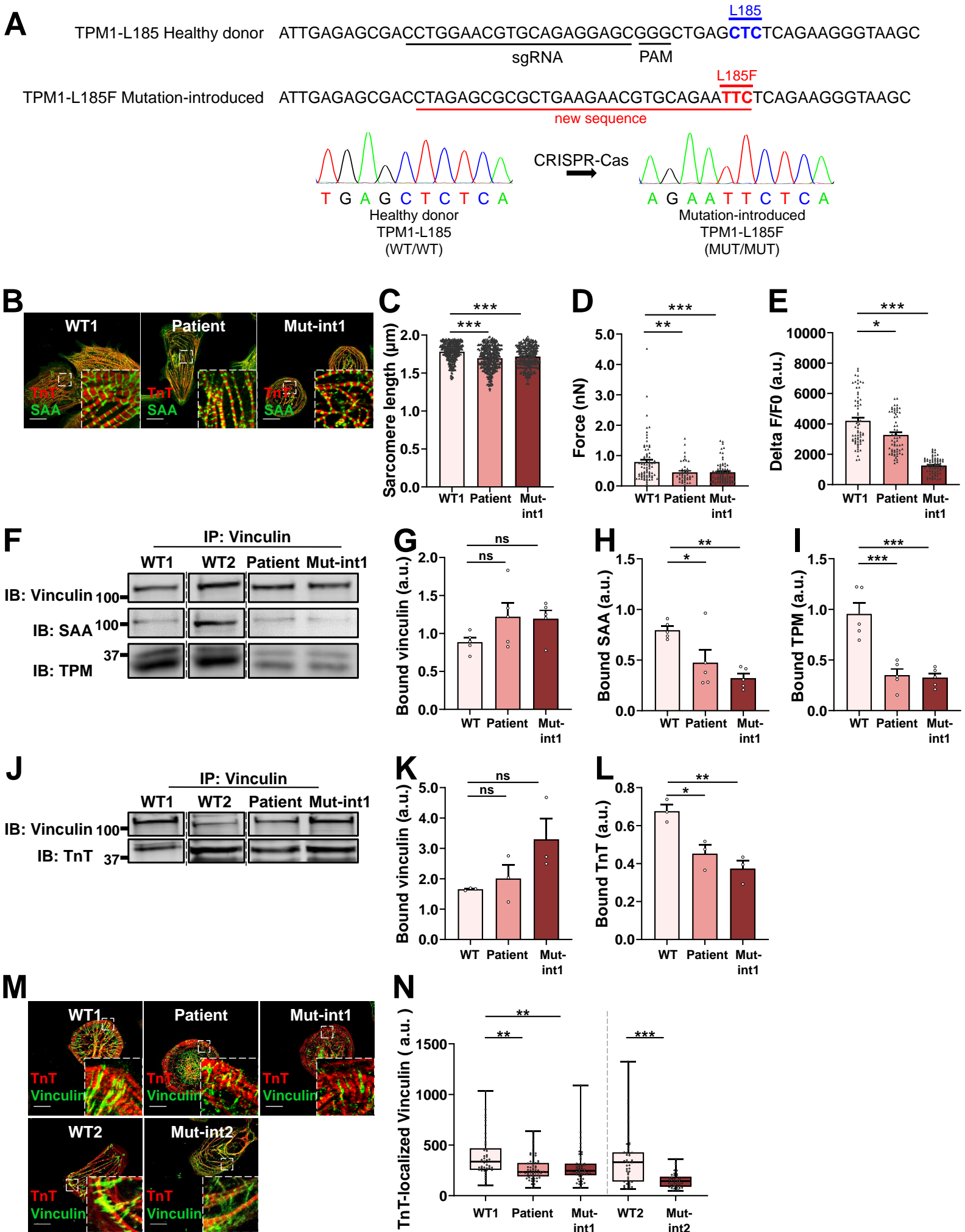
Fig. 2

Fig. 3

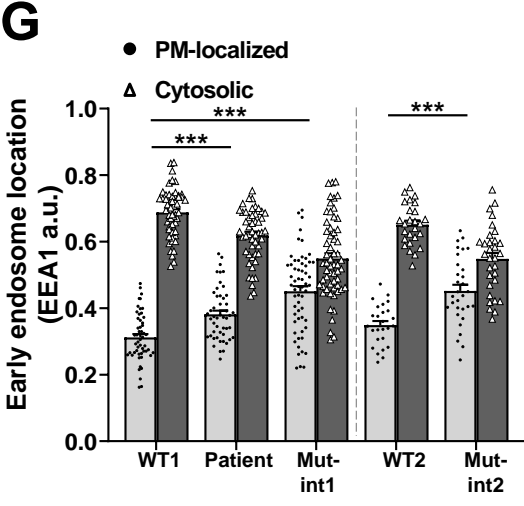
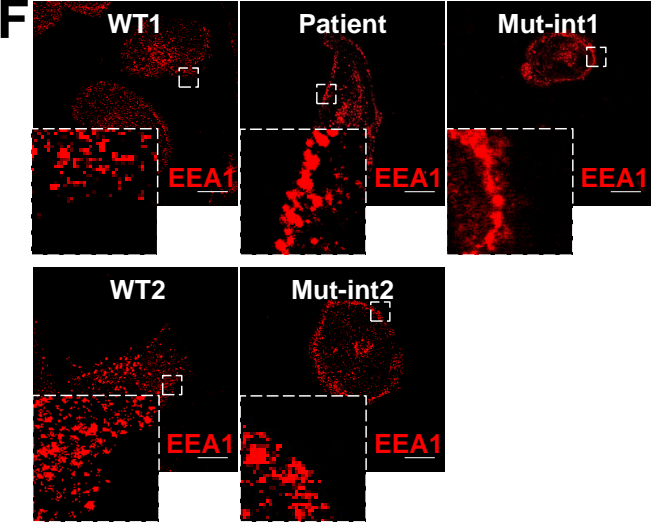
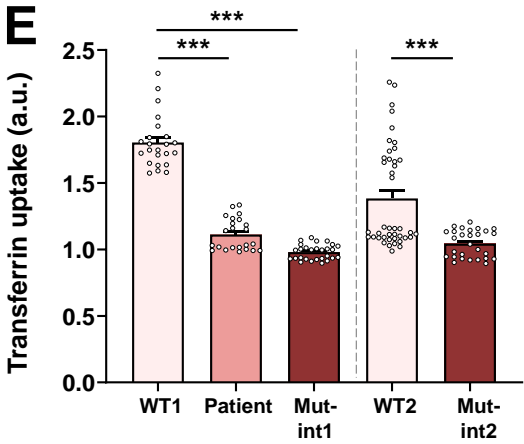
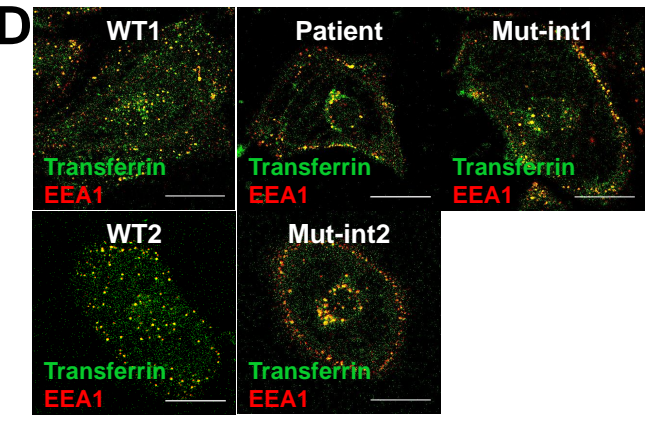
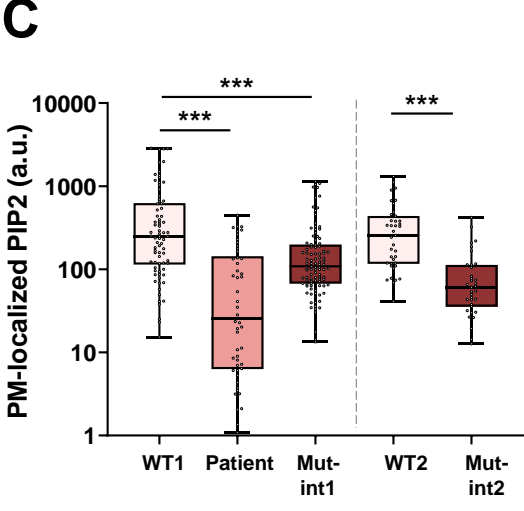
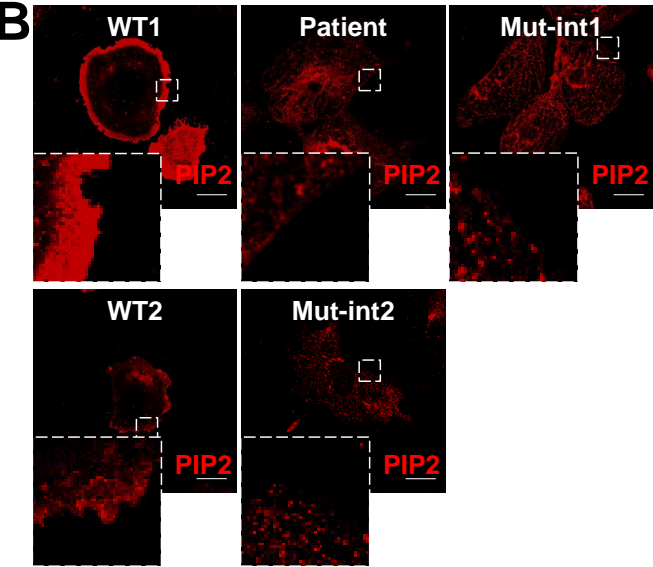
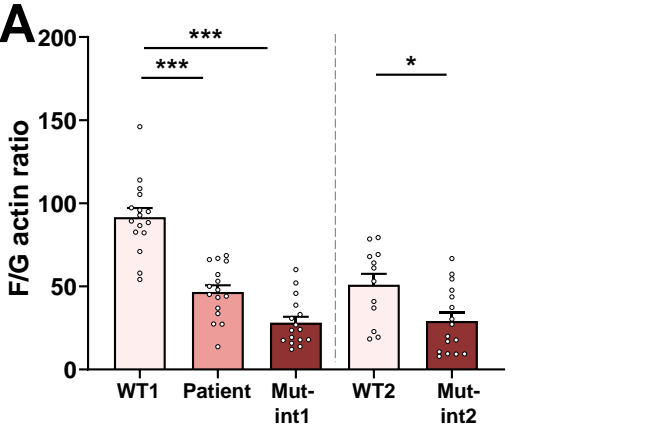


Fig. 4

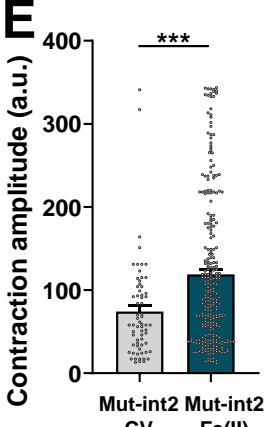
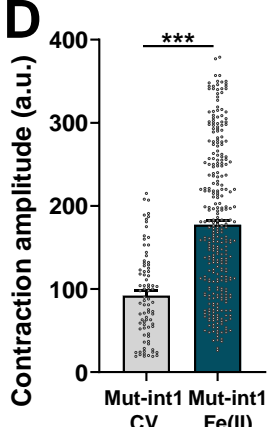
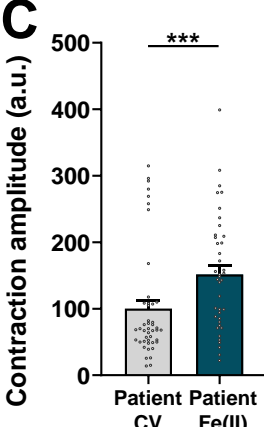
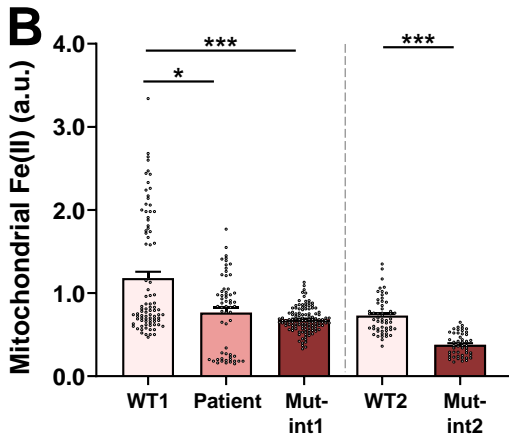
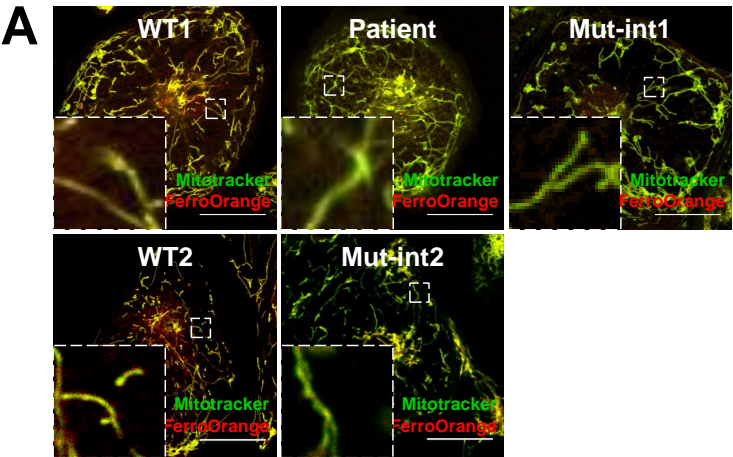


Fig. 5

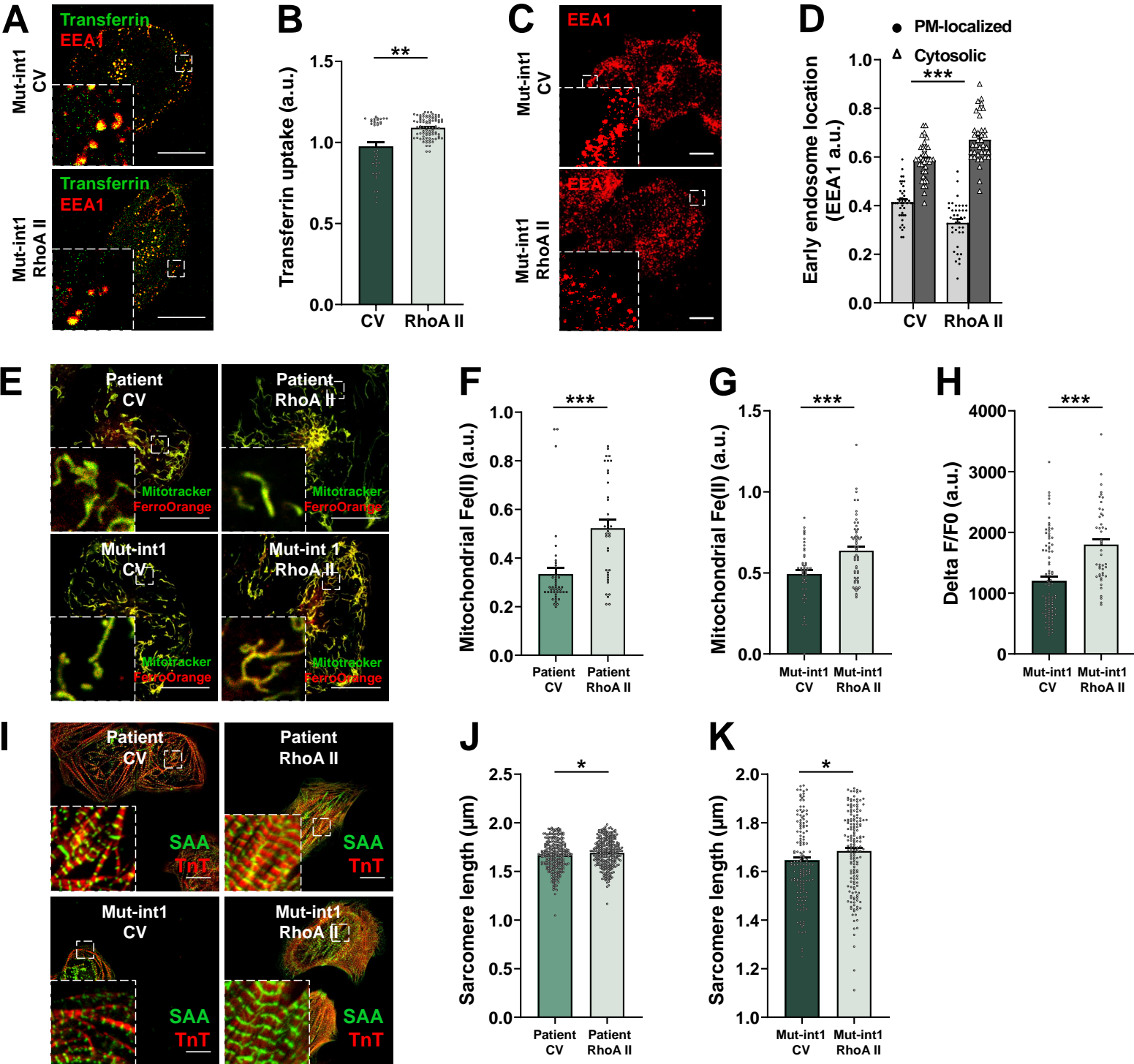
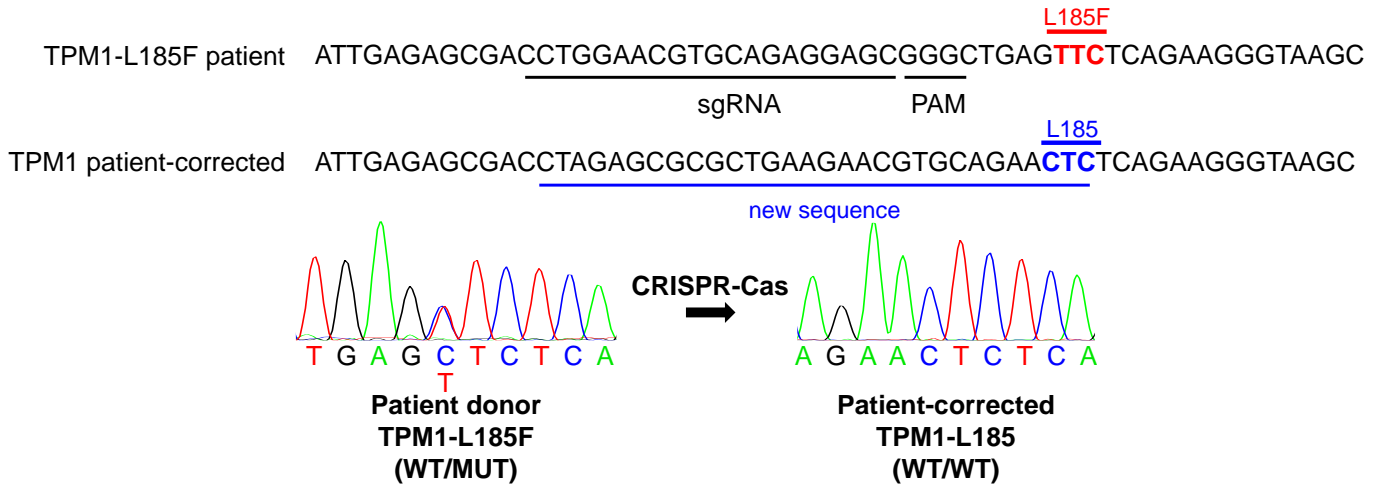
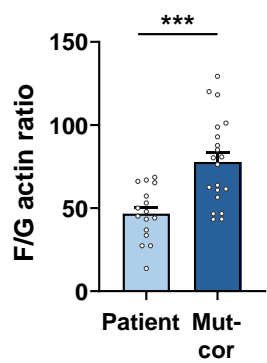


Fig. 6

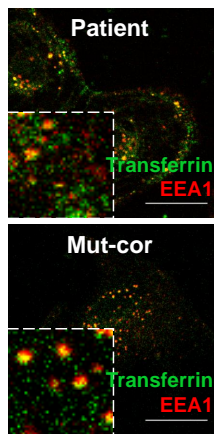
A



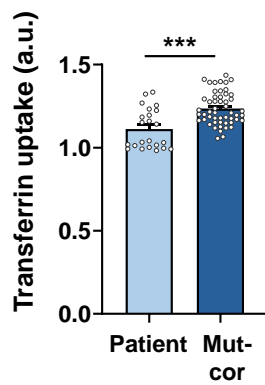
B



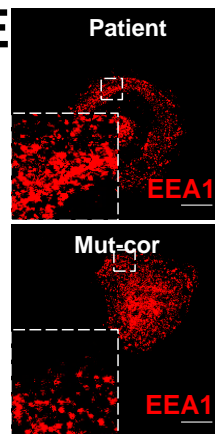
C



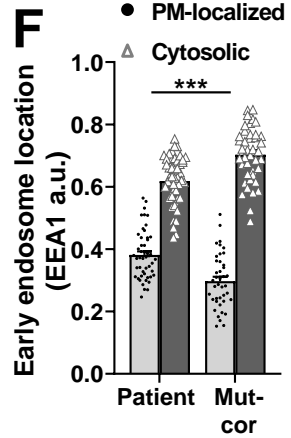
D



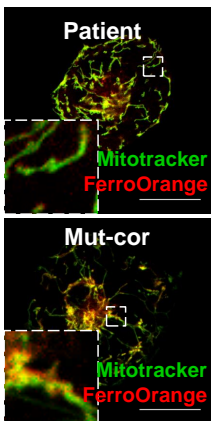
E



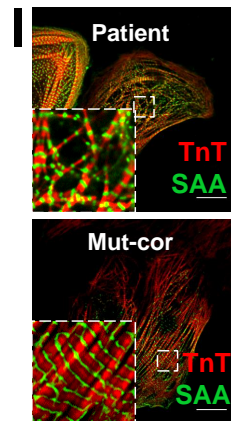
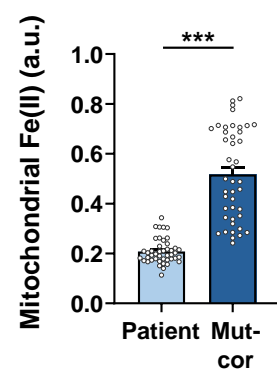
F



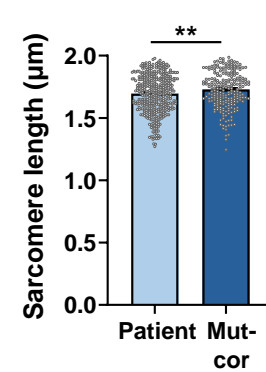
G



H



J



K

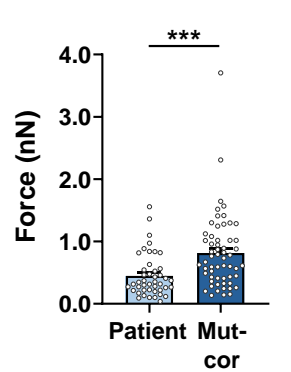


Fig. 7

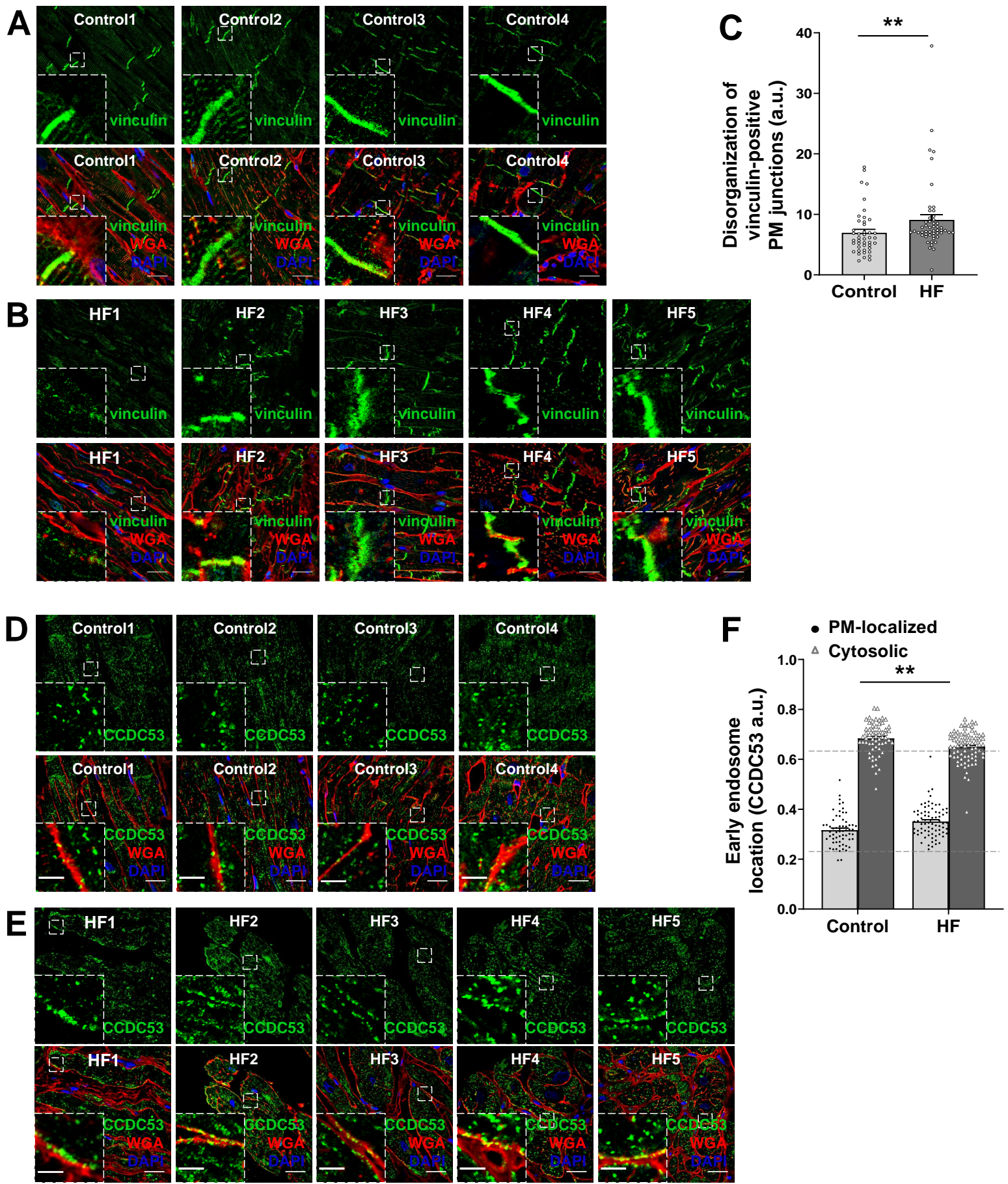
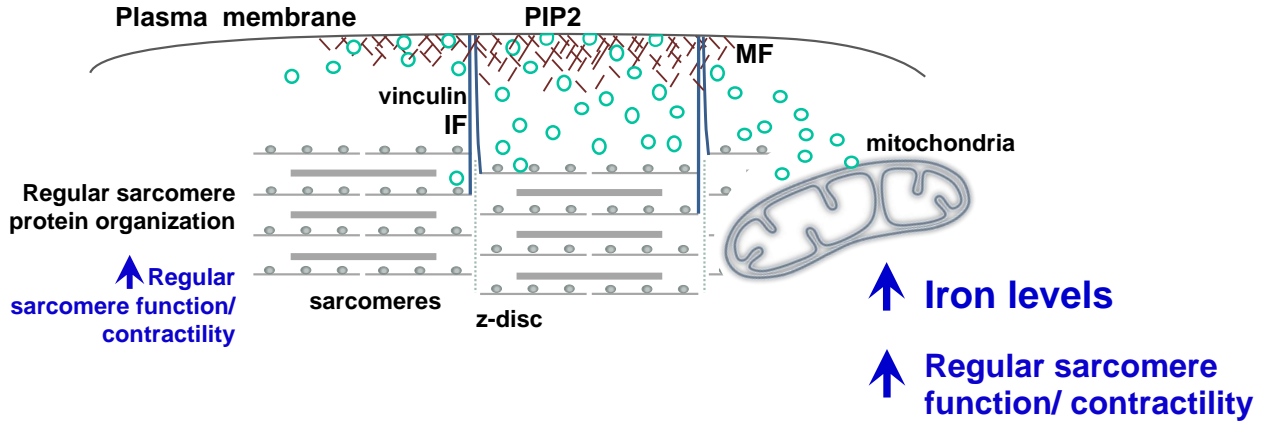
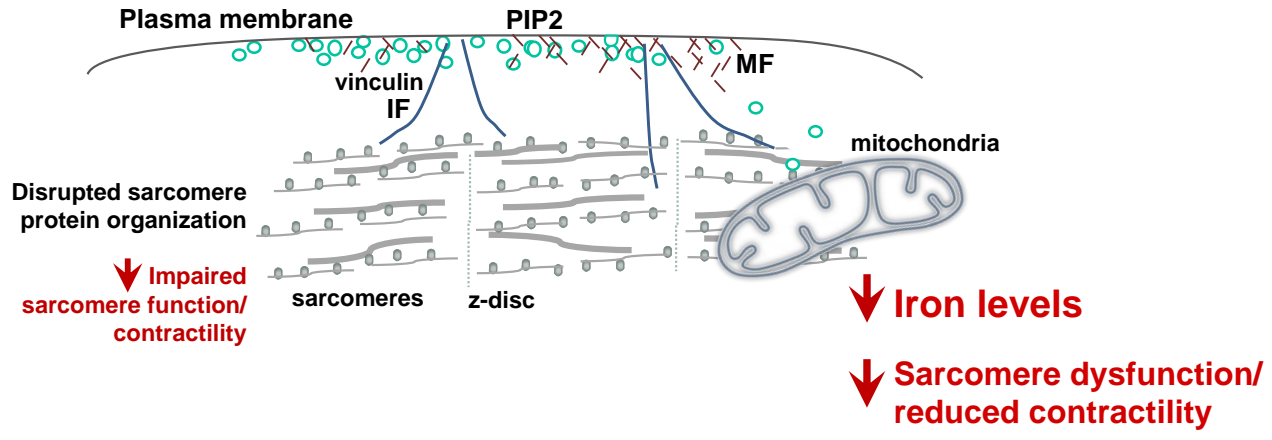


Fig. 8

WT



DCM (MUT)



- Early endosomes
- IF: Intermediate filaments
- MF: Microfilaments
- PIP2: Phosphatidylinositol 4,5-bisphosphate-enriched microdomains

Fig. S1

A

		At diagnosis				At latest follow up					
ID	BSA (m2)	Age(year)	LVEDD (mm)	LVEF (%)	ECG	Age(year)	LVEDD (mm)	LVEF (mm)	ECG	Medical therapy	NYHA class
I-1	n/a	62	n/a	n/a	n/a	n/a	n/a	n/a	n/a	n/a	n/a
II-2	1.81	47	61	50	SR, LVH	57	61	45	nsVT	ARB	2
II-5	1.95	53#	60	52	SR	63	67	27	nsVT, PVC (10%)	ARB, BB, MRA, D, ICD#	3
II-7	2.42	39	65	50	SR	50	63	50	SR	ARB, BB	1
III-1	n/a	<1§	n/a	n/a	n/a	-	-	-	-	-	-
III-3	1.82	15	74	15	SR	28	68	40	SR	ACEI, BB, MRA, DI, D	2
III-4	2.08	23	61	52	SR	30	60	51	SR	ACEI	1
III-5	n/a	15	73	15	SR, nsVT	-	-	-	-	HTx#	-

B

Normal ECG
Healthy sibling of II-4



C

Severe DCM
III-5

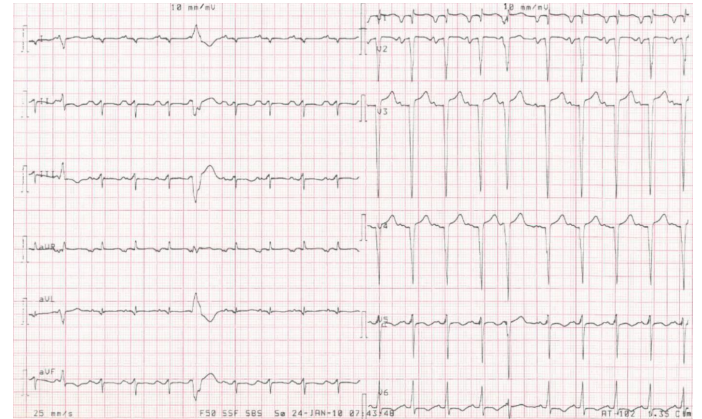


Fig. S2

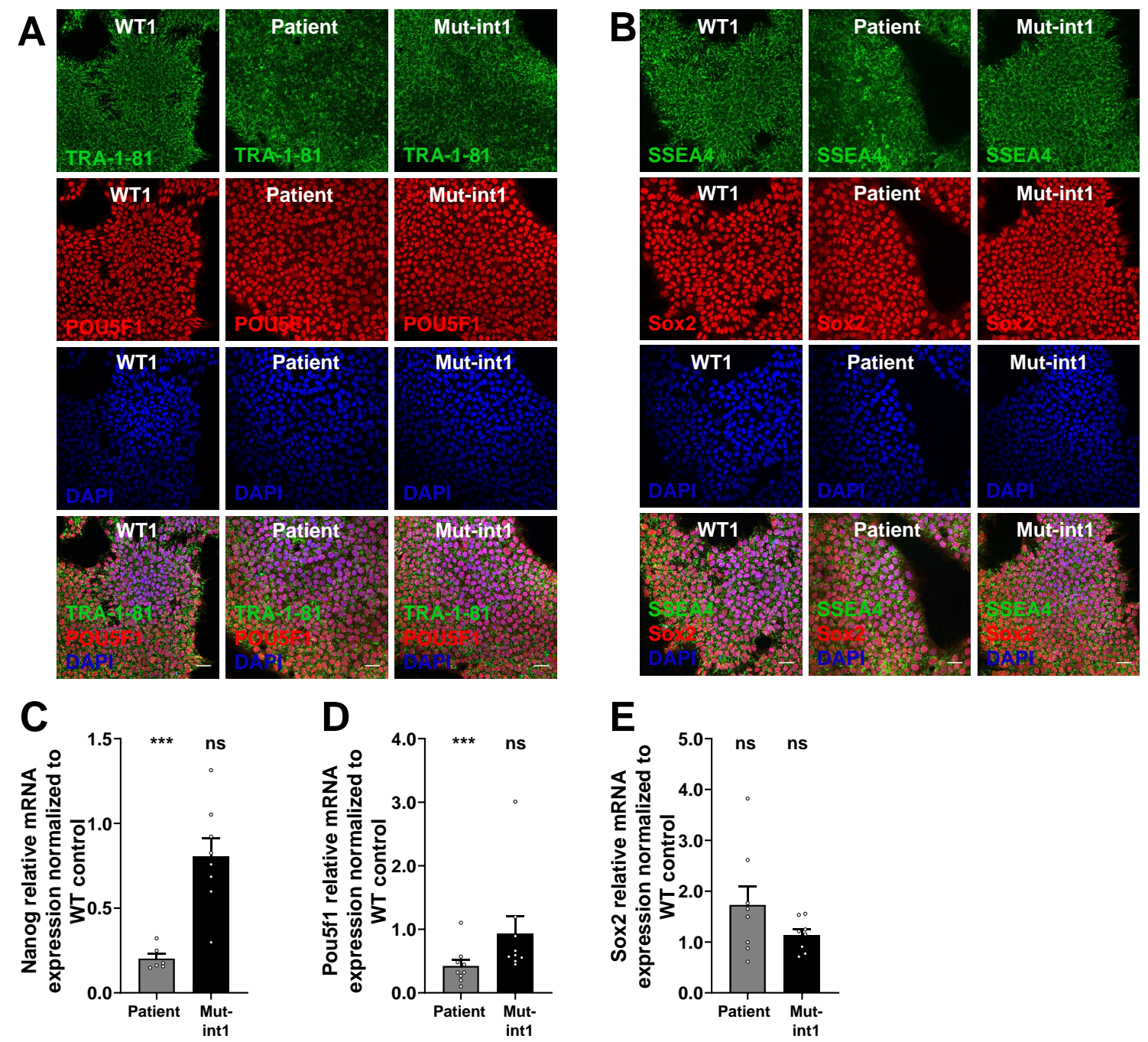


Fig. S3

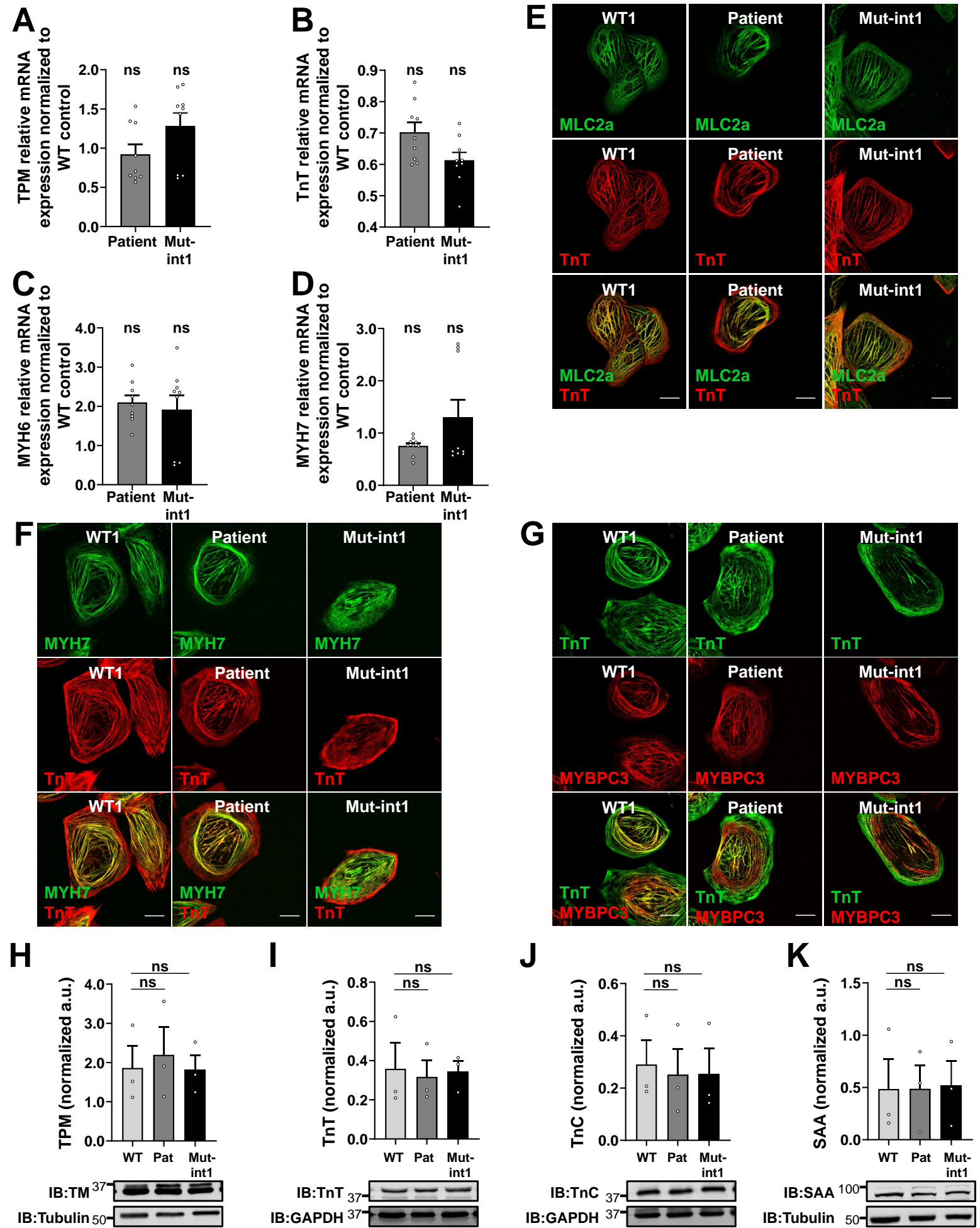


Fig. S4

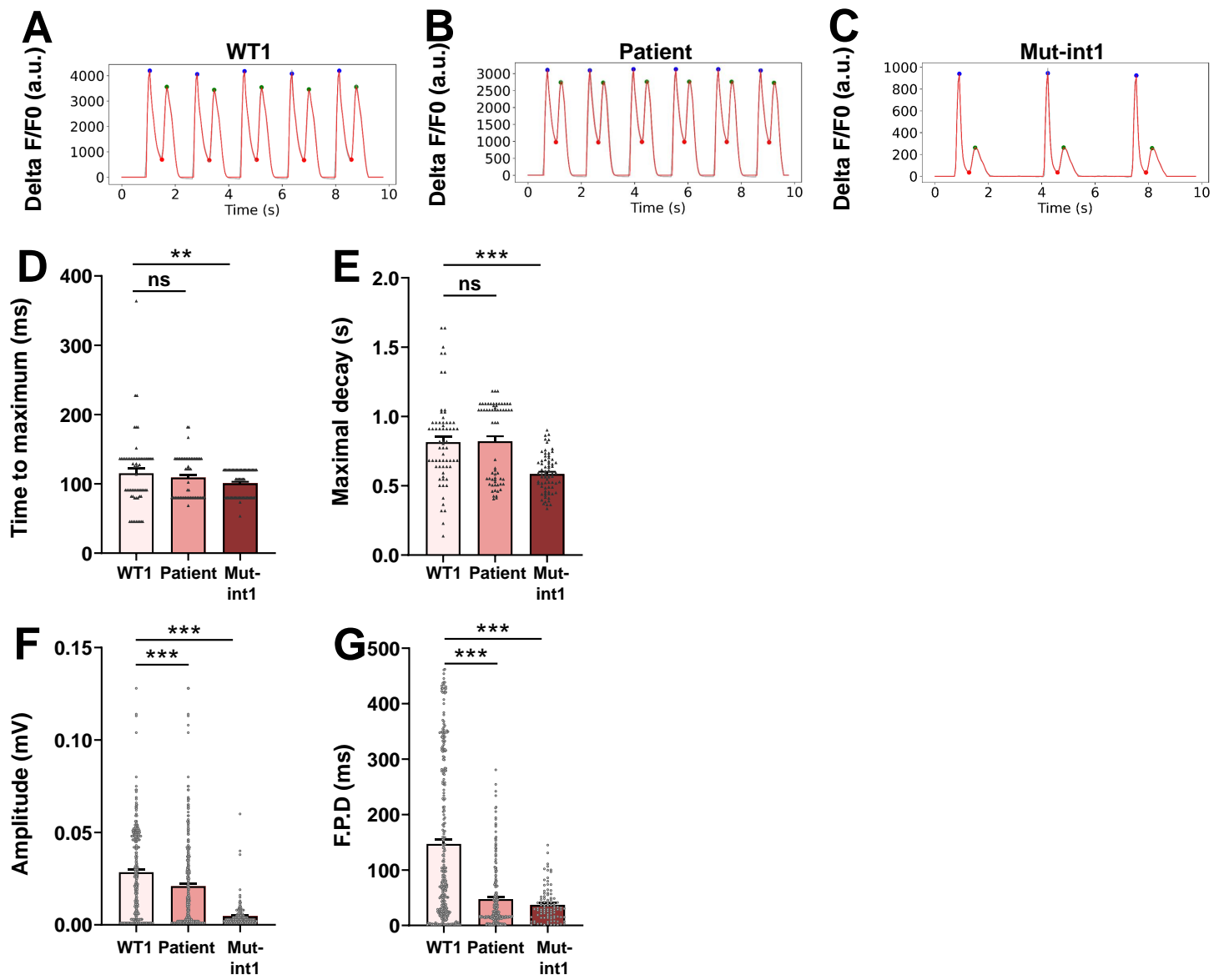


Fig. S5

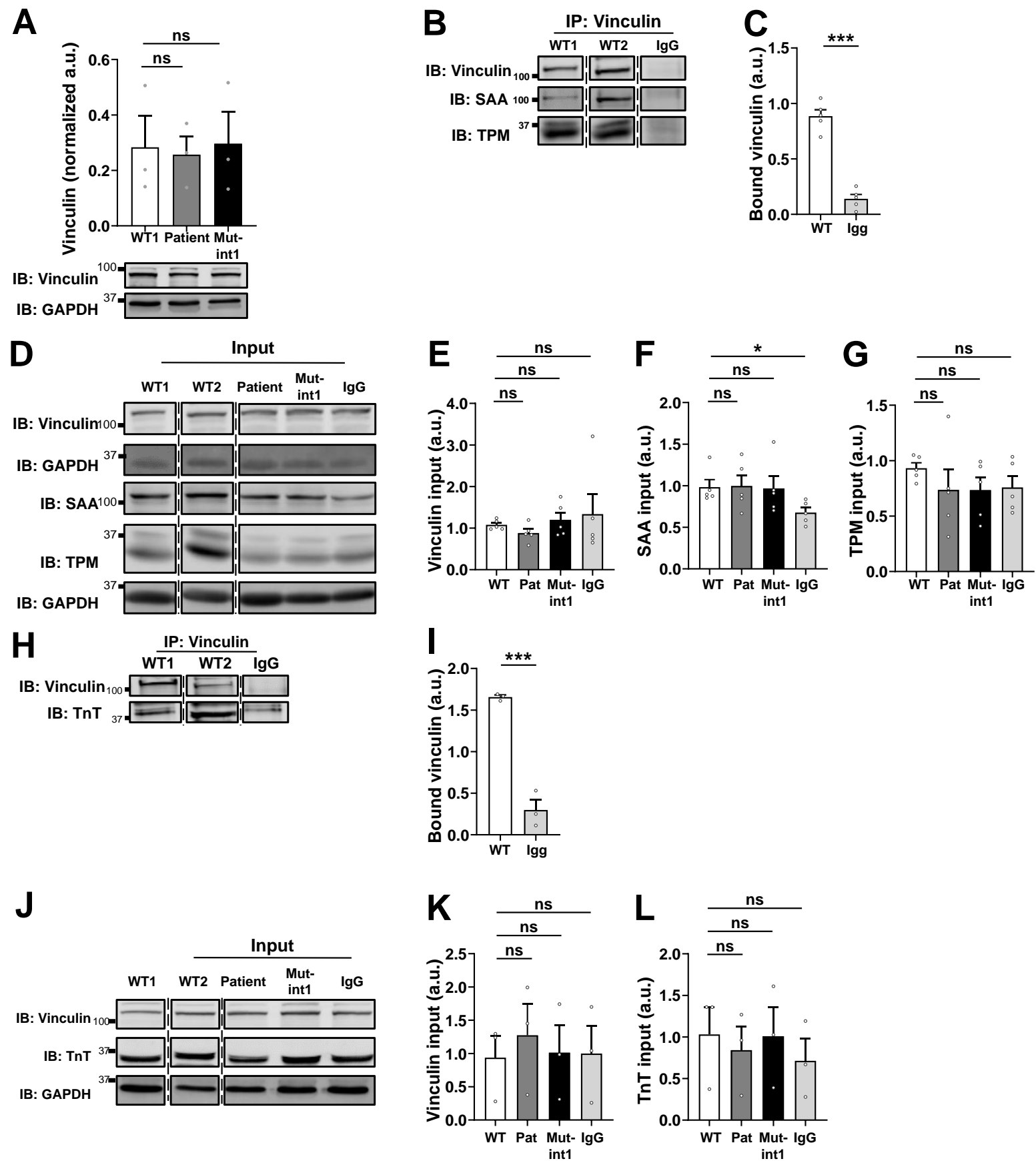


Fig. S6

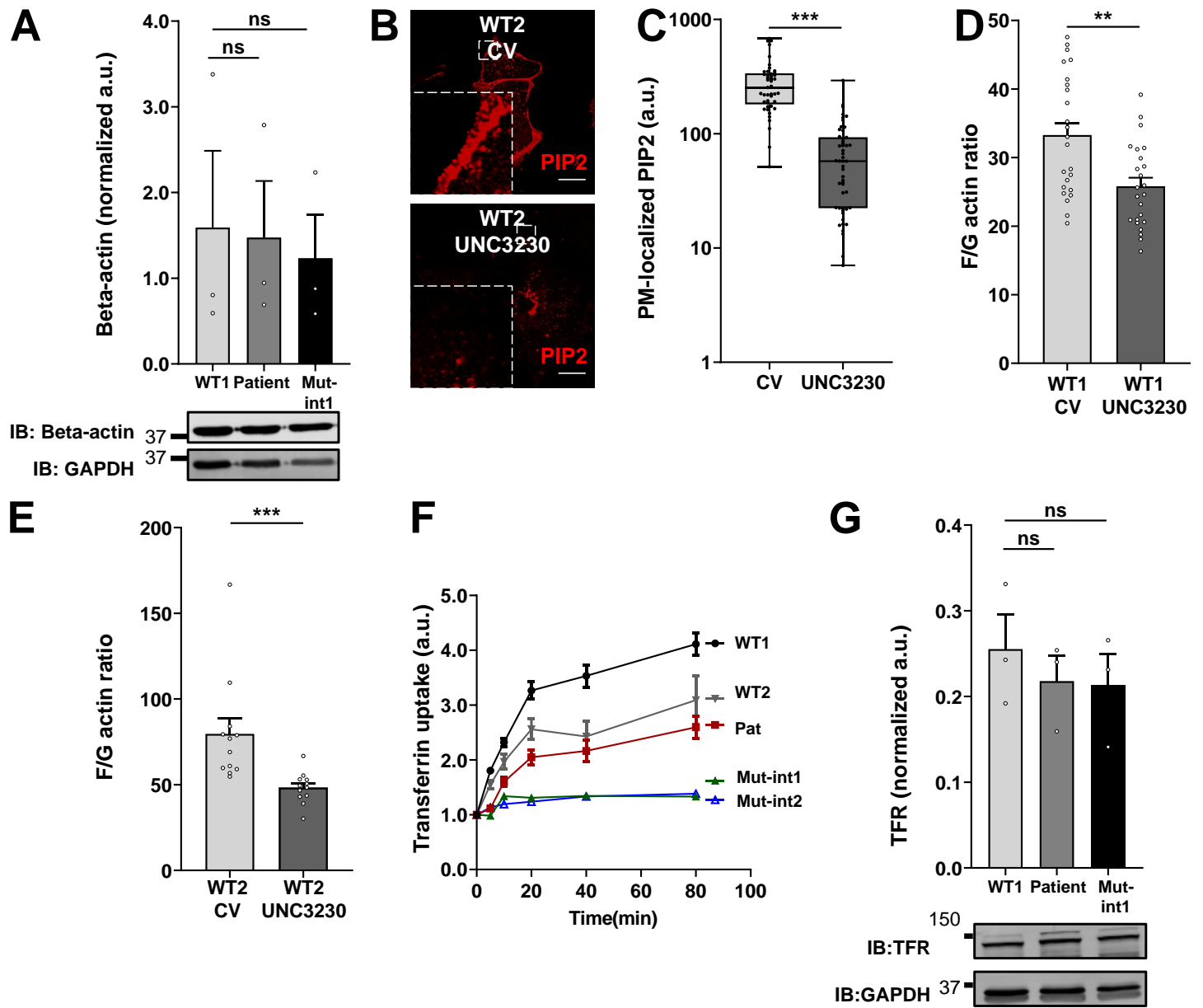


Fig. S7

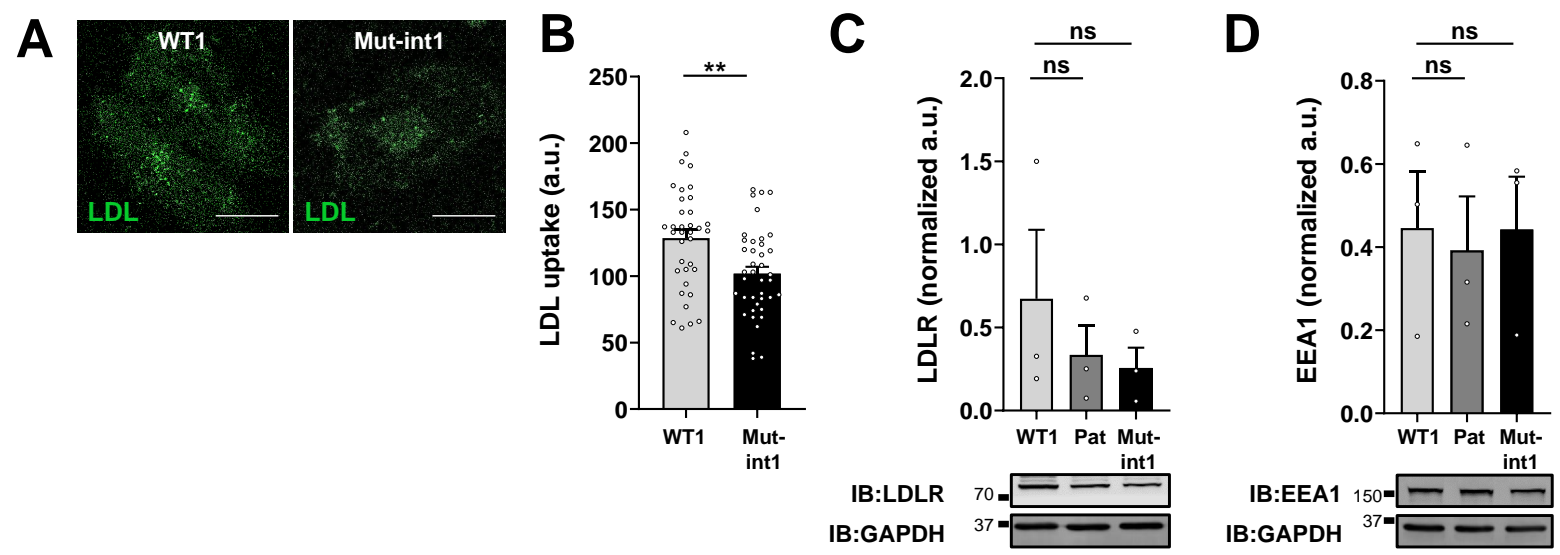


Fig. S8

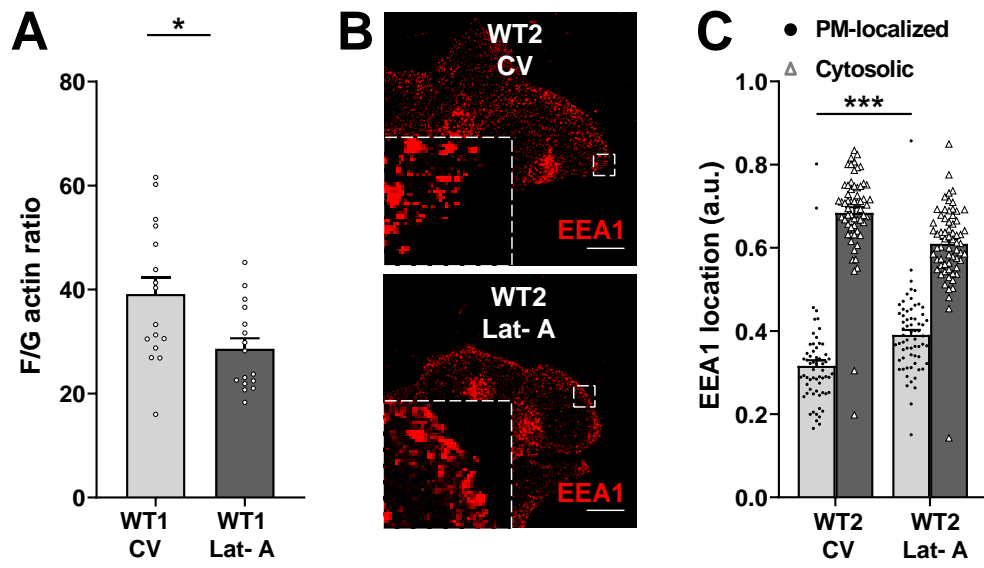


Fig. S9

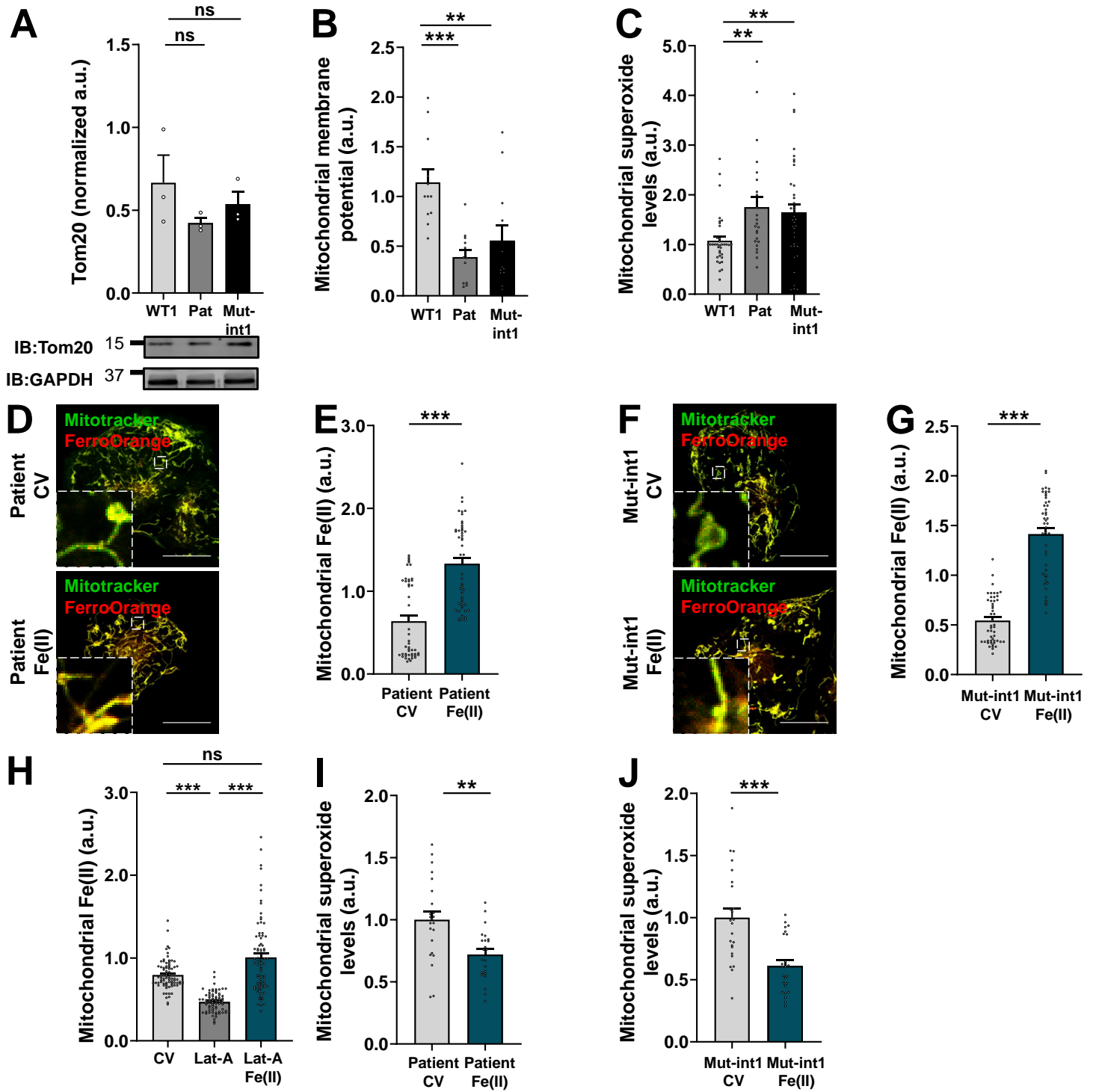


Fig. S10

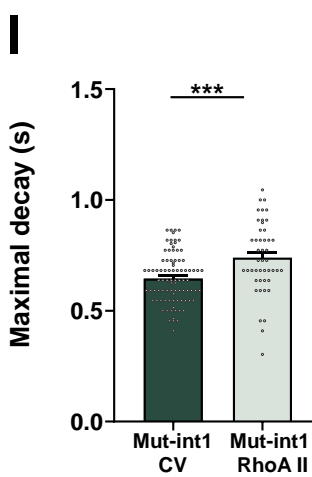
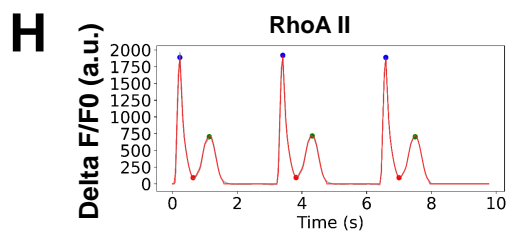
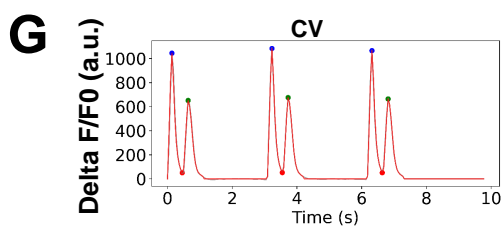
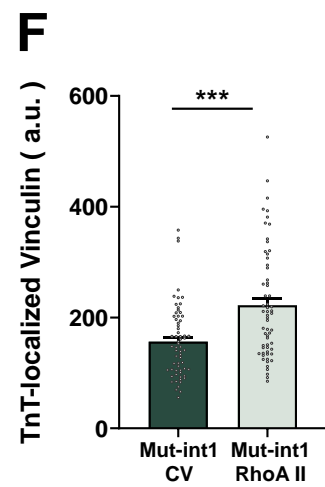
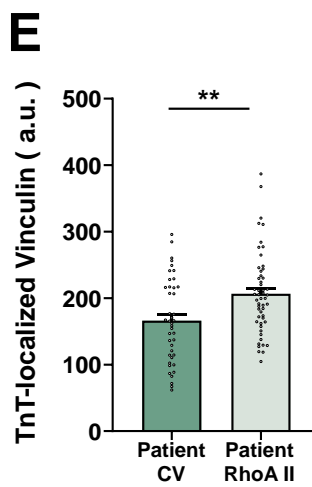
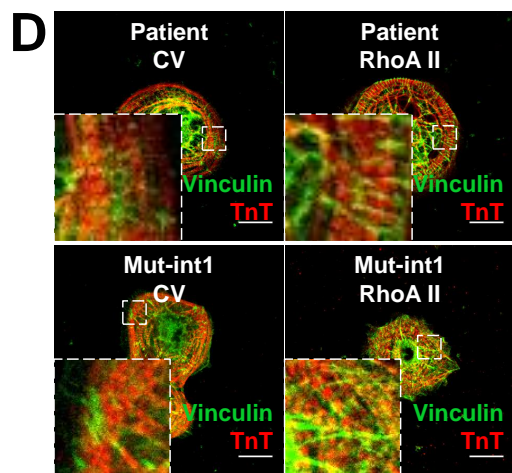
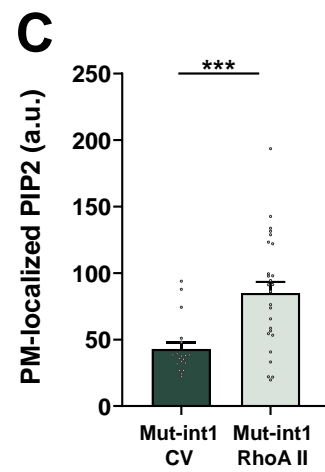
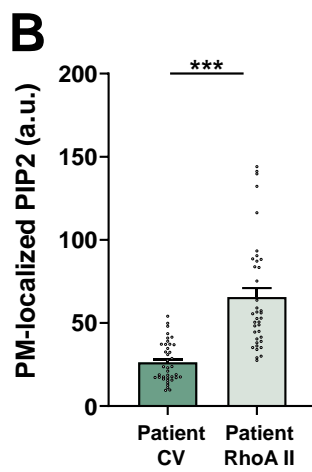
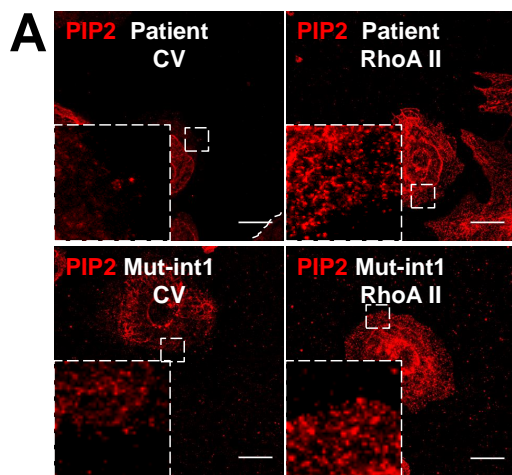


Fig. S11

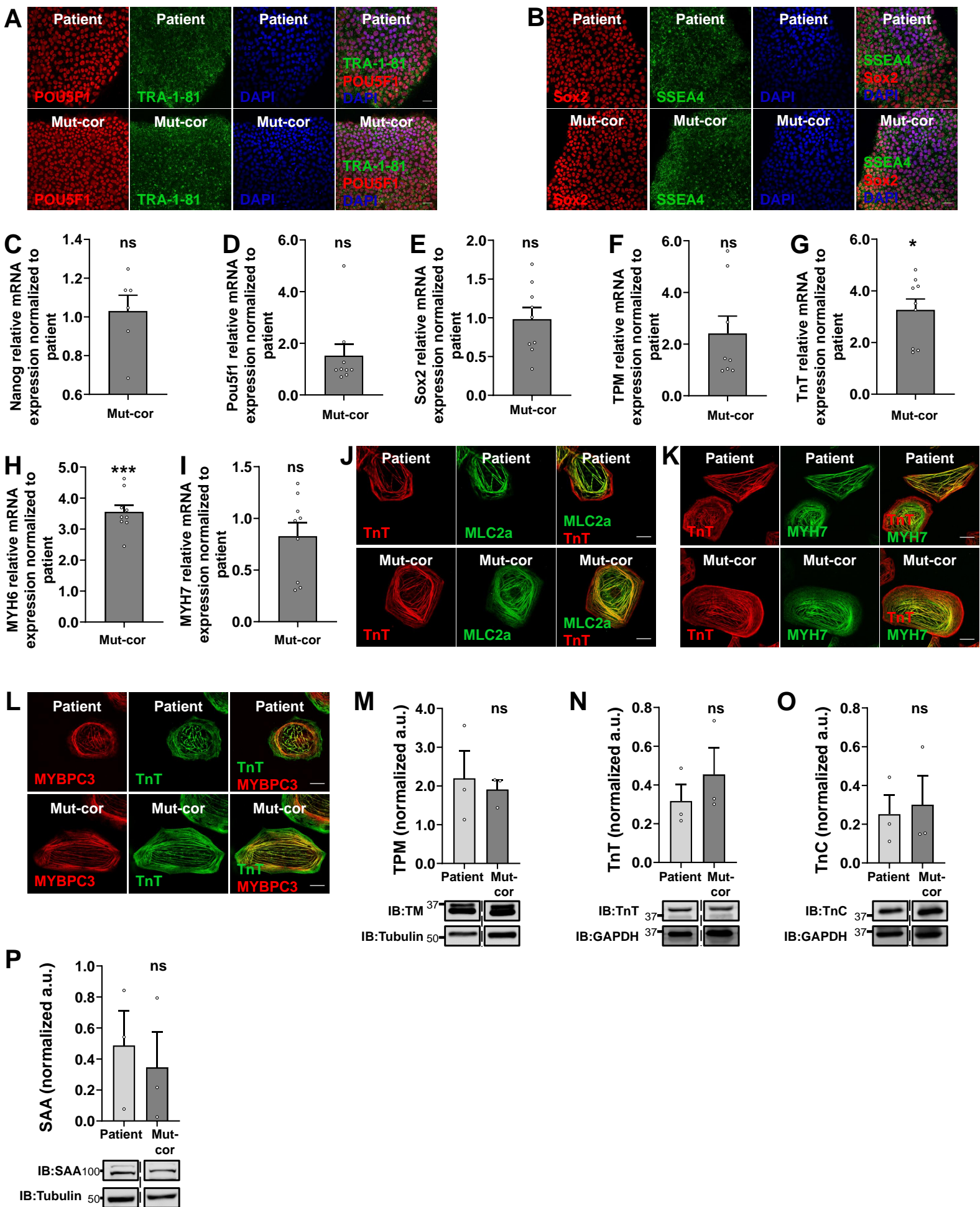


Fig. S12**A**

	ID	Conditions of patients
Control 1	Nr.19	severe aortic valve stenosis with compensated LV function that underwent surgical valve replacement
Control 2	Nr.19-3	severe aortic valve stenosis with compensated LV function that underwent surgical valve replacement
Control 3	Nr.20	severe aortic valve stenosis with compensated LV function that underwent surgical valve replacement
Control 4	Nr.31	severe aortic valve stenosis with compensated LV function that underwent surgical valve replacement
HF 1	Nr.60-4	heart transplantation because of severe heart failure due to dilated cardiomyopathy
HF 2	Nr.62-1	heart transplantation because of severe heart failure due to dilated cardiomyopathy
HF 3	Nr.73-2	heart transplantation because of severe heart failure due to dilated cardiomyopathy
HF 4	Nr.74-2	heart transplantation because of severe heart failure due to dilated cardiomyopathy
HF 5	Nr.68-2	heart transplantation because of severe heart failure due to dilated cardiomyopathy

B

	Control	HF
Indication for heart surgery	Aortic valve implantation + CABG	Heart transplantation
Count (n)	4	5
Clinical characteristics		
Age (years)	73.8 ± 3.0	58.6 ± 6.9
Sex, female, n (%)	1 (25)	1 (20)
Body mass index (kg/m ²)	24.3 ± 0.7	24.2 ± 3.9
LV ejection fraction (%)	58.5 ± 7.4	19.3 ± 9.3
LV assist device, n (%)	0 (0)	2 (40)
ICD, n (%)	0 (0)	3 (60)
Coronary artery disease, n (%)	4 (100)	0 (0)
Prior myocardial infarction, n (%)	2 (50)	0 (0)
Prior CABG, n (%)	0 (0)	0 (0)
Hypertension, n (%)	3 (75)	1 (20)
Hyperlipidemia, n (%)	3 (75)	0 (0)
Diabetes, n (%)	1 (25)	0 (0)
Atrial fibrillation, n (%)	2 (50)	4 (80)
Peripheral vascular disease, n (%)	0 (0)	0 (0)
Prior cerebral ischemia event, n (%)	0 (0)	0 (0)
Chronic pulmonary disease, n (%)	1 (25)	1 (20)
Medication		
ACE inhibitors	2 (50)	3 (60)
AT1 blockers	2 (50)	1 (20)
Beta-blockers	2 (50)	5 (100)
Calcium channel inhibitors	2 (50)	0 (0)
Digitalis	0 (0)	0 (0)
Lipid-lowering drugs	3 (75)	0 (0)
Mineralocorticoid-receptor antagonists	0 (0)	4 (80)
Other diuretics	1 (25)	4 (80)

Fig. S13

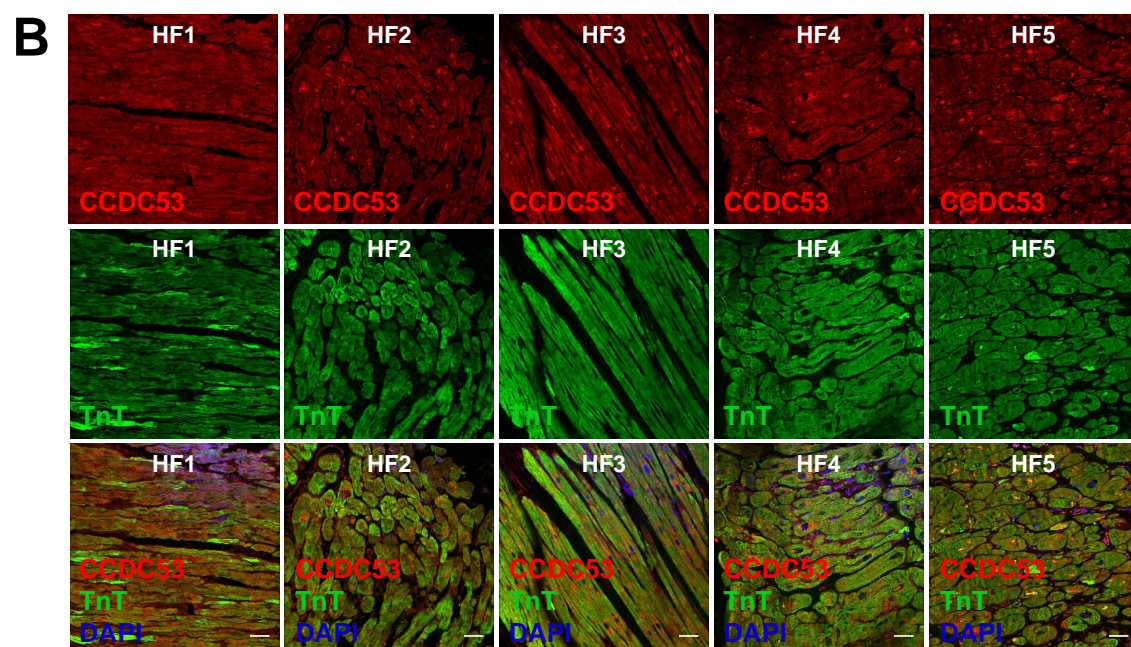
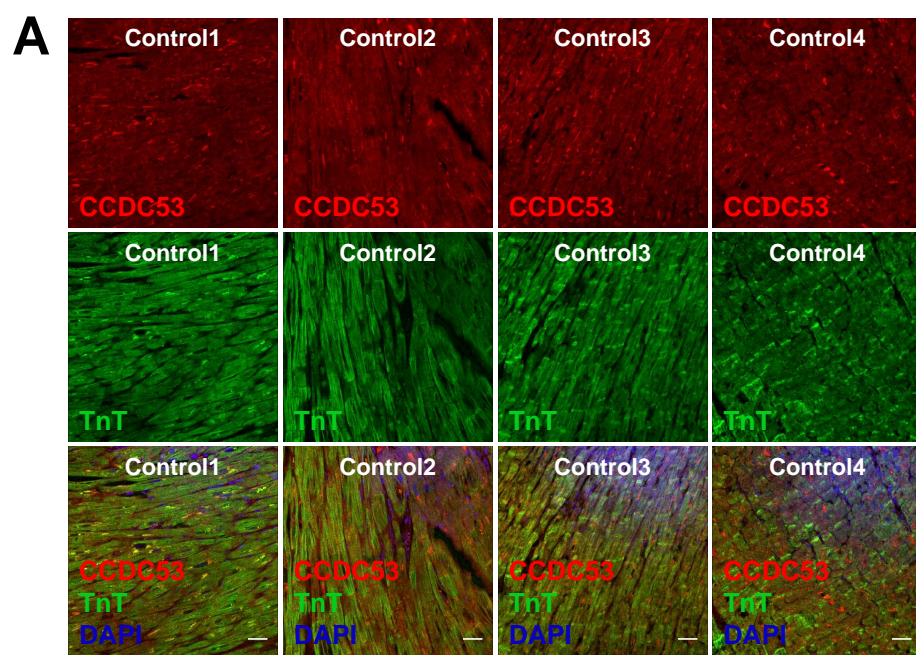
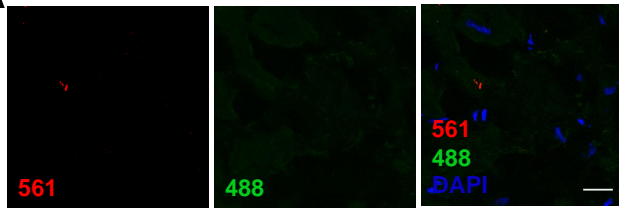
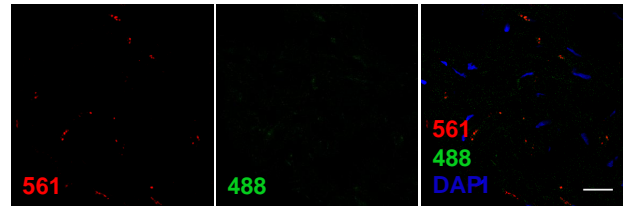


Fig. S14

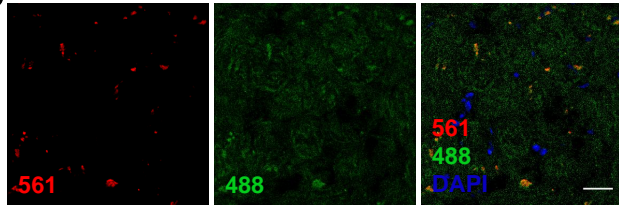
A CCDC53(Rabbit)+Alexa Fluor 488 anti-mouse antibody



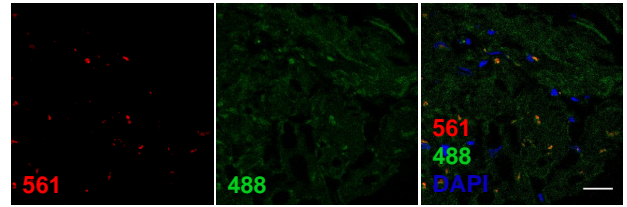
B TnT(mouse) and Alexa Fluor 561 anti-rabbit antibody



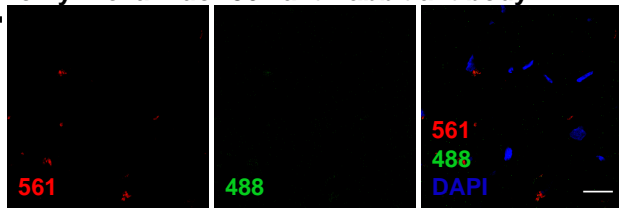
C only Alexa Fluor 488 anti-rabbit antibody



D only Alexa Fluor 488 anti-mouse antibody



E only Alexa Fluor 561 anti-rabbit antibody



SUPPLEMENTARY MATERIALS

An alternative mechanism of subcellular iron uptake deficiency in cardiomyocytes and treatment approach in heart failure

Yuanyuan Dai^{1,2}, Nadezda Ignatyeva^{1,2}, Hang Xu^{1,2}, Ruheen Wali^{1,2}, Karl Toischer^{1,2,3}, Sören Brandenburg^{1,2,3}, Christof Lenz⁴, Samuel Sossalla⁵, Niels Voigt^{2,6,7}, Elisabeth M. Zeisberg^{1,2},
Andreas Janshoff⁸, Henning Urlaub^{4,9}, Torsten Bloch Rasmussen¹⁰, Jens Mogensen¹¹,
Stephan E. Lehnart^{1,2,7}, Gerd Hasenfuss^{1,2,3}, Antje Ebert^{1,2}

¹ Heart Research Center Goettingen, Department of Cardiology and Pneumology, University Medical Center Goettingen, Georg-August University of Goettingen, Goettingen, Germany;

²DZHK (German Center for Cardiovascular Research), partner site Goettingen, Germany;

³Heart Center, Department of Cardiology and Pneumology, University Medical Center Goettingen, Goettingen University, Germany; ⁴Institute of Clinical Chemistry, University Medical Center, Goettingen University; ⁵Department for Internal Medicine II, University Medical Center Regensburg; ⁶Institute of Pharmacology and Toxicology University Medical

Center, Goettingen University; ⁷Cluster of Excellence “Multiscale Bioimaging: from Molecular Machines to Networks of Excitable Cells” (MBExC), Goettingen University;

⁸Institute for Physical Chemistry, Goettingen University, Germany; ⁹Bioanalytical Mass Spectrometry, Max Planck Institute for Biophysical Chemistry, Goettingen; ¹⁰Department of

Cardiology, Regional Hospital West Jutland, Herning, Denmark; ¹¹Department of Cardiology,
Aalborg University Hospital, Aalborg, Denmark.

Correspondence: Antje Ebert, Goettingen University Medical Center, Goettingen University,
Robert-Koch-Strasse 40, 37075 Goettingen, Germany. Email: [antje.ebert@med.uni-
goettingen.de](mailto:antje.ebert@med.uni-goettingen.de)

DETAILED METHODS

Human iPSC reprogramming and culture. The protocols for the studies with iPSC were approved by the Goettingen University Ethical Board (15/2/20 and 20/9/16An) and the Odense University Ethical Board (Projekt ID S-20140073HLP). Informed consent was obtained from all participants and all research was performed in accordance with relevant guidelines and regulations. Approval for the study of human myocardial samples was granted by the Goettingen University Ethical Board (No. 21/10/00 and 31/9/00), and written informed consent was obtained from all patients. The procedures used in this study adhere to the tenets of the Declaration of Helsinki. A TPM1-L185F family cohort was recruited for this study and five mutation carriers as well as four healthy donors donated a skin biopsy. From all skin biopsies, fibroblasts were derived and employed for iPSC reprogramming. The skin punch biopsies were dissociated, and isolated skin fibroblasts were kept in Dulbecco's modified Eagle's medium (Life Technologies) supplied with 10% fetal bovine serum (Gibco) under sterile culture conditions at 37°C. For generation of the human iPSC lines, human fibroblasts from skin biopsies were reprogrammed to hiPSCs using the CytoTune™-iPS 2.0 Sendai Reprogramming Kit (Thermo Fisher Scientific) and colonies with stem cell-like morphology were picked and expanded (1-4). Individuals II-4 and III-5 and the corresponding human iPSC lines control WT 1 (WT/WT) and DCM patient-specific TPM1-L185F (WT/MUT) were selected for this study. Individual II-4 is a 55-year-old male who presented with no phenotype or symptoms and was negative for the TPM1-L185F mutation (WT/WT). Individual III-5 is a 27-year-old female patient with severe DCM who presented with non-sustained ventricular tachycardia and received a heart transplantation when 15 years old due to end-stage heart failure. Patient III-5

genotyped positive for the TPM1-L185F mutation (WT/MUT). WT/WT iPSCs from control WT 1 and DCM patient-specific TPM1-L185F iPSCs (WT/MUT) were utilized to generate a set of isogenic control lines that diverge from the respective parental line only in the site of the TPM1-L185F mutation. WT/WT iPSCs were used as parental line to generate TPM1-L185F MUT-introduced iPSCs (MUT-int/MUT-int). WT/MUT patient-specific iPSCs were employed to generate TPM1-L185F MUT-corrected iPSCs (WT-cor/WT-cor). The iPSC line control WT 2, a kind gift by Joseph C. Wu (Stanford University, CA), was reported and characterized previously (1, 5, 6). The derivation of the TnT-R141W CRISPR/Cas9 mutation-introduced iPSC line, TnT-R141W MUT-int/MUT-int, has been described before (6). The isogenic parental line for TnT-R141W MUT-int/MUT-int is the iPSC line control WT 2 (6). The iPSC lines have been deposited at the Goettingen University Medical Center Biobank (control WT 1, DCM patient-specific TPM1-L185F) or the Stanford Cardiovascular Institute Biobank (control WT 2). Human iPSCs were grown as described previously on Matrigel-coated plates (ES qualified, BD Biosciences) using chemically defined E8 medium (3, 7, 8). The culture medium was changed daily, and iPSCs were passaged every four days using EDTA (Life Technologies).

Cardiac differentiation of human iPSC. Human iPSCs were grown to 80–90% confluence using matrigel-coating and chemically defined E8 medium (7). Subsequently, iPSCs were differentiated into beating cardiomyocytes with a small molecule–based monolayer method described previously (9, 10). Briefly, a GSK inhibitor, Chir (Selleckchem) was applied for 24–48 h, followed by addition of a canonical Wnt-signaling inhibitor, IWR1 (Selleckchem). From

day 7-10 onward, beating iPSC-derived cardiomyocytes (iPSC-CMs) were observed. Subsequently (from day 7 onward), human iPSC-CMs were cultured in RPMI medium plus B-27 Supplement (Life Technologies). Following 20-22 days of cardiac differentiation, beating iPSC-CM monolayers were dissociated using TrypleE (Life Technologies) and plated in suitable assay formats.

CRISPR/Cas9 genetic engineering, molecular cloning, and plasmid sources.

CRISPR/Cas9-mediated gene editing via homology-directed repair to introduce the TPM1-L185F mutation into WT/WT iPSCs or correct this mutation in the DCM patient-specific TPM1-L185F WT/MUT iPSCs was performed as described before (6, 11-13). In brief, the sgRNA sequence (5'-CCTGGAACGTGCAGAGGAGC-3') was subcloned into the pSpCas9(BB)-2A-Puro plasmid. Subsequently, to produce TPM1-L185F MUT-introduced iPSCs (MUT-int/MUT-int), sgRNA and the new sequence (5'-CTAGAGCGCGCTGAAGAACGTGCAGAATTC-3' in a pUC vector backbone) containing the single nucleotide exchange C to T, which results in TPM1-L185F, were transfected into iPSCs via electroporation. Likewise, to generate TPM1-L185F MUT-corrected iPSCs (WT-cor/WT-cor), the sgRNA and respective new sequence (5'-CTAGAGCGCGCTGAAGAACGTGCAGAACTC-3' in a pUC vector backbone), were transfected into iPSCs. Single clones were isolated and sequence verified.

Nanion CardioExcyte 96 measurements. Human iPSC-CMs on day 17-19 of differentiation were washed with PBS and dissociated using TrypleE (Life Technologies). After spinning

iPSC-CMs for 5min at 200g, 37°C, cells were resuspended in culture medium supplemented with 5% FBS and seeded on Nanion CardioExcyte 96 Plates. Cells were allowed to recover from the passage for 6-7 days. Plates were recorded using a Nanion CardioExcyte 96 instrument with temperature control. Data were acquired and analyzed via CardioExcyte Control software.

Immunoprecipitation and immunoblotting. Vinculin-specific antibody (Thermo Fisher Scientific) was immobilized on Dyna beads (Thermo Fisher Scientific) according to the manufacturer's instructions. Lysates from WT and patient iPSC-CMs were prepared for immunoprecipitation binding with washing buffer (25 mM Tris, NaCl 150 mM, EDTA 1mM, pH=7.5). Eluted protein solutions as well as lysate input were subjected to SDS-PAGE and transferred to PVDF membranes. Membranes were scanned in LI-COR machine after incubated with primary and secondary antibodies (LI-COR). Quantification was done by Image Studio Lite Ver 5.2.

Confocal live imaging, Fe measurements, continuous transferrin uptake, and LDL uptake. Human iPSC-CMs were plated into imaging chambers 2-3 days before the experiments and with Mitotracker Green (Cell Signaling Technology) at 37°C as by the manufacturer's instructions, then incubated cells with 100 μM ammonium Fe²⁺ (Santa Cruz) and subsequently incubated with FerroOrange (Dojindo EU GmbH) as by the manufacturer's instructions. Images were acquired using a confocal microscope (Carl Zeiss, LSM 710 Meta, Göttingen, Germany). To measure transferrin uptake, iPSC-CMs were starved for 1h at 37°C in RPMI

medium containing human albumin and ascorbic acid as described before (4). Cells were incubated with 20µg/mL transferrin (Alexa Fluor™ 488 Conjugate, Thermo Fisher Scientific) for indicated times at 37°C. Following a PBS wash, cells were fixed for 20 min at room temperature for each individual time point. Z-stack images were taken under a 20x (plan apochromat) confocal objective (Carl Zeiss, LSM 710 Meta, Göttingen, Germany). Mean fluorescence from each time point is normalized by the data acquired at 0 min. To measure LDL uptake, cells were incubated with LDL-BODIPY (Thermo Fisher Scientific) as by the manufacturer's instructions for 0 min or 10 min at 37°C. Subsequently, cells were washed with PBS and fixed for 20 min at room temperature. Images were acquired under a 63x (plan apochromat oil) objective from a confocal microscope (Carl Zeiss, LSM 710 Meta, Göttingen, Germany) and ZEN software (Carl Zeiss) as well as ICY software was used for data analysis.

Immunohistochemistry (IHC) staining and confocal microscopy. Cells were grown on glass coverslips (Thermo Fisher Scientific), fixed with 4% glyoxal (17) or 4% PFA, permeabilized in 0.01% digitonin 20min or 0.2% TritonX-100 60min at room temperature (RT). Afterwards cells were incubated with primary antibodies: POU5F1 (Cell Signaling Technology), TRA-1-60 (Chemicon), SSEA4 (R&D systems), EEA1 (Cell signaling Technology), PI3P (Echelon Biosciences), TnT (Thermo Fisher Scientific), SAA (Sigma), TPM (Abcam), vinculin (Sigma), PIP2 (Echelon Biosciences), CCDC53 (ProteinTech) overnight at 4°C and secondary antibodies (Alexa Fluor dyes, Thermo Fisher Scientific) at RT 2 hours. Coverslips were mounted onto a glass slide in FluroMount mounting medium (Thermo Fisher Scientific). Images were taken with 63x (plan apochromat oil) objectives from a

confocal microscope (Carl Zeiss, LSM 710 Meta, Göttingen, Germany) and ZEN software (Carl Zeiss).

SUPPLEMENTAL FIGURE LEGENDS

Fig. S1. Clinical data of individuals from the recruited family carrying the TPM1-L185F variant

(A) Clinical data from family carrying TPM1-L185F mutation. BSA, body surface area; LVEDD, left ventricular end-diastolic diameter; LVEF, left ventricular ejection fraction; ECG, electrocardiogram; NYHA, New York Heart Association. ARB, angiotensin receptor blocker; BB, beta receptor blocker; MRA, mineralocorticoid receptor blocker; D, diuretic; DI, digoxin; ICD, implantable cardioverter defibrillator; SR, sinus rhythm; LVH, left ventricular hypertrophy; nsVT, non-sustained ventricular tachycardia; PVC, premature ventricular contractions; HTx, heart transplantation. §, died nine months old of dilated cardiomyopathy. #, ICD for primary prevention. No therapies for ventricular tachycardia or -fibrillation delivered at follow up. ☐, underwent subacute heart transplantation following diagnosis. (B-C) Electrocardiograms (ECGs) for a healthy sibling of II-4 (healthy donor, HD) (B) and patient III-5, a 15-year-old male carrier who received a heart transplantation. ECG displayed non-sustained ventricular tachycardia and poor precordial R-wave progression (C).

Fig. S2. Characterization of iPSCs

(A-E) iPSCs show regular expression of stem cell marker, such as POU5F1, TRA-1-81, SOX2 and SSEA-4. (A-B) Representative 20x confocal images of human iPSC following immunostaining for pluripotency markers (A) 20x confocal images of human iPSCs clones stained with POU5F1 and TRA-1-81 antibodies; scale bar, 40 μ m. (B) Representative 20x confocal images of human iPSCs clones stained with SOX2 and SSEA-4 antibodies. Scale bar, 40 μ m. (C-E)

iPSCs show regular expression of pluripotency markers at mRNA levels, such as Nanog (C), Pou5f1 (D) and Sox2 (E). (C) ***P<0.001 for WT control (WT1, WT/WT) vs. DCM patient-derived (Pat) iPSC-CMs; ns, not significant for WT1 vs. TPM1-L185F mutation-introduced iPSC-CMs (Mut-int1, MUT-int/MUT-int) iPSC-CMs (one-way ANOVA and Dunn's multiple comparisons test). (D) ***P<0.001 for WT1 vs. patient; ns, not significant for WT1 vs. Mut-int1 iPSC-CMs (one-way ANOVA and Sidak's multiple comparisons test). (E); ns, not significant for WT1 vs. patient and WT1 vs. Mut-int1 iPSC-CMs (one-way ANOVA and Dunn's multiple comparisons test). Data are shown as mean \pm sem.

Fig. S3. Expression levels of cardiac markers are comparable in iPSC-CMs carrying the TPM1-L185F mutation versus WT

(A-D) Human iPSC-CMs displayed regular expression of cardiac markers at mRNA levels, such as (A) TPM, (B) TnT, (C) MYH6 and (D) MYH7. (A, C) ns, not significant for WT control (WT1, WT/WT) vs. DCM patient-derived (Pat, WT/MUT) and WT1 vs. TPM1-L185F mutation-introduced iPSC-CMs (Mut-int1, MUT-int/MUT-int) iPSC-CMs (one-way ANOVA and Dunn's multiple comparison test). (B, D) ns, not significant for WT1 vs. patient and WT1 vs. TPM1-L185F Mut-int1 iPSC-CMs (one-way ANOVA and Sidak's multiple comparisons test). (E-G) iPSC-CMs displayed regular expression of cardiac markers. (E) Representative 63x confocal images of iPSC-CMs following immunostaining with MLC2a and TnT antibodies. (F) Representative 63x confocal images of iPSC-CMs following immunostaining with MYH7 and TnT antibodies. (G) Representative 63x confocal images of iPSC-CMs following immunostaining with MYBPC3 and TnT antibodies; scale bar, 20 μ m. (H-K) iPSC-CMs

display regular expression of cardiac markers at protein levels. Representative scans of immunoblots and quantification from cardiac markers, such as (H) TPM, (I) TnT, (J) TnC and (K) SAA. Bargraphs displayed averages of n=3 experiments and representative immunoblots were shown below; ns, not significant for WT1 vs. patient and WT1 vs. Mut-int 1 iPSC-CMs (one-way ANOVA and Sidak's multiple comparisons test). Data are shown as mean \pm sem.

Fig. S4. The TPM1-L185F mutation results in defective contractility as well as reduced field potential duration and amplitude

(A-E) Reduced contractility in DCM patient-derived (Pat, WT/MUT) and TPM1-L185F mutation-introduced iPSC-CMs (Mut-int1, MUT-int/MUT-int). (A-C) Representative recordings from each group. TPM1-L185F mutation-introduced iPSC-CMs (Mut-int1) showed reduced time to maximum (D) and maximal decay (E). (D) ns, not significant for WT1 vs. patient; **P<0.01 WT1 vs. Mut-int1. (E) ns, not significant for WT1 vs. patient; ***P<0.001 WT1 vs. Mut-int1. (FG) Nanion electrophysiology analysis. (F) Reduced amplitude in patient and TPM1-L185F MUT-int1 iPSC-CMs. ***P<0.001 for WT1 vs. patient and WT1 vs. Mut-int1. (G) Reduced field potential duration in patient and TPM1-L185F mutation-introduced iPSC-CMs (Mut-int1). ***P<0.001 for WT1 vs. patient and WT1 vs. Mut-int1. One-way ANOVA and Dunn's multiple comparisons test was used to calculate the statistics. Data are shown as mean \pm sem.

Fig. S5. Relative controls for immunoprecipitation of vinculin for interactions with sarcomeric proteins (relating to main figure 2)

(A) The protein levels of vinculin were not significantly different among groups. Representative membrane scans of blots and quantification were shown. Data were normalized by GAPDH. ns, not significant for WT1 vs. DCM patient-derived (Pat) t and WT control (WT1, WT/WT) vs. TPM1-L185F mutation-introduced iPSC-CMs (Mut-int1, MUT-int1/MUT-int) (one-way ANOVA and Sidak's multiple comparisons test). (B-C) IgG control showed significantly reduced binding ability with vinculin compared to WT groups. (B) Representative membrane scans were shown. (C) Quantification of (B). ***P<0.001 for WT vs. IgG (unpaired t test). (D-G) The protein levels of vinculin (E), SAA (F) and TPM (G) were not significantly different in DCM patient-derived (Pat, WT/MUT) and TPM1-L185F mutation-introduced iPSC-CMs (Mut-int1, MUT-int1/MUT-int) compared to WT group in input fractions. (D) Representative membrane scans of membranes from input samples. (E) ns, not significant for WT vs. patient, WT vs. Mut-int1 iPSC-CMs and WT vs. IgG. (F) ns, not significant for WT vs. patient and WT vs. Mut-int1. *P<0.05 for WT vs. IgG. (G) ns, not significant for WT vs. patient, WT vs. Mut-int1 and WT vs. IgG (one-way ANOVA and Sidak's multiple comparisons test). Data were normalized by GAPDH. (H-I) IgG control showed significantly reduced binding ability with vinculin compared to WT group. (H) Representative membrane scans were shown. (I) Quantification of (H). ***P<0.001 for WT vs. IgG (unpaired t test). (J-L) Protein levels for vinculin (K) and TnT (L) were not significantly different between groups. (J) Representative membrane scans of input samples were shown. (K) ns, not significant for WT vs. patient, WT vs. Mut-int1 and WT vs IgG (one-way ANOVA and Sidak's multiple comparisons test). (L) ns, not significant for WT vs. patient, WT vs. Mut-int1 and WT vs igg. Statistics were calculated by one-way ANOVA and Dunn's multiple comparisons test unless indicated otherwise. Data

were normalized by GAPDH. Data are shown as mean \pm sem.

Fig. S6. Plasma membrane-PIP2 levels are critical for F-actin polymerization

(A) Quantification of protein levels for beta-actin showed no significant difference between groups. Representative images of immunoblots were shown. ns, not significant for WT1 vs. DCM patient-derived (Pat) and WT1 vs. Mut-int1 iPSC-CMs (one-way ANOVA and Sidak's multiple comparisons test). (B-C) Reduction of PIP2 levels around the PM in WT2 iPSC-CMs treated with UNC3230, a PIP5K inhibitor. (B) 63x confocal images of WT2 iPSC-CMs treated with CV and UNC3230 (10 μ M, 24 h) followed by a PIP2-specific immunostaining. (C) Quantification of (B), ***P<0.001 for CV vs. UNC323 WT2 iPSC-CMs (Mann-Whitney test). (D) Reduction of F-actin content in UNC3230 treated WT1 iPSC-CMs compared with CV. ** P<0.01 for CV WT1 vs. UNC323 WT1 (Mann-Whitney test). (E) Reduction of F-actin content in UNC3230-treated WT2 iPSC-CMs compared with CV. * P<0.05 for CV vs. UNC323 WT2 iPSC-CMs (Mann-Whitney test). (F) Kinetics of continuous transferrin uptake. Quantification of 20x confocal Z stack images acquired from individual time point. Data were normalized by number from 0 min. (G) Protein levels of transferrin receptor were not significantly different among groups. Representative membrane scans of blots and quantification were shown. ns, not significant for WT1 vs. patient and WT1 vs. Mut-int1 iPSC-CMs (one-way ANOVA and Sidak's multiple comparisons test). Data are shown as mean \pm sem.

Fig. S7. Supplemental Figure VII: TPM1-L185F mutation-introduced iPSC-CMs are characterized by impaired LDL uptake

(A-B) LDL-BODIPY uptake was impaired in TPM1-L185F mutation-introduced iPSC-CMs (Mut-int1, MUT-int1/MUT-int) vs. WT control (WT1). (A) Representative 63x confocal images of continuous LDL-BODIPY uptake. (B) Quantification of (A), quantification is done using spot detection plugin in ICY software with 63x confocal images. **P<0.01 for WT1 vs. Mut-int 1 iPSC-CMs (Unpaired t test). (C-D) LDL receptor (C) and EEA1 (D) protein expression levels were not significantly different between groups. Representative membrane scans of blots and quantification were shown. ns, not significant for WT1 vs. DCM patient-derived (Pat) and WT1 vs. Mut-int1 iPSC-CMs (one-way ANOVA and Sidak's multiple comparisons test). Data are shown as mean \pm sem.

Fig. S8. Supplemental Figure VIII: Actin polymerization is critical for proper early endosome distribution.

(A) Reduction of F-actin content in Lat-A treated WT control (WT1, WT/WT) iPSC-CMs compared with CV. * P<0.05 for CV vs. Lat-A WT1. (B-C) Inhibition of actin polymerization via Lat-A treatment results in abnormal EE distribution in WT control (WT2, WT/WT) iPSC-CMs. Confocal images(B) and quantification(C) of WT2 cells treated with Lat-A (3 μ M) followed by immunostaining with an anti-EEA1 antibody; scale bar, 20 μ m. ***P<0.001 for CV WT2 vs. Lat-A WT2. Statistics were calculated by a Mann-Whitney test. Data are shown as mean \pm sem.

Fig. S9. Supplemental Figure IX: Mitochondrial dysfunction and increased oxidative stress in DCM patient-derived and TPM1-L185F mutation-introduced iPSC-CMs

(A) Protein expression levels of a mitochondrial marker, Tom20, were not significantly altered between groups. Representative membrane scans of blots and quantification are shown. ns, not significant for WT1 vs. DCM patient-derived (Pat) and WT control (WT1, WT/WT) vs. TPM1-L185F mutation-introduced iPSC-CMs (Mut-int1, MUT-int1/MUT-int) (one-way ANOVA and Sidak's multiple comparisons test). (B) Mitochondrial membrane potential (MMP) was measured via JC-1 staining using a multi-well plate reader. Data were calculated as the red/green JC-1 fluorescence intensity ratio. In patient and TPM1-L185F mutation-introduced iPSC-CMs (Mut-int1), a reduced MMP was detected. *** $P < 0.001$ for WT1 vs. Patient, ** $P < 0.01$ for WT1 vs Mut-int1 iPSC-CMs (one-way ANOVA and Dunn's multiple comparisons test). (C) Mitochondrial superoxide levels were increased in patient (WT/MUT) and TPM1-L185F mutation-introduced iPSC-CMs (Mut-int1) measured via MitoSox staining in a high-content plate reader. ** $P < 0.01$ for WT1 vs. patient and WT1 vs. Mut-int1 iPSC-CMs (one-way ANOVA and Dunn's multiple comparisons test). (D-G) Fe(II) treatment can replenish mitochondrial Fe levels in patient (WT/MUT) and TPM1-L185F mutation-introduced iPSC-CMs (Mut-int1). Representative 63x confocal images (D, F) and quantification (E, G) Mitotracker and FerroOrange labelling following treatment with CV or ammonium Fe (II) sulfate (100 μ M, 30min). Scale bar, 20 μ m. (D-E) *** $P < 0.001$ for CV vs. Fe(II) patient and CV vs. Fe(II) Mut-int1 iPSC-CMs (Mann-Whitney test). (H) Fe(II) treatment rescued reduced mitochondrial Fe(II) levels induced by Lat-A treatment (1 μ M, 1 hours) in WT1 iPSC-CMs. *** $P < 0.001$ for CV vs. Lat-A and Lat-A vs. Lat-A+ Fe(II); ns, not significant for CV vs. Lat-A + Fe(II) (one-way ANOVA and Dunn's multiple comparisons test). (I-J) Fe(II) treatment reduced mitochondrial superoxide levels in patient (WT/MUT) and TPM1-L185F mutation-

introduced iPSC-CMs (Mut-int1). ****P<0.01** for CV vs. Fe(II) patient iPSC-CMs (unpaired t-test) and *****P<0.001** for CV vs. Fe(II) Mut-int1 iPSC-CMs (Mann-Whitney test). Data are shown as mean \pm sem.

Fig. S10. Recovering actin polymerization via RhoA activation rescues PM-localized PIP2 levels and sarcomere connections with the plasma membrane

(A-C) Increased PIP2 around the PM after Rho activator II treatment in both DCM patient-derived (Pat) and TPM1-L185F mutation-introduced iPSC-CMs (Mut-int1, MUT-int1/MUT-int). (A) Representative 63X confocal images of Patient and TPM1-L185F mutation-introduced (Mut-int1) iPSC-CMs treated with CV and Rho activator II (3 μ g/mL, 3 hours) followed by an immunostaining with a PIP2 antibody. (B-C) Quantification of (A); scale bar, 20 μ m. *****P < 0.001** for CV vs. RhoA II Patient and CV vs. Rho A II Mut-int 1 iPSC-CMs (Mann-Whitney test). (D-F) RhoA II treatment facilitates TnT-vinculin interaction in patient and TPM1-L185F mutation-introduced (Mut-int1) iPSC-CMs. (D) Representative 63X confocal images of TPM1-L185FMut-int1 iPSC-CMs treated with CV and RhoA II (3 μ g/mL, 16 hours) followed by immunostaining with vinculin and TnT antibodies; scale bar, 20 μ m. (E-F) ROI based quantification of (D). ****P<0.01** for CV vs. RhoAII Patient and *****P<0.001** for CV vs. RhoA II Mut-int1 iPSC-CMs (Mann-Whitney test). (G-I) Rho activator II treatment improved the contractility in TPM1-L185F mutation-introduced (Mut-int1) iPSC-CMs. (G-H) Representative recordings are shown for each group. Maximal decay (I) improvement following Rho activator II treatment (3 μ g/mL, 3 hours). *****P<0.001**, CV vs. RhoA II Mut-int 1 iPSC-CMs (Mann-Whitney test). Data are shown as mean \pm sem.

Fig. S11. Characterization of TPM1-L185F MUT-corrected iPSCs and iPSC-CMs

(A-E) DCM patient-derived (Pat) and mutation-corrected (mut-cor, WT-cor/WT-cor) iPSCs showed regular expression of stem cell marker, such as OCT3/4, TRA-1-81, Sox2 and SSEA4.

(A-B) Representative 20x images of human iPSC clones immuno-stained with pluripotency markers. (A) Representative 20x confocal images of human iPSCs co-stained with POU5F1 and TRA-1-81 antibodies; scale bar, 40 μ m. (B) Representative 20x confocal images of DCM patient-derived (Pat) and mutation-corrected (mut-cor) iPSCs clones co-stained with Sox2 and SSEA4 antibodies; scale bar, 40 μ m. (C-E) DCM patient-derived (Pat) and mutation-corrected (mut-cor) iPSCs showed regular expression of pluripotency markers at mRNA levels, such as Nanog (C), Pou5f1 (D) and Sox2 (E). ns, not significant for Pat vs. mut-cor iPSC-CMs as calculated by unpaired t test. (F-I) Patient and Mut-cor iPSC-CMs display regular expression of cardiac markers at mRNA levels, such as (F) TPM, (G) TnT, (H) MYH6 and (I) MYH7. (F, I) ns, not significant for Patient vs. Mut-cor (Mann Whitney test). (G) *P < 0.05, for Patient vs. Mut-cor iPSC-CMs (H) ***P < 0.001, for Patient vs. Mut-cor iPSC-CMs (unpaired t test). Statistics were calculated by Mann Whitney test unless indicated otherwise. (J-L) DCM patient-derived (Pat) and mutation-corrected (mut-cor) iPSC-CMs display regular expression of cardiac markers. (J) Representative 63x confocal images of iPSC-CMs stained with MLC2a and TnT antibodies; scale bar, 20 μ m. (K) Representative 63x confocal images of iPSC-CMs stained with MYH7 and TnT antibodies. (L) Representative 63x confocal images of iPSC-CMs stained with MYBPC3 and TnT antibodies; scale bar, 20 μ m. (M-P) DCM patient-derived (Pat) and mutation-corrected (mut-cor) iPSC-CMs displayed regular expression of cardiac markers

at protein levels, such as (M) TPM, (N) TnT, (O) TnC and (P) SAA. Representative scans of immunoblots and quantification were shown. (M, N, P) ns, not significant for patient vs. Mut-cor iPSC-CMs (unpaired t test). (O) ns, not significant for patient vs. Mut-cor iPSC-CMs (Mann Whitney test). Data are shown as mean \pm sem.

Fig. S12. Clinical data from controls and HF patients

(Corresponding to Figure 7) LV heart tissue from patients with dilated cardiomyopathy who received a heart transplantation due to end-stage heart failure (indicated as “heart failure”, HF, or heart transplantation) was analyzed (Figure 7). In comparison, LV heart tissue from patients with preserved LV function that underwent aortic valve replacement (severe valve stenosis) and coronary artery bypass graft surgery was used in the control group (“control”). (A) Conditions of patients in the control and HF groups; (B) Clinical data from controls and HF patients. Data are represented as mean \pm sem. ACE, angiotensin-converting enzyme; AT1, angiotensin II receptor type 1; CABG, coronary artery bypass grafting; ICD, implantable cardioverter defibrillator; LV, left-ventricular.

Fig. S13. Heart tissues show regular expression of CCDC53 and TnT

(A-B) Heart tissues show regular expression of CCDC53 and TnT. Representative 20X confocal images of tissues from controls and HF patients stained with TnT and CCDC53 antibodies. control, n=4 patients; HF, n=5 patients; scale bar, 40 μ m.

Fig. S14. Relative controls in human heart tissue staining

(A-E) Relative controls in human heart tissue staining. (A) Representative 63x confocal images from slides stained with CCDC53 (rabbit) and Alexa Fluor 488 goat anti-mouse antibody, scale bar, 20 μm . (B) Representative 63x confocal images from slides stained with TnT (mouse) and Alexa Fluor 561 goat anti-rabbit antibody; scale bar, 20 μm . (C) Representative 63x confocal images from slides stained with Alexa Fluor 488 goat anti-rabbit antibody only; scale bar, 20 μm . (D) Representative 63x confocal images from slides stained with Alexa Fluor 488 goat anti-mouse antibody only; scale bar, 20 μm . (E) Representative 63x confocal images from slides stained with Alexa Fluor 561 goat anti-rabbit antibody only; scale bar, 20 μm .

Supplementary Table 1:
Number of experiments and statistics for each figure

Supplementary Table 2:
Raw data for experiments with sample size less than 20

SUPPLEMENTAL REFERENCES

1. N. Sun, M. Yazawa, J. Liu, L. Han, V. Sanchez-Freire, O. J. Abilez, E. G. Navarrete, S. Hu, L. Wang, A. Lee, A. Pavlovic, S. Lin, R. Chen, R. J. Hajjar, M. P. Snyder, R. E. Dolmetsch, M. J. Butte, E. A. Ashley, M. T. Longaker, R. C. Robbins, J. C. Wu, Patient-specific induced pluripotent stem cells as a model for familial dilated cardiomyopathy. *Sci Transl Med* **4**, 130ra147 (2012).
2. F. Lan, A. S. Lee, P. Liang, V. Sanchez-Freire, P. K. Nguyen, L. Wang, L. Han, M. Yen, Y. Wang, N. Sun, O. J. Abilez, S. Hu, A. D. Ebert, E. G. Navarrete, C. S. Simmons, M. Wheeler, B. Pruitt, R. Lewis, Y. Yamaguchi, E. A. Ashley, D. M. Bers, R. C. Robbins, M. T. Longaker, J. C. Wu, Abnormal calcium handling properties underlie familial hypertrophic cardiomyopathy pathology in patient-specific induced pluripotent stem cells. *Cell Stem Cell* **12**, 101-113 (2013).
3. A. D. Ebert, K. Kodo, P. Liang, H. Wu, B. C. Huber, J. Riegler, J. Churko, J. Lee, P. de Almeida, F. Lan, S. Diecke, P. W. Burridge, J. D. Gold, D. Mochly-Rosen, J. C. Wu, Characterization of the molecular mechanisms underlying increased ischemic damage in the aldehyde dehydrogenase 2 genetic polymorphism using a human induced pluripotent stem cell model system. *Sci Transl Med* **6**, 255ra130 (2014).
4. P. W. Burridge, E. Matsa, P. Shukla, Z. C. Lin, J. M. Churko, A. D. Ebert, F. Lan, S. Diecke, B. Huber, N. M. Mordwinkin, J. R. Plews, O. J. Abilez, B. Cui, J. D. Gold, J. C. Wu, Chemically defined generation of human cardiomyocytes. *Nat Methods* **11**, 855-860 (2014).
5. A. V. Malkovskiy, N. Ignatyeva, Y. Dai, G. Hasenfuss, J. Rajadas, A. Ebert, Integrated Ca(2+) flux and AFM force analysis in human iPSC-derived cardiomyocytes. *Biol Chem* **402**, 113-121 (2020).
6. H. Xu, R. Wali, C. Cheruiyot, J. Bodenschatz, G. Hasenfuss, A. Janshoff, M. Habeck, A. Ebert, Non-negative blind deconvolution for signal processing in a CRISPR-edited iPSC-cardiomyocyte model of dilated cardiomyopathy. *FEBS Lett*, (2021).
7. G. Chen, D. R. Gulbranson, Z. Hou, J. M. Bolin, V. Ruotti, M. D. Probasco, K. Smuga-Otto, S. E. Howden, N. R. Diol, N. E. Propson, R. Wagner, G. O. Lee, J. Antosiewicz-Bourget, J. M. Teng, J. A. Thomson, Chemically defined conditions for human iPSC derivation and culture. *Nat Methods* **8**, 424-429 (2011).
8. Y. Dai, A. Amenov, N. Ignatyeva, A. Koschinski, H. Xu, P. L. Soong, M. Tiburcy, W. A. Linke, M. Zaccolo, G. Hasenfuss, W. H. Zimmermann, A. Ebert, Troponin destabilization impairs sarcomere-cytoskeleton interactions in iPSC-derived cardiomyocytes from dilated cardiomyopathy patients. *Sci Rep* **10**, 209 (2020).
9. X. Lian, C. Hsiao, G. Wilson, K. Zhu, L. B. Hazeltine, S. M. Azarin, K. K. Raval, J. Zhang, T. J. Kamp, S. P. Palecek, Robust cardiomyocyte differentiation from human pluripotent stem cells via temporal modulation of canonical Wnt signaling. *Proc Natl Acad Sci U S A* **109**, E1848-1857 (2012).
10. X. Lian, J. Zhang, S. M. Azarin, K. Zhu, L. B. Hazeltine, X. Bao, C. Hsiao, T. J. Kamp, S. P. Palecek, Directed cardiomyocyte differentiation from human pluripotent stem cells by modulating Wnt/beta-catenin signaling under fully defined conditions. *Nat Protoc* **8**, 162-175 (2013).
11. A. Hendel, R. O. Bak, J. T. Clark, A. B. Kennedy, D. E. Ryan, S. Roy, I. Steinfield, B. D. Lunstad, R. J. Kaiser, A. B. Wilkens, R. Bacchetta, A. Tsalenko, D. Dellinger, L. Bruhn, M. H. Porteus, Chemically modified guide RNAs enhance CRISPR-Cas genome editing in human primary cells. *Nat Biotechnol* **33**, 985-989 (2015).
12. R. O. Bak, D. P. Dever, M. H. Porteus, CRISPR/Cas9 genome editing in human hematopoietic stem cells. *Nat Protoc* **13**, 358-376 (2018).
13. K. Kodo, S. G. Ong, F. Jahanbani, V. Termglinchan, K. Hirano, K. InanlooRahatloo, A. D. Ebert, P. Shukla, O. J. Abilez, J. M. Churko, I. Karakikes, G. Jung, F. Ichida, S. M. Wu, M. P. Snyder, D. Bernstein, J. C. Wu,

- iPSC-derived cardiomyocytes reveal abnormal TGF-beta signalling in left ventricular non-compaction cardiomyopathy. *Nat Cell Biol* **18**, 1031-1042 (2016).
14. I. Atanassov, H. Urlaub, Increased proteome coverage by combining PAGE and peptide isoelectric focusing: comparative study of gel-based separation approaches. *Proteomics* **13**, 2947-2955 (2013).
 15. J. P. Lambert, G. Ivosev, A. L. Couzens, B. Larsen, M. Taipale, Z. Y. Lin, Q. Zhong, S. Lindquist, M. Vidal, R. Aebersold, T. Pawson, R. Bonner, S. Tate, A. C. Gingras, Mapping differential interactomes by affinity purification coupled with data-independent mass spectrometry acquisition. *Nat Methods* **10**, 1239-1245 (2013).
 16. Y. Zhang, A. Bilbao, T. Bruderer, J. Luban, C. Strambio-De-Castillia, F. Lisacek, G. Hopfgartner, E. Varesio, The Use of Variable Q1 Isolation Windows Improves Selectivity in LC-SWATH-MS Acquisition. *J Proteome Res* **14**, 4359-4371 (2015).
 17. K. N. Richter, N. H. Revelo, K. J. Seitz, M. S. Helm, D. Sarkar, R. S. Saleeb, E. D'Este, J. Eberle, E. Wagner, C. Vogl, D. F. Lazaro, F. Richter, J. Coy-Vergara, G. Coceano, E. S. Boyden, R. R. Duncan, S. W. Hell, M. A. Lauterbach, S. E. Lehnart, T. Moser, T. F. Outeiro, P. Rehling, B. Schwappach, I. Testa, B. Zapiec, S. O. Rizzoli, Glyoxal as an alternative fixative to formaldehyde in immunostaining and super-resolution microscopy. *EMBO J* **37**, 139-159 (2018).
 18. T. Wilhelmi, X. Xu, X. Tan, M. S. Hulshoff, S. Maamari, S. Sossalla, M. Zeisberg, E. M. Zeisberg, Serelaxin alleviates cardiac fibrosis through inhibiting endothelial-to-mesenchymal transition via RXFP1. *Theranostics* **10**, 3905-3924 (2020).
 19. S. Brandenburg, T. Kohl, G. S. Williams, K. Gusev, E. Wagner, E. A. Rog-Zielinska, E. Hebisch, M. Dura, M. Didié, M. Gotthardt, V. O. Nikolaev, G. Hasenfuss, P. Kohl, C. W. Ward, W. J. Lederer, S. E. Lehnart, Axial tubule junctions control rapid calcium signaling in atria. *J Clin Invest* **126**, 3999-4015 (2016).

4 Discussion

To ensure cellular homeostasis, membranes separate the extracellular environment from define compartments with different functions inside the cell¹. Together with the plasma membrane, cytoskeleton elements perform coordinated nutrient uptake as well as signal transduction events. One of the processes where membranes and cytoskeleton work in a coordinated manner is endocytosis². While endocytic vesicles bud off the plasma membrane, microfilaments are critical for vesicle formation and subsequent distribution of cargo transported by vesicles. Inherited mutations, such as mutations in genes encoding sarcomere proteins have been identified as frequent causes of cardiac diseases such as DCM¹⁸¹. DCM is clinically characterized by left ventricular or biventricular dilation and impaired contraction, excluding the cases due to abnormal loading conditions¹⁸². In cardiomyocytes, sarcomere misalignment is one of the key phenotypes caused by DCM mutations¹⁸³. Disrupted interactions between sarcomeres and other cytoskeleton filaments have been demonstrated as potential mechanisms of heart failure^{8,171}. In this study, a human iPSC-CM model carrying TnT-R173W, TnT-R141W or TPM1-L185F mutations combined with CRISPR/Cas9 genome editing was employed to study the underlying disease mechanism.

This study elucidated how mutations in sarcomeric proteins can lead to dysfunction of sarcomeric microdomains, impaired sarcomere-cytoskeleton-PM interactions, cargo uptake, and abnormal early endosome distribution. This resulted in iron deficiency and ultimately impaired cardiomyocyte function. CRIPSR/Cas9-based mutation-introduced and mutation-corrected iPSC lines were created and used to introduce or rescue molecular disease phenotypes, respectively. For example, decreased stability of the Tn-TPM complex was found, indicated by reduced binding of TnT with TPM in presence of a sarcomeric DCM mutation (TnT-R173W) which further enhanced disorganisation of sarcomeres. In addition, reduced binding of PKA to TnT in presence of a contractile mutation caused diminished Tnl phosphorylation at Ser 23/24 locations. Moreover, sarcomere-cytoskeleton interactions were disturbed in presence of sarcomeric DCM mutations, indicated by impaired TnT-filamin C and TnT-MYH7 interactions. Importantly, the co-localization of TnT-filamin C was rescued by the AMPK activator treatment.

Moreover, additional downstream effects resulting from defective sarcomere-cytoskeleton interactions were discovered. Firstly, DCM-causing mutations, such as TPM1-L185F or TnT-R141W led to disrupted interactions of the

sarcomere/cytoskeleton with the PM. This was supported by reduced binding of sarcomeric proteins including TPM, SAA, and TnT to vinculin in presence of a sarcomeric mutation. Consequently, vinculin-mediated actin polymerization in PIP2-enriched microdomains at the PM was impaired in presence of the DCM mutations. The dysfunction of F-actin/PIP2-enriched microdomains led to defective CME of cargoes such as transferrin and LDL. Importantly, early endosomes displayed an abnormal distribution in presence of DCM-causing mutations. Defective CME and impaired distribution of endosome-transported cargoes resulted in depletion of mitochondrial iron levels in presence of the DCM mutation.

Secondly, treating WT iPSC-CMs with Lat-A, a small molecule-inhibitor of actin polymerization, caused defective actin polymerization, defects in early endosome distribution, and reduced mitochondrial iron levels. Thus, Lat-A treatment in WT iPSC-CMs introduced the molecular dysfunctions observed previously in DCM iPSC-CMs. Furthermore, RhoA activation by treatment with Rho activator II, which activates PIP5K⁸², replenished PIP2 levels at the PM and rescued CME, early endosome distribution, and mitochondrial iron levels in DCM iPSC-CMs. Besides, iron supplementation rescued reduced iron levels in mitochondria as well as cardiomyocyte contractility in DCM iPSC-CMs.

Thirdly, these phenotypic dysfunctions, such as actin polymerization defects, abnormal early endosome distribution, reduced iron levels in mitochondria, and decreased contractile force were recovered following CRISPR/Cas9-based correction of the DCM mutation TPM1-L185F.

Last but not least, the cardiac myocytes of left ventricular tissues from DCM patients with end-stage heart failure were found to display abnormal endosome distribution compared to left ventricular tissues from patients with preserved systolic left-ventricular function. Therefore, these findings confirm that this phenotype, which had been observed in DCM iPSC-CMs, may also be present in adult heart tissue from DCM patients with heart failure. This suggests that abnormal early endosome distribution may potentially represent a more general mechanism in systolic heart failure due to DCM, but future studies are needed to ascertain this point.

4.1 Sarcomeric protein disorganisation results in microdomain dysfunction

As noted, sarcomere disorganization caused by sarcomeric DCM mutations results in several severe molecular pathogenic events¹⁸⁴. Consistently, in this study, sarcomeric mutations such as TnT-R173W, TPM1-L185F or TnT-R141W destabilized the troponin complex on thin filaments, resulting in disrupted sarcomere protein alignment. Moreover, force generation and contractility were impaired in presence of sarcomeric DCM mutations. This can be a consequence of impaired Tn-TPM complex interactions in presence of sarcomeric DCM mutations as those interactions are critical for TPM to release the actin binding site on the thin filaments and initiate cross-bridge formation.

Moreover, reduced binding of TnT with PKA as observed in DCM iPSC-CMs contributed to dysregulation of local sarcomeric microdomains such as decreased PKA-mediated Ser 23/24 phosphorylation of TnI. This reduction of phosphorylation could lead to defective β -adrenergic signaling and impaired contractility upon β -adrenergic stimulation. This is in line with published data showing β -adrenergic signaling is blunted in DCM iPSC-CMs³⁸. In addition, local cAMP levels at sarcomeric microdomains were increased in DCM iPSC-CMs. This might be a compensatory effect due to reduced TnI phosphorylation at Ser 23/24. Moreover, a substantial increase of PDE protein expression was observed in immunoblot assays, consistent with a previous study showing that upregulation of PDE expression could be the cause of impaired β -adrenergic activation in DCM iPSC-CMs³⁸. Together, sarcomeric cAMP elevation could not compensate effects due to impaired PKA-sarcomere interactions in DCM iPSC-CMs, which therefore may contribute to impaired contractility and force generation (Figure 7).

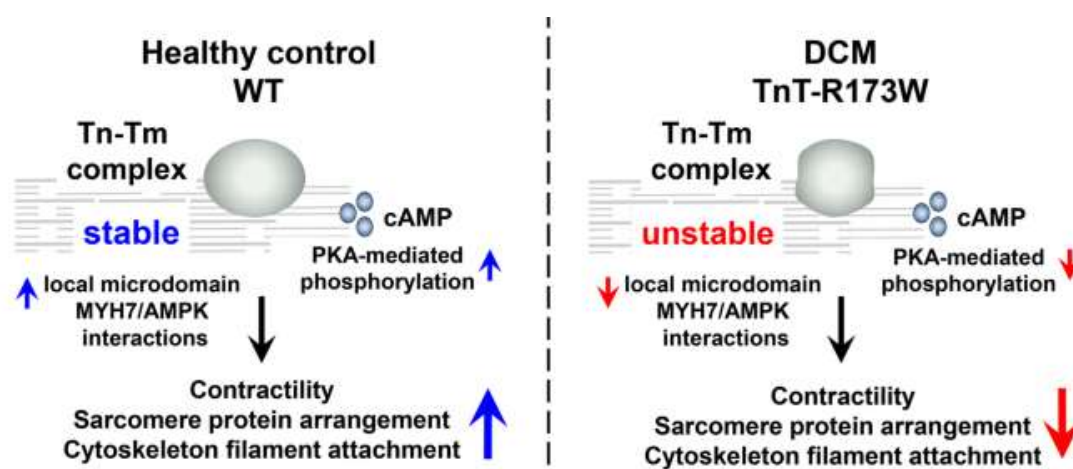


Figure 7: Disorganized sarcomeric proteins result in dysfunction of sarcomeric microdomains.

A schematic displaying effects of impaired protein-protein interactions at sarcomere microdomains due to the DCM mutation TnT-R173W. In presence of TnT-R173W, reduced binding of TnT-R173W to TPM and PKA impairs local microdomain signaling, such as sarcomere protein misalignment and reduced TnI phosphorylation at locations Ser 23/24. Additionally, the DCM mutation causes defective sarcomere-cytoskeleton filament interactions indicated by defective TnT-filament C and TnT-MYH7 interactions. This further leads to impaired MYH7-AMPK interaction. Importantly, AMPK activation rescues these molecular disease phenotypes. This image is adapted after Dai Y et al. *Sci Rep.* 2020 Jan 14;10(1):209.¹⁷¹

4.2 Sarcomere disorganisation leads to impaired interactions with the PM

It has been shown that sarcomere-cytoskeleton-PM interactions play an essential role in maintenance of cardiac function and structure¹⁸⁵. Elements including costameres, IFs, and microfilaments have been well-documented in terms of their functions in signaling transmission and force transduction between sarcomeres and the PM¹⁸⁵. Dysfunction of those essential elements causes cardiac diseases including DCM¹⁸⁵. The interactions between sarcomere, cytoskeleton-associated proteins (such as vinculin, MYH7), and IFs (such as filamin-C) were impaired in presence of a sarcomeric mutation. Here, in presence of a sarcomeric mutation, connections among sarcomere, cytoskeleton, and the PM were found to be impaired. This was supported by the disturbed TnT-filament C, TnT-MYH7, and TPM-SAA-vinculin interactions. Both AMPK, a key intracellular signaling modulator, and sarcomeric TnT can interact with MYH7⁵⁷⁻⁶⁰. The disturbed interaction observed between TnT and MYH7 destabilized the interaction between MYH7 and AMPK. Consequently, destabilized AMPK further led to defective AMPK-mediated remodeling of cytoskeleton filaments. Those findings thus suggested that AMPK, a protein critically involved in regulation of the cytoskeleton organization, was negatively affected by disturbed sarcomere-cytoskeleton interactions in DCM iPSC-CMs. Activation of AMPK by a small molecule rescued the impaired sarcomere-cytoskeleton interactions. This was supported by the recovered colocalization between TnT and filamin C in DCM iPSC-CMs (Figure 7). Additionally, AMPK activation improved the contractility and sarcomere protein alignment in presence of a contractile DCM mutation, TnT-R173W. This further confirmed the regulatory connection between AMPK and sarcomeres, and its critical role for sarcomere-cytoskeleton interactions and cardiomyocyte function.

Vinculin, a key element of costameres in cardiomyocytes, links sarcomeres, microfilaments, and the PM. In presence contractile DCM mutations, reduced binding of vinculin with sarcomeric proteins such as SAA, TPM, and TnT demonstrated that interactions among sarcomeres, microfilaments, and the PM were impaired. Moreover, colocalization between vinculin and TnT was found to be reduced in DCM iPSC-CMs.

Those data further confirmed that sarcomere/microfilament interactions with the PM were impaired. This also provides an additional explanation for defective force generation in presence of sarcomeric DCM mutations, since proper connections between the sarcomeres and the PM are essential for force generation and transduction. Importantly, sarcomere misalignment and impaired force generation were rescued by genomic correction of the TPM1-L185F mutation by CRISPR/Cas9 gene editing.

4.3 Defective sarcomere-microfilament-PM interactions cause impaired CME and abnormal early endosome distribution

Proper sarcomere-microfilament-PM interactions are essential for signaling between sarcomere and the PM as well as function of the cytoskeleton¹⁸⁵. Those interactions were found to be disturbed in presence of DCM mutations. Interestingly, actin polymerization was found to be defective, as indicated by reduced F/G actin ratio in DCM iPSC-CMs carrying a contractile mutation, compared to WT controls. Reduced F-actin levels were in line with substantially reduced PIP2 levels at the PM in presence of sarcomeric DCM mutations. PIP2-enriched microdomains are essential for the initiation of CME⁹⁹. Dysfunction of PIP2-enriched microdomains and defective actin polymerization were previously suggested to lead to defective CME^{186,187}. In line with this, disturbed uptake of cargoes, such as transferrin and LDL through CME, were observed in DCM iPSC-CMs due to decreased PIP2 levels on the PM and defective actin polymerization at the PM. Furthermore, actin polymerization as well as cargo uptake were rescued upon genomic correction of the contractile DCM mutation, TPM1-L185F. This supported that in DCM iPSC-CMs carrying sarcomeric mutations, pathogenic downstream signaling disrupted cytoskeleton functions, impairing processes such as actin polymerization, F-actin connections at the PM, and consequently cargo uptake via CME.

Interestingly, early endosome cargo carriers accumulated at the PM in DCM iPSC-CMs, distributing abnormally throughout the cytoplasm. Previously actin polymerization was suggested to play a role in the distribution of early endosomes¹⁰⁹. Thus, the abnormal early endosome distribution observed in presence of DCM mutations could present a consequence of impaired actin polymerization, F-actin connections at the PM, and defective sarcomere interactions. Importantly, the Lat-A treatment induced defective early endosome distribution in WT iPSC-CMs, thereby introducing the phenotype observed in DCM iPSC-CMs. Of note, the abnormal early

endosome distribution was rescued following CRISPR/Cas9-based genomic correction of the contractile DCM mutation, TPM1-L185F. This supported that abnormal early endosome distribution is a consequence of the sarcomeric DCM mutation. Taken together, impaired sarcomere-microfilament-PM interactions in presence of sarcomeric mutations led to impaired cargo uptake and abnormal early endosome distribution (Figure 8).

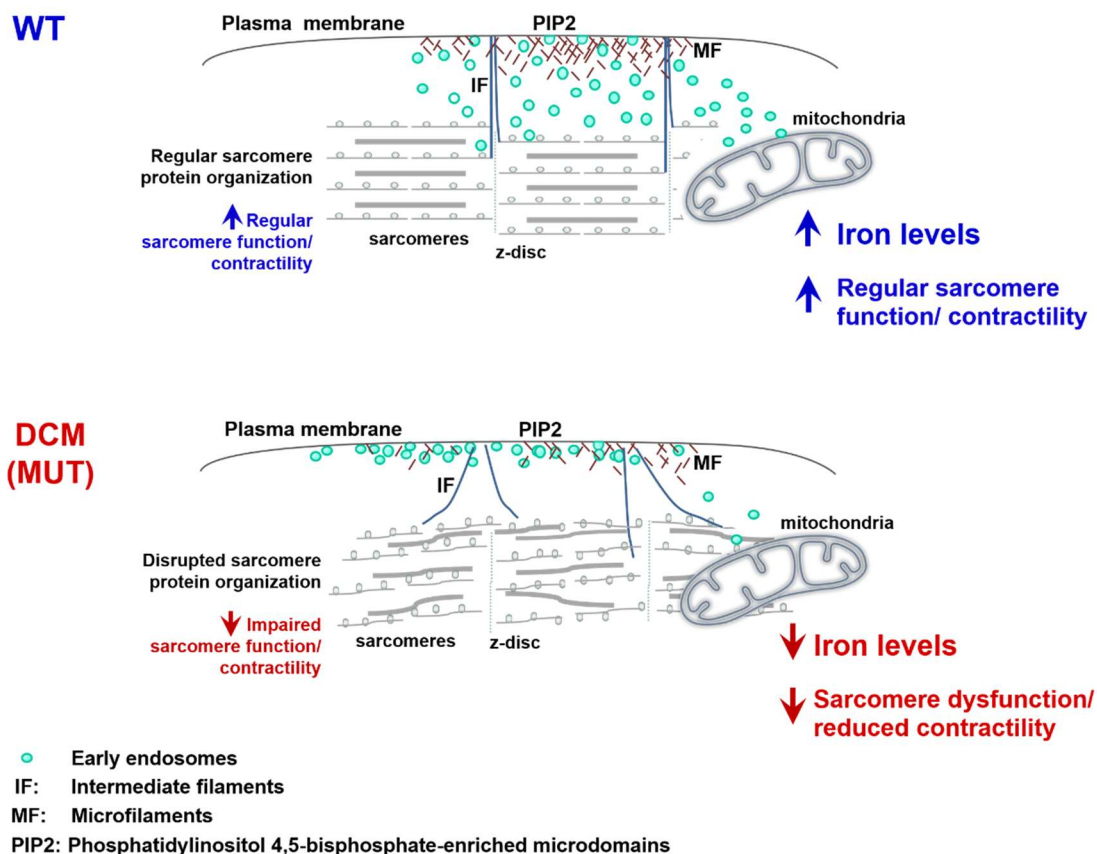


Figure 8: Defective endocytosis and endosome distribution result in mitochondrial iron deficiency in presence of DCM mutations.

A schematic showing effects of disrupted sarcomere protein structure caused by sarcomeric mutations such as TnT-R173W, TnT-R141W or TPM1-L185F. In WT cells, organized sarcomeric structure facilitated the proper sarcomere-cytoskeleton-PM interactions. This is essential for actin polymerization in PIP2-enriched microdomains on the PM. Actin polymerisation assisted the normal process of CME through which transferrin could enter the cell. Transferrin uptake contributed to maintaining an adequate amount of iron and thus normal mitochondrial functions. In contrast, disorganised sarcomeric proteins lost their proper connections with the cytoskeleton and PM. Defective actin polymerisation due to defective protein-protein interactions leads to reduced transferrin uptake. This further resulted in reduced iron levels in mitochondria and impaired cardiac function ultimately. IF, intermediate filaments; MF, microfilaments around the PM (red lines); PM, plasma membrane; PIP2, PIP2-enriched PM microdomains; green circles, endosomes containing transferrin-bound iron; grey circles on sarcomeres, Tn-TPM complexes. This image is adapted after Dai Y et al. Submitted to *Circulation Research*.2022.¹⁸⁸

4.4 Sarcomeric mutations result in impaired cargo uptake and depletion of iron levels in mitochondria

In presence of DCM mutations, dysfunction of PIP2-enriched microdomains and defective actin polymerization resulted in impaired CME-dependent cargo uptake such as transferrin and LDL. Transferrin uptake via CME is an essential process for cardiomyocytes to take up iron^{102,149}. Mitochondria utilize a major amount of intracellular iron as Fe/S clusters and heme groups are essential for the function of electron transport chain complexes I–IV¹⁸⁹. Here, in DCM iPSC-CMs with sarcomeric mutations, iron levels in mitochondria were depleted (Figure 8). Importantly, iron supplementation rescued contractility in iPSC-CMs carrying a DCM-causing mutation, which was in line with previous studies¹⁵⁰. This suggested that an adequate amount of iron was essential to perform normal cardiomyocyte functions, such as contractility, and insufficient iron levels impaired the mitochondrial function of cardiomyocytes^{143,190}. Of note, the mitochondrial iron levels were restored in mutation-corrected iPSC-CMs. Moreover, treatment with Lat-A decreased mitochondrial iron levels in WT iPSC-CMs, introducing the disease phenotype observed in DCM iPSC-CMs as a consequence of abnormal early endosome distribution and defective actin polymerization. Those data indicated that actin polymerization was important for early endosome distribution and maintenance of adequate iron levels in mitochondria in iPSC-CMs. Importantly, decreased iron levels in mitochondria due to the Lat-A treatment were rescued by iron supplementation. This confirmed that iron supplementation helped to recover the adequate amount of iron required for in mitochondria in DCM iPSC-CMs.

To sum up, depletion of intracellular iron levels was observed in presence of sarcomeric mutations (Figure 8). This can be a consequence of impaired transferrin uptake through CME due to defective actin polymerization and dysfunction of PIP2-enriched microdomains on the PM. In addition, replenishing iron rescued reduced iron levels in mitochondria and impaired contractility in DCM iPSC-CMs. This indicated that iron deficiency was linked to defective contractility and an adequate amount of iron was essential for normal cardiomyocyte functions. Drugs modulating this pathway present potential therapeutic strategies for treatments of patients with DCM due to sarcomeric mutations.

4.5 Novel therapeutic implications and directions of this study

It has been reported that omecamtiv mecarbil, a selective and direct cardiac myosin activator, improves cardiac function in patients with heart failure and reduces the death

from disease with cardiovascular causes^{191,192}. Omecamtiv mecarbil targets myosin, increases cardiac actomyosin activity, and stabilizes actin-bound myosin¹⁹¹. Here, A769662¹⁹³, an AMPK activator, was found to improve contractility and sarcomere alignment in presence of a contractile mutation without directly targeting contractile proteins. This could be due to beneficial signaling mediated by AMPK activation and presents a direction for further translational research. In line with this, drugs which activate AMPK and improve cardiac energy supply, such as trimetazidine, have displayed beneficial effects for patients with idiopathic dilated cardiomyopathy¹⁹⁴.

Previous studies demonstrate that in response to chronic pressure overload, cardiomyocyte-specific deletion of RhoA results in accelerated DCM and increases the severity of heart failure outcome⁸⁵. Low levels of constitutively activated RhoA in cardiomyocytes exhibits increased tolerance against ischemia/reperfusion (I/R) injury⁸⁶. However, its sustained overactivation could result in pathological consequences⁸⁷. cardiac-specific overexpression of RhoA ultimately induces DCM with impaired contractility⁸⁸. Therefore, a basal amount of RhoA activity is required for normal cardiac function. In this study, RhoA activation via Rho activator II treatment improved contractility in presence of a contractile mutation. In addition, RhoA activation replenished PIP2 levels on the PM and rescued transferrin uptake as well as mitochondrial iron levels. Activation of RhoA facilitated early endosome distribution which was a result of restored PIP2 levels and F-actin content around the PM. Moreover, RhoA activation assisted to recover sarcomere-PM interactions indicated by increased colocalization between vinculin and TnT. Finally, sarcomere protein organization was improved by RhoA activation. In addition, iron supplementation rescued the depleted iron levels in mitochondria as well as contractility in DCM iPSC-CMs.

Together, these data indicated that the maintenance of proper connections among sarcomeres, cytoskeleton, and the PM was critical for both sarcomere function directly and resulting signaling mechanisms affecting other critical cardiomyocyte functions. RhoA activation in a well-balanced manner might be a potential therapeutic direction to follow up with in future studies.

4.6 Conclusions and outlook

This study has elucidated that in presence of sarcomeric DCM mutations such as TnT-R173W, TnT-R141W or TPM1-L185F, sarcomere misalignment led to impaired

interactions at sarcomeric microdomains and the connected signaling pathways. This included impaired sarcomere-PKA and sarcomere-MYH7 interactions. Furthermore, the interaction between sarcomeres, PM, and cytoskeleton were found to be disturbed in DCM iPSC-CMs. This suggested that disorganised sarcomeres lost their proper connections with the PM and cytoskeleton, resulting in defective downstream signaling pathways such as defective actin polymerization and disrupted PIP2-enriched microdomains at the PM. Further observed consequences were defective CME and transferrin uptake. This resulted in the depletion of iron levels in mitochondria, because the CME of transferrin is essential for cardiac myocytes to maintain iron availability (Figure 8). Importantly, left ventricular tissues from patients with end-stage heart failure due to DCM displayed abnormal endosome distribution compared to left ventricular tissues from patients with preserved systolic left-ventricular function. This suggested that iron deficiency due to defective endocytosis may present a more general mechanism in patients with systolic heart failure due to DCM. Importantly, AMPK activation rescued molecular disease phenotypes, including sarcomere disorganization and sarcomere-cytoskeleton interactions. Of note, Rho activation rescued disease phenotypes, including the impaired function of F-actin/PIP2 enriched microdomains, depletion of mitochondrial iron levels, and reduced contractility in DCM iPSC-CMs. Thus, Rho activation presents a potential therapeutic direction in the future for the treatment of patients with inherited sarcomeric DCM mutations. This study also showed that at cellular levels, replenishing iron could restore the depleted iron levels in mitochondria as well as impaired contractility in DCM iPSC-CMs. This provided additional evidence for the benefit of applying iron supplementation, which is currently used as a treatment strategy in patients with heart failure. Here, a human iPSC-CM model of inherited DCM mutations was used. Subsequent studies in animal models represent the next steps to further validate the findings of this study.

It has been suggested that cytoskeleton-associated proteins such as filamin C and vinculin play an important role in sarcomere interactions with other cytoskeleton elements and the PM¹⁸⁵. This work further supported that the link between sarcomeres and other parts of the cytoskeleton was essential for normal cardiomyocyte functions. Moreover, as organised sarcomeres ensure proper connections between sarcomeres and cytoskeleton, the sarcomere protein disorganization observed in presence of DCM mutations resulted in defective downstream interactions and dysfunctions of signaling pathways. In addition, this study has proposed a potential new cellular pathomechanism contributing to iron deficiency in cardiomyocytes from heart failure

patients: Impaired CME due to dysfunction of F-actin/PIP2-enriched microdomains resulted in defects in transferrin uptake and subsequently depletion of iron levels in mitochondria.

Further studies will be needed to address if iron supplementation and Rho activator II treatment can rescue the disease phenotypes described above also in populations of patients with heart failure due to other reasons than inherited mutations. In addition, future studies in small animal models and, subsequently, large animal models such as the swine could further validate the relevance of this patho-mechanism and also their potential importance as a basis for future translational applications.

5 Own contributions

Publication 1 Troponin destabilization impairs sarcomere-cytoskeleton interactions in iPSC-derived cardiomyocytes from dilated cardiomyopathy patients

Authors: Yuanyuan Dai, Asset Amenov, Nadezda Ignatyeva, Andreas Koschinski, Hang Xu, Poh Loong Soong, Malte Tiburcy, Wolfgang A Linke, Manuela Zaccolo, Gerd Hasenfuss, Wolfram-Hubertus Zimmermann, Antje Ebert

Status: Published

Own contributions: Y.D. performed biochemical experiments including troponin expression, interaction, local PKA signaling, AMPK activation, and microdomain interaction. P.L.S., M.T., Y.D., A.E. and W.H.Z. performed EHM experiments. A.K., Y.D. and M.Z. performed FRET sensor experiments.

Publication 2 An alternative mechanism of subcellular iron uptake deficiency in cardiomyocytes and treatment approach in heart failure

Authors: Yuanyuan Dai, Nadezda Ignatyeva, Hang Xu, Ruheen Wali, Karl Toischer, Sören Brandenburg, Christof Lenz, Samuel Sossalla, Niels Voigt, Elisabeth M. Zeisberg, Andreas Janshoff, Henning Urlaub, Torsten Bloch Rasmussen, Jens Mogensen, Stephan E. Lehnart, Gerd Hasenfuss, Antje Ebert

Status: Submitted to Circulation Research

Own contributions: Y.D. performed characterization of iPSCs and iPSC-CMs (IHC staining of stem cell markers, IHC staining and immune-blot of cardiac markers, and sarcomere length analysis); protein-protein interaction studies, including co-immunoprecipitation, immuno-blot, IHC staining and co-localization analysis; measurement of PM-localized PIP2 levels after Rho activator II treatment; characterization of cargo uptake (transferrin and LDL uptake), endosome distribution, mitochondrial iron levels under baseline and after drug treatments such as Fe (II) and RhoA activator II; characterization of F/G actin ratio under baseline and after UNC3230 or Lat-A treatment; measurements of contractility, sarcomere length and mitochondrial iron levels after Fe (II) or RhoA activator II treatment; assessment of vinculin organization and endosome distribution in adult human heart tissue; characterization of protein expression levels of vesicular trafficking related proteins, such as EEA1, beta-actin, LDL receptor and transferrin receptor; characterization of mitochondria function, such as respiration, membrane potential and superoxide levels under baseline and after drug treatment; data analysis; manuscript writing. H.X., R.W., and Y.D. performed contractility and force recording experiments. C.L., Y.D., and H.U. performed MS experiments.

6 List of publications

1. **Dai Y**, Amenov A, Ignatyeva N, Koschinski A, Xu H, Soong PL, Tiburcy M, Linke WA, Zaccolo M, Hasenfuss G, Zimmermann WH, Ebert A. Troponin destabilization impairs sarcomere-cytoskeleton interactions in iPSC-derived cardiomyocytes from dilated cardiomyopathy patients. *Sci Rep.* 2020 Jan 14;10(1):209.
2. **Dai Y**, Ignatyeva N, Xu H, Wali R, Toischer K, Brandenburg S, Lenz C, Sossalla S, Voigt N, Zeisberg E, Janshoff A, Urlaub H, Rasmussen T, Mogensen J, Lehnart S, Hasenfuss G, Ebert A. An alternative mechanism of subcellular iron uptake deficiency in cardiomyocytes and treatment approach in heart failure. Submitted to *Circ Res.* 2022
3. Ebert A, Joshi AU, Andorf S, **Dai Y**, Sampathkumar S, Chen H, Li Y, Garg P, Toischer K, Hasenfuss G, Mochly-Rosen D, Wu JC. Proteasome-dependent regulation of distinct metabolic states during long-term culture of human iPSC-derived cardiomyocytes. *Circ Res.* 2019 Jun 21;125(1):90-103.
4. Malkovskiy AV, Ignatyeva N, **Dai Y**, Hasenfuss G, Rajadas J, Ebert A. Integrated Ca^{2+} flux and AFM force analysis in human iPSC-derived cardiomyocytes. *Biol Chem.* 2020 Oct 27;402(1):113-121.

7 References

- 1 Cooper & M, G. *The Cell: A Molecular Approach. 2nd edition.*, (2000).
- 2 Kumari, S., Mg, S. & Mayor, S. Endocytosis unplugged: multiple ways to enter the cell. *Cell Res* **20**, 256-275, doi:10.1038/cr.2010.19 (2010).
- 3 Xiang, Y. & Kobilka, B. The PDZ-binding motif of the beta2-adrenoceptor is essential for physiologic signaling and trafficking in cardiac myocytes. *Proc Natl Acad Sci U S A* **100**, 10776-10781, doi:10.1073/pnas.1831718100 (2003).
- 4 Gurevich, V. V. *et al.* Arrestin interactions with G protein-coupled receptors. Direct binding studies of wild type and mutant arrestins with rhodopsin, beta 2-adrenergic, and m2 muscarinic cholinergic receptors. *J Biol Chem* **270**, 720-731, doi:10.1074/jbc.270.2.720 (1995).
- 5 Moore, C. A., Milano, S. K. & Benovic, J. L. Regulation of receptor trafficking by GRKs and arrestins. *Annu Rev Physiol* **69**, 451-482, doi:10.1146/annurev.physiol.69.022405.154712 (2007).
- 6 Estadella, I. *et al.* Endocytosis: A Turnover Mechanism Controlling Ion Channel Function. *Cells* **9**, doi:10.3390/cells9081833 (2020).
- 7 Karnik, R. *et al.* Endocytosis of HERG is clathrin-independent and involves arf6. *PLoS One* **8**, e85630, doi:10.1371/journal.pone.0085630 (2013).
- 8 Hein, S., Kostin, S., Heling, A., Maeno, Y. & Schaper, J. The role of the cytoskeleton in heart failure. *Cardiovasc Res* **45**, 273-278, doi:10.1016/s0008-6363(99)00268-0 (2000).
- 9 Clark, K. A., McElhinny, A. S., Beckerle, M. C. & Gregorio, C. C. Striated muscle cytoarchitecture: an intricate web of form and function. *Annu Rev Cell Dev Biol* **18**, 637-706, doi:10.1146/annurev.cellbio.18.012502.105840 (2002).
- 10 Eisner, D. A., Caldwell, J. L., Kistamás, K. & Trafford, A. W. Calcium and Excitation-Contraction Coupling in the Heart. *Circ Res* **121**, 181-195, doi:10.1161/CIRCRESAHA.117.310230 (2017).
- 11 Yin, Z., Ren, J. & Guo, W. Sarcomeric protein isoform transitions in cardiac muscle: a journey to heart failure. *Biochim Biophys Acta* **1852**, 47-52, doi:10.1016/j.bbadis.2014.11.003 (2015).
- 12 Katrukha, I. A. Human cardiac troponin complex. Structure and functions. *Biochemistry (Mosc)* **78**, 1447-1465, doi:10.1134/S0006297913130063 (2013).
- 13 Cheng, Y. & Regnier, M. Cardiac troponin structure-function and the influence of hypertrophic cardiomyopathy associated mutations on modulation of contractility. *Arch Biochem Biophys* **601**, 11-21, doi:10.1016/j.abb.2016.02.004 (2016).
- 14 Gangadharan, B. *et al.* Molecular mechanisms and structural features of cardiomyopathy-causing troponin T mutants in the tropomyosin overlap region. *Proc Natl Acad Sci U S A* **114**, 11115-11120, doi:10.1073/pnas.1710354114 (2017).
- 15 Marston, S. & Zamora, J. E. Troponin structure and function: a view of recent progress. *J Muscle Res Cell Motil* **41**, 71-89, doi:10.1007/s10974-019-09513-1 (2020).
- 16 Tardiff, J. C. Thin filament mutations: developing an integrative approach to a complex disorder. *Circ Res* **108**, 765-782, doi:10.1161/CIRCRESAHA.110.224170 (2011).

-
- 17 Takeda, S., Yamashita, A., Maeda, K. & Maéda, Y. Structure of the core domain of human cardiac troponin in the Ca(2+)-saturated form. *Nature* **424**, 35-41, doi:10.1038/nature01780 (2003).
- 18 Matyushenko, A. M. & Levitsky, D. I. Molecular Mechanisms of Pathologies of Skeletal and Cardiac Muscles Caused by Point Mutations in the Tropomyosin Genes. *Biochemistry (Mosc)* **85**, S20-S33, doi:10.1134/S0006297920140023 (2020).
- 19 Cabral-Lilly, D., Tobacman, L. S., Mehegan, J. P. & Cohen, C. Molecular polarity in tropomyosin-troponin T co-crystals. *Biophys J* **73**, 1763-1770, doi:10.1016/S0006-3495(97)78206-7 (1997).
- 20 Whitby, F. G. & Phillips, G. N. Crystal structure of tropomyosin at 7 Angstroms resolution. *Proteins* **38**, 49-59 (2000).
- 21 Chang, A. N., Greenfield, N. J., Singh, A., Potter, J. D. & Pinto, J. R. Structural and protein interaction effects of hypertrophic and dilated cardiomyopathic mutations in alpha-tropomyosin. *Front Physiol* **5**, 460, doi:10.3389/fphys.2014.00460 (2014).
- 22 Frank, D. & Frey, N. Cardiac Z-disc signaling network. *J Biol Chem* **286**, 9897-9904, doi:10.1074/jbc.R110.174268 (2011).
- 23 Luther, P. K. The vertebrate muscle Z-disc: sarcomere anchor for structure and signalling. *J Muscle Res Cell Motil* **30**, 171-185, doi:10.1007/s10974-009-9189-6 (2009).
- 24 Glukhov, A. V. *et al.* Direct Evidence for Microdomain-Specific Localization and Remodeling of Functional L-Type Calcium Channels in Rat and Human Atrial Myocytes. *Circulation* **132**, 2372-2384, doi:10.1161/CIRCULATIONAHA.115.018131 (2015).
- 25 Balycheva, M., Faggian, G., Glukhov, A. V. & Gorelik, J. Microdomain-specific localization of functional ion channels in cardiomyocytes: an emerging concept of local regulation and remodelling. *Biophys Rev* **7**, 43-62, doi:10.1007/s12551-014-0159-x (2015).
- 26 Pasqualini, F. S., Nesmith, A. P., Horton, R. E., Sheehy, S. P. & Parker, K. K. Mechanotransduction and Metabolism in Cardiomyocyte Microdomains. *Biomed Res Int* **2016**, 4081638, doi:10.1155/2016/4081638 (2016).
- 27 Surdo, N. C. *et al.* FRET biosensor uncovers cAMP nano-domains at beta-adrenergic targets that dictate precise tuning of cardiac contractility. *Nat Commun* **8**, 15031, doi:10.1038/ncomms15031 (2017).
- 28 Maron, B. J. *et al.* Contemporary definitions and classification of the cardiomyopathies: an American Heart Association Scientific Statement from the Council on Clinical Cardiology, Heart Failure and Transplantation Committee; Quality of Care and Outcomes Research and Functional Genomics and Translational Biology Interdisciplinary Working Groups; and Council on Epidemiology and Prevention. *Circulation* **113**, 1807-1816, doi:10.1161/CIRCULATIONAHA.106.174287 (2006).
- 29 Layland, J., Solaro, R. J. & Shah, A. M. Regulation of cardiac contractile function by troponin I phosphorylation. *Cardiovasc Res* **66**, 12-21, doi:10.1016/j.cardiores.2004.12.022 (2005).

- 30 Metzger, J. M. & Westfall, M. V. Covalent and noncovalent modification of thin filament action: the essential role of troponin in cardiac muscle regulation. *Circ Res* **94**, 146-158, doi:10.1161/01.RES.0000110083.17024.60 (2004).
- 31 Strang, K. T., Sweitzer, N. K., Greaser, M. L. & Moss, R. L. Beta-adrenergic receptor stimulation increases unloaded shortening velocity of skinned single ventricular myocytes from rats. *Circ Res* **74**, 542-549, doi:10.1161/01.res.74.3.542 (1994).
- 32 Kentish, J. C. *et al.* Phosphorylation of troponin I by protein kinase A accelerates relaxation and crossbridge cycle kinetics in mouse ventricular muscle. *Circ Res* **88**, 1059-1065 (2001).
- 33 Saeki, Y., Shiozawa, K., Yanagisawa, K. & Shibata, T. Adrenaline increases the rate of cross-bridge cycling in rat cardiac muscle. *J Mol Cell Cardiol* **22**, 453-460, doi:10.1016/0022-2828(90)91480-u (1990).
- 34 Hoh, J. F., Rossmann, G. H., Kwan, L. J. & Hamilton, A. M. Adrenaline increases the rate of cycling of crossbridges in rat cardiac muscle as measured by pseudo-random binary noise-modulated perturbation analysis. *Circ Res* **62**, 452-461, doi:10.1161/01.res.62.3.452 (1988).
- 35 Fentzke, R. C. *et al.* Impaired cardiomyocyte relaxation and diastolic function in transgenic mice expressing slow skeletal troponin I in the heart. *J Physiol* **517 (Pt 1)**, 143-157, doi:10.1111/j.1469-7793.1999.0143z.x (1999).
- 36 Jin, J. P. & Chong, S. M. Localization of the two tropomyosin-binding sites of troponin T. *Arch Biochem Biophys* **500**, 144-150, doi:10.1016/j.abb.2010.06.001 (2010).
- 37 Jeon, Y. H. *et al.* Phosphodiesterase: overview of protein structures, potential therapeutic applications and recent progress in drug development. *Cell Mol Life Sci* **62**, 1198-1220, doi:10.1007/s00018-005-4533-5 (2005).
- 38 Wu, H. *et al.* Epigenetic Regulation of Phosphodiesterases 2A and 3A Underlies Compromised beta-Adrenergic Signaling in an iPSC Model of Dilated Cardiomyopathy. *Cell Stem Cell* **17**, 89-100, doi:10.1016/j.stem.2015.04.020 (2015).
- 39 Sumandea, C. A. *et al.* Cardiac troponin T, a sarcomeric AKAP, tethers protein kinase A at the myofilaments. *J Biol Chem* **286**, 530-541, doi:10.1074/jbc.M110.148684 (2011).
- 40 Noland, T. A. & Kuo, J. F. Protein kinase C phosphorylation of cardiac troponin I and troponin T inhibits Ca(2+)-stimulated MgATPase activity in reconstituted actomyosin and isolated myofibrils, and decreases actin-myosin interactions. *J Mol Cell Cardiol* **25**, 53-65, doi:10.1006/jmcc.1993.1007 (1993).
- 41 Herrmann, H., Strelkov, S. V., Burkhard, P. & Aebi, U. Intermediate filaments: primary determinants of cell architecture and plasticity. *J Clin Invest* **119**, 1772-1783, doi:10.1172/JCI38214 (2009).
- 42 Tsikitis, M., Galata, Z., Mavroidis, M., Psarras, S. & Capetanaki, Y. Intermediate filaments in cardiomyopathy. *Biophys Rev* **10**, 1007-1031, doi:10.1007/s12551-018-0443-2 (2018).
- 43 Goldmann, W. H. Intermediate filaments and cellular mechanics. *Cell Biol Int* **42**, 132-138, doi:10.1002/cbin.10879 (2018).
- 44 Mao, Z. & Nakamura, F. Structure and Function of Filamin C in the Muscle Z-Disc. *Int J Mol Sci* **21**, doi:10.3390/ijms21082696 (2020).

- 45 Koteliansky, V. E. *et al.* Identification of a filamin-like protein in chicken heart muscle. *FEBS Lett* **125**, 44-48, doi:10.1016/0014-5793(81)80992-1 (1981).
- 46 Head, B. P. *et al.* Microtubules and actin microfilaments regulate lipid raft/caveolae localization of adenylyl cyclase signaling components. *J Biol Chem* **281**, 26391-26399, doi:10.1074/jbc.M602577200 (2006).
- 47 Dalkilic, I., Schienda, J., Thompson, T. G. & Kunkel, L. M. Loss of FilaminC (FLNc) results in severe defects in myogenesis and myotube structure. *Mol Cell Biol* **26**, 6522-6534, doi:10.1128/MCB.00243-06 (2006).
- 48 Begay, R. L. *et al.* Filamin C Truncation Mutations Are Associated With Arrhythmogenic Dilated Cardiomyopathy and Changes in the Cell-Cell Adhesion Structures. *JACC Clin Electrophysiol* **4**, 504-514, doi:10.1016/j.jacep.2017.12.003 (2018).
- 49 Dominguez, R. & Holmes, K. C. Actin structure and function. *Annu Rev Biophys* **40**, 169-186, doi:10.1146/annurev-biophys-042910-155359 (2011).
- 50 Yarmola, E. G., Somasundaram, T., Boring, T. A., Spector, I. & Bubb, M. R. Actin-latrunculin A structure and function. Differential modulation of actin-binding protein function by latrunculin A. *J Biol Chem* **275**, 28120-28127, doi:10.1074/jbc.M004253200 (2000).
- 51 Patel, V. B. *et al.* PI3K α -regulated gelsolin activity is a critical determinant of cardiac cytoskeletal remodeling and heart disease. *Nat Commun* **9**, 5390, doi:10.1038/s41467-018-07812-8 (2018).
- 52 Efimova, N. *et al.* Branched actin networks are assembled on microtubules by adenomatous polyposis coli for targeted membrane protrusion. *J Cell Biol* **219**, doi:10.1083/jcb.202003091 (2020).
- 53 Mullins, R. D., Heuser, J. A. & Pollard, T. D. The interaction of Arp2/3 complex with actin: nucleation, high affinity pointed end capping, and formation of branching networks of filaments. *Proc Natl Acad Sci U S A* **95**, 6181-6186, doi:10.1073/pnas.95.11.6181 (1998).
- 54 Svitkina, T. M. & Borisy, G. G. Arp2/3 complex and actin depolymerizing factor/cofilin in dendritic organization and treadmilling of actin filament array in lamellipodia. *J Cell Biol* **145**, 1009-1026, doi:10.1083/jcb.145.5.1009 (1999).
- 55 Duleh, S. N. & Welch, M. D. WASH and the Arp2/3 complex regulate endosome shape and trafficking. *Cytoskeleton (Hoboken)* **67**, 193-206, doi:10.1002/cm.20437 (2010).
- 56 Moon, S., Han, D., Kim, Y., Jin, J. & Ho, W. K. Interactome analysis of AMP-activated protein kinase (AMPK)- α 1 and - β 1 in INS-1 pancreatic beta-cells by affinity purification-mass spectrometry. *Sci Rep* **4**, 4376, doi:10.1038/srep04376 (2014).
- 57 Miranda, L. *et al.* AMP-activated protein kinase induces actin cytoskeleton reorganization in epithelial cells. *Biochem Biophys Res Commun* **396**, 656-661, doi:10.1016/j.bbrc.2010.04.151 (2010).
- 58 Chatterjee, A., Villarreal, G., Jr., Oh, D. J., Kang, M. H. & Rhee, D. J. AMP-activated protein kinase regulates intraocular pressure, extracellular matrix, and cytoskeleton in trabecular meshwork. *Invest Ophthalmol Vis Sci* **55**, 3127-3139, doi:10.1167/iovs.13-12755 (2014).

- 59 Bairwa, S. C., Parajuli, N. & Dyck, J. R. The role of AMPK in cardiomyocyte health and survival. *Biochim Biophys Acta* **1862**, 2199-2210, doi:10.1016/j.bbadis.2016.07.001 (2016).
- 60 Johnston, J. R., Chase, P. B. & Pinto, J. R. Troponin through the looking-glass: emerging roles beyond regulation of striated muscle contraction. *Oncotarget* **9**, 1461-1482, doi:10.18632/oncotarget.22879 (2018).
- 61 Guyon, J. R. *et al.* Calpain 3 cleaves filamin C and regulates its ability to interact with gamma- and delta-sarcoglycans. *Muscle Nerve* **28**, 472-483, doi:10.1002/mus.10465 (2003).
- 62 Gontier, Y. *et al.* The Z-disc proteins myotilin and FATZ-1 interact with each other and are connected to the sarcolemma via muscle-specific filamins. *J Cell Sci* **118**, 3739-3749, doi:10.1242/jcs.02484 (2005).
- 63 Peter, A. K., Cheng, H., Ross, R. S., Knowlton, K. U. & Chen, J. The costamere bridges sarcomeres to the sarcolemma in striated muscle. *Prog Pediatr Cardiol* **31**, 83-88, doi:10.1016/j.ppedcard.2011.02.003 (2011).
- 64 Zemljic-Harpf, A., Manso, A. M. & Ross, R. S. Vinculin and talin: focus on the myocardium. *J Investig Med* **57**, 849-855, doi:10.2310/JIM.0b013e3181c5e074 (2009).
- 65 Grimes, K. M., Prasad, V. & McNamara, J. W. Supporting the heart: Functions of the cardiomyocyte's non-sarcomeric cytoskeleton. *J Mol Cell Cardiol* **131**, 187-196, doi:10.1016/j.yjmcc.2019.04.002 (2019).
- 66 Bakolitsa, C. *et al.* Structural basis for vinculin activation at sites of cell adhesion. *Nature* **430**, 583-586, doi:10.1038/nature02610 (2004).
- 67 Borgon, R. A., Vonrhein, C., Bricogne, G., Bois, P. R. & Izard, T. Crystal structure of human vinculin. *Structure* **12**, 1189-1197, doi:10.1016/j.str.2004.05.009 (2004).
- 68 van den Bout, I. & Divecha, N. PIP5K-driven PtdIns(4,5)P₂ synthesis: regulation and cellular functions. *J Cell Sci* **122**, 3837-3850, doi:10.1242/jcs.056127 (2009).
- 69 Ziegler, W. H., Liddington, R. C. & Critchley, D. R. The structure and regulation of vinculin. *Trends Cell Biol* **16**, 453-460, doi:10.1016/j.tcb.2006.07.004 (2006).
- 70 Boujemaa-Paterski, R. *et al.* Talin-activated vinculin interacts with branched actin networks to initiate bundles. *Elife* **9**, doi:10.7554/eLife.53990 (2020).
- 71 DeMali, K. A., Barlow, C. A. & Burridge, K. Recruitment of the Arp2/3 complex to vinculin: coupling membrane protrusion to matrix adhesion. *J Cell Biol* **159**, 881-891, doi:10.1083/jcb.200206043 (2002).
- 72 Hagiwara, M. *et al.* Vinculin and Rab5 complex is required [correction of required] for uptake of Staphylococcus aureus and interleukin-6 expression. *PLoS One* **9**, e87373, doi:10.1371/journal.pone.0087373 (2014).
- 73 Bucci, C. *et al.* The small GTPase rab5 functions as a regulatory factor in the early endocytic pathway. *Cell* **70**, 715-728, doi:10.1016/0092-8674(92)90306-w (1992).
- 74 Thompson, P. M. *et al.* A Structural Model for Vinculin Insertion into PIP. *Structure* **25**, 264-275, doi:10.1016/j.str.2016.12.002 (2017).
- 75 Halstead, J. R. *et al.* Rac controls PIP5K localisation and PtdIns(4,5)P₂ synthesis, which modulates vinculin localisation and neurite dynamics. *J Cell Sci* **123**, 3535-3546, doi:10.1242/jcs.062679 (2010).

- 76 Sechi, A. S. & Wehland, J. The actin cytoskeleton and plasma membrane connection: PtdIns(4,5)P(2) influences cytoskeletal protein activity at the plasma membrane. *J Cell Sci* **113 Pt 21**, 3685-3695 (2000).
- 77 Czech, M. P. PIP2 and PIP3: complex roles at the cell surface. *Cell* **100**, 603-606, doi:10.1016/s0092-8674(00)80696-0 (2000).
- 78 Suh, B. C. & Hille, B. PIP2 is a necessary cofactor for ion channel function: how and why? *Annu Rev Biophys* **37**, 175-195, doi:10.1146/annurev.biophys.37.032807.125859 (2008).
- 79 Mandal, K. Review of PIP2 in Cellular Signaling, Functions and Diseases. *Int J Mol Sci* **21**, doi:10.3390/ijms21218342 (2020).
- 80 Fruman, D. A., Meyers, R. E. & Cantley, L. C. Phosphoinositide kinases. *Annu Rev Biochem* **67**, 481-507, doi:10.1146/annurev.biochem.67.1.481 (1998).
- 81 Shibasaki, Y. *et al.* Massive actin polymerization induced by phosphatidylinositol-4-phosphate 5-kinase in vivo. *J Biol Chem* **272**, 7578-7581, doi:10.1074/jbc.272.12.7578 (1997).
- 82 Oude Weernink, P. A. *et al.* Stimulation of phosphatidylinositol-4-phosphate 5-kinase by Rho-kinase. *J Biol Chem* **275**, 10168-10174, doi:10.1074/jbc.275.14.10168 (2000).
- 83 Miyamoto, S. *et al.* Revisited and revised: is RhoA always a villain in cardiac pathophysiology? *J Cardiovasc Transl Res* **3**, 330-343, doi:10.1007/s12265-010-9192-8 (2010).
- 84 Kilian, L. S., Voran, J., Frank, D. & Rangrez, A. Y. RhoA: a dubious molecule in cardiac pathophysiology. *J Biomed Sci* **28**, 33, doi:10.1186/s12929-021-00730-w (2021).
- 85 Lauriol, J. *et al.* RhoA signaling in cardiomyocytes protects against stress-induced heart failure but facilitates cardiac fibrosis. *Sci Signal* **7**, ra100, doi:10.1126/scisignal.2005262 (2014).
- 86 Xiang, S. Y. *et al.* RhoA protects the mouse heart against ischemia/reperfusion injury. *J Clin Invest* **121**, 3269-3276, doi:10.1172/JCI44371 (2011).
- 87 Loirand, G., Guérin, P. & Pacaud, P. Rho kinases in cardiovascular physiology and pathophysiology. *Circ Res* **98**, 322-334, doi:10.1161/01.RES.0000201960.04223.3c (2006).
- 88 Sah, V. P. *et al.* Cardiac-specific overexpression of RhoA results in sinus and atrioventricular nodal dysfunction and contractile failure. *J Clin Invest* **103**, 1627-1634, doi:10.1172/JCI6842 (1999).
- 89 Matsui, T. *et al.* Rho-associated kinase, a novel serine/threonine kinase, as a putative target for small GTP binding protein Rho. *EMBO J* **15**, 2208-2216 (1996).
- 90 Surma, M., Wei, L. & Shi, J. Rho kinase as a therapeutic target in cardiovascular disease. *Future Cardiol* **7**, 657-671, doi:10.2217/fca.11.51 (2011).
- 91 Shimizu, T. & Liao, J. K. Rho Kinases and Cardiac Remodeling. *Circ J* **80**, 1491-1498, doi:10.1253/circj.CJ-16-0433 (2016).
- 92 McLaughlin, S., Wang, J., Gambhir, A. & Murray, D. PIP(2) and proteins: interactions, organization, and information flow. *Annu Rev Biophys Biomol Struct* **31**, 151-175, doi:10.1146/annurev.biophys.31.082901.134259 (2002).
- 93 van den Bogaart, G. *et al.* Membrane protein sequestering by ionic protein-lipid interactions. *Nature* **479**, 552-555, doi:10.1038/nature10545 (2011).

- 94 Wang, Y. H. *et al.* Divalent cation-induced cluster formation by polyphosphoinositides in model membranes. *J Am Chem Soc* **134**, 3387-3395, doi:10.1021/ja208640t (2012).
- 95 Frost, A., Unger, V. M. & De Camilli, P. The BAR domain superfamily: membrane-molding macromolecules. *Cell* **137**, 191-196, doi:10.1016/j.cell.2009.04.010 (2009).
- 96 Mattila, P. K. *et al.* Missing-in-metastasis and IRSp53 deform PI(4,5)P₂-rich membranes by an inverse BAR domain-like mechanism. *J Cell Biol* **176**, 953-964, doi:10.1083/jcb.200609176 (2007).
- 97 Wu, T. & Baumgart, T. BIN1 membrane curvature sensing and generation show autoinhibition regulated by downstream ligands and PI(4,5)P₂. *Biochemistry* **53**, 7297-7309, doi:10.1021/bi501082r (2014).
- 98 Hilgemann, D. W. & Ball, R. Regulation of cardiac Na⁺,Ca²⁺ exchange and KATP potassium channels by PIP₂. *Science* **273**, 956-959, doi:10.1126/science.273.5277.956 (1996).
- 99 Kaksonen, M. & Roux, A. Mechanisms of clathrin-mediated endocytosis. *Nat Rev Mol Cell Biol* **19**, 313-326, doi:10.1038/nrm.2017.132 (2018).
- 100 Alberts B, J. A., Lewis J, et al. *Molecular Biology of the Cell. 4th edition.*, (New York: Garland Science, 2002).
- 101 Sorkin, A. & von Zastrow, M. Endocytosis and signalling: intertwining molecular networks. *Nat Rev Mol Cell Biol* **10**, 609-622, doi:10.1038/nrm2748 (2009).
- 102 Lane, D. J. *et al.* Cellular iron uptake, trafficking and metabolism: Key molecules and mechanisms and their roles in disease. *Biochim Biophys Acta* **1853**, 1130-1144, doi:10.1016/j.bbamcr.2015.01.021 (2015).
- 103 Go, G. W. & Mani, A. Low-density lipoprotein receptor (LDLR) family orchestrates cholesterol homeostasis. *Yale J Biol Med* **85**, 19-28 (2012).
- 104 Antonescu, C. N., Aguet, F., Danuser, G. & Schmid, S. L. Phosphatidylinositol-(4,5)-bisphosphate regulates clathrin-coated pit initiation, stabilization, and size. *Mol Biol Cell* **22**, 2588-2600, doi:10.1091/mbc.E11-04-0362 (2011).
- 105 Zoncu, R. *et al.* Loss of endocytic clathrin-coated pits upon acute depletion of phosphatidylinositol 4,5-bisphosphate. *Proc Natl Acad Sci U S A* **104**, 3793-3798, doi:10.1073/pnas.0611733104 (2007).
- 106 Di Paolo, G. *et al.* Impaired PtdIns(4,5)P₂ synthesis in nerve terminals produces defects in synaptic vesicle trafficking. *Nature* **431**, 415-422, doi:10.1038/nature02896 (2004).
- 107 Traub, L. M. Tickets to ride: selecting cargo for clathrin-regulated internalization. *Nat Rev Mol Cell Biol* **10**, 583-596, doi:10.1038/nrm2751 (2009).
- 108 Boulant, S., Kural, C., Zeeh, J. C., Ubelmann, F. & Kirchhausen, T. Actin dynamics counteract membrane tension during clathrin-mediated endocytosis. *Nat Cell Biol* **13**, 1124-1131, doi:10.1038/ncb2307 (2011).
- 109 Mooren, O. L., Galletta, B. J. & Cooper, J. A. Roles for actin assembly in endocytosis. *Annu Rev Biochem* **81**, 661-686, doi:10.1146/annurev-biochem-060910-094416 (2012).
- 110 Smythe, E. & Ayscough, K. R. Actin regulation in endocytosis. *J Cell Sci* **119**, 4589-4598, doi:10.1242/jcs.03247 (2006).

- 111 Kaksonen, M., Toret, C. P. & Drubin, D. G. Harnessing actin dynamics for clathrin-mediated endocytosis. *Nat Rev Mol Cell Biol* **7**, 404-414, doi:10.1038/nrm1940 (2006).
- 112 Cauvin, C. *et al.* Rab35 GTPase Triggers Switch-like Recruitment of the Lowe Syndrome Lipid Phosphatase OCRL on Newborn Endosomes. *Curr Biol* **26**, 120-128, doi:10.1016/j.cub.2015.11.040 (2016).
- 113 Wandinger-Ness, A. & Zerial, M. Rab proteins and the compartmentalization of the endosomal system. *Cold Spring Harb Perspect Biol* **6**, a022616, doi:10.1101/cshperspect.a022616 (2014).
- 114 Mu, F. T. *et al.* EEA1, an early endosome-associated protein. EEA1 is a conserved alpha-helical peripheral membrane protein flanked by cysteine "fingers" and contains a calmodulin-binding IQ motif. *J Biol Chem* **270**, 13503-13511, doi:10.1074/jbc.270.22.13503 (1995).
- 115 Vicinanza, M. *et al.* OCRL controls trafficking through early endosomes via PtdIns4,5P₂-dependent regulation of endosomal actin. *EMBO J* **30**, 4970-4985, doi:10.1038/emboj.2011.354 (2011).
- 116 Seaman, M. N., Gautreau, A. & Billadeau, D. D. Retromer-mediated endosomal protein sorting: all WASHed up! *Trends Cell Biol* **23**, 522-528, doi:10.1016/j.tcb.2013.04.010 (2013).
- 117 Jia, D. *et al.* WASH and WAVE actin regulators of the Wiskott-Aldrich syndrome protein (WASP) family are controlled by analogous structurally related complexes. *Proc Natl Acad Sci U S A* **107**, 10442-10447, doi:10.1073/pnas.0913293107 (2010).
- 118 Padrick, S. B., Doolittle, L. K., Brautigam, C. A., King, D. S. & Rosen, M. K. Arp2/3 complex is bound and activated by two WASP proteins. *Proc Natl Acad Sci U S A* **108**, E472-479, doi:10.1073/pnas.1100236108 (2011).
- 119 Rodnick-Smith, M., Luan, Q., Liu, S. L. & Nolen, B. J. Role and structural mechanism of WASP-triggered conformational changes in branched actin filament nucleation by Arp2/3 complex. *Proc Natl Acad Sci U S A* **113**, E3834-3843, doi:10.1073/pnas.1517798113 (2016).
- 120 Benesch, S. *et al.* Phosphatidylinositol 4,5-biphosphate (PIP₂)-induced vesicle movement depends on N-WASP and involves Nck, WIP, and Grb2. *J Biol Chem* **277**, 37771-37776, doi:10.1074/jbc.M204145200 (2002).
- 121 Vivot, R. M., Goitia, B., Usach, V. & Setton-Avruj, P. C. DMT1 as a candidate for non-transferrin-bound iron uptake in the peripheral nervous system. *Biofactors* **39**, 476-484, doi:10.1002/biof.1088 (2013).
- 122 Motley, A., Bright, N. A., Seaman, M. N. & Robinson, M. S. Clathrin-mediated endocytosis in AP-2-depleted cells. *J Cell Biol* **162**, 909-918, doi:10.1083/jcb.200305145 (2003).
- 123 Núñez, M. T., Gaete, V., Watkins, J. A. & Glass, J. Mobilization of iron from endocytic vesicles. The effects of acidification and reduction. *J Biol Chem* **265**, 6688-6692 (1990).
- 124 Ohgami, R. S. *et al.* nm1054: a spontaneous, recessive, hypochromic, microcytic anemia mutation in the mouse. *Blood* **106**, 3625-3631, doi:10.1182/blood-2005-01-0379 (2005).

-
- 125 Ohgami, R. S. *et al.* Identification of a ferrireductase required for efficient transferrin-dependent iron uptake in erythroid cells. *Nat Genet* **37**, 1264-1269, doi:10.1038/ng1658 (2005).
- 126 Lambe, T. *et al.* Identification of a Steap3 endosomal targeting motif essential for normal iron metabolism. *Blood* **113**, 1805-1808, doi:10.1182/blood-2007-11-120402 (2009).
- 127 Gruenheid, S., Cellier, M., Vidal, S. & Gros, P. Identification and characterization of a second mouse Nramp gene. *Genomics* **25**, 514-525, doi:10.1016/0888-7543(95)80053-o (1995).
- 128 Torti, F. M. & Torti, S. V. Regulation of ferritin genes and protein. *Blood* **99**, 3505-3516, doi:10.1182/blood.v99.10.3505 (2002).
- 129 von Haehling, S., Ebner, N., Evertz, R., Ponikowski, P. & Anker, S. D. Iron Deficiency in Heart Failure: An Overview. *JACC Heart Fail* **7**, 36-46, doi:10.1016/j.jchf.2018.07.015 (2019).
- 130 Cappellini, M. D. *et al.* Iron deficiency across chronic inflammatory conditions: International expert opinion on definition, diagnosis, and management. *Am J Hematol* **92**, 1068-1078, doi:10.1002/ajh.24820 (2017).
- 131 Rizzo, C., Carbonara, R., Ruggieri, R., Passantino, A. & Scrutinio, D. Iron Deficiency: A New Target for Patients With Heart Failure. *Front Cardiovasc Med* **8**, 709872, doi:10.3389/fcvm.2021.709872 (2021).
- 132 Ponikowski, P. *et al.* Beneficial effects of long-term intravenous iron therapy with ferric carboxymaltose in patients with symptomatic heart failure and iron deficiency†. *Eur Heart J* **36**, 657-668, doi:10.1093/eurheartj/ehu385 (2015).
- 133 Yiannikourides, A. & Latunde-Dada, G. O. A Short Review of Iron Metabolism and Pathophysiology of Iron Disorders. *Medicines (Basel)* **6**, doi:10.3390/medicines6030085 (2019).
- 134 Camaschella, C., Nai, A. & Silvestri, L. Iron metabolism and iron disorders revisited in the hepcidin era. *Haematologica* **105**, 260-272, doi:10.3324/haematol.2019.232124 (2020).
- 135 Harrison, P. M., Banyard, S. H., Hoare, R. J., Russell, S. M. & Treffry, A. The structure and function of ferritin. *Ciba Found Symp*, 19-40, doi:10.1002/9780470720325.ch2 (1976).
- 136 Levi, S. *et al.* A human mitochondrial ferritin encoded by an intronless gene. *J Biol Chem* **276**, 24437-24440, doi:10.1074/jbc.C100141200 (2001).
- 137 Nemeth, E. *et al.* Hepcidin regulates cellular iron efflux by binding to ferroportin and inducing its internalization. *Science* **306**, 2090-2093, doi:10.1126/science.1104742 (2004).
- 138 Donovan, A. *et al.* The iron exporter ferroportin/Slc40a1 is essential for iron homeostasis. *Cell Metab* **1**, 191-200, doi:10.1016/j.cmet.2005.01.003 (2005).
- 139 Billesbølle, C. B. *et al.* Structure of hepcidin-bound ferroportin reveals iron homeostatic mechanisms. *Nature* **586**, 807-811, doi:10.1038/s41586-020-2668-z (2020).
- 140 Drakesmith, H., Nemeth, E. & Ganz, T. Ironing out Ferroportin. *Cell Metab* **22**, 777-787, doi:10.1016/j.cmet.2015.09.006 (2015).

- 141 Muckenthaler, M., Gray, N. K. & Hentze, M. W. IRP-1 binding to ferritin mRNA prevents the recruitment of the small ribosomal subunit by the cap-binding complex eIF4F. *Mol Cell* **2**, 383-388, doi:10.1016/s1097-2765(00)80282-8 (1998).
- 142 Meyron-Holtz, E. G. *et al.* Genetic ablations of iron regulatory proteins 1 and 2 reveal why iron regulatory protein 2 dominates iron homeostasis. *EMBO J* **23**, 386-395, doi:10.1038/sj.emboj.7600041 (2004).
- 143 Lakhal-Littleton, S. Mechanisms of cardiac iron homeostasis and their importance to heart function. *Free Radic Biol Med* **133**, 234-237, doi:10.1016/j.freeradbiomed.2018.08.010 (2019).
- 144 Muckenthaler, M. U., Rivella, S., Hentze, M. W. & Galy, B. A Red Carpet for Iron Metabolism. *Cell* **168**, 344-361, doi:10.1016/j.cell.2016.12.034 (2017).
- 145 Rouault, T. A. The role of iron regulatory proteins in mammalian iron homeostasis and disease. *Nat Chem Biol* **2**, 406-414, doi:10.1038/nchembio807 (2006).
- 146 Cerri, S., Milanese, C. & Mastroberardino, P. G. Endocytic iron trafficking and mitochondria in Parkinson's disease. *Int J Biochem Cell Biol* **110**, 70-74, doi:10.1016/j.biocel.2019.02.009 (2019).
- 147 Richardson, D. R. *et al.* Mitochondrial iron trafficking and the integration of iron metabolism between the mitochondrion and cytosol. *Proc Natl Acad Sci U S A* **107**, 10775-10782, doi:10.1073/pnas.0912925107 (2010).
- 148 Braymer, J. J. & Lill, R. Iron-sulfur cluster biogenesis and trafficking in mitochondria. *J Biol Chem* **292**, 12754-12763, doi:10.1074/jbc.R117.787101 (2017).
- 149 Xu, W. *et al.* Lethal Cardiomyopathy in Mice Lacking Transferrin Receptor in the Heart. *Cell Rep* **13**, 533-545, doi:10.1016/j.celrep.2015.09.023 (2015).
- 150 Hoes, M. F. *et al.* Iron deficiency impairs contractility of human cardiomyocytes through decreased mitochondrial function. *Eur J Heart Fail* **20**, 910-919, doi:10.1002/ejhf.1154 (2018).
- 151 Ebert, A. D., Diecke, S., Chen, I. Y. & Wu, J. C. Reprogramming and transdifferentiation for cardiovascular development and regenerative medicine: where do we stand? *EMBO Mol Med* **7**, 1090-1103, doi:10.15252/emmm.201504395 (2015).
- 152 Takahashi, K. & Yamanaka, S. Induction of pluripotent stem cells from mouse embryonic and adult fibroblast cultures by defined factors. *Cell* **126**, 663-676, doi:S0092-8674(06)00976-7 [pii] 10.1016/j.cell.2006.07.024 (2006).
- 153 Musunuru, K. *et al.* Induced Pluripotent Stem Cells for Cardiovascular Disease Modeling and Precision Medicine: A Scientific Statement From the American Heart Association. *Circ Genom Precis Med* **11**, e000043, doi:10.1161/HCG.0000000000000043 (2018).
- 154 Chen, G. *et al.* Chemically defined conditions for human iPSC derivation and culture. *Nat Methods* **8**, 424-429, doi:10.1038/nmeth.1593 nmeth.1593 [pii] (2011).
- 155 Lian, X. *et al.* Robust cardiomyocyte differentiation from human pluripotent stem cells via temporal modulation of canonical Wnt signaling. *Proc Natl Acad Sci U S A* **109**, E1848-1857, doi:10.1073/pnas.1200250109 1200250109 [pii] (2012).

-
- 156 Lian, X. *et al.* Directed cardiomyocyte differentiation from human pluripotent stem cells by modulating Wnt/beta-catenin signaling under fully defined conditions. *Nat Protoc* **8**, 162-175, doi:10.1038/nprot.2012.150 nprot.2012.150 [pii] (2013).
- 157 Horvath, P. & Barrangou, R. CRISPR/Cas, the immune system of bacteria and archaea. *Science* **327**, 167-170, doi:10.1126/science.1179555 (2010).
- 158 Ran, F. A. *et al.* Genome engineering using the CRISPR-Cas9 system. *Nat Protoc* **8**, 2281-2308, doi:10.1038/nprot.2013.143 (2013).
- 159 Garneau, J. E. *et al.* The CRISPR/Cas bacterial immune system cleaves bacteriophage and plasmid DNA. *Nature* **468**, 67-71, doi:10.1038/nature09523 (2010).
- 160 Hale, C. R. *et al.* RNA-guided RNA cleavage by a CRISPR RNA-Cas protein complex. *Cell* **139**, 945-956, doi:10.1016/j.cell.2009.07.040 (2009).
- 161 Makarova, K. S. *et al.* Evolution and classification of the CRISPR-Cas systems. *Nat Rev Microbiol* **9**, 467-477, doi:10.1038/nrmicro2577 (2011).
- 162 Kotyk, A., Venkov, P. & Dvoráková, M. Membrane transport in an osmotically fragile mutant of *Saccharomyces cerevisiae*. *Yeast* **4**, 241-247, doi:10.1002/yea.320040402 (1988).
- 163 Liang, F., Han, M., Romanienko, P. J. & Jasin, M. Homology-directed repair is a major double-strand break repair pathway in mammalian cells. *Proc Natl Acad Sci U S A* **95**, 5172-5177, doi:10.1073/pnas.95.9.5172 (1998).
- 164 Nambiar, T. S. *et al.* Stimulation of CRISPR-mediated homology-directed repair by an engineered RAD18 variant. *Nat Commun* **10**, 3395, doi:10.1038/s41467-019-11105-z (2019).
- 165 Davis, A. J. & Chen, D. J. DNA double strand break repair via non-homologous end-joining. *Transl Cancer Res* **2**, 130-143, doi:10.3978/j.issn.2218-676X.2013.04.02 (2013).
- 166 Savoji, H. *et al.* Cardiovascular disease models: A game changing paradigm in drug discovery and screening. *Biomaterials* **198**, 3-26, doi:10.1016/j.biomaterials.2018.09.036 (2019).
- 167 McNally, E. M. & Mestroni, L. Dilated Cardiomyopathy: Genetic Determinants and Mechanisms. *Circ Res* **121**, 731-748, doi:10.1161/CIRCRESAHA.116.309396 (2017).
- 168 Yutzey, K. E. & Robbins, J. Principles of genetic murine models for cardiac disease. *Circulation* **115**, 792-799, doi:10.1161/CIRCULATIONAHA.106.682534 (2007).
- 169 Rudolph, F. *et al.* Deconstructing sarcomeric structure-function relations in titin-BioID knock-in mice. *Nat Commun* **11**, 3133, doi:10.1038/s41467-020-16929-8 (2020).
- 170 Swist, S. *et al.* Maintenance of sarcomeric integrity in adult muscle cells crucially depends on Z-disc anchored titin. *Nat Commun* **11**, 4479, doi:10.1038/s41467-020-18131-2 (2020).
- 171 Dai, Y. *et al.* Troponin destabilization impairs sarcomere-cytoskeleton interactions in iPSC-derived cardiomyocytes from dilated cardiomyopathy patients. *Sci Rep* **10**, 209, doi:10.1038/s41598-019-56597-3 (2020).
- 172 Sun, N. *et al.* Patient-specific induced pluripotent stem cells as a model for familial dilated cardiomyopathy. *Sci Transl Med* **4**, 130ra147, doi:10.1126/scitranslmed.3003552 (2012).

- 173 Xu, H. *et al.* Non-negative blind deconvolution for signal processing in a CRISPR-edited iPSC-cardiomyocyte model of dilated cardiomyopathy. *FEBS Lett*, doi:10.1002/1873-3468.14189 (2021).
- 174 Dieseldorff Jones, K. M. *et al.* Pathogenic troponin T mutants with opposing effects on myofilament Ca. *Arch Biochem Biophys* **661**, 125-131, doi:10.1016/j.abb.2018.11.006 (2019).
- 175 Li, D. *et al.* Novel cardiac troponin T mutation as a cause of familial dilated cardiomyopathy. *Circulation* **104**, 2188-2193 (2001).
- 176 Hinson, J. T. *et al.* HEART DISEASE. Titin mutations in iPS cells define sarcomere insufficiency as a cause of dilated cardiomyopathy. *Science* **349**, 982-986, doi:10.1126/science.aaa5458 (2015).
- 177 Gupte, T. M. *et al.* Mechanistic heterogeneity in contractile properties of α -tropomyosin (TPM1) mutants associated with inherited cardiomyopathies. *J Biol Chem* **290**, 7003-7015, doi:10.1074/jbc.M114.596676 (2015).
- 178 Chang, A. N., Harada, K., Ackerman, M. J. & Potter, J. D. Functional consequences of hypertrophic and dilated cardiomyopathy-causing mutations in alpha-tropomyosin. *J Biol Chem* **280**, 34343-34349, doi:10.1074/jbc.M505014200 (2005).
- 179 Bai, F., Groth, H. L. & Kawai, M. DCM-related tropomyosin mutants E40K/E54K over-inhibit the actomyosin interaction and lead to a decrease in the number of cycling cross-bridges. *PLoS One* **7**, e47471, doi:10.1371/journal.pone.0047471 (2012).
- 180 Lakdawala, N. K. *et al.* Familial dilated cardiomyopathy caused by an alpha-tropomyosin mutation: the distinctive natural history of sarcomeric dilated cardiomyopathy. *J Am Coll Cardiol* **55**, 320-329, doi:10.1016/j.jacc.2009.11.017 (2010).
- 181 Chang, A. N. & Potter, J. D. Sarcomeric protein mutations in dilated cardiomyopathy. *Heart Fail Rev* **10**, 225-235, doi:10.1007/s10741-005-5252-6 (2005).
- 182 Schultheiss, H. P. *et al.* Dilated cardiomyopathy. *Nat Rev Dis Primers* **5**, 32, doi:10.1038/s41572-019-0084-1 (2019).
- 183 Garfinkel, A. C., Seidman, J. G. & Seidman, C. E. Genetic Pathogenesis of Hypertrophic and Dilated Cardiomyopathy. *Heart Fail Clin* **14**, 139-146, doi:10.1016/j.hfc.2017.12.004 (2018).
- 184 McNally, E. M., Golbus, J. R. & Puckelwartz, M. J. Genetic mutations and mechanisms in dilated cardiomyopathy. *J Clin Invest* **123**, 19-26, doi:62862 [pii] 10.1172/JCI62862 (2013).
- 185 Sequeira, V., Nijenkamp, L. L., Regan, J. A. & van der Velden, J. The physiological role of cardiac cytoskeleton and its alterations in heart failure. *Biochim Biophys Acta* **1838**, 700-722, doi:10.1016/j.bbamem.2013.07.011 (2014).
- 186 Boucrot, E., Saffarian, S., Massol, R., Kirchhausen, T. & Ehrlich, M. Role of lipids and actin in the formation of clathrin-coated pits. *Exp Cell Res* **312**, 4036-4048, doi:10.1016/j.yexcr.2006.09.025 (2006).
- 187 Merrifield, C. J. & Kaksonen, M. Endocytic accessory factors and regulation of clathrin-mediated endocytosis. *Cold Spring Harb Perspect Biol* **6**, a016733, doi:10.1101/cshperspect.a016733 (2014).
- 188 Yuanyuan Dai, N. I., Hang Xu, Ruheen Wali, Karl Toischer, Sören Brandenburg, Christof Lenz, Samuel Sossalla, Niels Voigt, Elisabeth M. Zeisberg, Andreas Janshoff,

-
- Henning Urlaub, Torsten Bloch Rasmussen, Jens Mogensen, Stephan E. Lehnart, Gerd Hasenfuss, Antje Ebert. An alternative mechanism of subcellular iron uptake deficiency in cardiomyocytes and treatment approach in heart failure. *submitted to Circulation Research* (2022).
- 189 Stehling, O., Sheftel, A. D. & Lill, R. Chapter 12 Controlled expression of iron-sulfur cluster assembly components for respiratory chain complexes in mammalian cells. *Methods Enzymol* **456**, 209-231, doi:10.1016/S0076-6879(08)04412-1 (2009).
- 190 Sato, T. *et al.* mRNA-binding protein tristetraprolin is essential for cardiac response to iron deficiency by regulating mitochondrial function. *Proc Natl Acad Sci U S A* **115**, E6291-E6300, doi:10.1073/pnas.1804701115 (2018).
- 191 Malik, F. I. *et al.* Cardiac myosin activation: a potential therapeutic approach for systolic heart failure. *Science* **331**, 1439-1443, doi:10.1126/science.1200113 (2011).
- 192 Teerlink, J. R. *et al.* Cardiac Myosin Activation with Omecamtiv Mecarbil in Systolic Heart Failure. *N Engl J Med* **384**, 105-116, doi:10.1056/NEJMoa2025797 (2021).
- 193 Moreno, D., Knecht, E., Viollet, B. & Sanz, P. A769662, a novel activator of AMP-activated protein kinase, inhibits non-proteolytic components of the 26S proteasome by an AMPK-independent mechanism. *FEBS Lett* **582**, 2650-2654, doi:10.1016/j.febslet.2008.06.044 (2008).
- 194 Tuunanen, H. *et al.* Trimetazidine, a metabolic modulator, has cardiac and extracardiac benefits in idiopathic dilated cardiomyopathy. *Circulation* **118**, 1250-1258, doi:10.1161/CIRCULATIONAHA.108.778019 (2008).

8 Acknowledgements

I have received a great amount of assistance and support throughout my PhD study and writing this assertion.

Firstly, I would like to thank SFB1002 which has been providing the funding for my work.

Secondly, I would like to express my deep gratitude to my supervisor PD Dr. Antje Ebert for her valuable suggestions and patience. Her insight feedbacks have guided me to finish my study.

Thirdly, I appreciate the help and advice I have received from Prof. Dr. Henning Urlaub, Prof. Dr. Silvio O. Rizzoli, and Dr. John Chua Jia En.

Fourthly, I am particularly grateful for the assistance and support provided by my lab members throughout my PhD study.

Fifthly, many thanks to Prof. Dr. Ralf Dressel, Prof. Dr. Dörthe Katschinski and Prof. Dr. André Fischer who have participated in my thesis examination and defence.

Last but not least, assistance provided by Dr. Felipe Opazo, Prof. Dr. Blanche Schwappach, Prof. Dr. Peter Rehling, Prof. Dr. Wolfram-Hubertus Zimmermann, Dr. Malte Tiburcy, Prof. Dr. Gerd Hasenfuß, Prof. Dr. Stephan Lehnart, Prof. Dr. Karl Toischer, Dr. Sören Brandenburg, Prof. Dr. Andreas Janshoff, Prof. Dr. Niels Voigt, and Prof. Dr. Elisabeth Zeilsberg was greatly appreciated.